Surface patterning by means of Soft Lithography for Molecular and Bio-Electronics

Von der Fakultät für Mathematik, Informatik und Naturwissenschaften der
Rheinisch-Westfälischen Technischen Hochschule Aachen
zur Erlangung des akademischen Grades eines Doktors
der Naturwissenschaften genehmigte Dissertation

vorgelegt von
Diplom-Physiker
Daniel Christian Johannes Wendelin Schwaab
aus Landau in der Pfalz

Berichter: Universitätsprofessor Dr. rer. nat. Andreas Offenhäusser
Universitätsprofessor Dr. rer. nat. Markus Morgenstern

Tag der mündlichen Prüfung : 12.01.2007

Diese Dissertation ist auf den Internetseiten der Hochschulbibliothek online verfügbar.

Surface Patterning by means of Soft Lithography for Molecular and Bio-Electronics

Daniel Schwaab

Berichte des Forschungszentrums Jülich ; 4242
ISSN 0944-2952
Institute of Bio- and Nanosystems (IBN)
Bioelectronics (IBN-2) Jül-4242
D 82 (Diss., RWTH Aachen, 2007)

Zu beziehen durch: Forschungszentrum Jülich GmbH · Zentralbibliothek, Verlag
D-52425 Jülich · Bundesrepublik Deutschland
☎ 02461/61-5220 · Telefax: 02461/61-6103 · e-mail: zb-publikation@fz-juelich.de

Vollständig frei verfügbar im Internet auf dem Jülicher Open Access Server (JUWEL)
unter http://www.fz-juelich.de/zb/juwel

Abstract

The aim of this thesis was establishing *Soft Lithography*, mainly *Microcontact Printing*, as a powerful patterning technique for *Molecular* and *Bio-Electronics*. Especially patterns having sub 100 nm dimensions were subject of this thesis. Therefore a main issue addressed was the adoption of stamp materials with a Young´s modulus larger than 100 MPa that allowed the transfer of patterns with low critical dimensions. The Young´s modulus of these materials was more than an order of magnitude larger than that of materials commonly used. From a functional point of view emphasis was laid on the transfer of proteins. A process was to be developed that allowed the transfer of fully functional protein patterns. In addition the influence of *Contact Inking* on the functionality of transferred proteins was investigated. Beside that, protein patterns were used to demonstrate the influence of sub 1 μm patterns on the cell culture of neurons. Another major object of this thesis was the establishment of a technique to transfer metal patterns to arbitrary surfaces. Commonly used methods only work with a specific choice of stamp material, metal and target surface. The concept proposed and demonstrated in this thesis was more universal. *Crossbar* junctions having molecular interlayers were demonstrated as one application for this process.

A special design was developed based on lines and spaces with variable widths and gaps, which allowed the detailed investigation of various scaling issues. This pattern was used as template for the fabrication of masters. A process compromising *Electron-Beam Lithography* of PMMA resist and megasonic development followed by a *Reactive Ion Etching* process using a hydrogen-bromide plasma to etch into polysilicon provided best results. Ideal passivation of masters was obtained by vapor deposition of a perfluoro-octyl-trichlorosilane. It formed a smooth monolayer on the master´s surface prohibiting sticking of the stamp. PDMS stamps were fabricated by *casting* the liquid pre-polymer against the master. Since PDMS has got a rather low Young´s modulus defects such as *Pairing* were observed for the pattern design used. Thermoplastic material Affinity VP polyolefin was used as stamp material patterned by *Hot Embossing*. Although its Young´s modulus is fifty times higher than that of PDMS *Pairing* was observed. Therefore thermoplastic materials with an even higher Young´s modulus were used, namely polyolefins Zeonor, Zeonex, Topas, ionomere Surlyn and methacrylate Plexiglas. All these materials could be used to obtain defect free replications of the master. For Surlyn the edges were slightly rounded, while for the other materials the shape of the stamp pattern were rectangular.

Alkanethiols served as model molecules to investigate the printing process since they are commonly used in various applications and widely studied. For printing octadecanethiol *Contact Inking* was performed. Diffusion of the molecules for printing with PDMS stamps was found in agreement with previous publications. For Affinity VP stamps however, the diffusion was found to be less pronounced due to the different composition of the stamp material. For printing with Surlyn, which is rather

hydrophilic compared to PDMS or Affinity, a special wetting behavior was observed. A transfer was only observed at the edges of the patterns resulting in 60 nm patterns.

Redox-active proteins cytochrome *c* and azurin served as model molecules with a very specific, easy accessible, fragile functionality. Laminin was used as model system with a binding functionality. ECM gel and polylysine were used as model molecules for cell adhesion proteins. Beside their functionality they were used to demonstrate the printing of sub 100 nm patterns, since their mobility at surfaces is rather low due to the huge mass. For the first time *Contact Inking* was demonstrated with proteins using various stamp materials. A longer transfer time was found to be necessary for a complete transfer. The binding functionality of laminin was proven to be unchanged. However, the redox activity of cyt *c* was lost, but this is also true for *Wet Inking*. Therefore a novel process called *In-situ μCP* was developed. It was shown, that this process allows to transfer cyt *c* in a patterned manner without loosing the functionality.

The applicability of the protein transfer for the guiding of neuron growth with sub 1 μm patterns was demonstrated. The direction of neurite growth was dominated by the pattern direction. Larger patterns were preferred against thinner lines. First results indicate, that certain patterns might initiate a splitting of neurite bundles or a change of growth direction.

Surlyn was used for the printing of octadecanthiol and various proteins by applying an extra load in the 0.1 MPa range. Its Young´s modulus is higher than any other stamp material used in μCP so far. In order to use materials with an even higher Young´s modulus and in order to achieve very homogeneous printing results a novel process called *Air-Cushion μCP* was introduced. For the first time usability of stamp materials with a Young´s modulus larger 100 MPa was demonstrated. Small defects and inhomogeneities in the stamps patterns were compensated. With these hard stamp materials protein pattern transfer smaller than 40 nm was demonstrated.

A novel process called *Shuttle-Transfer Printing* was developed in order to transfer pre-patterned metal films with low kinetic energy to arbitrary substrates. The applicability of this process for the formation of *Crossbar* junctions was demonstrated. Therefore molecular layers were sandwiched between two gold electrodes. For alkanethiol molecules a tunneling like behavior was found, as expected. For long thiols the tunneling parameters were in agreement with various publications, while for shorter molecules the characteristic was dominated by the roughness of the electrodes. For junction with a cytochrome *c* interlayer also a tunneling behavior was observed. The tunneling parameters indicate, that the *Superexchange* mechanism makes major contributions to the charge transfer process.

Kurzfassung

Ziel der vorliegenden Arbeit war es *Weiche Lithographie*, insbesondere *Mikrokontakt-Drucken*, als leistungsfähige Strukturierungsmethode in der *Molekular-* und *Bio-Elektronik* zu etablieren mit Schwerpunkt auf der Übertragung von Strukturen kleiner als 100 nm. Ein Hauptpunkt war die Nutzung von Stempelmaterialen mit einem Youngs Modulus größer als 100 MPa. Bei den zu übertragenden Molekülen wurde der Schwerpunkt auf Proteine gelegt. Ein Prozess wurde entwickelt, der es erlaubt Proteine zu übertragen ohne deren Funktionalität zu beeinflussen. Zusätzlich wurde der Einfluss von *Contact Inking* auf die Funktionalität untersucht. Die Anwendung von Proteinmustern mit Dimensionen kleiner als 1 μm auf die Zellkultur von Neuronen wurde demonstriert. Ein weiterer Schwerpunkt der Arbeit war die Entwicklung einer Methode für die Übertragung von Metallmustern auf willkürliche Oberflächen. Bisher verwendete Methoden stellen sehr spezielle Anforderungen an die Stempelmaterialen, Metalle und Oberflächen. In dieser Arbeit wurde ein universelles Konzept entwickelt. Als Anwendung konnten *Crossbar*-Kontakte mit Molekül-Zwischenschichten gezeigt werden.

Ein spezielles Muster basierend auf Linien mit unterschiedlichen Breiten und Abständen wurde entwickelt, welches die vereinfachte Untersuchung verschiedener Skalierungsprobleme ermöglichte. Dieses Muster wurde als Vorlage für die Herstellung von Mastern benutzt. Master wurden mit standard Reinraum-Verfahren erzeugt. Das beste Resultat wurde mit Polysilizium-Substrat erreicht, welche in einem Prozess bestehend aus *Elektronenstrahl-Lithographie* von PMMA Lacken gefolgt von *Megaschall-Entwicklung* und *Reaktivem Ionenätzen* mit einem Bromwasserstoff-Plasma strukturiert wurden. Eine optimale Passivierung der Master wurde mit Vakuum-Deposition von Perfluoro-Oktyl-Trichlorsilan erreicht. Dabei konnte eine Monolage auf der Master-Oberfläche erreicht werden, die das Anhaften des Stempels verhindert. PDMS Stempel wurden durch *Abguss* mit flüssigem Vorpolymer vom Master erzeugt. Da PDMS einen relativ geringen Youngs Modulus hat, wurden Defekte wie z.B. *Pairing* beobachtet. Das thermoplastische Polyolefin Affinity VP wurde mit Hilfe von *Heissprägen* strukturiert. Obwohl der Youngs Modulus 50-mal größer ist als bei PDMS wurde dennoch *Pairing* beobachtet. Daher wurden weitere Materialen mit noch größerem Youngs Modulus wie z.B. die Polyolefine Zeonor, Zeonex und Topas, das Ionomer Surlyn oder das Methacrylat Plexiglas verwendet. Es konnten defektfreie Stempel mit allen Materialen geformt werden.

Alkanthiole wurde als Modelmoleküle für die Untersuchung des Druckprozesses benutzt, da diese sehr gut untersucht sind und für viele Anwendungen als Modellsystem benutzt werden. Oktadecanthiol wurde mit dem *Contact Inking* Verfahren übertragen. Für den Übertrag mit PDMS Stempeln wurde Diffusion in Übereinstimmung mit anderen Veröffentlichungen beobachtet. Für den Übertrag mit Affinty VP Stempel war die Diffusion allerdings geringer ausgeprägt. Beim Drucken mit Surlyn-

Stempeln wurde eine charakteristische Benetzung der Randbereiche beobachtet. Dies lässt sich mit der unterschiedlichen Benetzbarkeit von Surlyn im Vergleich zu PDMS und Affinty VP erklären. Nur im Randbereich der Muster wurden Moleküle übertragen. Dies führte zu Mustern im 60 nm-Bereich.

Die redoxaktiven Proteine Cytochrome *c* und Azurin wurden als Modellmoleküle benutzt wegen ihrer spezifischen, einfach messbaren, fragilen Funktionalität; Laminin mit seiner Bindungsfunktionalität; ECM-Gel und Polylysine als Modelmoleküle für Zelladhesions-Proteine. Daneben dienten die Proteine dazu das Drucken von Mustern kleiner als 100 nm zu demonstrieren, da ihre Mobilität an der Oberfläche durch ihre große Masse sehr gering ist. Zum ersten Mal konnte *Contact Inking* mit Proteinen gezeigt werden. Die Funktionalität von Laminin blieb dabei unverändert. Bei Cytochrome *c* hingegen ging sie verloren, was aber auch mit der *Wet Inking* Methode der Fall war. Eine neuartige Methode wurde entwickelt, nämlich *In-situ μCP*. Es konnte gezeigt werden, dass diese Methode das Drucken von Cytochrome *c* Mustern erlaubt ohne dabei die Funktionalität zu beeinflussen.

Die Anwendung von übertragenen Proteinmustern mit Mustern kleiner als 1 μm für das ausgerichtete Wachstum von Neuronen konnte gezeigt werden. Die Richtung des Neuriten-Wachstums wurde hauptsächlich durch das Muster vorgegeben. Größere Muster wurden gegenüber Kleineren bevorzugt. Erste Ergebnisse deuten darauf hin, dass spezielle Muster eine Aufteilung von Neuritenbündeln oder einen Wechsel der Wachstumsrichtung initiieren.

Surlyn-Stempel wurden für das Drucken von Oktadecanthiol und verschiedenen Proteinen benutzt. Es hat einen größeren Youngs Modulus als alle anderen bisher für *μCP* verwendeten Stempelmaterialen. Um Stempel mit größeren Youngs Modulus benutzen zu können wurde ein neuartiger Prozess entwickelt, nämlich *Air-Cushion μCP*. Dieser erlaubt gleichmäßige Druckergebnisse. Zum ersten Mal konnte die Anwendung von Stempelmaterialen mit einem Youngs Modulus größer 100 MPa gezeigt werden. Damit wurden Proteinmuster kleiner 40 nm übertragen.

Ein neuartiger Prozess zur Übertragung von vor-strukturierten Metallfilmen auf willkürliche Oberflächen wurde entwickelt, nämlich *Shuttle-Transfer Printing*. Die Anwendbarkeit dieses Prozesses für die Herstellung von *Crossbar*-Kontakten wurde gezeigt. Dazu wurden verschiedene Molekülschichten zwischen zwei Goldelektroden gebracht. Für Alkanthiole konnte wie erwartet ein tunnelartiges Verhalten beobachtet werden. Die gemessenen Tunnelparameter für langkettige Thiole stimmten mit anderen Veröffentlichungen überein, während das Verhalten für kürzere Thiolmoleküle von der Rauhigkeit der Elektroden dominiert wurde. An Kontakten mit Cytochrome *c* Zwischenschichten wurde ebenfalls Tunneln beobachtet. Die Auswertung der Tunnelparameter deutet darauf hin, dass der Superexchange-Mechanismus den größten Anteil am Ladungstransfer darstellt.

We have found a strange footprint on the shores of the unknown. We have devised profound theories, one after another, to account for its origins. At last, we have succeeded in reconstructing the creature that made the footprint. And lo! It is our own.

Sir Arthur Eddington (1882 - 1944)

Contents

Chapter 1

Introduction

Since the invention of the electron tube by J.A. Fleming in 1904 the triumphal procession of electronics was unstoppable. Today, there is almost no field of every day life, where electronics do not play a major role. The major trend in electronics is currently miniaturization. This does not only lead to smaller, but also cheaper devices with a higher processing speed and less power-consumption. This trend was described by G.E. Moore[1]. The final miniaturization step is yet known, namely *Molecular Electronics* (ME). Since single molecules are the smallest stable parts of matter, there could not be a smaller electronic device, than one that consists of only a single molecule. But ME does not only mean smaller devices, it also means new types of devices with novel architectures and new functionalities. There are molecules for example, that have moveable parts, such as rotoxanes, that could directly act as switches.
Another trend in today´s research is bionics[2]. Nature provides a huge repertory of materials and ideas, which can be used or applied for engineering or electronics. One of the most prominent examples for electronics are neuronal networks. No matter how fast and powerful computers are, there are operations, which are easy to perform by a brain, but very difficult for an artificial system. Image recognition is such an operation. The usage of biological components to perform electronic processing is called *Bio-Electronics* (BE). Furthermore BE compromises the combination of electronic and biological systems, e.g. for implants or sensors.
The major challenge in BE as well as ME is lithography, namely the patterning. ME demands precise patterning capabilities with very high resolutions, since the molecules are so small. In addition most molecules require special handling. BE demands gentle patterning processes, since biomolecules are fragile and require very specific conditions to keep their functionality, namely physiologic conditions.

[1] G.E. Moore predicted 1965 a doubling of the number of transistors on integrated circuits every 2 years. This trend still holds

[2] bionic = **bio**logy + electro**nics**

Presently, *Optical Lithography* (OL) is the most commonly used lithography technique in development and production of microelectronic devices. Its resolution is mainly limited by the wavelength of the light used. To reach sub 100 nm dimensions *Extreme UV* or *X-ray* light sources have to be used, which will lead to an enormous cost increase because of very expensive optical projection systems. It is thus doubtful, whether OL can be expanded to be useful for ME. Due to the rather harsh conditions, namely different organic solvents are involved, OL is only useful for BE in rare cases.
An alternative is a set of new emerging techniques, namely *Nanoimprint Lithography* (NIL). It was introduced as a patterning technique on the ITRS[3] roadmap for the 32 nm node and below. It compromises a bunch of techniques, which all make use of the mechanical deformation of resists. *Soft Lithography* (SL) is a special subgroup, which combines different approaches to use flexible, "soft" polymers for the imprint process. This allows a very gentle, precise processing. A very promising technique described in SL is *Microcontact Printing* (μCP). It allows the transfer of biomolecules and thus can be used as lithographic method. So far it was used for the patterning of proteins down to a few hundred nm. Several issues, such as the functionality of proteins or the maximum resolution were only addressed in very specific cases. On the other hand μCP is used to transfer organic molecules or even metals and thus is capable of building ME devices. This has only been shown in a few specific cases.
The main objective of this thesis was to establish *Soft Lithography* as a powerful sub 100 nm patterning technique[4]. Its potential usage in *Bio-Electronics* as well as *Molecular Electronics* was to be expanded. A first emphasis was laid on the fabrication of masters and stamps with appropriate patterns. Processes based on *Electron Beam Lithography* and *Reactive Ion Etching* were applied to fabricate masters/templates. New polymers, about 2000 times stiffer than the commonly used PDMS, were investigated as stamp materials. A new printing process was developed to investigate the dependency of the printing process to the applied pressure. Organic molecules served as model molecules to implement the new materials and techniques. Proteins were used as high molecular weight objects for the printing of sub 100 nm patterns. A second emphasis was laid on the transfer of proteins using different inking and printing techniques. The growth of neurons on protein patterns with sub micron dimensions was investigated. In addition a new in-situ printing process was developed to investigate the conservation of protein functionality. Here the metalloproteins cytochrome *c* and azurin with their redox activity served as model molecules. A third emphasis was laid on the advancement of *Nanotransfer Printing*. The knowledge gained in the development of *Nanocontact Printing* was used to build *Crossbar Arrays* with molecular interlayers. Alkanethiols and cytochrome *c* were used as interlayers to demonstrate direct tunneling through such devices.

[3] **I**nternational **T**echnology **R**oadmap for *S*emiconductors
[4] *Microcontact Printing* below 100 nm is also known as *Nanocontact Printing*

Chapter 2

Fundamentals and Methods

2.1 Soft Lithography

Lithography is a description for all processes used in semiconductor industry to pattern surfaces. The most widely-used method is *Optical Lithography* (OL). Its main advantage is, that it is a highly parallel process. This means, that a certain area can be patterned in a single step (up to 6 inch). The maximum resolution achievable is limited by the wavelength λ of light used. Classically this limitation is given by $\frac{\lambda}{2 \cdot A}$, with A being the aperture of the system. Since smaller structures generally mean cheaper and faster devices, the industry tries to further decrease this limitation. One approach is to reduce the wavelength by using ArF-lasers (193 nm) or even extreme UV sources (11 - 14 nm) to scale the limits down, on the other hand advanced techniques such as *Phase-Shift* masks, optical *Proximity Correction*, *Wave-Front Engineering* or *Immersion* are used to reduce the limit given by $\lambda/2$. It is expected, that 193 nm light sources could lead to structures with 65 nm haft-pitch. Nonetheless these new methods are getting more expensive and more difficult to achieve.
Likewise electrons can be used instead of light. According to de Broglie a wavelength can be associated to electrons with a certain energy due to wave-particle dualism; e.g. 10 kV electrons correspond to a wavelength of 12 pm. The drawback of electron writing is, that it is a serial process. The whole pattern has to be scanned with the electron beam. Nevertheless *Electron-Beam Lithography* (EBL) is the method of choice for R&D and small series production, if sub micron patterns are needed with arbitrary designs. A solution to increase the processing time is *Electron Beam Projection Lithography*. Here the beam is split and can thus write several patterns at the same time, but this is still rather slow compared to *Optical Lithography*.
Over the years many lithographic and patterning techniques have been proposed

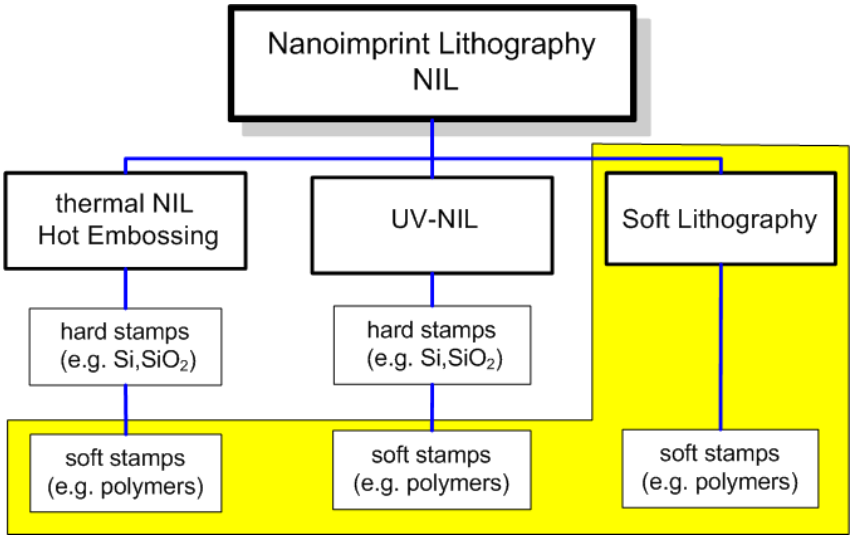

Figure 2.1: Categories of *Nanoimprint Lithography*

for a variety of different purposes. Reviews are given by [Gates et. al. 2004] and [Geissler et. al. 2004]. Basically resolution and throughput (speed) are correlated. There are rather slow methods, which allow the creation of patterns with very small critical dimensions (such as *Dip-Pen* or *Scanning Probe Techniques*), and there are others, which allow a rather high speed patterning at cost of larger critical dimensions. An empiric formula gives a power law[1] for the throughput as function of resolution [Marrian et. al. 2003]. One group of methods, which ranges outside this trend, is *Nanoimprint Lithography* (NIL). It combines a rather high resolution with a fast processing speed.

The general idea behind NIL is mechanical deformation of resists. A template called master is fabricated using conventional techniques such as OL or EBL. The master thus has a three dimensional pattern on its surface. In a replication process the negative pattern of the master is mechanically formed into a resist on a substrate (such as a silicon wafer). Subsequently this resist could serve either as an etch protection layer or as a layer for a lift-off process. Three different methods are known in NIL: thermal NIL, UV NIL and *Soft Lithography* (Fig.2.1).

In thermal NIL the resist is typically made of a thermoplastic material. The resist is press-formed by subsequential heating the setup over the glass-transition temperature of the resist, embossing it with the master and cooling everything down to room-temperature. This process is also known as *Hot Embossing* (HE). 25 nm patterns on a 270 mm^2 area were reported by [Chou et. al 1996a], [Chou et. al 1996b]. Using special preparation methods for the templates, 6 nm half-pitch structures were reported [Austin et. al. 2005] and sub 40 nm patterns by

[1] $R = 23 \cdot T^{0.2}$ with R: resolution in nm; T: throughput in μm^2/h

[Tallal et. al. 2005]. Contrarily in UV-NIL the resist is typically a UV-sensitive material. It is applied to the wafer as a liquid. The master is transparent and after a conformal contact between substrate and master is established, the resist is cured by UV-light illumination. Sub 60 nm were demonstrated by [Bender et. al. 2000]. A stepping process was demonstrated by [Colburn et. al 1999].
The results, namely the fidelity of patterns or the thickness of the residual layer, strongly depend on the flow of resist during the NIL process. The flow on the other hand depends on the viscoelastic properties of the resist as well as on the nanorheology. They are influenced by the master geometry as well as by the imprint parameters. A more detailed description is given by [Sotomayor Torres *Ed*. 2003].

Soft Lithography will be described in more details in the next section. The main advantage of NIL is, that a whole area can be patterned with small features in a single, parallel process. Since the master can be used several times (up to thousands), the fabrication cost per number of imprint processes is low. Although the template/master for NIL might be more expensive than an OL mask, resists and equipment for NIL are much cheaper than the equipment for sub 500 nm OL. The price for the "expensive" template/master can be distributed to all imprints and thus the price for a substrate in mass production is rather low.

2.1.1 Techniques in Soft Lithography

The general idea behind SL is, that a deformable, elastomeric material is capable of making a conformal contact to a rigid substrate. For OL it is known, that the contact between the rigid quartz-mask and the rigid wafer is a problem. Due to imperfections, dust grains, tensions or a temperature gradient gaps are formed between the mask and the resist leading to non-perfect exposure. It is generally not easy to bring two rigid flat surfaces into a uniform contact on a nanoscopic scale. In SL this problem is solved, because the flexible stamp is able

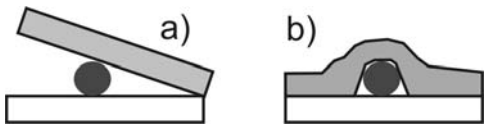

Figure 2.2: Barrier tolerance of *Soft Lithography*
a) Hard Stamp: a dust-grain or another barrier leads to a wedge shaped spacing between a hard stamp and a substrate.
b) Soft Stamp: a soft stamp can adopt to the barrier, only leading to a small area of non-contact.

to adjust to most imperfections [Bietsch et. al. 2000]. A dust grain for example only results in a small circular shaped defect and not in a large wedge error (Fig. 2.2 and Fig.4.50). More than that, with these flexible stamps one can also pattern non-flat surfaces, such as surfaces, which are already patterned, or even round and cylindrical surfaces [Xia et. al. 1998].

At first sight *Soft Lithography* compromises NIL processes (either thermal or UV) where the template/master is made out of an elastic, deformable (and thus "soft") material. Using these soft templates a high uniformity on large areas is achieved [Chang et. al 2005]. Besides that SL compromises other techniques capable of patterning resists on substrates. Across-the-board SL compromises all techniques, which make use of a deformable material to pattern anything on a substrate. This includes methods, which uses the soft material to transfer objects such as molecules or metals. The mostly used techniques of SL (besides the NIL applications) are shown and illustrated in Fig.2.3. These categories were first introduced by [Xia et. al. 1998]. Basically SL also starts with a template/master. This master is used to form a copy out of a deformable material. This copy is called the stamp and thus carries the negative patterns. A thermal process to fabricate the stamp is called *Hot Embossing*. The process of making the stamp out of a liquid pre-polymer mixtures is called *Casting*. A variety of SL techniques have been proposed and realized. Among others: *Microcontact Printing* (μCP) is a method in which the stamp is used to transfer molecules on a target substrate (more details will be given in the next section).

Replica Molding (REM) is a method in which the stamp itself is used as a master for a casting or embossing process (Fig.2.3A). The stamp is formed by *Casting*, *Hot Embossing* or any other technique. Also thermal and UV NIL with elastomeric templates can be thought of as replica molding.

Microtransfer Molding (μTM) is a method in where the suppressions of the stamp are filled with a material, which is later on molded onto a substrate (Fig.2.3B).

Micromolding in Capillaries (MIMIC) is a method where a stamp is placed on a substrate and then the resulting channels are filled with a material, which is molded onto the substrate (Fig.2.3C). This method is also known as Inverse Microcontact Printing.

Solvent-assisted Micromolding (SAMIM) is a method in which a solvent is placed into the suppressions of the stamp (Fig.2.3D). The substrate carries a polymer sensitive to this solvent. After bringing both into contact the solvent removes this polymer in the suppressions.

In recent years more and more variations of the previous mentioned techniques were reported, among others: *Nanotransfer Lithography* (nTP)

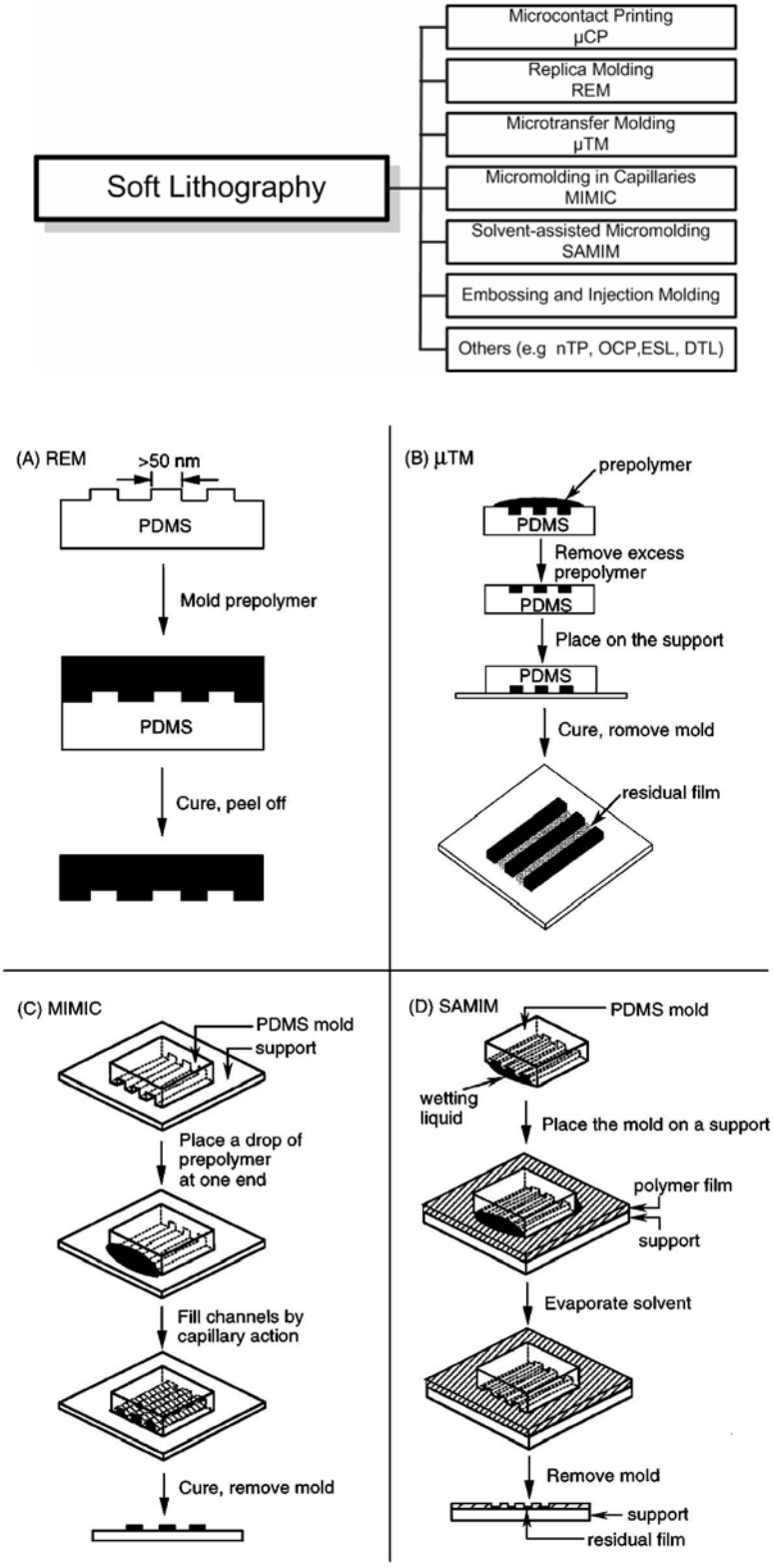

Figure 2.3: Categories of *Soft Lithography* and schematics of some techniques; taken from [Xia et. al. 1998]

(more details will be given in the next section), *Overpressure Contact Lithography* (OCL) [Guo et. al. 2004], *Edge Transfer Lithography* (ETL) [Cherniavskaya et. al. 2002], *Microdisplacement Printing* [Dameron et. al 2005], *electrical μCP* [Jacobs et. al. 2001] or *Decal Transfer Lithography* (DTL) [Childs et. al 2005]. All techniques have their specific advantages or drawbacks and are useful for specific applications.

Beside the patterning of resist there is a variety of things, which can be patterned or transferred with SL: organic molecules (such as self assembled monolayers (SAM) of thiols or silanes) [Kumar et. al. 1993]; biomolecules (such as proteins, DNA or lipids) [Bernard et. al. 1998]; metals (such as gold) [Loo et. al. 2002a]; macromolecules (such as dendrimers) [Li et. al. 2002]; polymers [Yan et. al. 1999]; nano-particles [Santhanam et. al. 2004]; lipid bilayers [Hovis et. al 2000] and many more.

This thesis is focused on the transfer of alkanethiol SAMs as model molecules, proteins and metals. For alkanethiols and proteins μCP is the method of choice and for metals nTP so far. The following sections will explain μCP and nTP in more details.

2.1.2 Microcontact Printing

Microcontact Printing (μCP) is one of the first and maybe the most important technique in Soft Lithography. An elastomeric stamp is formed of a solid template called master. Molecules are immobilized to this stamp by inking techniques and are subsequently transferred to a substrate by printing. Terms, which recur for μCP and most other SL techniques as well, are:

- Master
- Release Agent
- Stamp
- Inking and Printing

These issues will be discussed in more details in subsequent sections.

μCP was introduced by [Kumar et. al. 1993]. An elastomeric stamp was used to transfer a layer of alkanethiols in a patterned manner onto gold. The molecules served as an etch barrier in a successive etching step [Kumar et. al. 1992]. Starting

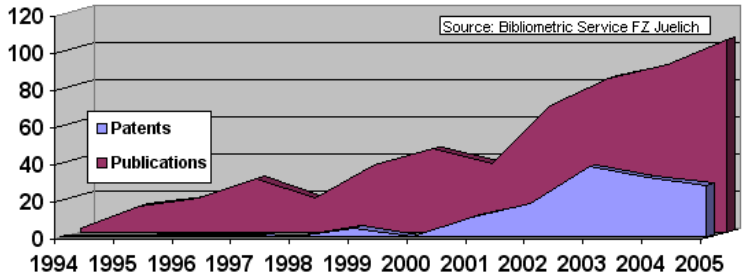

Figure 2.4: Number of publications dealing with μCP

from here over the next years the printing process, as well as the etching process have been further improved [Geissler et. al. 2002]. The next step was to investigate methods to perform μCP on large areas (80 cm^2 and more) with good homogeneity [Decre et. al. 2004]. In industrial applications this method is employed for building *TFT-LCD*[2] [Burdinski et. al. 2005]. Another direction was to use the principles of μCP for other molecules such as proteins [Bernard et. al. 1998]. In this concern an application is to pattern proteins such as antibodies for diagnostic applications [Renault et. al. 2003] or proteins such as ECM gel[3] for the guiding of cells [Yeung et. al. 2001], [Lauer et. al. 2001]. Proteins can also be patterned for applications in molecular electronic devices [Maruccio et. al. 2005]. To overcome the limitations of diffusion (Chapter 2.1.7) more heavy weight molecules such as dendrimers were investigated [Li et. al. 2002]. Another approach to reduce diffusion using contact times of sub 50 ms was reported by [Helmuth et. al 2006]. Patterning of different molecules was demonstrated through sequential printing or by using a microfluidic network [Bernard et. al. 2000], [Crozatier et. al 2006].

Since 1993 the number of publications and patents dealing with μCP is still increasing (Fig.2.4) as well as the number of different molecules utilized or the number of applications.

2.1.3 Nanotransfer Printing

For the transfer of metals to target surfaces a modification of μCP was proposed, namely nTP. The classical approaches of bringing patterned metal layers onto target substrates are *Shadow-Evaporation*, *Lift-Off* or wet/dry etching of metal layers. All these methods have in common, that the metal is directly evaporated onto the target substrate. In *Nanotransfer Printing* (nTP) a metal layer is evaporated onto a

[2] **T**hin **F**ilm **T**ransistor **L**iquid **C**rystal **D**isplay
[3] **E**xtra **C**ellular **M**atrix gel

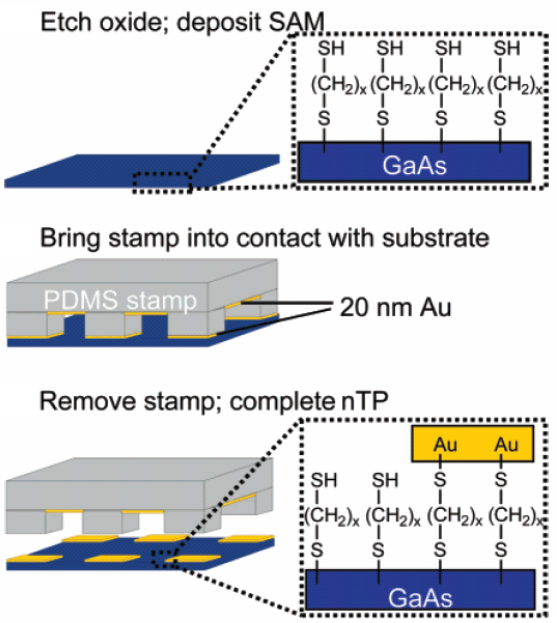

Figure 2.5: Schematic of *Nanotransfer Printing*; taken from [Loo et. al. 2003a]

stamp and transferred in a subsequent step to a target substrate under ambient conditions. The metal-layer should only weakly bind to the stamp, but strongly to the target substrate. Thus a transfer of metal from the stamp to the substrate is possible. However, the stamp and substrate have to be chosen such, that the adhesion of gold is weak on the stamp and strong on the substrate. This can either be achieved by a difference in the surface free energy [Hur et. al. 2004] or by covalent binding of the metal to the target substrate. nTP proved to be useful, when the target substrate contains special functionalities, such as molecule layers, that may be affected by direct evaporation processes. nTP was introduced by [Loo et. al. 2002a,b,c]. Like in μCP a master is used to form a stamp, but instead of inking the stamp with a molecule solution, a metal layer is evaporated on top of the stamp. The stamp thus has the metal on its surface and inside the suppressions. The stamp is then brought into contact with a substrate and the metal on the protruding patterns of the stamp is transferred while the metal inside the suppressions of the stamp is not. Therewith a metal pattern is transferred having the same pattern than the stamp and master. In reality this process is a bit more complex. So far *polydimethylsiloxane* (PDMS) was used as stamp material (more details about PDMS are given in Section 2.1.6) and gold as metal. Loo et. al. used the covalent binding. There the target substrate is modified such that covalent binding between gold and substrate is achieved. Covalent binding is the strongest interaction possible between two atoms besides ionic or electrostatic interactions. Sulfur containing molecules are the molecules of choice for the covalent binding of gold, because the S-Au bond is rather strong. In order to

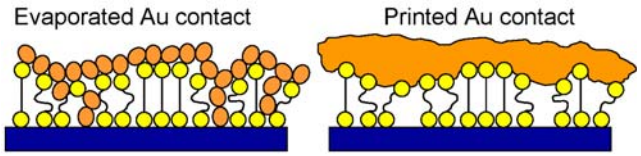

Figure 2.6: Schematic differences between evaporated and printed metal layers; taken from [Loo 2003b]

have a substrate surface with a high coverage of sulfur group mercapto-silanes on silicon and dithiols on GaAs were used. These organic molecules form SAMs on the surface. The process as reported by [Loo et. al. 2003a] is shown in Fig.2.5.

Of great importance for this thesis are *Molecular Electronic* devices with molecular functions such as *Crossbars* with molecular interlayers. Since evaporation processes are performed under UHV conditions, molecules can be harmed (especially proteins). Direct filaments could be created due to imperfections in the molecular layer (Fig.2.6 left). The molecular layer could even be damaged due to the energy of the evaporated atoms. This is avoided by nTP, since the transfer process takes place under ambient conditions. The metal layer is supposed to span small imperfections in the molecular layer (Fig.2.6 right). A comparison between directly evaporated gold layers onto molecular layers and nTP transferred layers is given by [Hsu et. al. 2003] and [Loo et. al. 2003a]. Their conclusion is, that direct contacts between the top gold layer and the substrate are formed by evaporated electrodes. These "shorts" dominate the IV-characteristic. nTP on the other hand is a gentle process. In addition it is a fast, cheap and capable method of transferring patterns down to a few hundred nm [Zaumseil et. al. 2003].

2.1.4 Master

The μCP stamps are replicated from templates called master or mold. In general masters are made of a rigid material like silicon or siliconoxide and patterned with any of the classical lithographic methods. For patterns in the hyper μm range *Optical Lithography* is the method of choice. For sub μm patterns *Electron-Beam Lithography* is often used (an introduction to EBL will be given in the next section). These methods create a three dimensional resist pattern on the substrate. The assembly of substrate and resist could either be directly used as master or the resist could be used as an etch mask to etch the pattern into the silicon/siliconoxide. The later results in a much harder and more defined surface. A silicon surface can easily be cleaned by plasma or acid treatment while a resist surface can only be cleaned with very gently methods. Other ways of fabricating masters are NIL, *Focussed Ion*

Beam Writing or *Soft Lithography* itself. In *Replica Molding* for example a stamp is used as a master.

Electron Beam Lithography

In order to define structures smaller than 500 nm *Electron Beam Lithography* (EBL)[4] is mostly used. A focused electron beam is moved over a resist surface exposing and thus modifying the resist, that it contacts. Exposed areas of the resist change their properties due to the energy that is deposited. An advantage of EBL is, that the wavelength of electrons depends on this energy. The electron beam has an energy of 1 - 100 kV. This corresponds to a de Broglie wavelength down to the pm range. Thus the maximum resolution only depends on the beam diameter and the properties of the resist. The drawback of EBL is the small throughput compared to OL or SL, which are able to pattern a whole wafer in one shot. The smallest generated patterns so far are a few nm, but these are rather special, limited cases. For more complex, arbitrary patterns the limit is between 10 - 20 nm [Marrian et. al. 2003].
Common variables used in EBL are: beam size, beam step size, dose and acceleration voltage. A commonly used system for electron beam writers is the *gaussian beam* system, which works in *vector-scan* mode. This means, that a circular shaped beam with a gaussian intensity distribution is moved just across the areas, which are to be exposed. Other systems work with rectangular or variable shaped beams. Another operation mode is the *raster-scan mode*. There the beam is moved over all parts of the sample and is blanked in areas where the resist should not be exposed.
The configuration of an electron-beam writer (Fig.2.7a) is similar to a *Scanning Electron Microscope*. An electron gun is mounted in an UHV chamber. Magnets, coils and cathodes are used to focus, shape and deflect the beam. The substrate is mounted on a moveable stage inside the chamber. The whole setup is vibrational isolated and electromagnetically shielded.
In order to define patterns with sharp edges, the beam size should be at least several times smaller than the structure size. The beam is scanned over the resist such, that every part of the design is exposed. Therefore the beam-size is chosen to be $\sqrt{2}$ times the beam-step size (Fig.2.8). The dose is the accumulated charge, which is brought into a certain area. It is measured in $\mu C/cm^2$. A common drawback of EBL is, that the dose is not only deposed in the area of the beam spot. Due to the gaussian shape of the beam spot, small amounts of charge are also deposited up to several μm away from the center. Electron scattering in the resist and the substrate lead to undesirable influence in the regions adjacent to those addressed by the electron beam. This effect is known as *proximity effect*. [Parikh 1979a,b,c] discusses several aspects of this effect in his studies. Proximity results in isolated

[4] An introduction is given in [Rai-Choudhury Ed. 1997].

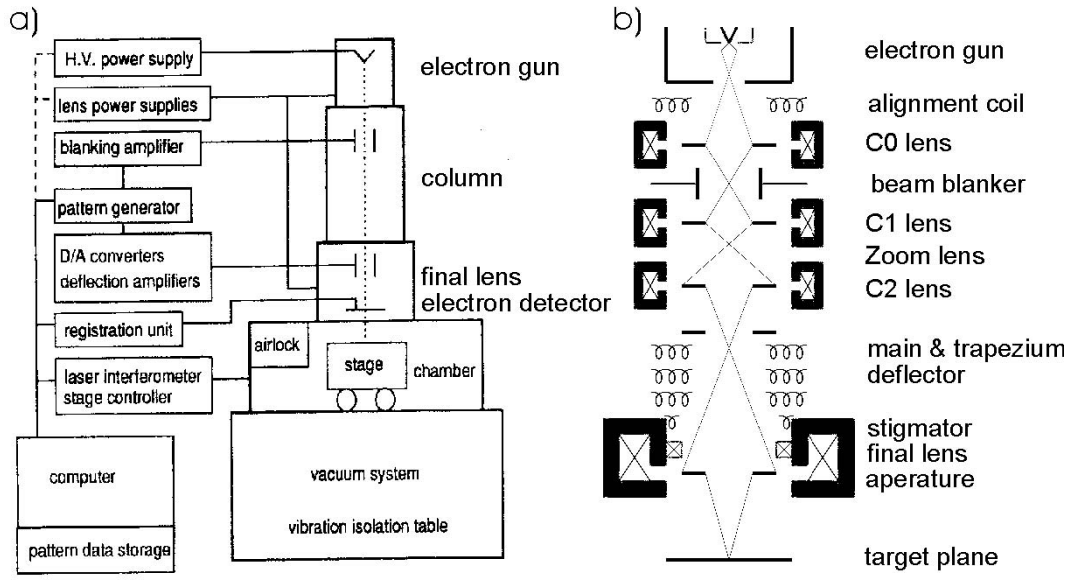

Figure 2.7: Configuration of an Electron-Beam Writer
a) major components, taken from [Rai-Choudhury Ed. 1997]
b) lens system for beam optics

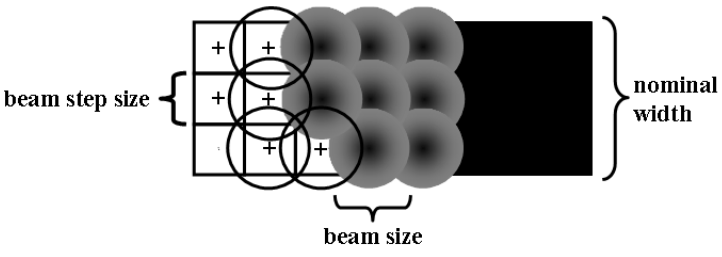

Figure 2.8: Schematic of the Gaussian Vector Scanning
beam-size = $\sqrt{2}\cdot$ beam-step size; here nominal width = $3\cdot$ beam-step size

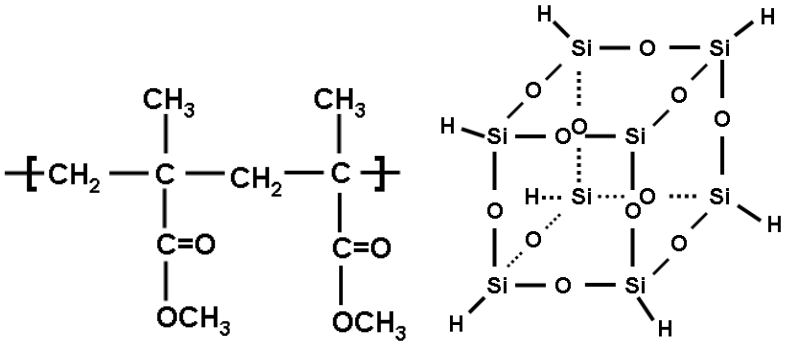

(a) PMMA (b) HSQ

Figure 2.9: Electron beam resists

patterns somewhat narrower than designed and lines in densely patterned areas somewhat wider than designed. The scattering of electrons can be simulated using *Monte Carlo methods*. Forward scattering in the resist leads to a spreading of the beam into an $\sim$100 nm distribution; backward scattering in the resist and substrate lead to a distribution of $\sim$1 - 2 μm [Parikh 1979a]. This problem affects single isolated lines as well as dense lines. To account for this problem proximity correction routines are used. Typically they change the doses for the individual patterns according to the expected proximity effect. Another option is to change the design of the pattern itself. Since electron scattering strongly depends on the type of resist, resist thickness, substrate and other parameters it is in general a long process to find a perfect correction routine. An example for a proximity corrected design file is given in Fig.B.6.

Many different types of resist are commercially available for EBL. Like in OL they are grouped into two classes: positive tone resists (PTR) and negative tone resists (NTR). For NTR the patterns, which are exposed, stay during development, while for PTR the exposed patterns are removed during development.
Two common resists optimized for EBL are polymethylmethacrylate (PMMA) as a PTR and hydrogene silesquioxane (HSQ) as a NTR.

PMMA is an organic polymer consisting of hydro-carbon chains with methacrylic moieties (Fig.2.9b). It is often used as an alternative for glass due to its unique properties, such like its transparency or that it does not shatter. Therefore it is also known as *Plexiglas*. PMMA is used as PTR since 1968 [Haller et. al. 1968]. The electron beam breaks the polymer into fragments. These fragments can be solved in a developer, while the unexposed parts are insoluble (Fig.2.10). Lines down to 4 nm were achieved [Hu et. al. 2004]. Transfer techniques such as *Lift-Off*

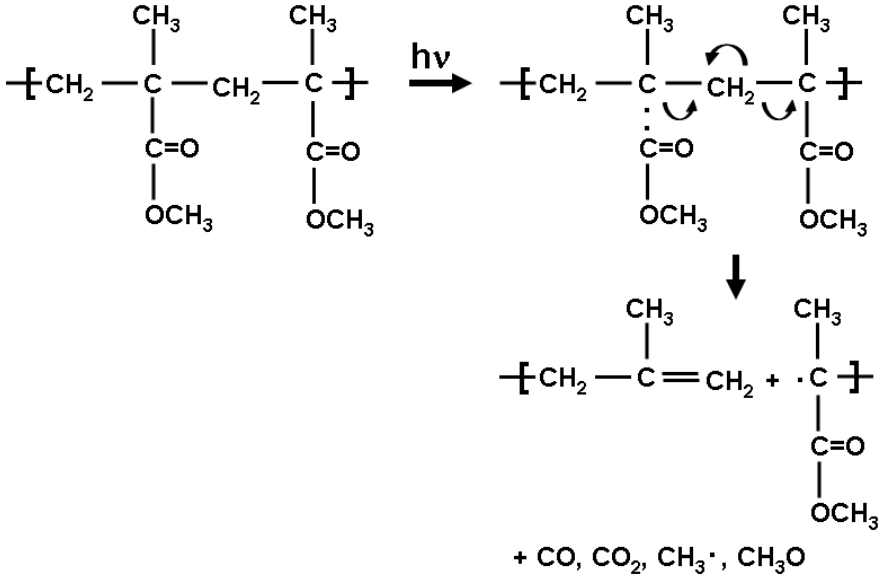

Figure 2.10: Electron beam induced reaction that occurs in PMMA; taken from http://www.azonano.com/details.asp?ArticleID=1208

and *Reactive Ion Etching* can be used to transfer the pattern to the wafer. Lift off processes down to 5 nm [Vieu et. al. 2000] are reported. Due to its thermoplastic properties it is also used in *Hot Embossing* and thermal *Nanoimprint Lithography* [Chou et. al 1996a].

HSQ $\left[HSiO_{(3/2)}\right]_8$ is an inorganic polysiloxane with eight silicon atoms arranged in a cube (Fig.2.9a). Thermal curing leads to a removal of hydrogen atoms and the formation of SiO_2 structures [Namatsu et. al. 1998]. Cured HSQ is a low-k dielectric material ($\varepsilon_r = 3$), which is used as spin-on dielectric coating or as planarization coating. Beside thermal curing also an electron beam can be used to transfer the HSQ structure to SiO_2 structure in NTR fashion [Namatsu et. al. 1998]. Up to now, single lines down to 7 nm [Maile et. al. 2000] and a resolution of 20 nm [van Delft et. al. 2000] were reported as well as aspect ratios[5] up to 4.4 [Henschel et. al 2003]. Besides EBL HSQ is also used for *Extreme UV Lithography* [Junarsa et. al. 2005], *Proton Beam Lithography* [van Kan et. al. 2006] as well as for *Nanoimprint* and *Nanotransfer* processes [Matsui et. al. 2003]. Using the HSQ on a silicon surface one obtains a high selectivity for silicon etch processes [Wahlbrink et. al. 2005].

[5] aspect ratio = height / width

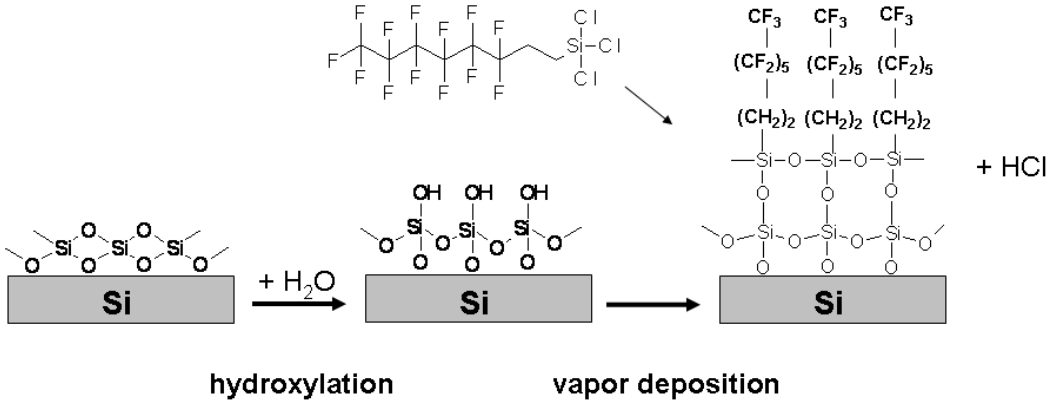

Figure 2.11: Silanization reaction
A freshly cleaned wafer exposes an oxygen terminated surface. During a reaction with water a hydroxylated surface layer is formed. Silane molecules are able to dock to this groups. In a case of silane with three chlorine groups, the chlorine is able to demerge forming HCl. The silane groups crosslink with the silicon-oxide and their next neighbor forming a monolayer.

2.1.5 Release Agent

After the master is fabricated its surface has to be modified with a layer of a low surface energy agent called lubricant or release agent. After curing the stamp polymer the surfaces of master and stamp perfectly match. Even median interactions (e.g. van der Waals) between the stamp and master surface lead to very strong sticking, which makes a separation impossible. In some cases, e.g. PDMS on silicondioxide surfaces, even covalent bonds are formed. In that case a separation could either damage the master or deform and destroy the stamp. Therefore a lubricant or release agent layer is needed, which eliminates covalent or most van der Waals interactions between the stamp and master surface. As already mentioned most masters are made of silicon or siliconoxide, thus the release agent layer of choice is a fluor containing self assembled monolayer. Basically two groups of molecules are reported in literature: Trichloro-silanes with CF_2 groups[Xia et. al. 1998] or CF_x molecules [Jaszewski et. al. 1999]. These molecules will cover the surface of the master with a dense monolayer exposing the fluor containing groups. Since fluor is an inert group, which does only weakly interact with other groups, the interaction between master and stamp is minimized. Covalent binding, hydrogen bonds between master and stamp are thus eliminated and van der Waals interactions are minimized. A homogenous release agent layer, at best a monolayer, is of major importance. A layer with aggregates could cover part of the structures of a master and one would transfer the undesired structure to the stamp. Up to 50 nm aggregates can often be found at lubricant layers

deposited under non-optimized conditions. The cleanness of the surface (in this case of the master´s surface) is important for the formation of a dense monolayer. Most common are dry-cleaning methods such as UV/Ozone or oxygen plasma and wet-cleaning methods such as RCA[6] cleaning. For the formation of silane layers two methods are known to coat the surface: liquid deposition and vapor deposition. Best results for silane layers were obtained using vapor deposition [Jung et. al. 2005]. The reaction that takes place is crosslinking between the silicon atoms with oxygen at an oxidized surface (Fig.2.11). This occurs due to a reaction of the -Si-O- bond with water to -Si-OH. The chlorine atoms of the silane demerge forming HCl and -Si-O-Si- bonds are formed between the silane and the surface as well as in between the silanes. While water is needed for the reaction to occur on the surface, to much water or water in the silane leads to a polymerization between the silane molecules, forming agglomerations. That is why environmental water is a critical parameter.

CF_x can also be deposited as a plasma polymerized film using CF_4 or C_4F_8 gas[7] or as ion sputtered film of a teflon target [Jaszewski et. al. 1999].
Often publications report the achievement of monolayer coverage measured by means of integrative methods such as ellipsometry. Such results only indicate, that the mean thickness is that of a monolayer, but they do not proof a closed monolayer without agglomerations. This proof has to be given with AFM or STM data. Therefore it is sometimes difficult to compare results reported by different groups.

2.1.6 Stamps

The stamp is a negative replication of the master. To achieve the benefits of SL as described earlier, the stamp is supposed to be made of an elastomeric, soft polymer material. In order to guarantee a conformal contact between stamp and target substrate the stamp material has to adhere to the surface. This is achieved by a low Young´s modulus and a high work of adhesion [Bietsch et. al. 2000]. In this context Young´s modulus is often used as a measure of the stiffness. It is given by the ratio of tensile stress to tensile strength:

$$Y = \frac{F/A}{\Delta l / l_0} \tag{2.1}$$

Here F is the force applied to a sample of initial length l_0 and cross-section A. Δl is the elongation observed. Note, that the relation stress/strain has different regions. The Young´s modulus can only be applied to the elastic linear part of

[6] method developed by the **R**adio **C**orporation of **A**merica
[7] The CF_x passivation is also used to cover the sidewalls in the *Bosch-process*.

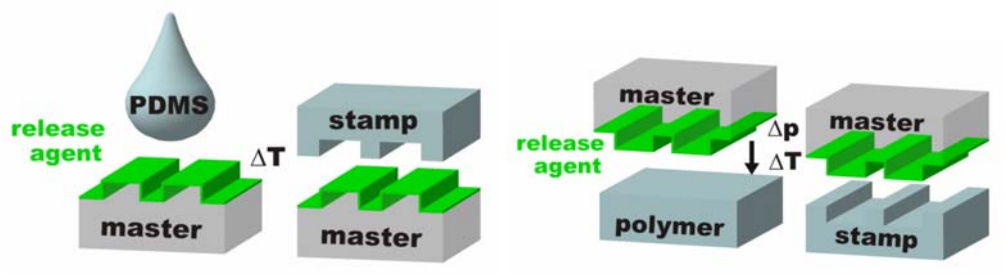

(a) Casting (b) Hot Embossing

Figure 2.12: Schematics for Casting and Hot Embossing
a) a liquid pre-polymer is poured over a master and cured with light or temperature.
b) a thermoplastic polymer is heated above its glass-transition temperature and pressed into a master.

the relation. While further expanded the polymers suffer a non-linear plastic deformation followed by fracture. For thermoplastic materials the linear region is rather pronounced, while for elastomeric rubbers it is difficult to assign a linear region.
On one hand the optimal material has to be soft enough to make a conformal contact to the substrate, while on the same time it has to be stiff enough to allow high resolution patterning and long-range accuracy. In general two methods for the fabrication stamps are used: *Casting* and *Hot Embossing* (Fig.2.12)
During *Casting* (CA) a liquid pre-polymer mixture is poured over a master. Curing is done either by heating above a certain temperature, using UV light, if it is UV sensitive, or just by time. The most commonly used material is polydimethylsiloxane (PDMS).
PDMS is a crosslinked silicone. It is available as a two component system; a base and a curing agent. Dimethylsiloxane molecules are crosslinked with crosslinker molecules using a platinum catalyst (Fig.2.13). After mixing and degassing the mixture is applicable for casting. By mixing the two components with different ratios or adding other chemicals one can change the stiffness of the PDMS. Since its Young´s modulus with a few MPa is rather low compared to other polymers, the application of the standard mixture is rather limited. For this reason a mixture, which leads to a stiffer PDMS called hard-PDMS or h-PDMS, was proposed [Schmid et. al. 2000]. With this mixture the Young´s modulus can be increase to about 10 MPa, but the material becomes very brittle. A more suitable combination is assembled by a multi-layer. h-PDMS is casted onto the master as a thin layer. In order to get a thicker stamp, it is backfilled with soft PDMS. If one needs to avoid bending of the stamp, one can also attach a glass slide as backplane on top of this assembly [Schmid et. al. 2000].

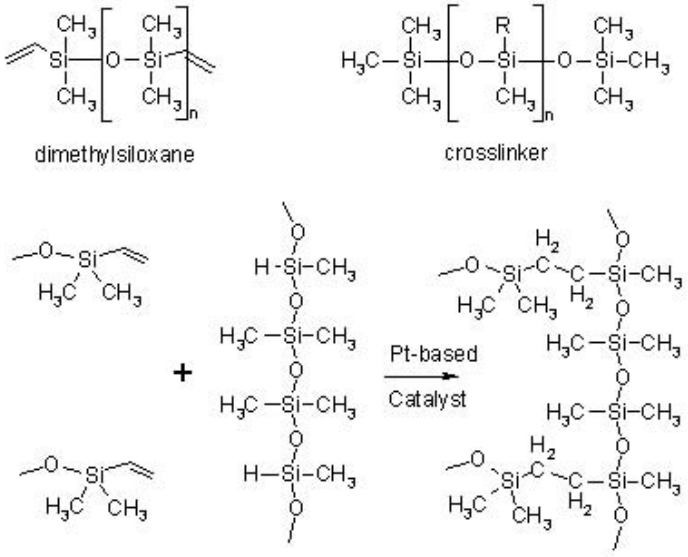

Figure 2.13: Polymerization of polydimethylsiloxane
A base (dimethylsiloxane) is mixed with a crosslinker. A Pt-based catalyst promotes the polymerization reaction.

Hot Embossing (HE) is a procedure similar to thermal NIL. A thermoplastic material is heated above its glass-transition temperature and is pressed into a master with a certain force [Heckele et. al 2004]. Master and stamp can be separated again after cooling down below the transition temperature. A class of materials, which is frequently used for HE are polyolefin plastomers (POP).
POP is made by polymerization of alkane chains with the help of a catalyst (Fig.2.14). The most prominent examples are polypropylene and polyethylene, which have countless applications in daily life. In contrast to PDMS POP consists of long chains, that are not crosslinked to each other but clewed. Such polymers are assigned to the class of thermoplastic materials, are much stiffer and can be patterned by means of HE. Since this is a single step process, it is much easier and faster to perform than making PDMS stamps consisting of several layers. So far only one special class of POP was used in μCP namely *Affinity* of Dow Chemical [Csucs et. al 2003]. It´s Young´s modulus is around 50 times larger than that of PDMS (Tab.4.1). Another thermoplastic materials, which was used for the fabrication of stamps, is a polystyrene block copolymer [Trimbach et. al. 2003]. Its Young´s modulus is in the same range than that of Affinity POP. These are the hardest materials used so far in μCP.

A problem associated with the stamps are contaminations as reported by

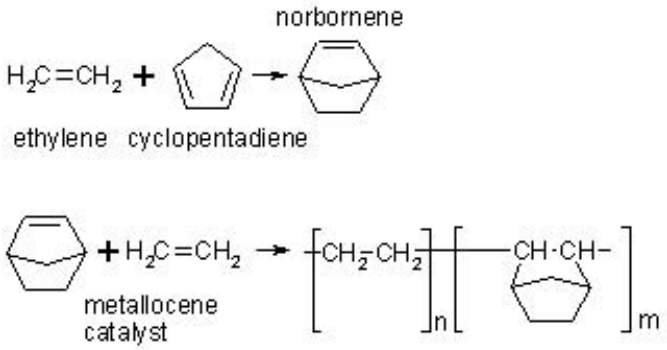

Figure 2.14: Polymerization of a polyolefin
This reaction shows the polymerization of *TOPAS*®, a material manufactured by Topas Advanced Polymers

[Graham et. al. 2002], [Glasmaestar et. al. 2003] and others. They report silicon containing contaminations after using PDMS as stamp material. This effect is illustrated in Fig.4.28. It is mainly due to low-weight, non-crosslinked molecules diffusing out of the PDMS. Several possibilities were proposed to get rid of these undesirable transfer: solution treatment, UV/ozone treatment [Glasmaestar et. al. 2003] and plasma treatment [Langowski et. al. 2005] of stamps. These methods are also used to change the surface properties such as the contact angle. To achieve optimal transfers for non-polar and polar inks, the surface properties of the stamp have to be chosen adequate as reported by [Hu et. al. 2004b], [Delamarche et. al. 2003] and [Trimbach et. al. 2004]. One advantage of using POP stamps is, that no contaminations during the printing process can be observed [Csucs et. al 2003]. Furthermore the surface properties of thermoplastic polymers can also be changed using above mentioned methods.
[Gates et. al. 2003] and [Hua et. al. 2004] indicate, that the ultimate resolution limit for the replication is near the theoretical cross-link distance, which for PDMS is 1 - 3 nm. [Hua et. al. 2004] could replicate SWNT[8] in PDMS. This leads to low aspect ratio structures that might not be applicable in μCP or nTP.

Stability of Stamps

The stability of a stamp is mainly depended on its Young´s modulus and its geometry. Consider a pattern of lines. The geometric information is given by the width of the lines **w**, the height of the lines (or depth of the trench) **h**, the length of a

[8] **S**ingle **W**alled **C**arbon **N**anotubes

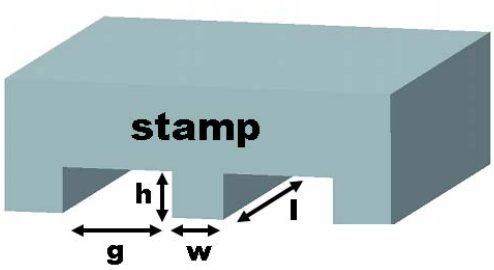

Figure 2.15: Geometry of stamps (for simplicity the pattern consists of parallel lines) **h** height of the pattern; **w** width of a line; **l** length of the pattern lines; **g** gap between neighboring lines;

line **l** and the gap between neighboring lines **g** (Fig.2.15). A parameter, which is of major interest, is the aspect ratio. It is the ratio of height vs. width. An aspect ratio of 2 means, that the line is twice as high as wide. It is clear, that there is a critical ratio for the structures to be stable depending on the stiffness of the material. If it is too high, deformations will occur. For PDMS stamps the ratio is typically in the range of two. This is also true for masters. Three major stability problems for stamps are known: Pairing, Sagging and Collapse.

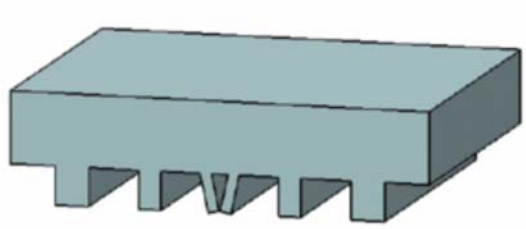

Figure 2.16: Pairing effect

Pairing (or lateral collapse) is an effect where neighboring patterns stick together. An analytical formula for the stability criterion is given in equation 2.2 according to [Hui et. al. 2002]:

$$\frac{h}{w} \cdot \left[\frac{8\gamma_S}{3E^* w}\right]^{\frac{1}{4}} < \sqrt{\frac{g}{w}} \tag{2.2}$$

Patterns are stable as long as the expression is true. Thus no pairing occurs as long as the left hand side is smaller than the right hand side. $E^* \equiv E/(1-\nu^2)$ is the plane strain modulus of the stamp material, where E is the Young´s modulus and ν is the Poisson´s ratio of the material. This can be approximated with $E^* \approx \frac{4E}{3}$. This

is true since the poisson ratio is typically between 0.3 and 0.5. For the materials used in this thesis ν is not available and thus the approximation is used. γ_S is the surface energy of the material. Obviously an increase of height will increase pairing, while increasing Young´s modulus will decrease it. This can be also achieved by increasing the gap or the width of patterns. A larger surface energy on the other hand leads to more pairing. The contribution of the height has got the largest impact on the stability.

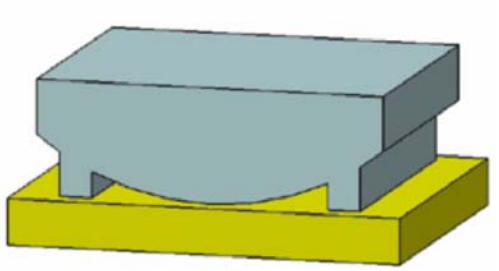

Figure 2.17: Sagging effect

Sagging (or roof collapse) occurs when the bottom of the stamps bends so much, that it contacts the substrate. An analytical formula for the stability criterion is given in equation 2.3 according to [Hui et. al. 2002]:

$$\frac{-2\sigma_\infty g}{\pi E^* h} \cdot \left(1+\frac{w}{g}\right) \cdot \cosh^{-1}\left[\sec\left(\frac{\pi g}{2(g+w)}\right)\right] < 1 \tag{2.3}$$

Patterns do not suffer sagging while the expression is true. Here σ_∞ is the uniform stress applied to the top of the stamp. It is obvious, that increasing the height or Young´s modulus will make the pattern more stable. It is also clear, that increasing the uniform stress will promote sagging. It can be seen, that increasing the width of patterns will decrease sagging, whilst increasing the gap will increase the sagging.

Another problem that can occur is buckling of lines, which might lead to a different shaped print or the rounding of lines or the complete collapse of patterns. This happens if the material is not capable to reproduce the patterns at all. A more detailed view on sagging is given by [Decre et. al. 2005] and [Huang et. al. 2005]. The collapse of high aspect ratio structures was investigated by [Roca-Cusachs et. al. 2005]. They state, that the maximum aspect ratio achievable is also depended on the width. For PDMS it is less than two in the sub micron regime.

Hydrophobicity of Stamps

The transfer of inks mainly depends on the surface properties of the stamp material. The method of choice to determine the wettability of a material is measuring the contact angle. The contact angle is given by Young´s equation:

$$\cos(\theta) = \frac{\gamma_{SV} - \gamma_{SL}}{\gamma_{LV}} \tag{2.4}$$

Here θ is the contact angle; γ is the interfacial energy between the solid-vapor, solid-liquid and liquid-vapor phases. This equation can be rewritten as Young-Dupré equation:

$$\gamma_{LV} \cdot (1 + \cos(\theta)) = \Delta W_{SLV} \tag{2.5}$$

Here W is the adhesion energy per unit area. A rule by thumb is, that a high surface free energy leads to a complete wetting. Adopting the rule *Similis Similibus Solvuntur* hydrophobic materials should be better suited for hydrophobic inks and vice versa. According to [Wu 1973] polar as well as non-polar interactions contribute to the interfacial energy. Thus the interfacial energy has to be decomposed into a polar and a dispersion component. This leads to a new set of equations. By measuring the contact angle with different solvents the work of adhesion can be determined.
Measuring the contact angle is a rather integrative method, since the solvent wets a rather large area. Small local changes in the surface chemistry of materials are difficult to observe. Polymers of a certain type are available with a huge variety of different bulk properties. They differ in the amount and type of additives and other components. For Surlyn, a material which was used in this thesis as stamp material, more than fifty different grades are available. The composition of these are company secrets and thus difficult to take into account. Thus the contact angle gives only a first indication of the surface properties, but the real interaction between ink and stamp has to be determined by printing experiments.

2.1.7 Printing

Since μCP is a printing technique, an inking step is needed first. Commonly the ink consists of a solution of molecules. As mentioned before, these could either be organic molecules such as alkanethiols in ethanol, proteins in an ionic buffer

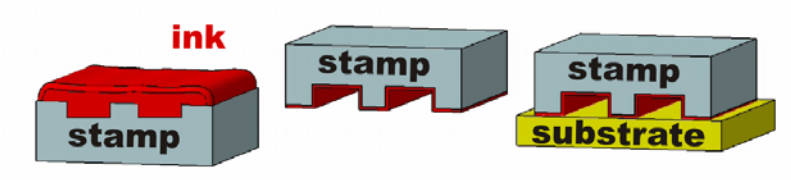

(a) Wet Inking

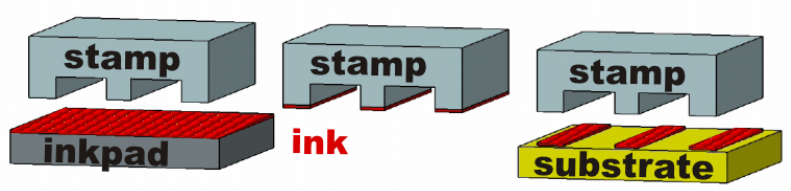

(b) Contact Inking

Figure 2.18: Inking methods

solution or others. In contrast to that there are also inkless methods like catalytic μCP [Li et. al. 2003b] or electrical μCP [Jacobs et. al. 2001]. The traditional and still common way of bringing the molecules onto the stamp and transferring them to a substrate is *Wet Inking* (Fig.2.18) [Kumar et. al. 1993]. There a stamp is placed into a solution for a certain time, mostly hours up to a day. The stamp is then blow dried in a nitrogen stream. Thus the molecules are dried onto the stamps surface. The transfer takes place by bringing the stamp into conformal contact with a substrate. This method allows a transfer of many molecules, since more than a monolayer of molecules is dried on the stamp. The drawback of this method is, that molecules are also inside the trenches of the stamp. Through sagging, diffusion (see next section) or other processes these molecules could be transferred onto the parts of those substrate where no transfer is desired. A method that accounts for this problem is *Contact Inking* (Fig.2.18) [Libioulle et. al. 1999]. There a flat unstructured piece of polymer (mostly PDMS) is placed into the ink solution. This is called an ink pad. The molecules assemble and are dried to the pad. The stamp is brought into contact with the ink pad. Thus molecules are only transferred on the parts of the stamp where it was in contact with the ink pad. The molecular layer on the stamp is thus thinner and the trenches are free of molecules. Subsequently the stamp is brought into contact with a substrate and the molecules are transferred. However, this approach was only used for organic molecules so far. A third approach makes use of the fact that ink molecules can diffuse through a PDMS stamp. That way, an ink reservoir is placed on the backside of the stamp. The stamp could thus be used for several successive printing cycles [Balmer et. al. 2005].
The mechanisms of the transfer of molecules between two polymers or between a polymer and another substrate are not fully understood. [Larsen et. al. 1997] and

[Graham et. al. 2002] showed, that the ordering effects in printed SAMs of alkanethiols mainly depend on the ink concentration. Monolayers could be transferred, which are indistinguishable of solution formed ones. A study for the transfer of non-covalently binding molecules onto mica is reported by [Workman et. al. 2004]. They state, that factors like humidity, temperature and vapor pressure play an important role there. [Andrade et. al. 1986] and [Young et. al. 1988] give an introduction to protein adsorption to polymers. The detailed processes involved during the printing steps are neither known in details nor discussed in any references. [Biasco et. al. 2005] showed, that for an azurin molecule the height is changed. They attribute this change to constraints due to several surfaces involved. In general a deeper understanding of the processes is needed. Especially the drying procedure of the ink on the stamp/ink-pad is definitely a problem concerning moisture dependence and stability of molecules, such as proteins. It is well known, that specific functionalities of certain proteins strongly depend on conformation and thus the hydrate-shell.

In order to employ small patterns of molecules, which can be transferred with μCP or nTP, it is important to address them directly to an complementary structure on the target surface. Therefore one has to perform the printing process in an aligned manner. This means, that one has to control the position of the printed structures with respect to other structures, which might already be present on the substrate. Conventionally alignment is performed by having marks like crosses on both objects, which should be aligned. The marks are adjusted to each other by moving one of the objects in x-y direction with micrometer screws under microscopical control. This principle is used in an *Optical Lithography* aligner for example. The accuracy of this method is given by the accuracy of the x-y movements, the resolution of the microscope and the accuracy of bringing the two objects into contact. Since alignment is done in a certain distance between the two objects, the ability to bring the two objects into contact while not introducing additional misplacement through mechanical clearance is very crucial. This could be limited by bringing them into an umpty micron separation. X-y movement accuracy can be improved to the sub femtometer range using piezoelectric elements. The critical point is the microscope resolution. Since the resolution is limited by the wavelength of light, which ranges between 400 nm-650 nm, alignment accuracy cannot be much better than half a micron. Moire patterns[9] as alignment marks can be utilized to break this boundary [Kawai et. al. 1998].

[9] interference pattern of two grids having a different mesh or at an angle

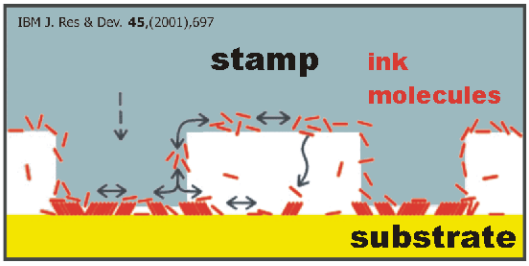

Figure 2.19: Various pathways for diffusion of ink during the contact between stamp and substrate; taken from [Delamarche et. al. 1998]

Diffusion

For printing patterns of molecules with small dimensions, diffusion processes are limiting parameters concerning the minimum dimensions of patterns. Diffusion processes depend on the mobility of molecules, which itself is depended on the mass. The diffusion process is given by Fick´s second law in one dimension as:

$$\frac{\partial c}{\partial t} = D\frac{\partial^2 c}{\partial^2 x} \tag{2.6}$$

Here D is the diffusion constant proportional to $\frac{1}{m}$; c is the concentration as a function of place x and time t; m is the mass of the object. Different pathways (Fig.2.19) for diffusion of molecules from the stamp surface to the substrate are possible [Delamarche et. al. 1998]. There, a clear dependency between the mass of the alkanethiol and the resulting resolution is shown. Therefore diffusion plays a major role for small organic molecules such as alkanethiols with M < 300 g/mol and limits the maximum resolution. A comparison of printing results obtained with octadecanethiol and hexadecanethiol is given by [Bass et. al. 2004]. Ink concentration and contact time also play a major role as described by [Sharpe et. al. 2004]. Diffusion is not a limitation for heavier molecules such as proteins [Bernard et. al. 2000] or dendrimers [Li et. al. 2003]. The limitations on the other hand can be used for the printing of chemical gradients [Kraus et. al. 2005].

2.2 Characterization Methods

Like *Optical Lithography* also *Optical Microscopy* is limited by $d = \frac{\lambda}{2 \cdot A}$. For a faithful imaging of the stamps, masters or substrates surface basically two methods can be applied: *Scanning Electron Microscopy* (SEM) and *Atomic Force Microscopy* (AFM)

SEM has the advantage, that samples can be moved freely in x,y,z direction as well as rotated or tilted. Thus a detailed 3D impression of the whole surface is achievable. The main disadvantage is a resolution in the umpty nm range. In addition samples have to be electrically conductive. Therefore stamps for example have to be coated with a metal layer. The advantage of AFM is, that it allows to measure a height profile with Angstrom resolution. In x-y scan direction molecular resolution can usually be obtained. The major drawback is, that just a small section of the sample can be scanned (e.g. a ten by ten micron area), which might not be representative of the whole surface. In addition such a scan takes several minutes, while it takes a few seconds with SEM. However, using both methods together allows to derive a realistic picture of the sample. SEM is used for a general impression of the surface and AFM for a detailed image.
The following two paragraphs give short introductions to SEM and AFM.

Scanning Electron Microscopy

A *Scanning Electron Microscope* is similar to an *Electron Beam Writer*[10]. In fact most SEMs are also used for EBL. Basically the primary electrons, which strike the surface, are inelastically scattered by the atoms (more precisely electron orbitals of the atoms). This scattering leads to a spreading of the electrons into a drop-shaped interaction volume. This volume contains Auger electrons, secondary electrons, back scattered electrons, characteristic X-Rays and a X-Ray continuum. For imaging, mainly backscatter and secondary electrons are detected. Some SEMs also have X-Ray detectors, which are used to obtain further information about the surface. In addition to the assembly of an electron beam writer (UHV chamber, electron gun, beam optics, stage) the SEM contains several electron detectors (Fig.2.20).
The *Inlense* detector is used to detect secondary electrons, which are going into the opposite beam direction. It is placed inside of the lens system. A scintillator/photomultiplier[11] assembly is used to detect these electrons. The *SE2* detector is used to detect backscatter and secondary electrons. It is placed aside the primary beam direction. A positively charged metallic grid attracts the electrons, which are directed to a scintillator/photomultiplier assembly. The backscattered electron detector (*BSE*) is placed directly above the sample. Thus imaging with a high contrast between different materials is possible since different materials have different backscattering coefficient. Like the *Inlense* detector the *EsB* (Energy and angle selective BSE) detector is placed inside the beam path. It is separated by a filtering grid and thus less sensitive to charges. All detectors have specific advantages and drawbacks. Depending on the beam energy and surface composition one or the

[10] A detailed introduction to SEM is given by [Goldstein et. al. 2003].
[11] A scintillator converts the electrons into photons. These photons are detected by the photomultiplier, which uses several dynodes to multiply the signal.

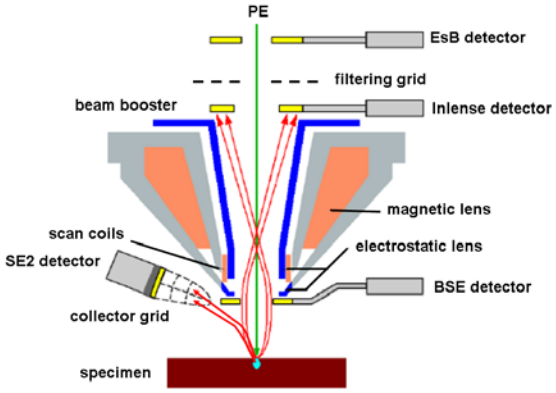

Figure 2.20: Configuration of the SEM detectors; taken from [Zeiss 2005]

other is more useful. [12]

Atomic Force Microscopy

Atomic Force Microscopy is one of the methods known as *Scanning Probe Microscopy*[13]. Another closely related method is *Scanning Tunneling Microscopy* STM. G. Binning, C. Quate and C. Geber introduced the AFM in 1986. A cantilever with a sharp tip on one side is moved over a surface at a certain hight. It is made of a very stiff material such as silicon (Si) or siliconnitride (Si_3N_4). At a certain distance to the surface while approaching the tip starts to exert atomic forces on the atoms of the sample surface. A typical force distance curve is shown in Fig.2.21b). These forces are deflecting the cantilever. A deflection is measured using a laser and detector (Fig.2.21a). Basically two different AFM operation modes are known: *Contact Mode* and *Tapping Mode*. In contact mode the force between tip and sample is kept constant by keeping the deflection constant. This deflection is a measure for the topography. In tapping mode an oscillation stimulates the cantilever near it´s resonance frequency. The oscillation is damped by the tip-surface interactions. The difference to the external oscillation is a measure for the topography. In order to get the topography of the sample surface the cantilever is scanning in x- and y-direction and displaced in z-direction. The movement is done using piezoelectric elements. Through the piezoelectric effect, movements with sub atomic resolution can be achieved.

[12] An overview of the detectors, their working principles and applications is given in [Zeiss 2005].
[13] An introduction is given in [Bonnell 2001].

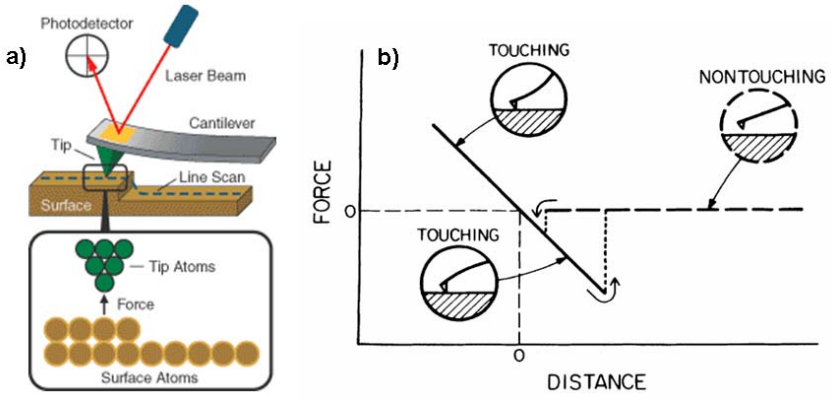

Figure 2.21: Configuration of an AFM;
a) taken from *www.molec.com/what_is_afm.html*
b) force vs distance curve ; taken from [Weisenhorn et. al. 1992]

2.3 Molecular Electronics (ME)

Molecular Electronics of molecular conduction. These theories were proposed by S. Mulliken and A. Szent-Gyorgi in the 1940s. They proposed a donor-acceptor charge transfer complex [Mulliken et. al. 1969] and the idea, that proteins might not be insulators [Szent-Gyorgi 1941]. The investigation of the conduction in proteins was carried on by [Evans et. al 1949] and D.D. Eley. Their work was focused on the iron containing protein cytochrome *c* (see Section 2.5). The idea to use the concepts of *Molecular Conduction* for information-processing systems on a molecular level started with R. Feynman´s famous lecture *There´s plenty of Room at the Bottom*[14]. The first tangible proposal in this direction was made by A. Aviram and M.A. Ratner [Aviram et. al. 1974]. They proposed to use a electron donor-acceptor molecule as a molecular diode. This step also transformed

[14] A transcript is available at www.zyvex.com/nanotech/feynman.html

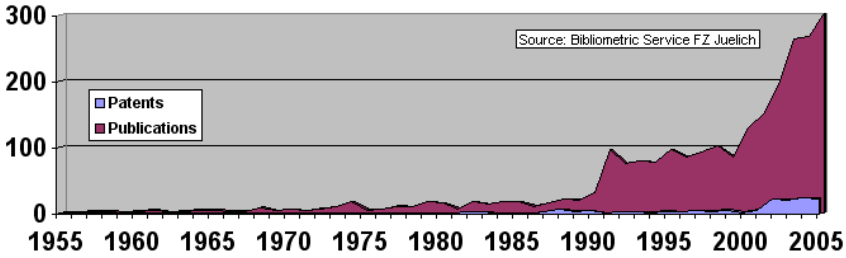

Figure 2.22: Number of publications and patents dealing with *Molecular Electronics*

Molecular Conductance into *Molecular Electronics*. F.L. Carter pushed the research on molecular wires, switches, molecular logic elements by his visionary ideas [Carter 1983]. From that point there was a surge in experimental research on ME as well as theoretical research (Fig.2.22). A more detailed historical overview is given by [Hush 2003].

Since *Molecular Electronics* is a highly interdisciplinary field, many groups of researchers are involved in the experimental research. Chemists have to provide the molecules. They not only prepare high purity molecules, but also synthesis molecules with the desired centers or functionalities. In addition they measure the macroscopic properties of these molecules with e.g. electrochemistry, spectroscopy or other methods. Biologists provide appropriate proteins and information about them. Engineers deal with the miniaturization of electrodes and circuitries. They also deal with the issues of integration and interconnections. From a theoretical point of view chemists and physicists calculate or simulate the properties of molecules using methods such as *Density Functional Theory* (DFT). Engineers develop concepts of architectures, logics or defect tolerance. This splitting can be seen all over the literature dealing with ME. There are publications focusing on all of these aspects separately. Only a few concepts totally describe a system from the properties of molecules to integration. The most promising is the concept of crossbar arrays (described in the next section). Besides the aspects of ME mentioned above the fabrication and measuring techniques are also of major interest. From an experimental point of view ME depends on measuring small currents, probing tiny devices and high resolution imaging. Most insights in conductance of single molecules was achieved with *Scanning Tunneling Microsopy*[15] (STM). For the fabrication of ME devices and circuitries three approaches can be taken: *Top-Down*, *Bottom-Up* or a mixture of both. The *Top-Down* approach describes the miniaturization of macroscopic techniques and devices to reach the final limitations, for example increasing the resolution limits of *Optical Lithography* or *Electron Beam Lithography*. The *Bottom-Up* approach uses the unique properties in the molecular world such as self-assembly[16] and self-organization to built up circuits of already pre-build components such as nanotubes, nanowires or buckyballs. Besides the intention of R. Feynman to use ME to perform information-processing as the ultimate miniaturization, ME can also serve to gain more insights into the behavior of molecules. A question to be answered is: How does a macroscopic amount of molecules behave with respect to a 2-dim accumulation, a 1-dim accumulation or a single molecule (0-dim)? Such a comparison can give major insights whether the interaction between molecules drives the functionality or if the properties of each single molecule just add up.

[15] An introduction is given by [Bonnell 2001].

[16] An introduction to self-assembled nanostructures is given by [Zhang et. al. 2002].

2.3.1 Approaches to ME

Self-assembled monolayers are the easiest systems to study electron transfer processes through molecular films [Holmlin et. al. 2001]. Commonly the electrochemical (EC) characterizations, such as *Cyclic Voltammetry*, of SAMs on electrodes are often used. They are well established and theoretically understood. However, since the area of electrodes used there is rather large, lots of defects contribute to these measurements. The information obtained represents an integration over the whole surface area including all these defects, thus the quality of information obtained about the molecules is limited. In particular it is difficult to deduce the behavior of a single molecule. Since the amount of defects scales with the size of the electrodes it is necessary to reduce the size. Six approaches are reported, which allow measurements with smaller areas and are thus suited to investigate molecular properties.

- *Mercury-Droplet*
- conductive AFM/STM
- *Nanopores*
- *Break-junctions*
- *Crossed-Wires*
- *Crossbars*

In the *Mercury-Droplet* method a metal/molecule/metal tunneling junction is formed between two mercury droplets. The droplets are covered with SAMs and brought into close distance [Slowinski et. al. 1999]. A current across the molecule layer is measured by contacting the droplets. Since the size of the droplets is only scalable to a certain extend and is limited, the usage of this technique is limited. Typical areas are in the range of $0.002\,cm^2$. Thus the information is also integrated over a huge amount of molecules. *Scanning Probe* and *Break-Junction* [Reed et. al. 1997] techniques are utilized for measuring single or up to a few molecules. Using conductive AFM or STM, molecules can directly be contacted. One special case of these experiments are STM *Break-junctions* [Xiao et. al. 2004]. These techniques give a detailed picture about single molecule properties but are difficult to handle. In addition several problems arise, such as very high electric fields, due to the small dimensions of electrodes or heating effects. These problems could effect the properties of the molecules and thus influence or change the information obtained. To get a detailed picture of molecular properties measurements have to be performed at different length scale. By comparing the results such problems can be traced and taken into account. Between $1 \cdot 10^{12}$ molecules measured in *Mercury-Droplet* junctions and 75 molecules measured with a conductive AFM

setup there is a huge gap of 11 orders of magnitude. *Crossed-Wire* and *Crossbar* techniques allow to investigate assemblies of molecules in this range. In both methods electrodes are placed on top of each other having a molecular layer in between. *Crossed-Wire* electrodes consist of nanowires [Kushmerick et. al. 2002]. Since the size and diameter of these wires are predetermined by the growth conditions an arbitrary scaling is not or just hardly possible. *Crossbar* devices will be discussed in Chapter 2.3.3. *Nanopores* arrays consist of electrodes separated by a siliconnitride membrane [Reed et. al. 1997]. The molecules are assembled inside the holes. Also this technique is only scalable to a certain extend.

EC methods, as well as *Mercury-Droplet* and *Scanning Probe* allow measurements of the electrical properties of molecules, but they are not suited for the fabrication of electronic devices or sensors based on molecules. *Break-junctions*, *Nanopores Crossed-Wires* and *Crossbars* on the other hand can be used for such applications.

From a device point of view tunneling junctions, negative differential resistors [Chen et. al 1999], electrically configurable switches [Collier et. al 1999], transistors made of CNT [Tans et. al. 1998] and transistors made of single molecules [Park et. al. 2002] were demonstrated. Basic memory and logic functions [Collier et. al 1999] were demonstrated on a circuit level. Molecular wires were investigated by [Leatherman et. al. 1999]. Using the just described devices the next step is the construction of logic elements (such as an adder) and architectures for computers. A review about possible architectures is given by [Ellenbogen et. al 2000].

Major steps in constructing devices for ME are: bringing spots of molecules to certain positions, producing these spots having certain dimensions (down to single molecules), addressing and contacting of these spots in a defined way. The first task is similar to what was discussed above in section Alignment. The second task is caused by the fact, that the number of defects scales with the area and thus the area should be as small as possible. Measuring electronic properties is another challenge since very small currents and capacitance are involved. Theoretical interpretation of the measured properties is another issue, since the measurement is a convolution of the measuring technique, the molecular properties and the electrodes.

Theoretical considerations often begin with ground-state electronic properties of the molecules. Therefore DFT is often used. [Di Felice et. al. 2005] showed, that time-dependent DFT can be used to simulate the charge transfer. Another possibility is to use DFT to determine the one-electron hamiltonian and then use non-equilibrium Green´s functions to calculate the electron transfer [Stokbro et. al. 2005]. This method has the disadvantage of being ab-initio. A com-

bination of non-equilibrium Green´s functions and density-functional-based tight binding is reported in [Di Carlo et. al. 2005]. The major problem is, that the electrodes are described by DFT in a physical context as a open delocalized system, while the molecules have to be treated by ab-initio methods in a chemical context as a confined system.

2.3.2 Electron Tunneling in SAMs

The demonstration of utilizing molecules as the active region of electronic devices is of major interest in ME. Several publications reporting molecular conduction through molecular layers turned out to be filamentary effects [Stewart et. al. 2004] or other premature problems. Another severe problem in dealing with molecules as active device components is characterizing their configuration, bonding or even their very presence [Wang et. al. 2005]. One of the best understood and most extensively studied molecular systems are alkanethiol SAMs on metals (metal/molecule/metal). They are widely used as model systems, because they have a well-understood classical transport mechanism. They are applied as a control for eliminating or understanding fabrication issues. Alkanethiols were characterized by STM, conductive AFM, *Nanopores*, *Mercury-Droplet* methods, *Crossed-Wire* junctions and electrochemical methods. A review and comparison is given by [Wang et. al. 2005]. More than that, the bulk properties of alkanethiol SAMs were widely studied and understood.
The current-voltage characteristic of charge transport through molecules is influenced by several parameters: molecular length, conformation, HOMO[17]-LUMO[18] gap, type of electrode contact and the work function of the electrode material.
The dominant current mechanism through molecular junctions is supposed to be *Through-Bond* tunneling, in which the current follows the bond overlaps along the molecule [Salomon et. al. 2003]. However, there will always be a component of *Through-Space* tunneling between the electrodes, where the molecules only serve as a dielectric medium.
The conventional one-dimensional picture of electron tunneling is, that of a potential step barrier of height V_0 and width L. In this picture an electron of energy $E = \hbar^2 k^2/2m$ and wavefunction $\exp(ikx)$ impings on the barrier. In the barrier the wavefunction becomes $\exp(-\kappa x)$ with $\hbar^2 k^2/2m = V_0 - E$[19]. The transmission probability is approximately proportional to $\exp(-\beta L)$ with $\beta = 2\kappa$ being the decay parameter. Thus the current passing through such a barrier is expected to decrease exponentially as the barrier thickness increases. The rate of decrease β depends on

[17] **H**ighest **O**ccupied **M**olecular **O**rbital
[18] **L**owest **U**noccupied **M**olecular **O**rbital
[19] Further discussions and more detailed derivations are given in quantum mechanics textbooks, e.g. J.J. Sakurai: Modern Quantum Mechanics

the electron energy as

$$\beta = 2\sqrt{\frac{2m\varphi_0}{\hbar^2}} = 1.02\sqrt{\frac{\varphi_0}{eV}} \tag{2.7}$$

where φ_0 is the barrier height $V_0 - E$.

Going to metal/molecule/metal junctions the classical barrier has to be replaced by a set of molecular orbitals of the molecule. Considering molecules as very long chains, the molecular orbitals become energy bands in which the energy has a momentum dependence parameterized by an effective mass m^*. An approximation for finite length molecules is to take the band states of the infinite chain but with wavelengths commensurate with the short chain. The barrier picture is thus modified to one where the mass m is replaced by the effective mass m^* and the barrier height is the energy difference of the electron in the contact and that of the molecular orbital [Tomfohr et. al. 2002].

A first approximation is, that the barrier height becomes $\varphi_0 = (E_{LUMO} - E)$ or $\varphi_0 = (E - E_{HOMO})$ for tunneling through the LUMO or HOMO. The energy plot is shown in Fig.2.23a). HOMO and LUMO can be related to electron affinity (EA) and ionization potential (IP). Δ corrects for energy differences between charged and uncharged states. Current is carried by electrons at the Fermi level E_F located below the vacuum by a quantity of energy equal to the work function Φ. The tunneling current density can be approximated by Simmons model [Simmons 1963] in the regime of $V < \varphi_0/e$ as:

$$\begin{aligned} J = \frac{e}{4\pi^2\hbar d^2} \Bigg\{ & \left(\varphi_0 - \frac{eV}{2}\right) \exp\left[-\frac{2(2m)^{1/2}}{\hbar}\alpha\left(\varphi_0 - \frac{eV}{2}\right)^{1/2} d\right] \\ & - \left(\varphi_0 + \frac{eV}{2}\right) \exp\left[-\frac{2(2m)^{1/2}}{\hbar}\alpha\left(\varphi_0 + \frac{eV}{2}\right)^{1/2} d\right] \Bigg\} \end{aligned} \tag{2.8}$$

Here d is the barrier width. α is a unitless adjustable parameter that is introduced to provide either a way of applying the tunneling model of a rectangular barrier to tunneling through a nonrectangular barrier, or an adjustment to account for the effective mass of the tunneling electrons through a rectangular barrier, or both. $\alpha = 1$ corresponds to the case for a rectangular barrier and bare electron mass. For rectangular barriers the effective mass m^* is given by $\alpha^2 m$ [Wang et. al. 2005]. Equation 2.8 can be approximated in two limits: low bias and high bias compared to φ_0:

$$J \approx \left(\frac{(2m\varphi_0)^{1/2} e^2 \alpha}{h^2 d}\right) V \exp\left[-\frac{2(2m)^{1/2}}{\hbar}\alpha(\varphi_0)^{1/2} d\right] \tag{2.9}$$

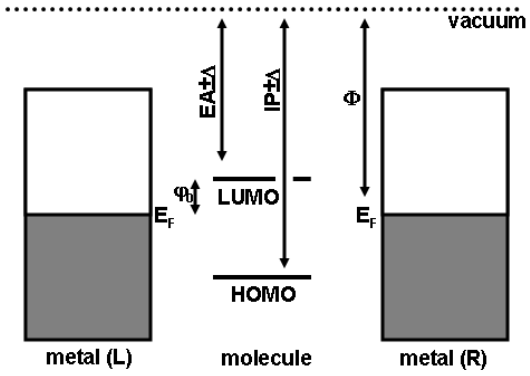

(a) weak-coupling

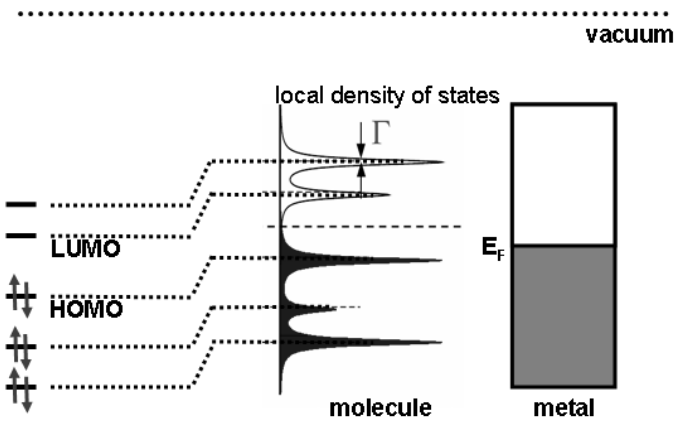

(b) strong-coupling

Figure 2.23: Energy plot for a metal/molecule/metal junction in the weak-coupling and strong-coupling approximation; a) adapted from [Lindsay 2005]

in case of low bias. The decay constant is given as:

$$\beta_0 = 2\frac{(2m)^{1/2}}{\hbar}\alpha(\varphi_0)^{1/2} \tag{2.10}$$

In case of high bias the current density is given by

$$J \approx \left(\frac{e}{4\pi^2\hbar d^2}\right)\left(\varphi_0 - \frac{eV}{2}\right)\exp\left[-\frac{2(2m)^{1/2}}{\hbar}\alpha\left(\varphi_0 - \frac{eV}{2}\right)^{1/2} d\right] \tag{2.11}$$

The decay constant is:

$$\beta_V = 2\frac{(2m)^{1/2}}{\hbar}\alpha\left(\varphi_0 - \frac{eV}{2}\right)^{1/2} = \beta_0\left(1 - \frac{eV}{2\varphi_0}\right)^{1/2} \tag{2.12}$$

At high bias β_V decreases as the bias increases, which results from the barrier lowering effect due to the applied bias.

Depending the kind of molecules and electrodes two different coupling strengths can be distinguished. For weak-coupling the interaction between molecular states and metal states is small. This might be case for example, if there is no chemical contact between the molecule and electrode. In case of strong-coupling between molecules and electrodes their states can hybridize. This means, that the formerly sharp molecular states become broadened and the energy levels shift (Fig.2.23b). Much of the electronic signal characteristic of a molecule is lost. Strong coupling should occur for covalently bound molecules. In case of molecules with large delocalized π-systems, such as aromatic molecules, the hybridization with the metal states should be easy. Often molecular junctions have different coupling strengths on both sides. This is the case when for example monothiols are used. Often this regime is called STM-setup, since for STM experiments it is typical to have a strong-coupling of the molecule to the substrate, but only weak-coupling to the tip.

The electronic transport can be understood by scattering theory[20]. The current is carried by scattering states. These extend from deep in one electrode over the molecule deep into the other electrode. The molecule is considered as a scatterer that mixes the eigenstates of the electrodes. Current-voltage curves can be described with the Landauer-Büttiker formalism [Büttiker et. al. 1985]:

$$I(V) = \frac{e^2}{\pi\hbar} \int dE\ T(E,V) \left[f\left(E - \frac{eV}{2}\right) - f\left(E + \frac{eV}{2}\right) \right] \tag{2.13}$$

where T(E,V) is the transmission function, f is the Fermi function and V the applied voltage. The transmission function is:

$$T(E,V) = tr\left[\Gamma_L \left(E - \frac{eV}{2}\right) G_M(E) \Gamma_R \left(E + \frac{eV}{2}\right) G_M^*(E) \right] \tag{2.14}$$

where G_M represents the Green´s function matrix elements for the coupled system. Note, that these matrix elements are exponentially sensitive to the geometry of bonding in the system. Therefore, the connection between metal and molecules can vary all the way between T=1 for well-connected systems to T=0 for components without a wavefunction overlap. Γ describes the coupling to the electrodes. It can be related to time τ it takes for an electron to escape to the metal electrode as $\Gamma = \hbar/\tau$. $\Gamma/\hbar$ can be interpreted as the rate at which electrons are injected into the molecule from the contact.

[20] Recently an review was given by [Nitzan 2001].

Beside direct tunneling, also other transport phenomena can contribute to the electron transfer. For higher applied voltages resonant tunneling modes occur. Other contributions are among others *Thermionic Emission* or *Hopping Conduction*. They differ from direct tunneling by a different voltage or temperature dependency. An overview and comparison is given by [Wang et. al. 2005].

2.3.3 Crossbar Arrays

A crossbar array (Xbar-Array) is a set of wires crossing each other with a functional layer in the crosspoints (junctions). Based on their ideas and experience with the *Teramac* computer and the *Field Programmable Gate Arrays* (FPGA) scientists at the *Hewlett-Packard Laboratories* proposed a similar architecture for nanoscale circuits [Heath et. al 1998]. Other Xbar arrays were reported by [Zhong et. al. 2003] and [Luo et. al. 2002]. An overview is given by [Kuekes et. al. 2005b]. The HP nanoscale circuit is based on a configurable crossbar architecture to connect molecular switches. This concept fulfills all major requirements of future nanoscale devices: it can switch a current on and off; it is a circuit that controllably links very large numbers of these devices with each other and with external systems to perform memory or logic functions; the wire dimensions can be continuously scaled down to molecular dimensions; $2N$ communication wires can address 2^N wires with a demultiplexer; it is a reconfigurable architecture and thus can be made defect tolerant; the simple physical structure makes the fabrication feasible and potentially inexpensive [Chen et. al 2003]. The Xbar arrays at HP were

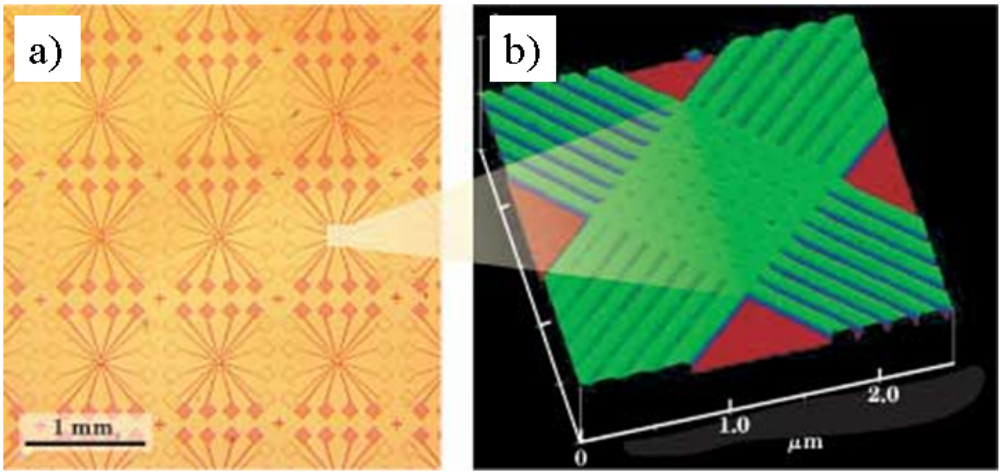

Figure 2.24: Images of crossbars fabricated at the HP labs; taken from [Chen et. al 2003]

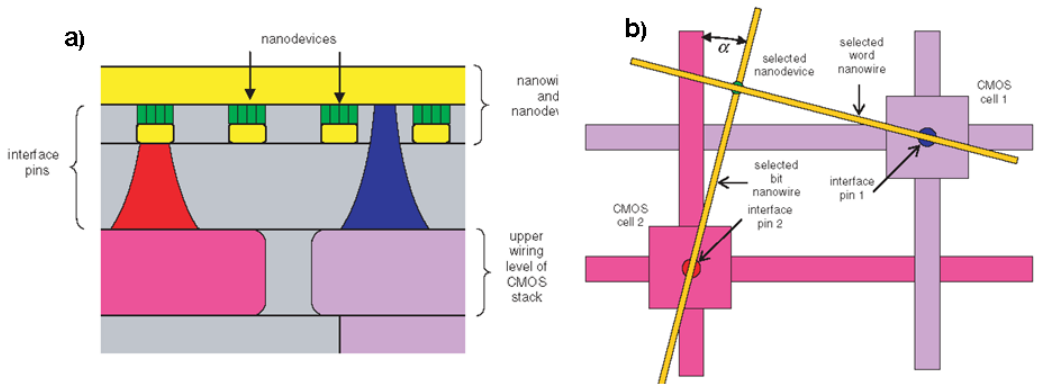

Figure 2.25: Concept of CMOL; taken from [Strukov et. al. 2005]

fabricated using NIL (Fig.2.24). A first NIL step was performed to pattern the first layer of electrodes (bottom-electrodes), then a molecular layer was deposited using the *Langmuir-Blodgett* method and subsequently a second electrode (top electrode) was patterned on top using an additional NIL step [Chen et. al 2003]. One kilobit Xbar arrays have already been fabricated [Wu et. al. 2005]. The smallest dimension of crossbar arrays fabricated so far had a half-pitch of 17 nm [Jung et. al. 2006]. [Stewart et. al. 2004] and [Richter et. al. 2005] reported, that the switching seen in the devices is more or less independent of the molecule layer used, it is rather given by the molecules and their interface to the electrodes. [Lau et. al. 2005] reported, that transport through the molecular device is dominated by nanoscale conducting channels, which can be described by a model that combines quantum tunneling and growth of nanoscale asperities.

Several concepts about the integration of crossbar arrays as potential nanoscale circuits were reported. The problem of signal restoration and inversion is solved with the architecture of crossbar latches [Kuekes et. al. 2005]. To integrate the Xbar arrays into today´s silicon technology the concept of CMOL was proposed [Strukov et. al. 2005]. There Xbar arrays with molecule interlayers are combined with CMOS technology (Fig.2.25). [Ziegler et. al. 2003] also report about the CMOS/Nano Co-Design. Nanoscale architectures are reported by [Choi et. al. 2004], [Stan et. al. 2003] and [Snider et. al. 2005]. Fundamental functions of data processing like adders can be fulfilled with simple Xbar circuits [Ellenbogen et. al 2000]. Approaches to deal with defect tolerance in Xbar arrays are given by [Kuekes et. al. 2006], [Lee et. al. 2004] and [Huang et. al. 2004].

2.4 Organic Molecules

Organic molecules are molecules that contain at least carbon and hydrogen atoms. In the context of *Soft Lithography* and *Molecular Electronics* organic molecules are mainly needed to serve as: model systems, etch barriers, binding sites for further reactions or as systems having special functionalities, such as redox centers. The molecules should form close, ordered monolayers. In addition they should be available with different properties, such as chain lengths. Therefore mainly molecules, which form self-assembled monolayers are used.[21] Due to their 2D structure they have a uniform arrangement at the surface and thus identical electronic properties. Molecules with different adsorption sites may have different electronic properties. Molecules bind covalently to a given surface and interact with each other forming an ordered monolayer. A typical sketch of SAM is shown in Fig.2.26. The molecules consist of a head-group, a tail and maybe some functional groups. Typically the molecules are amphiphilic. At a liquid/gas interface, they build *Langmuir* films. In contact with a surface, where the head-group can covalently bind, van der Waals interaction between the chains causes them to build an upright standing (or tilted) layer. The tails arrange such that opposite hydrogen atoms can form hydrogen bonds. Two groups of organic molecules are of major interest, namely alkanethiolates and alkylsiloxanes. Thiol groups bind strongly (83 - 145 kJ/mol) to gold and other metals, while alkylsiloxanes bind to siliconoxide. For each of these molecules a variety of different chain lengths is available as well as a huge variety of different functional groups on the outer termini of the molecule. There are for example plain carbon chains, acid groups, alcohol groups, amino groups and much more. Some molecules are shown in Fig.2.27.

[21] Reviews about various SAMs, structural information and growth conditions are given by [Schreiber 2000], [Smith et. al. 2004] and [Yan et. al. 2004].

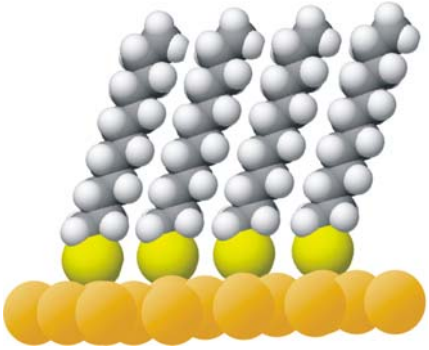

Figure 2.26: Sketch of a self-assembled monolayer of dodecanethiol on gold

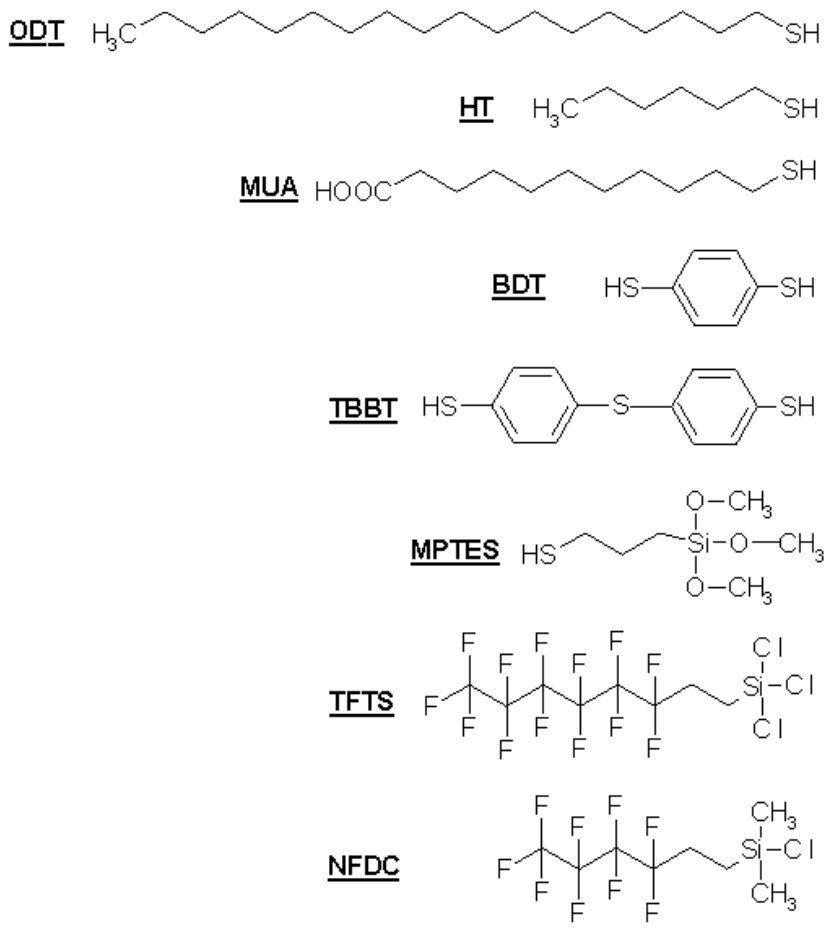

Figure 2.27: Formulas of organic molecules
ODT: octadecanethiol; HT: hexanethiol; MUA: 11-mercapto-undecanoicacid; BDT: 1,3-benzene-dithiol; TBBT: 4,4´-thiobisbenzenethiol; MPTES: mercapto-propyl-triethoxysilane; TFTS: tridecafluoro-octyl-trichlorosilane; NFDC: nonofluoro-hexly-dimethylchlorosilane

2.5 Proteins for ME and μCP

Proteins are complex, high molecular-weight biomolecules. They consist of amino acid sequences, which are linked by peptide bonds. An amino acid is a molecule that has an amino group and carboxylic acid functional group attached to neighboring carbon atoms. Twenty-three amino acids are known as building blocks for proteins. Beside the primary structure given by the amino acid sequence also the secondary structure (α helix or β sheet), the tertiary structure (overall shape of a single protein molecule) and the quaternary structure (the shape or structure that results from the union of more than one protein molecule) play a major role in functionality and behavior of a protein.[22]
Proteins are more than just building blocks of cells, they are also involved in almost all cell functions, such as signal transduction or the metabolism, transmembrane transport proteins (ion channels), hormones, enzymes, cell adhesion proteins, cytoskeletal proteins, metalloproteins (described in the next section) and many more. Besides their main functionality proteins often have additional functional units like different binding sides for capturing or immobilizing the proteins.
Typically proteins have masses up to hundreds of kilo Dalton and are a few nm in size. This makes them ideal nano-sized objects. The fact, that some proteins are easy to extract and can be obtained with high purity, makes them promising candidates for nanotechnology and molecular electronics. In addition the functionality and surface binding sites can be chosen to a certain extend or even be manipulated by mutation.

Metalloproteins

Metalloproteins are a special class of proteins, which contain prosthetic groups with one or more metal ions. The metal ion often has an influence on the proteins structure and stability, as well as it allows the protein to fulfill special tasks. They play a major role in the metabolism, respiration, signal transduction, muscle contraction or photosynthesis. Since transition metals are stable in different oxidation states, they can serve as catalysts or charge shuttles. Cytochrome *c* (cyt c) is an electron carrier in the mitochondrial respiration cycle. Here the prosthetic group consists of a heme group, which is composed of four pyrol rings forming a π-conjugated ring system. An iron ion is anchored via four N-coordinations in the center of the ring. Two additional coordinations are realized via the sulfur of a methionine and the nitrogen of a histidine group. The iron ion interconverts between Fe^{2+} (reduced) and Fe^{3+} (oxidized) states.

$$Fe^{3+} + e^{-} \rightarrow Fe^{2+}$$

[22] For an introduction to the nature of proteins see [Berg et. al. 2006].

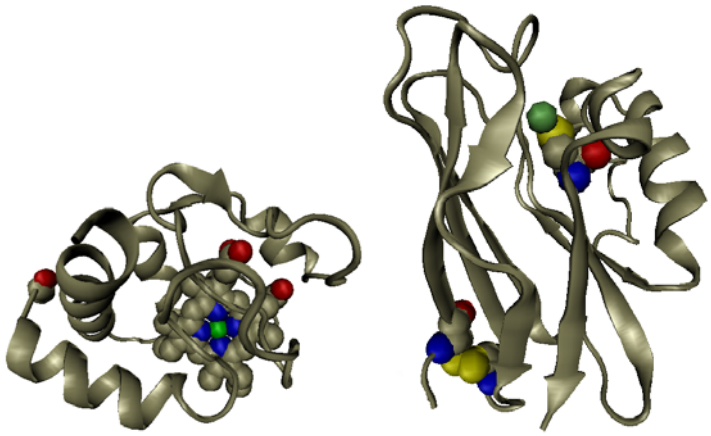

(a) cytochrome *c* (b) azurin

Figure 2.28: 3D representation of cytochrome *c* and azurin
cytochrome *c*: the iron atom in the heme-group is colored in green, the lysine group is colored in red.
azurin: the copper ion is colored in green, the sulfur atoms of the cystein groups are shown in yellow.
Information is taken from the RCBS protein data bank, images were made with the VMD program.

It is capable of performing oxidation and reduction, and thus acts as catalyst for various reactions. The primary structure of proteins depends on the respective organism. Bovine heart cytochrome *c* for instance contains a cystein group at the opposite side of the heme group. Horse heart cytochrome *c* does not have this group. This cystein group might cause differences in the coordination properties of the protein to metal surfaces. Recently redox behavior as well as different immobilization strategies for cytochrome *c* were investigated by [Salomon 2006].

Azurin from Pseudomonas aeruginosa is another electron-transfer protein. Its physiological function is not precisely known, although experiments suggest, that it is an electron donor to nitrite reductase in stress situations. Since it contains a copper ion as prosthetic group, it is widely studied as a model electron-transfer protein, in particular with respect to the coordination of the copper ion. The copper ion is anchored via two histidine groups, a cystein group and a methionine group. An additional anchoring is done via coulomb interaction with a glycine group. The electronic coupling is only done via one of the histidine groups. The copper ion interconverts between Cu^{1+} (reduced) and Cu^{2+} (oxidized) states.

$$Cu^{2+} + e^{-} \rightarrow Cu^{1+}$$

The redox behavior as well as different immobilization strategies were studied in various publications and recently by [Kandallu.R.S. 2006].

Chapter 3

Materials and Devices

In the scope of this thesis a brought variety of different chemicals, biomolecules and solid materials was used. All chemicals were used as purchased without further purification. Purified water with a specific resistance of 18.2 MΩ was used for aqueous solutions and rinsing. (Elix and MilliQ system of Millipore). 99.8 % nitrogen was used for dry-blowing and blow-off of dirt. Standard chemicals such as acetone, isopropanol, ethanol were purchased from KMF Laborchemie and used in the grade p.a. All lithographic work was done in class 10 and class 100 cleanrooms with permanent control of particle number, temperature and humidity.

Master

Masters are templates made of a rigid material carrying a pattern on their surface. They serve as mold in a replication process. In this thesis they were made of silicon and fabricated using standard silicon technology.
All silicon wafers were purchased from Si-Mat. PMMA resists of the AR-P series and PMMA developer AR 600.55 were bought from Allresist. HSQ resist FOx-12 and thinner MIBK from Dow Corning were used. A 4:1 mixture of FOx-12 and MIBK was employed. HSQ developer MF-CD-26 was purchased from Micro Resist Technology. The *Optical Lithography* resists AZ-5214 and Az-nLOF were bought from Microchemicals.
Layouts were designed using AutoCAD 2000Lt. During the first 18 months of this thesis a Leica EBPG 5HR electron beam writer was used. Later it was replaced by an EBPG 5000Plus writer. An acceleration voltage of 50 kV was chosen. *Optical Lithography* was performed on a MA6 mask-aligner of SUSS Microtec with an i-line (365 nm) light source. Silicon was etched using a Plasma Lab 100 (RIE) from Oxford Instruments with a HBr plasma. Siliconoxide was etched with CHF_3/CF_4 plasma in a AMR RIE from Oxford Instruments. Metal deposition was done with

a PLS 500 evaporation chamber from Balzers. The development was done with a 2 MHz megasonic 4 in transducer system from Sonosys. Wafer were oxidized to different thicknesses using an oxidation oven of Tempress B.V. In some applications polysilicon and siliconnitrid were deposited onto wafers with a LPCVD of Centrotherm.
Detailed recipes for the master fabrication are described in Appendix C.

Release Agent

A release agent is needed to passivate the master so that the stamp can be easily removed after the replication process.
For this purpose trichloro(1H,1H,2H,2H-perfluorooctyl)-silane 97 % was purchased from ABCR and nonafluoro-hexly-dimethyl-chlorsilane of Sigma-Aldrich and applied to the master.
The silanes were handled inside a glovebox system of MBraun in an argon 99.99 % atmosphere. Vacuum components necessary for the vacuum setup were supplied by Leybold Vacuum.
Samples were previously cleaned with a 200 W oxygen plasma. For liquid deposition the silanes were dissolved in toluene, which was dried over a molecular sieve. For the vapor deposition samples were placed inside a desiccator together with 40 μL of silane. The desiccator was evacuated to a pressure of 4.5 kPa, for 1 h. After that the samples were rinsed with MilliQ water and dry-blown.

Stamp

Stamps are polymeric materials, which were formed of the master, and thus carry the opposite pattern on their surface.
PDMS Sylgard 184 was purchased from Dow Corning. Base and curing agent were mixed in a ratio of 10:1. The prepolymer was left 10min in a flat dish for degassing. Then it was poured over a master. Ink-pads were prepared in a flat dish. It was cured in an oven at 60 $^{\circ}C$ for 12h and then at 110 $^{\circ}C$ for another hour. Microset 101RF was purchased from Microset Products Ltd. After applying it to a master it cured at room temperature within several minutes. h-PDMS was prepared according to [Schmid et. al. 2000] using HMS-301, VDT-731 and SIP 6831.1 supplied by ABCR. 3.4 g VDT-731 were mixed with 18 μl SIP 6831.1 and a drop of tetramethyltetravinylcyclotetrasiloxane. Afterwards 3 g of HMS-301 were added. Everything was mixed, degassed and cured at 60 °C for 12 h and 120 °C for 1 h.
Hot Embossing polymer Topas 8007 was supplied by Topas Advanced Polymers, Zeonor 1020 by Zeon, Surlyn 1702 by DuPont and Plexiglas 99530 by Roehm/Degussa. Affinity VP8770 was supplied by Dow Chemicals as a resin.

The resin was pressed into slabs of different thickness by the Institute of Plastics Processing at RWTH Aachen University. They used a maximum pressure of 3 MPa and 200 °C. HE was performed on a glass device heated by four 100W light bulbs. Pressure was applied by adding brass weights. Zeonex was embossed at 160 °*C* / 0.2 MPa; Zeonor at 160 °*C* / 0.2 MPa; Affinity at 85 °*C* / 0.2 MPa; Surlyn at 120 °*C* / 0.2 MPa. Before embossing the polymers were cleaned in isopropanol. The temperature was kept constant for 5 min, then the device was allowed to cool.
Before usage the stamps were briefly rinsed in ethanol and dry-blown with nitrogen.

Inking and Printing

Inking and printing are the steps performed in order to bring molecules onto the stamps surface and to transfer them onto a substrate.
Unless stated otherwise all chemicals used were purchased from Sigma-Aldrich. Alkenethiols were used as model molecules for printing and as molecular interlayers for Xbars. A standard solution of 1mM in ethanol was used for all alkanethiols. An ultrasonic bath was used for mixing. 1-propanethiol, 1-butanethiol, 1-hexanethiol, 1-octanethiol, 1,8-octanedithiol, 1-dodecanethiol, 1-hexadecanethiol and 1-octadecanethiol were used. The wet etch solution for gold was prepared according to [Xia et. al. 1995] of 1 M potassium-hydroxide, 0.1 M sodium-thiosulphate, 0.01 M potassium-ferricyanide and 0.001 M potassium-ferrocyanide in MilliQ water.
Mercapto-undecanoic acid was used as an immobilization layer for cytochrome *c*. 1,4-benzenedithiol was purchased from TCI. Horse heart >95 % and bovine heart >95 % cytochrome *c* were diluted in a buffer solution of sodium-dihydrogenphosphate and sodium-hydrogenphosphate with a ratio of 1.6:1 at a pH of 7 using MilliQ water. Azurin from pseudomonas aeruginosa >80 % was prepared in a potassium-acetate buffer solution at pH 4.6 using MilliQ water. Phosphate buffered salt solution (PBS) was prepared of 137 mM sodium-chloride, 2.7 mM potassium-chloride, 8.1 mM sodium-hydrogenphosphate, 1.5 mM potassium-hydrogenphosphate at pH 7.3 in MilliQ water. Bovine serum albumin was diluted to a 1 % mixture with PBS. Anti-mouse laminin-1 antibody and mouse laminin were purchased from R&D Systems and diluted in PBS. Anti-rat secondary antibody from goat fused with CY3[1] was purchased from Dianova and diluted in PBS.
Gold colloids 5 nm and 20 nm were purchased from Sigma-Aldrich. PAMAM and PAMAM-OS dendrimers of different generations were supplied by Dendritech.
The printing was done onto silicon chips with native oxide, silicon chips covered with 5nm chromium and 50 nm gold or glass coverslips. Prior to usage the sub-

[1] Indocarbocyanin (CY3) is a fluorescence marker with an excitation of 550 nm and an emission of 570 nm.

strates were freshly cleaned using sulfuric acid, followed by rinsing in MilliQ water and dry-blowing with nitrogen. Afterwards a short flame annealing was performed. For the aligned μCP a Fineplacer of Finetech was used.
For *Air Cushion μCP* a NX-2000 nanoimprint tool from Nanonex was used. Substrate and stamp were placed onto a silicone foil, a second silicone foil on a tender was placed on top of it. This assembly was placed into the chamber. Vacuum was applied for 10 s, afterwards a pressure of 0.2 MPa was applied for 10 s followed by a higher pressure for 1 min. Then pressure was released and substrate and stamp were separated.
Substrates for the printing of cyt *c* were immersed into mercapto-propionic acid (MPA) or 10 mM ethanolic mercapto-undecanoic acid (MUA) for 10 min, then rinsed and dried. Ink-pads and stamps were rinsed in ethanol and dry-blown.
Unpatterned slabs of Sylgard PDMS were used as ink-pad. For *Wet Inking* the stamps were immersed for at least 2 h. For *Contact Inking* the ink-pad was immersed in the solution for 4 h-overnight. The stamp were brought into contact with the ink-pad for 2 min. The contact between the substrate and the stamp while printing was varied between 5 s and 5 min. Ink solutions were used at the most on three successive days.
Xbar top and bottom electrodes were prepared as described in Appendix C. The bottom electrodes were cleaned by gentle flame annealing and immersed into a solution of the molecules of choice. Afterwards they were rinsed with ethanol, MilliQ water and dry-blown. The top electrodes were transferred onto a piece of Affinity VP8770 POP by pressing it onto the top electrodes for 30 s. Prior the POP was flattened by pressing it between to silicon wafers. Afterwards this assembly was separated by immersing it into isopropanol. The POP was gently removed of the top electrode wafer. That way the electrodes stuck on the POP. It was placed on the chuck of the FinePlacer and the bottom electrode wafer with the molecular layer was placed on the lever. A droplet of hexane was dripped onto the POP. After 5 s the bottom electrodes were pressed with 50 kPa onto the POP. Subsequently the POP was gently removed after 30 s. Instead of POP also Microset PDMS was used. In that case hexane was not needed.

Characterization

Optical Microscopy was done with a Zeiss microscope with an incident light setup. Fluorescence images of CY3 marked antibodies were taken with a Rhodamin-filter having 545 nm excitation, 570 nm beam splitter and 605 nm emission. AFM investigations were done with a Nanosope IV multimode AFM/STM device from Veeco Instruments. The AFM was mounted in a vibration isolated faraday cage. Tapping mode cantilevers RTESP5 from Veeco were used. SEM images were taken with a Gemini 1550 VP from Leo/Zeiss. Top-View images were recorded

with the Inlense detector; tilted images with the SE2 detector. Master and stamps were imaged at an acceleration voltage of 10 kV, printed molecules and proteins at 2 kV. Non-conductive samples such as stamps were sputtered with gold for 40s with a SCD-050 sputter coater from Balzers. XPS spectra were taken with a XPS 5600 of Physical Electronics. For measuring the thickness of molecular layers a scanning ellipsometer with a 632 nm laser from Nanofilms was used. Contact angle measurements were performed on an OCA from Dataphysics. Electrical characterization of Xbar electrodes was done with a PM5 probe station from SUSS Microtec and a 4200 Semiconductor Analyzer with a Preamp from Keithley Instruments. Samples were probed using tungsten tips from SUSS Microtec. Non-eutectic gallium-indium from Alfa Aesar was used to repair broken wires or to enhance the contact between tip and electrodes.

Chapter 4

Experimental Section

The first part of this chapter deals with the experimental details on the development of μCP with dimensions smaller 100 nm. The second part introduces three novel printing methods developed during the course of this thesis.

4.1 Design

During this thesis serval applications for μCP were performed or developed. For each application a design for master and stamps was created using AutoCad.
A special design was developed to address problems associated with the down scaling of μCP below 100 nm. It is made up of three different areas:

Variable Gap	lines with equal widths are separated by gaps with variable widths
Variable Width	lines with variable widths are separated by gaps with equal widths
Variable Both	the widths of gaps and lines are varied the same time

The design is based on 1 μm to 75 nm wide lines (Fig.B.4). The line-pattern is repeated up to an 800 μm by 800 μm area.

The following issues were learned from this design: The impact of the pattern on the doses needed in EBL as well as on the proximity effect were investigated. It turned out, that for small gap sizes the development of exposed patterns becomes a critical issue. An influence of the design on the results of *Reactive Ion Etching* could not be observed. However, the design proved to be very useful to find the limitations for stamp materials concerning sagging and pairing. In addition diffusion of molecules were investigated. All aforesaid issues will be discussed and illustrated in more detail through the course of this chapter.
For the fabrication of *Crossbar* electrodes a special design was developed con-

sisting of three parts: 100 μm bondpads, taper-triangles and wires. The wires are connected with the bondpads through the taper-triangles. These tapers are supposed to avoid the breaking of wires at the connection points. A wire that is directly attached to a bondpad could generate a breaking-point due to an abrupt change of size. The design comprises electrodes with one, two and three wires running between the pads. This allows to prove and investigate electrical scaling laws. Furthermore it is also helpful to have spare wires, if one wire is broken during the transfer steps. The wires have widths of 100 nm, 250 nm, 500 nm and 1 μm respectively. The design is shown in Fig.B.8.
Other designs used during the course of this thesis for different applications are shown in Appendix B.

4.2 Master

The master serves as templates for the replication of stamps and carries the design on their surface. Thus they are of fundamental importance for all further fabrication steps. The fabrication was chosen so that the masters fulfill following requirements: they should be stiff, flat at the bottom of the trenches, temperature and pressure stable in order to use them for hot embossing and easy to fabricate by means of standard techniques. Therefore they were produced on the basis of *Silicon Technology*, since this is state-of-the-art. Silicon is stiff, easy to clean and can be coated in a precise, reproducible way. Since it is the aim of this thesis to scale down below 100 nm, *Electron Beam Lithography* was the method of choice for prototyping of masters. Three main lithographic steps had to be optimized to obtain ideal masters: lithography, development and etching.
The first step was to choose the electron beam resists. In order to be flexible to make various patterns, while keeping the writing time at a minimum, a positive and a negative resist were used. PMMA was chosen as a positive resist, because it is well-established and often used in EBL. HSQ was chosen as negative resist since it allows high resolution patterning and has the great advantage of being a silicon based material. All deployed wafers used were standard 3 inch or 4 inch p-doped $\langle 100 \rangle$ wafers. Depending on the experiment they were either used as supplied without modifications, oxidized with a thermal oxide layer, or a siliconnitrid/n-polysilicon stack was deposited using *Low Pressure Chemical Vapor Deposition* (LPCVD). The resists were spin-coated onto the wafers at various speeds. An adhesion promoter, such as hexamethyldisilazane (HMDS), was found to be not necessary for the samples fabricated here. Thus it was never applied. Prior to coating the wafers were backed at 150 $^{\circ}C$ - 180 $^{\circ}C$ for 5 min in order to remove the water layer.

For all experiments the acceleration voltage of the electron beam was fixed

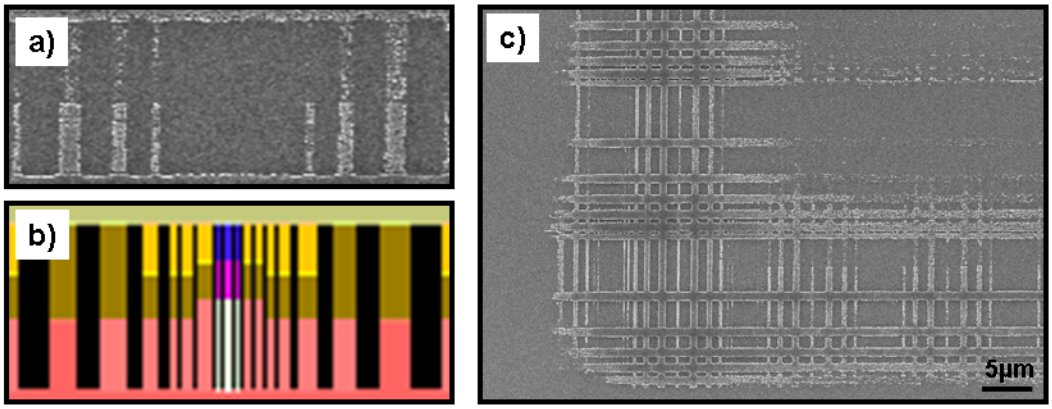

Figure 4.1: Proximity correction for HSQ
a) SEM image (10 kV) of HSQ on silicon after development with design Fig.B.4.
b) Proximity Correction used for a); each color represents a different dose
c) SEM image (10 kV) of a corner region

at 50 kV. Beam size and beam-step size were chosen according to the design. A 25 nm beam-step size for example was used for writing 75 nm patterns. For each design dose variations were performed to find the optimum exposure doses. Comparing results with and without proximity correction revealed, that for the designs used in this thesis PMMA resist did not require a correction, while for HSQ it was found to be crucial (Fig.A.1). Here a strong halo was present due to the proximity effect. Since HSQ is a negative resist the areas subject to scatting are thus exposed and stay after development. The height of this halo however was not as high as the true patterns, because the accumulated charge is much smaller (Fig.A.1b). For reducing this effect a proximity correction was performed using Proxecco[1]. Energy deposition was simulated and fifty different doses were used for the correction. The impact on the design is shown in Fig.B.6. It is obvious, that the doses are mainly changed in the outer parts of the design, while only the 75 nm lines in the inner part receive a different dose. The basis-dose was varied between 110 μC/cm^2 and 150 μC/cm^2 (Fig.4.2). Note, that in this specific experiment the 75 nm lines were replaced by 100 nm lines separated by 100 nm gaps. It can be seen, that at 110 μC/cm^2 the pattern is underexposed. Resist lines smaller than 200 nm are missing[2]. At 150 μC/cm^2 the pattern is overexposed. Trenches smaller than 150 nm are completely filled. It can be also seen, that there is no dose, where the pattern is exposed in the right way. This problem is mostly due to a non-perfect proximity correction. This is also apparent close to the border area of the design (Fig.4.1). Lines that receive different correction parameters, look

[1] program distributed by PDF Solutions GmbH
[2] For a negative resist only exposed patterns stay after development.

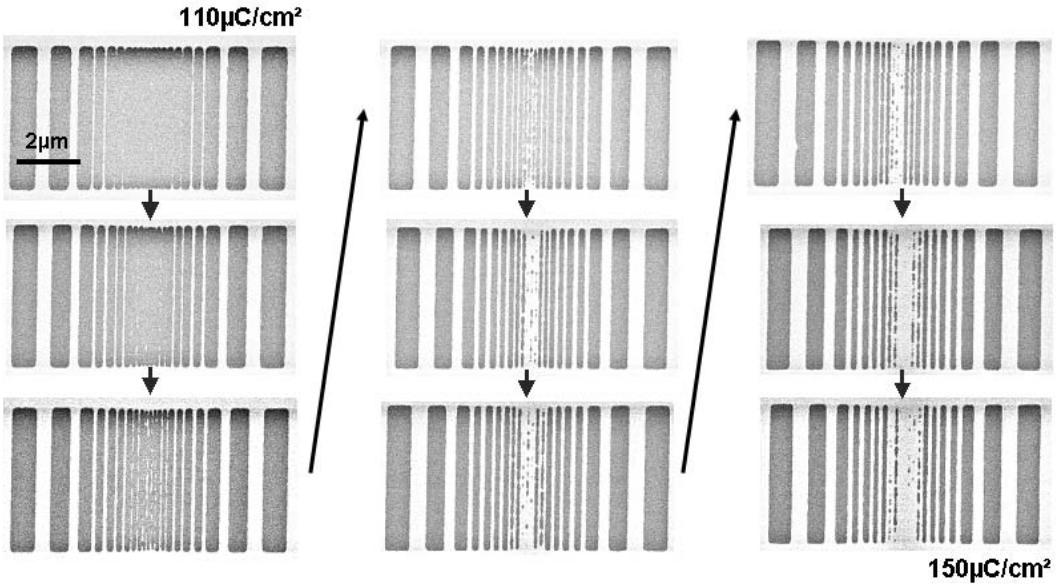

Figure 4.2: Dose series for HSQ resist
SEM images (10 kV) of HSQ on a silicon after development with design Fig.B.4. A proximity correction was used. The dose was varied between 110 μC/cm^2 and 150 μC/cm^2 in 5 μC/cm^2 steps.

completely different, although the correction parameters are supposed to avoid this problem. In principle the correction has to be adjusted so, that the dose of each line is changed particularly in the inner parts. This problem is caused by the fact, that the correction function used does not account for all effects that contribute to the charge deposition. Finding an ideally adjusted function is a complex issue especially for the facts that will be discussed in the next paragraphs. Note, that HSQ was mostly used for separated lines so far. The design shown in Fig.B.4 with its variable gaps and widths is expected and found to be more challenging.

Another severe problem is, that HSQ was found to be very sensitive to small variations in the dose. 5 μC/cm^2 changes led to completely different results. The three different areas of the design Fig.B.4 required different doses (Fig.4.3). At 110 μC/cm^2 **Variable Width** was exposed in the right way and **Variable Gap** was underexposed. In addition all trenches (widths) in Fig.4.3a) are to broad. This is because the gaps, formed by the exposed resist are to small due a underexposure of lines[3]. At 150 μC/cm^2 the **Variable Gap** was exposed in the right way, **Variable Width** was overexposed. For **Variable Both** a dose in between was needed. All widths have approximately the right size. This indicates, that in principle the dose

[3] The measured widths are given in a table below Fig.4.3.

Figure 4.3: Comparison of the 75 nm design in different resists
SEM images (10 kV) of
a) HSQ on silicon written with a dose of 110 μC/cm^2
b) HSQ on silicon written with a dose of 150 μC/cm^2
c) PMMA on silicon written with a dose of 250 μC/cm^2. The master was covered with a sputtered gold film.

width$^\natural$	1000	800	600	400	200	150	100	75	300G†	300W‡
a)	1070	890	710	510	n.a	n.a	n.a	n.a	175	430
b)	1000	805	598	402	205	152	n.a	n.a	303	295
c)	1000	815	603	405	197	148	105	70	301	302

all values in nm; the error is $\sim \pm 10\,nm$; $\natural$ nominal values for the widths in the **Variable Both** part; † size of 300 nm gaps in the **Variable Width** part; ‡ size of 300 nm widths in the **Variable Gap** part

is right. The overexposure of sub 150 nm patterns is due to the proximity effect. To solve the problem of different required doses two modifications of the design were introduced: for the **Variable Both** region the 75 nm lines were replaced by 100 nm and the three areas were splitted into three separated areas (Fig.A.2). Note, that an optimal proximity correction should allow having patterns with a wide variety of dimensions on the same design. Besides the sensitivity on the dose the age of the HSQ resist and the time between spin-coating and exposure contribute to the performance [van Delft 2002]. The author relates the properties of the resist to the adsorption of contaminates such as ammonia. [Henschel et. al 2003] discuss the impact of baking temperature and developer concentration on the contrast and sensitivity. The bake temperature of 220 °C chosen here has a high selectivity, but a low contrast compared to a bake at 90 °C. This low contrast could be responsible for the proximity correction not to be effective. The authors also report, that the time between spin-coating and writing is a critical parameter. A few days more or less change the properties of HSQ completely. This is also reported by [Henschel et. al 2003]. Using HSQ of a different batch or at a different age could also lead to a basis-dose, that has to be changed by tenths of μC/cm^2. As described by [Trellenkamp 2003] the storage conditions (the resist has to be cooled at all times) are difficult to handle. Opening the cooled resist under ambient conditions might introduce a certain water content into the resist. This might also be a reason for such problems. For the above mentioned experiments several of these issues were not taken into account.

In conclusion the process parameters (high baking temperature and low developer concentration) as well as unconsidered issues (time between baking and writing) led to amiss results. The proximity correction routine did not seem to improve these results. Therefore it can be concluded, that the experiments were done in a unsuited process window. In addition the proximity correction function needs to be adapted. Up to now only single, isolated lines as well as dense lines with fixed pitch have been reported using HSQ. Since the designs used here are far more complex it is not clear, whether there are ideal process conditions. Since the resist is sensitive to small changes in the quality, age and process parameters it is not clear, whether it is possible to achieve a high reproducibly using this technology even while having an ideal set of parameters. The next important step, after writing of patterns, is the development of exposed resists. There are no apparent problems for HSQ. Since it is a negative resist, everything which is not exposed is washed during development. Resist residues could only be found next to patterns and are a result of overexposure or proximity effects.

The dependence of PMMA on dose changes is not as strong. A dose around 250 μC/cm^2 was found to be best. It is sufficient for all three parts of the design to be

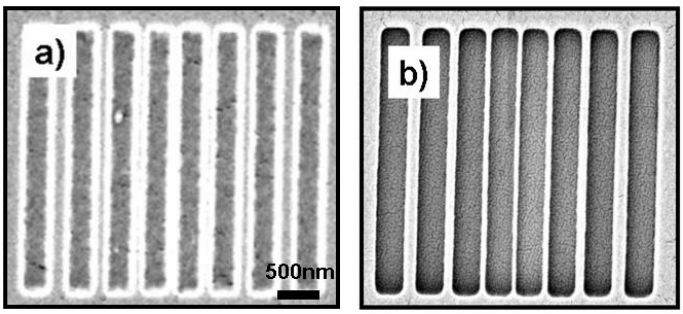

Figure 4.4: Comparison of development with and without megasonic assistance
SEM images (10 kV) developed PMMA masters with a height height of 230 nm. Shown here is the **Variable Gap** region.
a) development by conventional dipping
b) development with a 2 MHz megasonic system

exposed in the right way (Fig.4.3c). Since the measured widths nicely correspond to the nominal widths, it can be concluded, that the dose is right. Proximity correction was not needed.

The development of PMMA is rather different compared to HSQ. Since it is a positive resist the exposed parts of the resist have to be washed away. The design described above consists of lines written into the resist. This means, that the resist has to be removed out of small trenches. It turns out, that it is rather difficult to bring the developer solution into these trenches and to remove the resist completely. Resist residues can be found on the bottom of trenches smaller than 500 nm (Fig.4.4a) and Fig.4.5a) using conventional dip development. In addition the size of the trenches is smaller than expected. During development the sample lay horizontally in the developer bath and was slowly moved up and down. The problem of residues for example is also known for the development of high aspect ratio structures done by LIGA technique, as reported by [Meyer et. al. 2002]. Different methods were tested to solve this problem: At first the container with the development solution was placed inside an ultrasonic bath. Ultrasonic treatment resulted in destroyed resist patterns. Resist lines smaller than 150 nm were partially or totally destroyed (Fig.4.5b). The trenches were slightly larger than expected. Obviously the patterns was exposed in the right way, but in a) some exposed resist still stuck to the edges of the trenches. The destruction of patterns is caused by cavitation[4]. To avoid this effect a megasonic bath was tested. The working principle of a megasonic sys-

[4] When a liquid is subject to tensile stress above a certain threshold it ruptures and forms vaporous cavities. These bubbles will collapse and form jets. The energy is the release in a bunched way destroying the patterns.

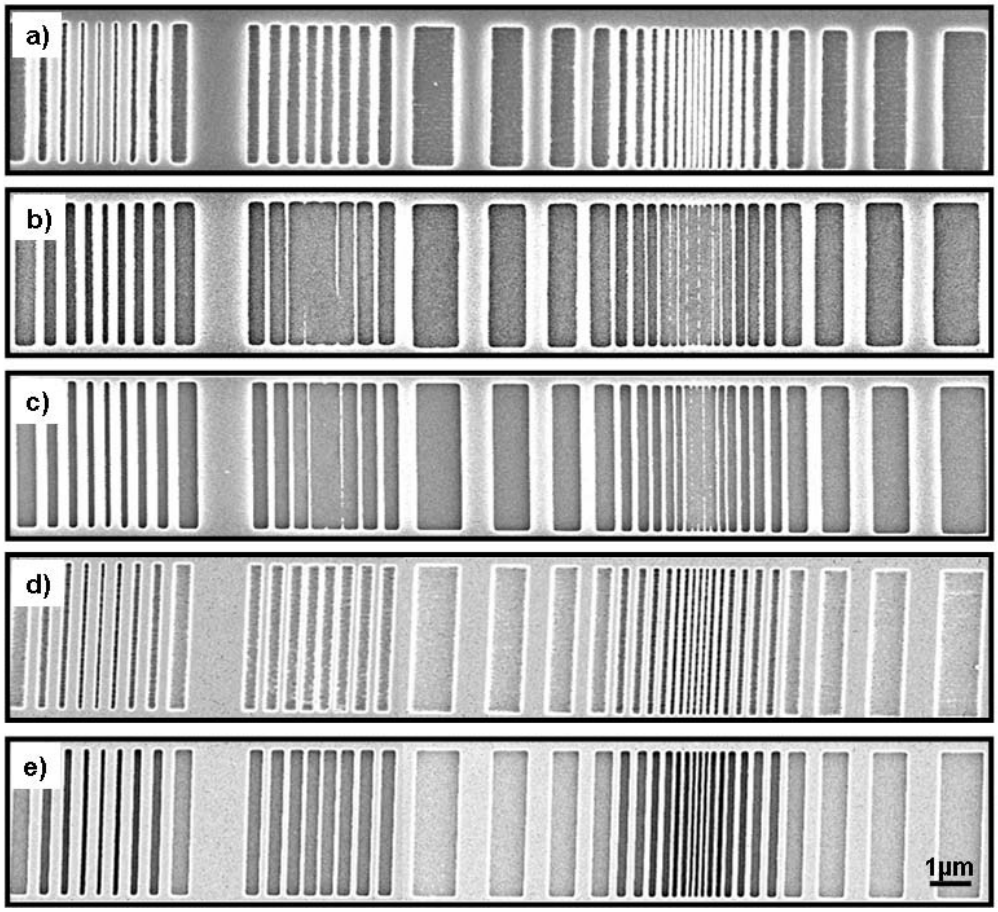

Figure 4.5: Comparison of different development recipes for PMMA masters
SEM images (10kV). The height of the PMMA layer was 230 nm. a) standard development without any assistance
b) development in a ultrasonic bath
c) development in a 1 MHz megasonic bath at 60 % power
d) development in a 2 MHz megasonic bath at 30 % power
e) development in a 2 MHz megasonic bath at 100 % power

width$^{\natural}$	1000	800	600	400	200	150	100	75	300W†	300G‡
a)	925	725	550	375	150	100	50	30	275	360
b)	1015	820	630	440	250	200	n.a	n.a	350	265
c)	1005	800	610	420	195	142	100	n.a	315	282
d)$^{\sharp}$	890	700	500	300	185	90	50	30	255	350
e)	998	800	595	400	190	145	100	65	295	305

all values in nm; the error is $\sim \pm 10\,nm$; $\natural$ nominal values for the widths in the **Variable Both** part; † size of 300 nm gaps in the **Variable Width** part; ‡ size of 300 nm widths in the **Variable Gap** part; $\sharp$ the contrast of the edges is smeared out, thus the values seem to be overestimated

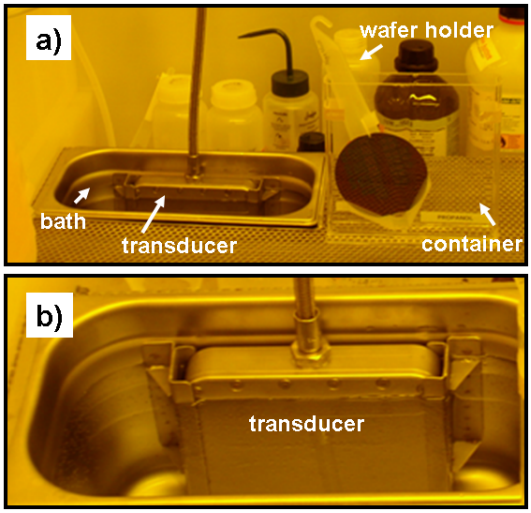

Figure 4.6: Setup of the megasonic bath
a) The transducer is mounted upright in a water bath. The developer solution is filled in a container. This container is placed inside the bath in front of the transducer.
b) closer view on the transducer in the water bath

tem is equivalent to an ultrasonic system except the frequency is in the megahertz range while it is around 20 kHz for ultrasound. However, using a 1MHz megasonic system also damaged small patters. At 300 W power resist patterns smaller than 100 nm were destroyed, but all resist residues were removed (Fig.4.5c). The sizes of the trenches was in the right range. Below 300 W all patterns were intact, but the resist residues were still present. Therefore a system with 2 MHz was used instead of 1MHz. At 300 W all resist patterns were intact and the bottom of the trenches looked clean (Fig.4.5e). The widths of the patterns are in good agreement with their nominal size. The cleanness of the trenches is clarified in Fig.4.4. At a power below 200 W resist residues were still present (Fig.4.5d). In addition the width of the trenches was smaller than expected comparable to Fig.4.5a). A quantitation of this results by means of the ratio of covered surface is not possible. In case of residues the whole floor of the trenches seems to be covered by residues. This impression is further strengthen by Fig.A.3. This makes a simple analysis by means of image processing using a threshold very difficult.

The effect of different frequencies can be understood, since the size of cavitation bubbles gets smaller for larger frequencies. Cavitation should not contribute to the cleaning for megasonic frequencies[5]. The cleaning effect occurs due to local agitation, the large pressure and local wetting. The megasonic setup has been

[5] A more detailed description of the megasonic process is given by [Shwartzman et. al. 1985].

installed such that the transducer was placed upright into a water bath (Fig.4.6). A rectangular shaped quartz container was placed inside this bath. The wafer or chip was dipped upright into the container. Thus the amount of development solution was limited. To guarantee a good coupling of the megasonic waves to the container and the development solution the walls of the container were chosen to be 3 mm thick [Straka 2005]. With this setup, together with a 2 MHz transducer, best results were obtained and thus it was used as standard for all further investigations.

In conclusion PMMA is an easy to write electron beam resist. A standard dose of 250 μC/cm^2 was suited to expose all parts of the design in a homogeneous way. No proximity correction was needed. The problem of resist residues inside small trenches after standard development could be solved by using a megasonic assisted development process.

Two possible routes were pursued after the development of masters: using the resist structures directly as a master or using them as etch masks. For HSQ the first route is straight forward since HSQ becomes silicondioxide like after a post-exposure bake at around 450 $^\circ C$ [Liou et. al. 1998]. It can be coated with a release agent; it can be cleaned by plasma, acid or flame annealing; it is stable during hot embossing against temperatures and pressures. Thus it fulfills all critical requirements. PMMA patterns can also be directly used as master. In doing so some intrinsic disadvantages appear: they can not be cleaned, since PMMA will be damaged by acids, organic solvents, plasma or temperature. A homogeneous coating with a release agent is not possible, since various different chemical groups are exposed at the surface of the PMMA. It is in general not possible to use these masters for hot embossing, because PMMA itself is a thermoplastic material and deforms above its glass transition temperature (T_g)[6].
A way to fabricate masters with more defined properties is using the resist patterns as etch masks. *Reactive Ion Etching* (RIE)[7] is the method of choice for the etching of sub micron features. Two different material systems were used: resist on siliconoxide and resist on silicon. In order to etch all patterns to the same depth an intrinsic etch stop was used. In case of siliconoxide etching it is sufficient to have a siliconoxide layer on top of a silicon wafer. This is done by thermal dry or wet oxidation. Selectivity between silicon and its oxide is rather good. This means, that the etch rate of siliconoxide is much faster than that of silicon. The oxide layer is subsequently etched while the etch process automatically stops, when the silicon is reached.

[6] Above T_g the polymer becomes rubbery and capable of elastic or plastic deformation without fracture, since non-covalent bonds between the polymer chains become weak in comparison to thermal motion.

[7] An introduction into the field of RIE is given by [Coburn et. al 1982].

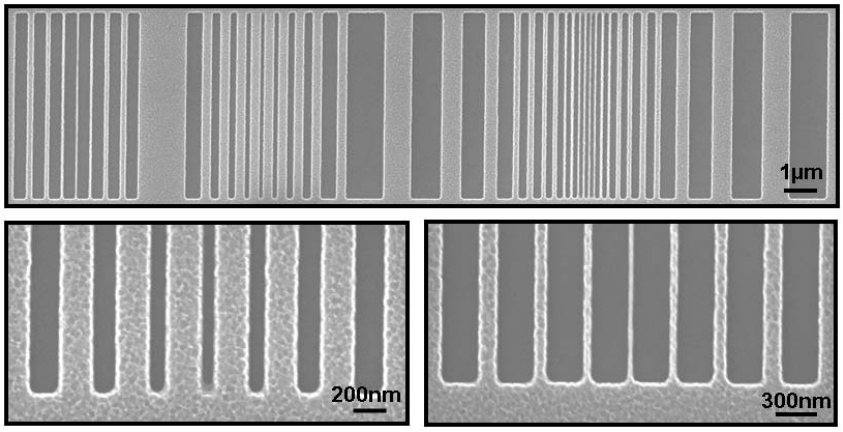

Figure 4.7: *Reactive Ion Etching* of siliconoxide through a PMMA mask
SEM image (10 kV) of 150 nm siliconoxide etched through a 150 nm PMMA layer with the design shown in Fig.B.4. A 1:1 mixture of CHF_3/CF_4 at 200 W for 5:15 min was used.
The lower images are magnifications of the **Variable Width** and **Variable Gap** part of the upper one.

width♮	1000	800	600	400	200	150	100	75	300W†	300G‡
	1010	815	611	408	215	132	113	95	310	275

all values in nm; the error is $\sim \pm 5\,nm$; ♮ nominal values for the widths in the **Variable Both** part; † size of 300 nm gaps in the **Variable Width** part; ‡ size of 300 nm widths in the **Variable Gap** part;

The process was performed using PMMA as resist and a gas mixture of tetrafluoromethane (CF_4) and trifluoromethane (CHF_3) at 200W in a RIE chamber. Etching was done under end-point detection, until no more changes in the signal could be observed. As can be seen in Fig.4.7 the patterns could be nicely reproduced. Only the width of the smallest patterns seems to be increased due to over-etching. However, the initial height of the siliconoxide of 150 nm was reduced to 110 nm. This indicates, that the 150 nm PMMA layer was etched faster than the siliconoxide. Obviously after the PMMA layer was gone the siliconoxide was continuously etched everywhere. This also explains the rather rough surface of the master also apparent in Fig.4.7. Changing the power or gas composition did not provide better results. Possible solutions would be to increase the resist height or to decrease the siliconoxide thickness. The height of the residual layer and the writing results would also change by changing the resist thickness. In this thesis the siliconoxide etching was not further pursued. Instead a promising etch process on silicon was chosen, as described in the next paragraph. HSQ can not be used in a process for oxide etching, since the etch rate is very close to the etch rate of oxide.

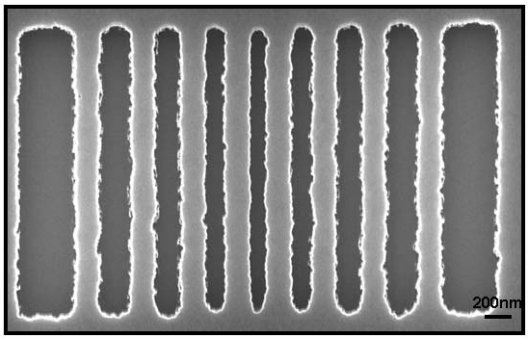

Figure 4.8: *Reactive Ion Etching* of polysilicon through a HSQ etch mask
SEM image (10 kV) of 150 nm polysilicon etched with a HBr plasma using HSQ as an etch mask
The **Variable Width** part of the design shown in Fig.B.4 is shown here.

nominal width♮	400	200	150	100	75
measured	454	272	180	145	125

all values in nm; the error is $\sim \pm 5\,nm$; ♮ nominal values for the widths in the **Variable Width** part;

For HSQ a highly selective etch process for the etching of silicon was reported by [Trellenkamp 2003]. This process used a hydrogen-bromide (HBr) plasma and was performed in an ICP-RIE[8]. In order to have a defined etch stop siliconoxide or siliconnitride were used. As mentioned the HSQ is siliconoxide like. After the etch process the HSQ has to be removed from the master with a 1 % HF dip. This dip would also damage the siliconoxide etch stop. Therefore siliconnitride was used instead, since it is not harmed by HF. The nitride was deposited using a LPCVD followed by the deposition of a n-polysilicon layer with a certain thickness. Prior to etching the samples were baked at 450 °C for 1h in a nitrogen atmosphere. The etching for HSQ was done in a two step process. The first step was pure HBr plasma at 50W bias and 750 W ICP for 30 s, then 1 part of oxygen was added to 25 parts of HBr at 100 W bias and 2000 W ICP until the etch-stop was reached. After the etching was finished, a certain HSQ was always left. It was stripped by HF as described above. As can be seen in Fig.4.8 the etching process stopped nicely at the nitride layer. However, the roughness of the lines shown in this Figure is striking. In addition the width of the trenches is to big compared to their nominal width. This indicates, that the HSQ is overexposed and thus the HSQ lines are too broad. To investigate whether the roughness is due to the HSQ, etch process or polysilicon, further tests were performed. An experiment on a SOI[9] wafer revealed the same roughness. Thus it is not due to the granular structure of the polysilicon.

[8] The **I**nductive **C**ouple **P**lasma technology allows more selective etch processes.
[9] **S**ilicon **o**n **I**nsulator

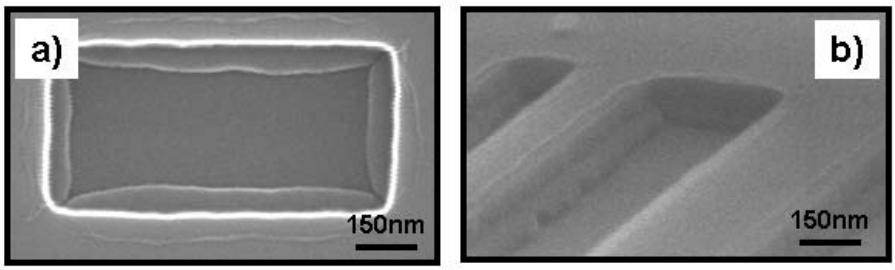

Figure 4.9: *Reactive Ion Etching* of polysilicon etched through a PMMA mask in a single step
SEM image (10 kV) of 150 nm polysilicon etched with a HBr plasma using PMMA as an etch mask. The etching was done in a 3:30 min step

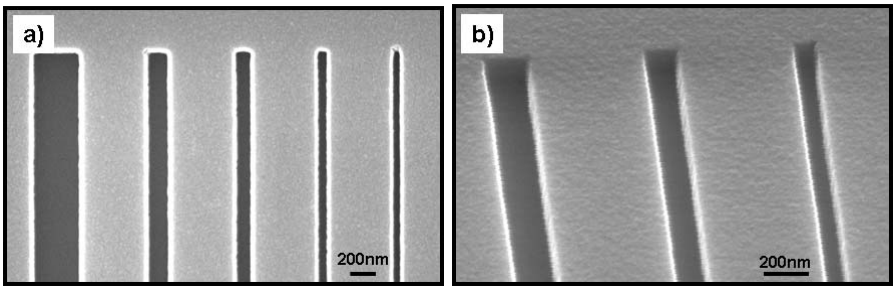

Figure 4.10: *Reactive Ion Etching* of polysilicon etched through a PMMA mask in several step
SEM image (10 kV) of 100 nm polysilicon etched with a HBr plasma using PMMA as an etch mask. The etching was done in a five 30 s steps.
a) top-view
b) taken under a 70° angle

The experiments using PMMA described in the next paragraph revealed much smoother edges. Thus the roughness can be clearly attributed to the HSQ itself and the writing process. As previously discussed this might also be due to the proximity effect. This further disqualifies HSQ as an useful resist for our purposes, namely the specific designs used.

Since the results of the etching were promising, the same process was used with PMMA as an etch mask. Instead of a two step process the first HBr step without oxygen was performed until the polysilicon was etched through. Fig.4.9 shows, that the patterns did not etch homogenously. After a depth of around 100 nm the trenches became smaller at a certain slope. This can be explained by the thermoplastic behavior of PMMA. After about half of the etching was done, the

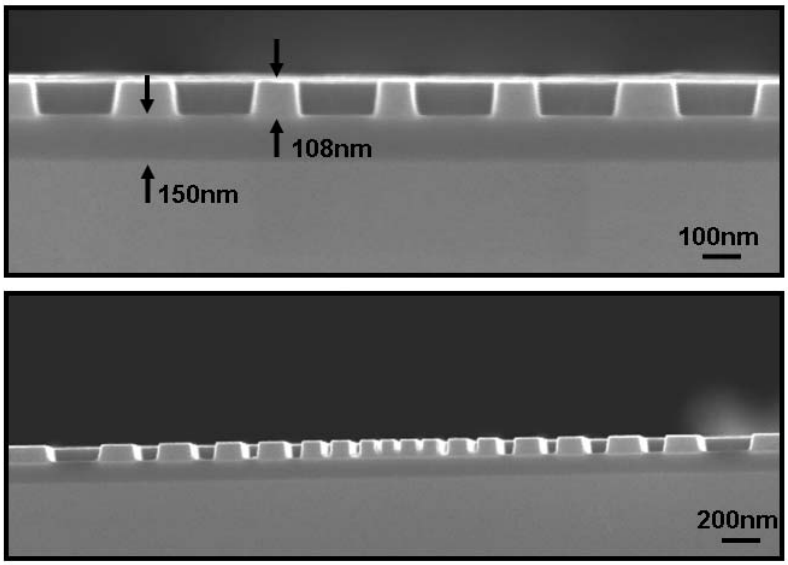

Figure 4.11: Cross-section through a master fabricated with the etching of polysilcion SEM images (10 kV) of the master shown in Fig.4.10 cut and imaged under a 90 °.

width	200	150	100	75
upper image♮	n.a.	175	125	100
lower image†	240	192	140	80

all values in nm; the error is $\sim \pm 5\,nm$; ♮ nominal values for the widths in the **Variable Gap** part; † size of gaps in the **Variable Both** part measured on top of the structures;

sample must have heated above the glass-transition temperature, which is around 160 °C. Then the resist must have slowly melted and flowed into the trenches. The only explanation for the heating is the thermal coupling, since the ICP-RIE process is specially designed to minimize the load on the sample. In the experiment described a 1 cm by 1 cm sample was placed onto a quartz dish in the RIE. It is quite reasonable, that the coupling of this small sample to the cooling chuck was quite bad. To account for this, four inch wafers were used for all further experiments. In addition the etching process was splitted into 30 s runs, followed by two minute breaks. That way the described problem was never observed again. The results for silicon etching using PMMA as etch mask (Fig.4.10) show, that the patterns are nicely etched to the etch stop and are free of any residues. Cross-section images reveal, that the siliconnitride was not harmed at all, since the height after etching is still around 150 nm (Fig.4.11). The polysilicon has also kept its initial height. The sides of the lines are slightly tilted. This can be attributed to PMMA, not having perpendicular sides after developing, since the HBr etching process is known to be highly unisotropic. The roughness of the edges is much smaller compared to HSQ.

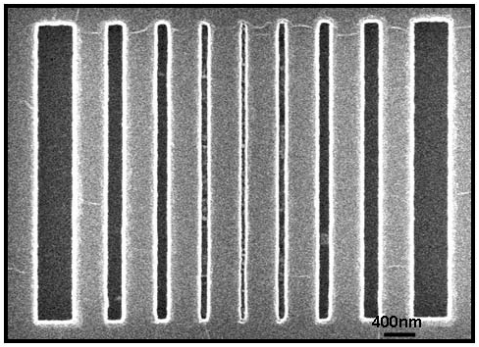

Figure 4.12: Master fabricated under non-perfect conditions
SEM image (10 kV) of a PMMA sample patterned with the design shown in Fig.B.4 at 250 μC/cm^2, developed using 2 MHz megasonic, etched with a HBr plasma into polysilicon. However, some residues are present in the trenches.

This proves, that neither the etching process nor the polysilicon is responsible for the roughness observed.

However the cross-section reveals, that the gaps are larger than expected and the 75 nm trenches are not completely etched to the siliconnitride. Since the edges are rather perpendicular this can not be explained by melting of PMMA as discussed above. Problems with the etch process itself lead to isotropic etching or over-etching, but in all these case the pattern lines would be thinner and not broader. Most probably the width of the trenches after writing and developing of these patterns must have been smaller. Note, that in this case the pattern was not investigated prior to etching. Also note, that all previously discussed results were obtained with a Leica EBPG 5HR electron beam writer, while the last results were obtained with a new EBPG 5000Plus writer. Several problems had to be solved after the exchange of the electron beam writers. Obviously the beam parameters were still not chosen adequate. But even if perfect parameters were found for all steps involved, the combination of all processes involved is far from being stable with the design used here, namely dense lines and space with sub 200 nm variable dimensions. Results obtained through the course of this thesis showed fluctuations. Fig.4.12 was performed with PMMA at the "right" dose, with megasonic development and using the HBr etching process. But residues can be seen in the sub 150 nm trenches. Most probably the electron beam parameter were somehow not adequate. This could have happened through a changing of the resist properties over time, through the exchange of the electron beam writers or through the change of electron beam parameters through time[10]. These changes have to be compensated. However, it is not always possible to keep pace with them,

[10] It is for example known, that the properties of the electron gun change with the age of the gun.

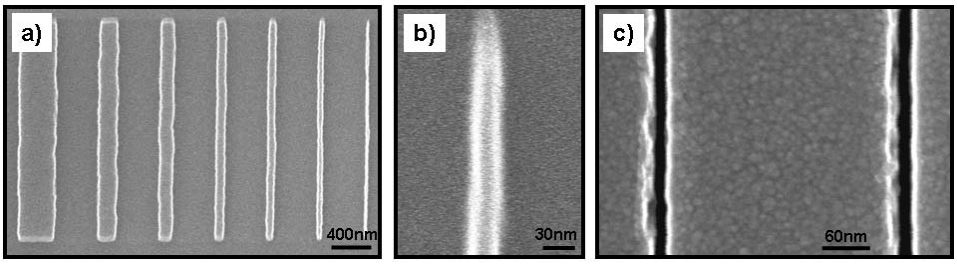

Figure 4.13: Master having sub 50 nm patterns
SEM images (10 kV) patterns of design shown in Fig.B.5
a) HSQ used as an etch mask to etch through a 150 nm polysilicon layer with the design shown in Fig.B.5 and etched with the HBr RIE process.
b) Zoom on a nominal 25 nm line
c) PMMA used as an etch mask to etch through a 100 nm polysilicon layer with the design shown in Fig.B.5 and etched with the HBr RIE process.

nominal width	400	200	150	100	75	50	35
measured	402	201	153	103	73	52	30

all values in nm; the error is $\sim \pm 5\,nm$;

especially since some are not understood. It is known form running systems, e.g. in production, that from time to time (weekly) test patterns need to be processed in order to adjust the parameters of the writing and etching processes.

Using the design Fig.B.5 for the HSQ process as well as the PMMA process 25 nm lines or trenches could be obtained (Fig.4.13). For HSQ a) the width of patterns matches perfectly their nominal width. This indicates, that the dose was chosen right. Note, that in this design the distance between lines was 500 nm. Therefore the proximity effect is much weaker. Single lines separated by a larger distance is the common application for HSQ as NTR. Fig.4.13c) shows, that trenches with a width below 40 nm could be obtained.

In conclusion the etching of silicon using an ICP RIE process with HBr and PMMA as etch mask is able to produce the quality of masters needed. Nice masters were obtained using the combination of PMMA developed with megasonic assistance and etched with HBr into silicon (Fig.4.14). These masters were used for all further investigations.

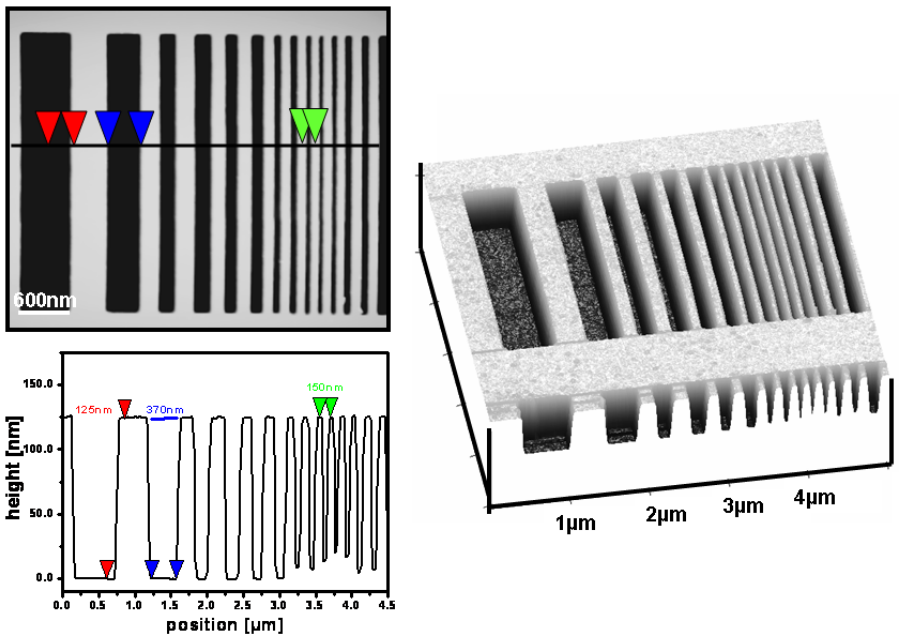

Figure 4.14: AFM (tapping mode) image of a perfect master
PMMA was patterned with the design shown in Fig.B.4 on silicon, developed using megasonic treatment and etched with HBr. Due to the geometry of the tip the small trenches could not be resolved.

4.3 Release Agent

The release agent layer should passivate the master surface and thus make sure, that master and stamp can easily be separated. Therefore it was chosen such, that it is chemically inert, robust, stable over many embossing steps and easy applicable. For that purpose fluor containing silanes were chosen, because they form densely packed monolayers on siliconoxide. Two different silanes were used: tridecafluor-octyl-trichlorosilane (TFTS) (Fig.2.27) and nonafluoro-hexyl-dimethyl-chlorosilane (NFDC). TFTS is widely used as a release agent in most NIL applications. Results obtained with TFTS were more reproducible than those obtained with NFDC. This is in agreement with [Angst et. al. 1991]. They state, that a trifunctionality is necessary to form tightly packed monolayers. That is why NFDC was discarded after the first experiments. Different silanization protocols were tested: deposition from solution, thermal evaporation of silane at ambient pressure and vapor deposition.
For the vapor deposition a vacuum silanization setup was built up (Fig.4.15). The silane was poured in a petri-dish located inside a desiccator. The samples were placed beside it. In order to avoid splashing of the liquid silane onto the sample the silane was covered with a splash-guard made of glass such, that it is closed next to

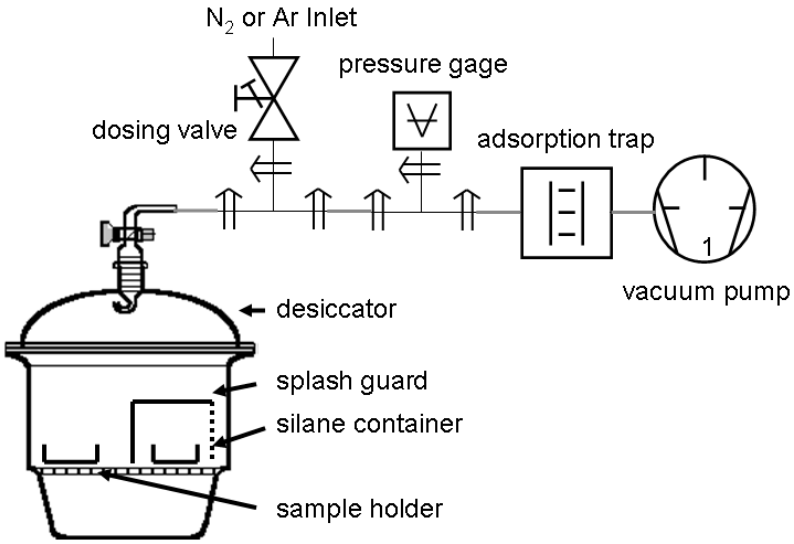

Figure 4.15: Vapor deposition setup for the silanization

the sample and open on the opposing side. The desiccator was evacuated with a conventional vacuum pump. In order to avoid pump-oil residues an adsorption-trap was placed in the vacuum line next to the pump, followed by a pressure gage. The pressure was adjusted by adjusting the inlet of argon with a dosing valve located next to the pump inlet. Since the silanization process and the silane itself are moisture dependent, the desiccator was placed inside a glovebox system having an argon atmosphere.

The drawback of this setup is, that the cleaning is performed outside the glovebox in a plasma chamber. The samples were later on transferred into the glovebox. Thus they were covered with an ubiquitarian amount of surface water. This amount strongly depends on the environmental conditions temperature and humidity, which were not controlled in these laboratories. [Habuka et. al. 2005] report, that the surface concentration of water linearly depends on the humidity, and that the saturation of water is reached after a few minutes. The time between cleaning and lock-in into the glovebox systems for the experiments presented here was between 2 - 30 min. This might have led to a different water concentration on the surface. However, a certain amount of water is needed in order to perform the reaction. If the amount of water is too low, the reaction can not occur at all. If it is too high aggregates will form. With the setup introduced here the amount cannot be controlled. One solution to this problem was introduced by [Jung et. al. 2005]. They apply the silane vapor for a certain time, followed by water vapor. Thus the amount of water in the silanization device can be adjusted. Based on this idea a

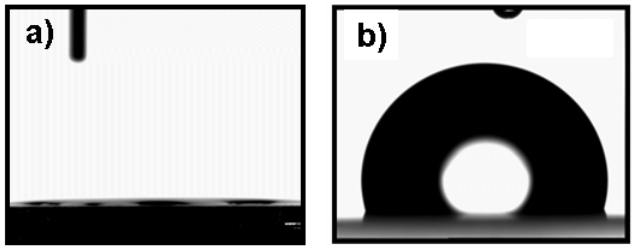

Figure 4.16: Comparison of the water contact angle before and after silanization
a) siliconoxide surface after oxygen plasma treatment
b) surface of a) after a fluoro-silanization

new setup is part of ongoing research. Plasma cleaning will be performed inside this device. Thus contaminations and surface water can be neglected. In addition further detailed studies of the silane layers by means of XPS and Ellipsometry are part of ongoing research [Gilles 2006]. For thermal deposition the silane was placed on a hot-plate inside a glove-pack. The sample was placed next to the silane and heated to 10 °C below its boiling point. This procedure resulted in thick silane layers, which could even after rinsing with toluene and ultrasonic assistance not be removed. Thus the thermal deposition was not pursued any more, especially since the handling with the glove-pack is very difficult. For the liquid deposition the silane was dissolved in dried toluene. The samples were immersed in the silane for 15 min and rinsed with dried toluene.

A crucial point of the silanization is the cleanness of the surface and the water content. The contact angle of a fresh silicon wafer taken out of a storage box was found to be around 65 °. Since siliconoxide is hydrophilic, this indicates, that the surface is partially covered by hydrophobic adsorbates. This is discussed by [Takahagi et. al. 1996]. They observed organic contaminations on the surface of a silicon wafer. These were attributed to antioxidants contained in the wafer case material, monomers and dimers form the plastic vessel material used for handling as well as organic solvents and plasticizer, which are present in the atmosphere. After a 30 s 200 W oxygen plasma treatment the contact angle was well below 10 ° (Fig.4.16a) indicating a clean surface. For shorter times the contact angle was between 10 ° - 65 °. AFM images of the siliconoxide surface after plasma treatment did not indicate an increased roughness. Thus this cleaning protocol was taken as standard for all further process steps. After fluoro-silanizations the contact angle was found to be between 105 ° - 115 ° (Fig.4.16b). These are common values for fluorinated smooth surfaces. This indicates a very hydrophobic surface. The contact angles for liquid and vacuum deposition were equal. However, AFM measurements revealed, that liquid deposition always caused aggregates on the surface (Fig.4.17b).

This might be caused by water in the solution. Although the toluene used was dried, a certain amount of water can never be avoided. This amount strongly depends on the humidity. As discussed by [Bunker et. al. 2000] hydrolyzed silane molecules can form aggregates in solution. These aggregates led to agglomerations on the surface. On one hand it was dependent on the solvent they used, on the other hand it was strongly dependent on the amount of water in the solution. As discussed above, it neither should be too high nor too low. Aggregations on the surface having dimensions up to 50 nm were observed. They can effect *Casting/Hot Embossing* results and thus should be avoided. Therefore the vacuum deposition was chosen as method of choice. At 100 Pa the silane was rapidly evaporated (75 μL / 5 min). By adapting van´t Hoff´s equation describing the vapor pressure as function of temperature the following equation can be derived:

$$T_S(p) = T_S(p_0) \cdot \left(1 - \frac{RT_S(p_0)}{\Lambda} \ln\left(\frac{p}{p_0}\right)\right)^{-1} \tag{4.1}$$

Here T_S is the boiling point at normal pressure p_0 or at a different pressure p. Λ is the enthalpy of evaporation. Since it is not available the Picat-Trouton approximation was used[11]. Thus using the boiling point of TFTS at normal pressure as 192 °C the enthalpy is calculated as $39.5\,kJmol^{-1}$ and this results in a boiling point at 1mbar of 4 °C. Since the process is performed at 20 °C the silane is thus heavily boiling. This led to a certain surface coverage with a monolayer, accompanied by larger aggregates (Fig.A.6b). It is concluded, that at 1mbar the silane evaporates too fast. Therefore the reaction was performed at a higher pressure of 4.5 kPa for a time period of 1h. Using equation 4.1 the boiling point is 80 °C at 4.5 kPa. Thus this is far away from the actual temperature of 20 °C and thus the evaporation of the silane is very slow. This result is further approved by the fact, that after 1h most of the liquid silane is still left in the petri-dish, while at 100 Pa everything is evaporated after 5 min.
The evaporation at 4.5 kPa led to a slow, uniform reaction. AFM images taken at the begin of this thesis indicate a multilayer coverage with bilayer and trilayer components, but absolutely no aggregates were present (Fig.A.6a). The AFM image clearly indicates island growth. This is in agreement with [Banga et. al. 1995]. They described an island growth for fluoro-silanes using liquid deposition. They also state, that the monolayer is created via an in-filling process, and that the formation of the fluoro-silane SAM is a rather fast process compared to silanes without fluoro-groups. The low coverage of the sample could be explained with a finding of [Balgar et. al. 2003]. They describe a discrepancy between in-situ methods and ex-situ AFM. Rinsing performed prior to ex-situ AFM measurements will remove physisorbed species, while in-situ methods will not distinguish between physisorbed and chemisorbed species. Physisorbed molecules are not grafted to the

[11] For molecules without hydrogen bonds the entropy of evaporation is approximately $85\,JK^{-1}mol^{-1}$. The enthalpy of evaporation Λ can be estimated as $\Lambda = T_S \cdot 85\,JK^{-1}mol^{-1}$.

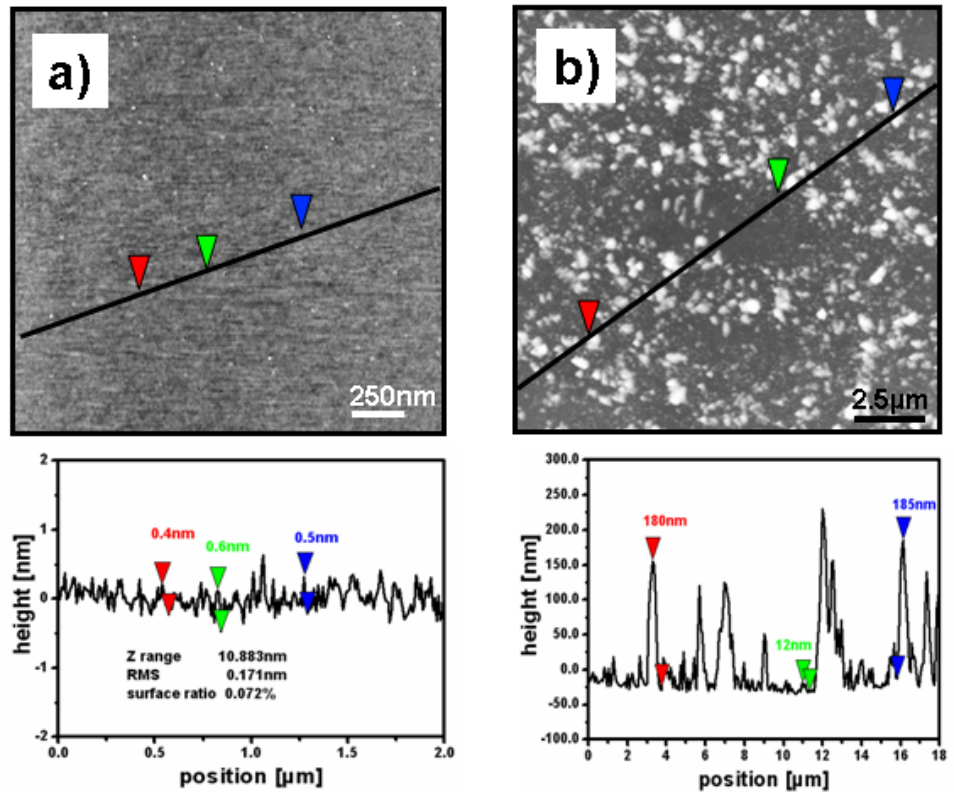

Figure 4.17: AFM image of fluoro-silanized surfaces
a) TFTS on a silcionoxide surface; vapor deposition at 4.5 kPa for 1 h; maximum z-scale (white contrast) 6 nm
b) TFTS on a siliconoxide surface, liquid deposition 0.02 vol% in dried toluene; maximum z-scale (white contrast) 400 nm

surface. This could in fact be due to a too low content of water and therefore too little hydroxyl-groups might be present on the surface. However, this experiment was performed outside the glovebox. Thus an uncontrollable amount of humidity was present in the desiccator. Also the silane in the bottle was affected by humidity forming large agglomerations in the bottle. In order to eliminate this problem experiments were performed inside the glovebox. Repeating the experiments with 4.5 kPa / 1 h and a fresh bottle of silanes revealed very flat surface layer (Fig.4.17a). The rms roughness of this layer was below 2 Å. This corresponds to 20 % of the molecule length. The rms roughness of the siliconoxide before silanization is around 1.5 Å [Mayer 2006]. It is reasonable for the roughness to slightly increase. This procedure fits all demands and was used as standard protocol for the release agent layer.

Using the protocols on master surface the easy separation of a stamp was always possible even for the surface with island coverage. Thus it is concluded, that no closed monolayer is needed. The functionality was also not harmed by *Hot Embossing* cycles. For temperatures up to 160 °C no changes in the separation ability could be observed. This is in agreement with [Devaprakasam et. al. 2004]. They report about the thermal stability of TFTS SAMs on aluminum substrates. Up to 150 °C they could only observe reversible changes. Above 150 °C they observed irreversible conformational and orientational disorder in a plane perpendicular to the carbon-axis.

In conclusion liquid deposition of silane resulted in lots of agglomerations on the silane surface, while for the vapor deposition no aggregates were seen. Vapor deposition is the method of choice. This is in good agreement with [Jung et. al. 2005]. The coverage observed by AFM seems to be conflicting. This can be explained with the uncontrolled amount of surface water on the samples. The passivation of a master and thus the ability to separate master and stamp easily seems not to be dependent on the monolayer coverage.

4.4 Stamps

The stamp is a replication of the master. Its patterns are covered with molecules or metal layers that are transferred to a substrate through a printing process. An ideal stamp should fulfill several requirements: it should be stiff enough to avoid the problems of sagging and pairing; it should be patternable at reasonable conditions with sub 100 nm patterns, it should be soft enough to guarantee a conformal contact to a substrate; the surface properties should be such, that molecules can be transferred. Two methods were used to form stamps: *Casting* and *Hot Embossing*. Different stamp materials were used having different properties:

material	E	θ_W	γ_S	method
Sylgard 184	0.001‡	110°	22♯	CA
h-PDMS	0.007♭	-	22♠	CA
Affinity VP8770	0.08‡	95°	30♮	HE
Topas 8007	2.6‡	90°	35†	HE
Zeonor 1420R	2.2‡	80°	33†	HE
Zeonex E48R	2.5‡	100°	33†	HE
Plexiglas 99530	2.0‡	75°	54†	HE
Surlyn 1702	0.19‡	70°	33♯	HE

Table 4.1: Comparison of the properties of stamp materials used
E: Young's modulus in GPa; θ_W: water contact angle measured; γ_S: surface free energy in mN/m ; CA: *Casting*; HE: *Hot Embossing*
‡ taken from the product datasheets
♭ taken from [Schmid et. al. 2000]
† taken from [Munzert et. al. 2003]
♯ taken from www.accudynetest.com/surface-energy-materials.html
♮ assuming standard PE or PP polymer
♠ assuming the same value as for Sylgard
contact angle and surface free energy will be discussed at the end of this section

Casting

In the scope of this thesis the most common polymeric material, which was used for *Casting* of stamps, was PDMS. Three different kinds of PDMS were tested: Sylgard 184, Microset 101RF and the so called h-PDMS. Microset comes as a two component system. After mixing, it cures at room temperature within several minutes. Microset is typically used as replication material for engineering inspections of any kind of technical surfaces. Thus it seems to have special anti-sticking additives. This makes it possible to cast Microset to any master without using additional release agent layers. The drawback with it is, that the transfer of non-crosslinked silicone components to the substrate surface while printing is rather prominent. Printing with a Microset stamp without applying any ink resulted in a pattern of silicone components on the substrate (Fig.A.8).

Sylgard 184 PDMS is also a two component system. It is the material used for more than 90 % of μCP results reported so far. The mixing ratio of curing agent and base is typically 1:10. A ratio of 1:2 led to slightly stiffer stamps, while a ratio of 1:40 led to a soft, sticky compound. After mixing precursor and crosslinker the compound was degassed by just letting it rest in a brought bowl. Afterwards it was cured by putting it into an oven at 60 °C for 14 h and subsequently 110 °C for 1h. The usage of PDMS as stamp material is limited by its rather low Young´s modulus, which is around 1 MPa. Pairing occurred for line patterns with the dimensions of i)

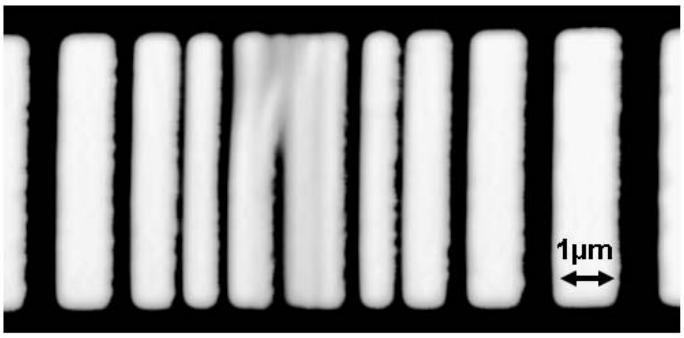

Figure 4.18: Pairing observed for a Sylgard PDMS stamp
AFM image (tapping mode) of a Sylgard 184 stamp. It was casted against a master having the design shown in Fig.B.3 with a depth of 440 nm.

	height	width	gap	Pairing†	left‡	right♮	expected♭
i)	440 nm	200 nm	200 nm	yes	1.5	1	yes
ii)	440 nm	400 nm	400 nm	no	0.6	1	no

† pairing observed; ‡ left hand side of equation 2.2; ♮ right hand side of equation 2.2;
♭ pairing expected according to equation 2.2;

(Fig.4.18). According to equation 2.2 pairing should occur since the left hand side of the equation 2.2 is larger than the right hand. The line pattern ii) did not show pairing. This is predicted by equation 2.2 since the left hand side is smaller than the right hand side. Obviously the equation accurately predicts pairing for PDMS. This is in good agreement with [Sharp et. al. 2004]. They could also demonstrate, that this formula predicts pairing for PDMS. A transfer of non-crosslinked silicone components (Fig.4.28) was observed using the PDMS stamps for printing of molecules. That is in agreement with [Glasmaestar et. al. 2003]. They reported a transfer of non-crosslinked, low-weight components. For these reasons Sylgard is not suitable for printing below 100 nm and was not investigated further as stamp material in this thesis, but rather served as a model system to get used to the technique and become aware of problems. Unpatterned Sylgard slabs were used for ink-pads or as backplanes for other stamp materials.

h-PDMS was prepared according to [Schmid et. al. 2000] material A. After degassing it was spincoated onto a master at a speed of 500 rpm. It was cured at 60 °C for a few minutes. Afterwards the mixture was back-filled with Sylgard 184 backplane. The later step was necessary because h-PDMS is quite brittle. A thick piece of it breaks immediately. But even for thin h-PDMS on a Sylgard slab breaking could be seen. Many patterns were destroyed and fragments could be found after printing. Even though the Young´s modulus was about 7 MPa, pairing could still be observed for i) (Fig.4.19) and iii) (Fig.4.20). Patterns of ii), iv) and v) did not indicate any pairing. The surface energy of h-PDMS was assumed to be equal to

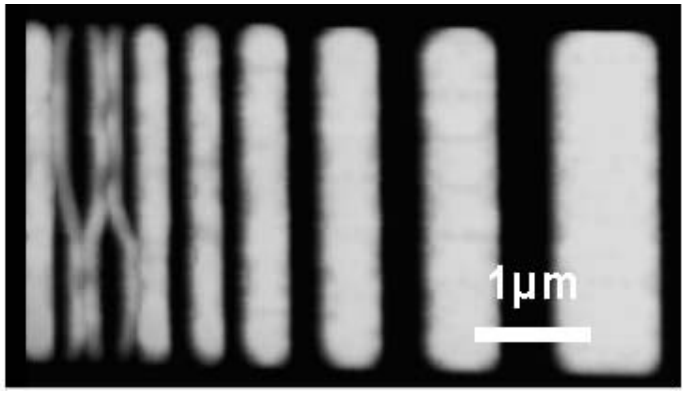

Figure 4.19: Pairing observed for a h-PDMS stamp
AFM image (tapping mode) of h-PDMS stamp with a depth of 440 nm and the design Fig.B.3; z-scale (white contrast) 500 nm

	height	width	gap	Pairing†	left‡	right♮	expected♭
i)	440 nm	200 nm	200 nm	yes	0.93	1	no
ii)	440 nm	400 nm	400 nm	no	0.39	1	no

† pairing observed; ‡ left hand side of equation 2.2; ♮ right hand side of equation 2.2;
♭ pairing expected according to equation 2.2;

Sylgard PDMS. The Young´s modulus was taken from [Schmid et. al. 2000]. Thus the choice of input values might not be 100 % accurate. In fact the Young´s modulus and surface free energy of h-PDMS and PDMS fluctuates for different publications. Since the stress/strain relation for rubbers is not linear, it is difficult to assign a Young´s modulus. Therefore these fluctuations might be due to different measurement procedures. Using equation 2.2 for i) and iii) the left hand side of the equation is smaller than the right hand side. However, the ratio of left to right hand side is around 90 % , for i) and iii), while it is 39 % for ii), 45 % for iv) and 31 % for v). So obviously i) and iii) do not satisfy equation 2.2, but they are rather close. The offset could be explained by none accurate input values. However, the offset could also be due to fact, that the analytical equation 2.2 does not account for all effects. For iv) and v) the left hand side is much smaller than the right hand side. As predicted by equation 2.2 small patterns with a larger gap (iv) and larger patterns with smaller gaps (v) are more stable than small patterns in close distance (i) and (iii).
This indicates, that h-PDMS is indeed stiffer than Sylgard 184, but it is not stiff enough for sub 100 nm printing of proximate structures. Nevertheless it could be used for the printing of larger patterns (Fig.4.29).

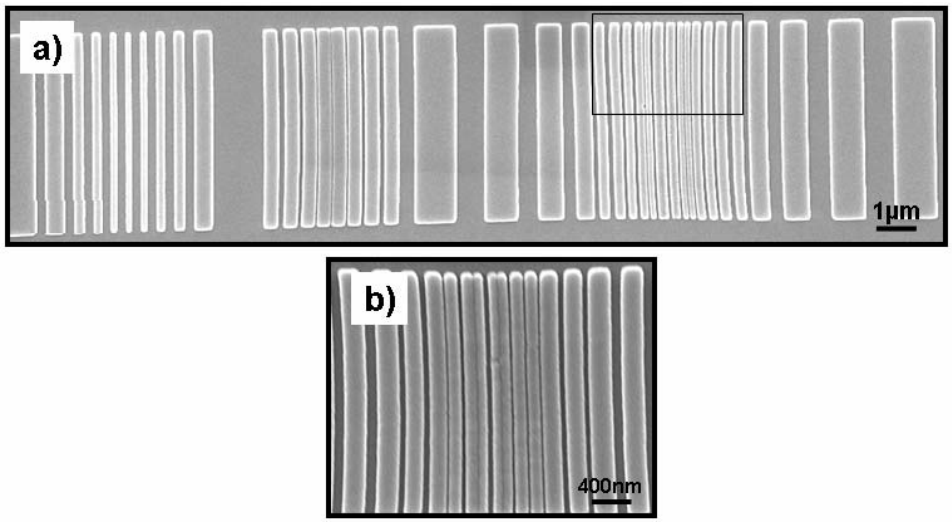

Figure 4.20: Pairing observed for a h-PDMS stamp
SEM image (10 kV) of a h-PDMS stamp with a depth of 100 nm and the design shown in Fig.B.4. The stamp was coated with a sputtered gold layer for imaging.
b) magnification of the highlighted area

	height	width	gap	Pairing†	left‡	right♮	expected♭
iii)	125 nm	75 nm	75 nm	yes	1.5	1	yes
iv)	125 nm	75 nm	300 nm	no	0.9	2	no
v)	125 nm	300 nm	75 nm	no	0.15	0.5	no

† pairing observed; ‡ left hand side of equation 2.2; ♮ right hand side of equation 2.2;
♭ pairing expected according to equation 2.2;

Hot Embossing

Since none of the materials used in *Casting* was found to be stiff enough to reproduce sub 100 nm patterns thermoplastic materials such as polyolefins Affinity VP8770, Topas 8007, Zeonor 1420R and Zeonex E48R, the ionomere Surlyn 1702 and the methacrylate Plexiglas 99530 were used. They are deformable by means of *Hot Embossing*. To perform HE in a precise, reproducible manner, it is necessary to adjust the pressure and temperature with good accuracy. Therefore a special device was constructed (Fig.4.21). The basic component is an optical heater based on halogen light bulbs. To directly heat the masters and stamp materials the bulbs are covered by glass[12]. Since glass and metals have different thermal expansion coefficients it was avoided to join glass with metal supports. Instead the whole device was made out of glass. This has the advantage, that not all parts of the

[12] Borofloat glass from Schott AG

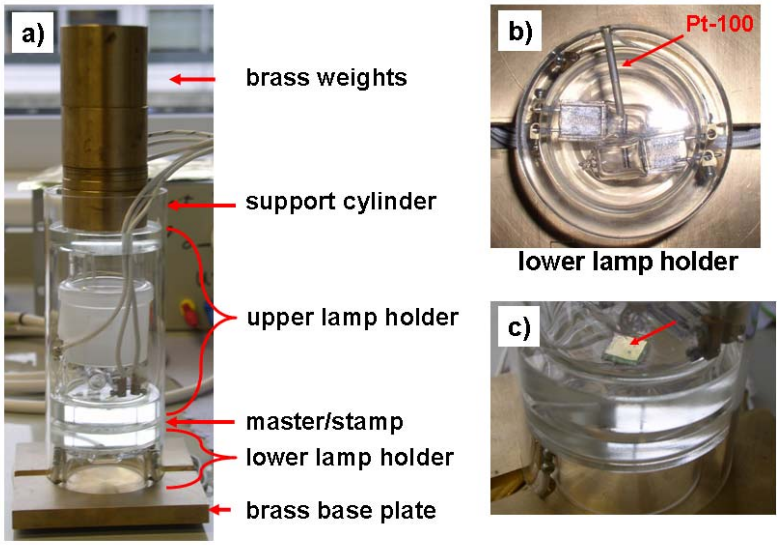

Figure 4.21: Images of the Hot Embossing device
a) side view of the whole device
b) top view of the lower lamp holder
c) side view of a master/stamp assembly inside the device

device are heated up due to a rather poor thermal conductivity of glass. More than that, since all parts have the same thermal expansion coefficients there is no non-uniform deformation of the device. Melting of the polymer can be observed through the glass. The master/stamp assembly is heated by two 100 W light bulbs from the bottom and two 100 W light bulbs from the top. The lamp power is controlled by two dimmers. The temperature is measured by measuring the resistance of Pt-100 elements inside the glass support between the light bulbs and the samples. Pt-100 elements are platinum wires with a defined cross section and length such, that they have a resistance of 100 Ω at 0 ° Celsius. The dependance of the resistance with respect to the temperature increase is rather linear. For applying a defined pressure onto the master/stamp assembly brass or lead weights with different masses are placed on top of the upper lamp holder. To avoid non-uniform pressure a glass cylinder is guiding the movement such, that tilting is avoided. The lamp holders are located inside the cylinder. The maximum pressure that can be applied to a 1 cm^2 piece is 1.0 MPa. About one minute is needed to heat the device from room temperature to 100 °C. Since there is no active cooling of the device, it takes approximately 15 min for the device to cool below 50 °C which is sufficient for separating master and stamp. A similar device is reported by [Seunarine et. al. 2006]. Their device was made of brass with a quartz window for heating. It had no possibility to monitor the temperature (except to place a sensor into the polymer). After melting the polymer, they applied a top-plate, which

pressed the polymer into the master and which cooled the polymer rapidly down at the same time, because it was not heated. They reported cycling times of a few minutes. The basic idea behind the device reported here is rather different. Instead of first heating the polymer, pressing and immediately cooling it again, the imprint pressure is applied all the time. The cycling time is thus longer, but the accuracy of pattern replication is supposed to be better. There is enough time for the stamp material to adapt to the master pattern. Hints for any tensions or stress in the stamp material after solidification could never be observed. A major advantage of the device is, that it is open. This means, that the polymer is able to freely flow to all sides after it is heated above the glass transition temperature. Thus the device can also be used to press thick polymer pieces to a certain thickness. The disadvantage is, that the pressure is applied through brass weight and is thus limited to about 0.1 - 1.0 MPa.

In order to apply higher pressures the NX-2000 Nanoimprint device was used. The NX-2000 is based on the *Air Cushion Press* technique [Chou 2002]. Master and stamp material are placed between two silicone foils inside a chamber. After evacuating the chamber the foils are sealed. Then a pressure of up to 4.3 MPa can be applied. In addition the sample can be heated up to 250 $^{\circ}C$. Main advantage of this device are a very homogenous pressure and a fast cycling time. A drawback of this device is, that due to the sealing the stamp material can not flow freely. The material can only fill the small cavity formed by the silicone foils. Thus the stamps prepared have a rounded backside. Results obtained with this device and the self-built device described above were equivalent. Critical process parameters like process pressure, temperature and initial thickness had to be chosen adequate.

For HE exclusively thermoplastic materials have been used in the scope of this thesis. The materials were used as few millimeter thick foils. A piece of the foil was put onto a master and both were placed into the embossing device. As a reference material polyolefin plastomer Affinity VP was used according to [Csucs et. al 2003]. It has a Young´s modulus of 80 MPa. SEM investigations after *Hot Embossing* reveal, that pairing defects are present (Fig.4.22). Lines patterns with of i) as well as ii) showed pairing (Fig.4.22a). Strangely this result is comparable to pairing observed with h-PDMS as previously discussed or even a little larger. Using equation 2.2 pairing is not expected to occur since the Young´s modulus of 80 MPa is 11 times larger than for h-PDMS and the surface energy is 30 mN/m, which is only a factor of 1.4 larger. Equation 2.2 clearly predicts, that pairing should not occur since the left hand side is much smaller than the right hand side. The ratio between left and right hand side of equation 2.2 is 16 % for i) and 26 % for ii). For patterns with a different height pairing was observed for patterns of iii) and iv) (Fig.4.22b). Here the ratio between left and right hand side of

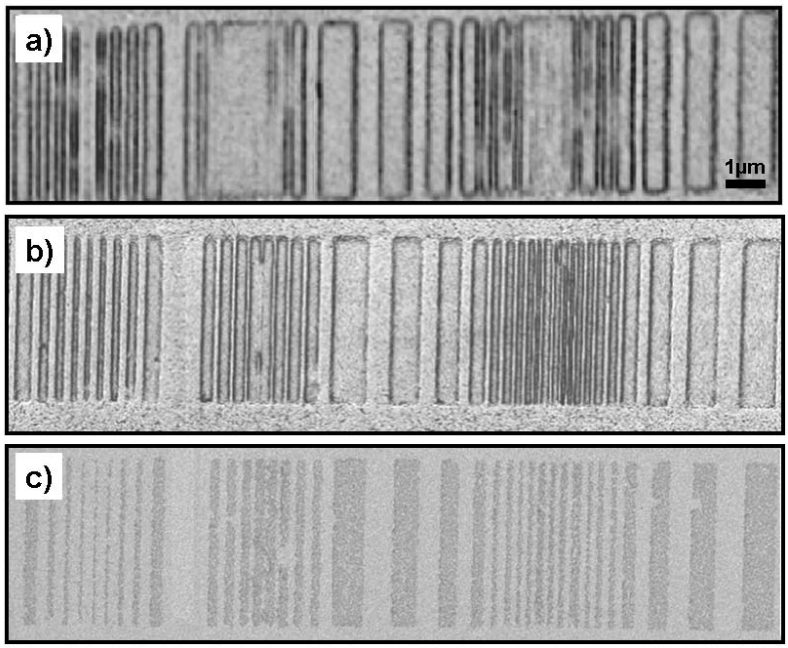

Figure 4.22: Pairing defects of POP stamps having the design shown in Fig.B.4
a) SEM image (10 kV) of the stamp with a depth of 150 nm
b) SEM image (10 kV) of a stamp with a depth of 100 nm
c) SEM image (2 kV) of cyt *c* printed with the stamp of a)
Stamps were coated with a sputtered gold film.

	height	width	gap	Pairing†	left‡	right♮	expected♭
a) i)	150 nm	300 nm	150 nm	yes	0.1	0.7	yes
a) ii)	150 nm	150 nm	150 nm	yes	0.3	1	no
b) iii)	125 nm	100 nm	100 nm	yes	0.4	1	no
b) iv)	125 nm	300 nm	75 nm	yes	0.1	0.5	no

† pairing observed; ‡ left hand side of equation 2.2; ♮ right hand side of equation 2.2;
♭ pairing expected according to equation 2.2;

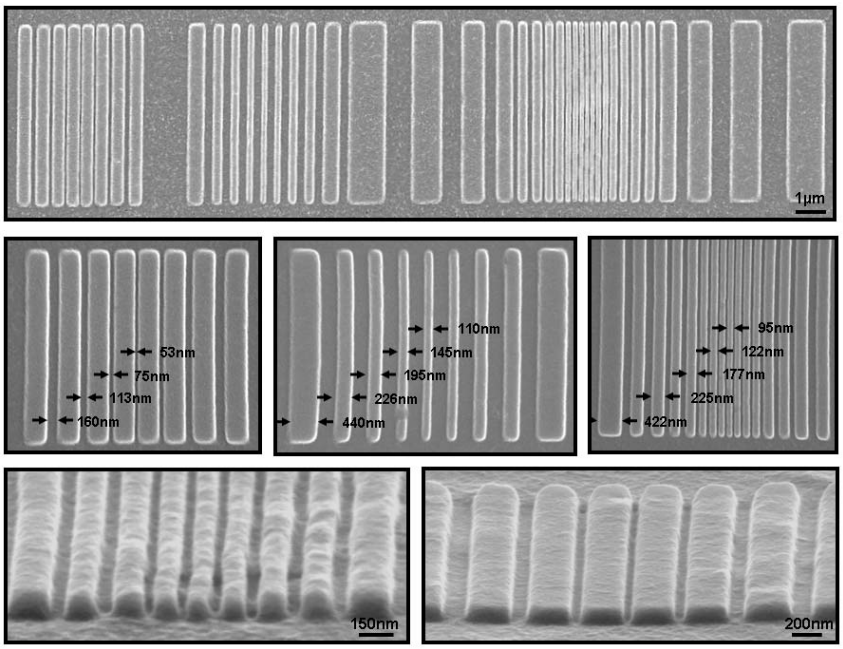

Figure 4.23: SEM (10 kV) images of a Surlyn stamp
Surlyn was embossed at 115 °C with 1.5 MPa using the NX-2000 tool. Stamps were covered with a sputtered gold layer for imaging

equation 2.2 is 37 % for iii) and 16 % for iv). So obviously pairing occurs in a range of 16 % to 37 %. Since the plastic materials such as polyolefins are fundamentally different to elastomeric materials such as PDMS it is quite reasonable, that equation 2.2 is not appropriate to describe both systems. [Csucs et. al 2003] used Affinity VP stamps having single lines with a wider spacing, and thus they did not observe any pairing. Therefore no reference about pairing for POP is available. Printing of proteins with these stamps indicated, that the pairing is not influenced by the printing process (Fig.4.22c).

Since the transfer of proteins and organic molecules was nice Affinity VP served as a reference system for printing experiments. However, harder stamp materials had to be found to realize the design shown in Fig.B.4.

Surlyn is an ethylene/methacrylic acid copolymer containing zinc ions. Its Young´s modulus is around 190 MPa. SEM images of the stamps reveal, that the stamp is stiff enough, that no deformations appear (Fig.4.23). Using patterns with height = 125 nm, width = 75 nm, gap = 75 nm to calculate equation 2.2 the ratio between left and right hand side is 46 %. This result indicates, that the functional dependency of an appropriate theory to describe pairing of thermoplastic materi-

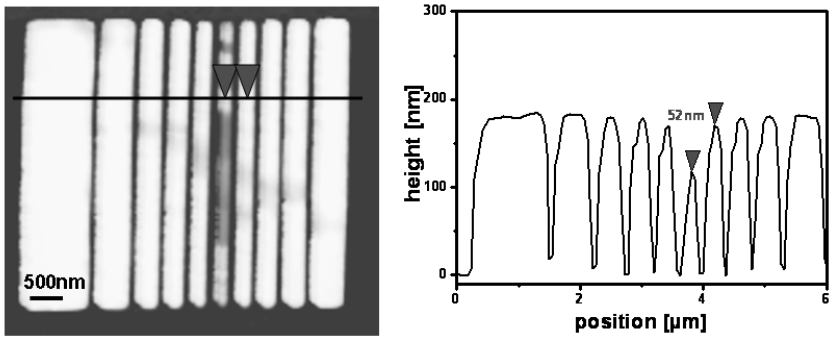

Figure 4.24: Tapping mode AFM image of a Surlyn stamp
Surlyn was embossed at 115 °C with 0.2 MPa using the glass HE device.

als must be significantly different from equation 2.2. From the finding for Affinity VP, which shows pairing for a ratio of $\approx 20\,\%$, one would expect pairing to occur for height = 125 nm, gap = 75 nm, width = 75 nm Surlyn patterns too. An alternative explanation could be, that equation 2.2 can be used for all types of materials, but something special happened for Affinity VP stamps. Their properties are rather unique. Among the polyolefin plastomers they are by far the ones with the lowest Young´s modulus. Thus their surface free energy might be special as well. Assuming, that equation 2.2 is correct and appropriate for Surlyn, the minimal pattern size for height = 125 nm would be width = 40 nm, gap = 40 nm. On the other hand Surlyn is still soft enough to adhere to a surface like POP and PDMS. It can be seen from Fig.4.23, that the dimensions of the lines correspond to the dimensions of the master, if one takes into account, that stamps are covered with a sputtered gold layer of approximately 10 nm thickness to avoid charging. Sometimes it happened, e.g. if the imprint pressure was too low, that the small lines were not of the same height than the larger patterns. Fig.4.24 is an extreme example showing a 52 nm shorter line. Such a problem is also discussed by [Sotomayor Torres *Ed*. 2003]. Since the design consists of many perpendicular trenches it might be difficult to completely fill all trenches homogeneously. In principle the imprint result strongly depends on the specific pattern used. Note, that also the problems observed for the master fabrication[13] as previously discussed could cause such results. But mostly smaller differences were observed. Note, that even just a 5 nm difference might lead to problems for the printing process, because the line does not "touch" the substrate. This problem was solved during the printing step and thus this slightly deviation in stamp quality was not further investigated

In order to increase the variety of stamp materials and further increase the maximum resolution even harder materials, in terms of higher Young´s modulus, were in-

[13] trenches not completely etched through; residues in the trenches

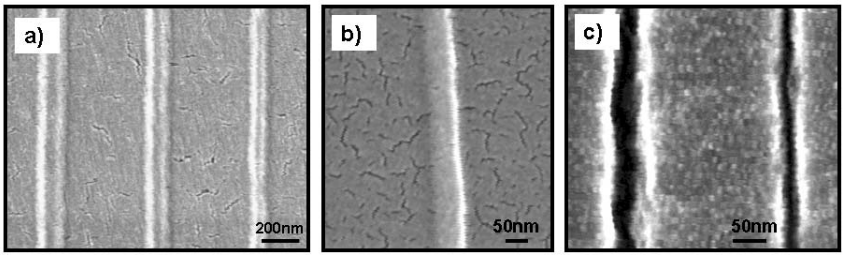

Figure 4.25: SEM images (10 kV) of stamps with sub 75 nm patterns
a) Topas embossed with a master having the design shown in Fig.B.5. The master was fabricated using the PMMA process.
b) closer view on a)
c) Surlyn embossed with a master having the design shown in Fig.B.5. The master was fabricated using the HSQ process. Therefore the design was inverted.

vestigated: Plexiglas 99530 as a methacrylate; Zeonor 1420R, Zeonex E48R, Topas 8007 as polyolefins. Their Young´s modulus is between 2 - 3 GPa (Tab.4.1). An estimation using equation 2.2 leads to critical dimension for pairing to occur at height = 125 nm to width = 23 nm, gap = 23 nm. Such patterns would have a aspect ratio of 5.5. This might be to large. Assuming a more realistic aspect ratio of 4 patterns with width = 10 nm, gap = 10 nm could be stable with height = 40 nm . This result is very promising. Of course the down-scaling does not only depend on the Young´s modulus but also on the intrinsic properties of the material such as chain length. Since PMMA (which is similar to Plexiglas) can be patterned by means of NIL or EBL in the sub 30 nm range, it should also be possible to achieve such resolutions for stamps. The materials used here are representatives for a huge variety of such polymers which are industrially available. They are available in different grades with slightly different properties such as Young´s modulus, glass transition temperature and many more. So for each application the material could be chosen accordingly. SEM images of stamps revealed, that for none of the materials pairing, sagging or other deformation were present (Fig.A.9). Especially the shape of the patterns was replicated very precisely. Due to their high stiffness the materials are not able to adhere themselves to a surface. This made it necessary to modify the μCP technique as described in the next section.

Master with sub 50 nm could be replicated with Surlyn and other materials. Lines of $\approx$ 50 - 60 nm could be imaged in SEM (Fig.4.25). Using master with a pattern consisting of sub 50 nm lines (compare Fig.4.13) sub 50 nm small trenches could be obtained. The increased line-width of patterns is most probably due to the coverage of the stamp with a sputtered gold layer.

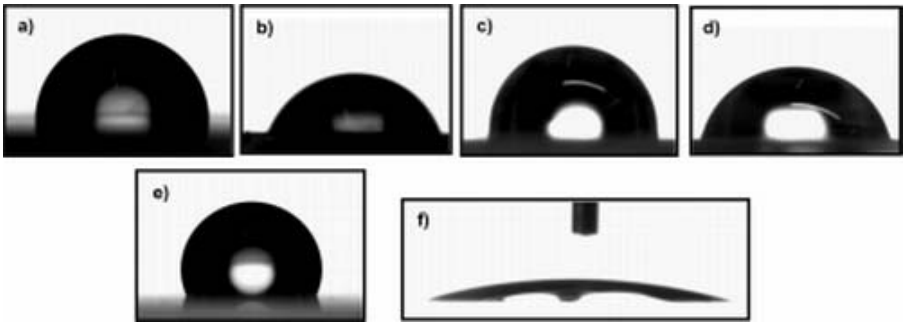

Figure 4.26: Water contact angle of stamp materials
a) Affinity POP, b) Surlyn, c) Topas POP, d) Zeonor POP, e) Sylgard PDMS untreated, f) Sylgard PDMS after 15 s oxygen plasma

The interaction between stamp and molecules is mainly determined by the hydrophobicity of the materials. The printing of molecules mostly compromises three surfaces involved: ink-pad, stamp and target substrate. The surface energy has to be chosen such, that a gradient is established. Molecules have to completely wet ink-pad, stamp and substrate. The adhesion to the stamp has to be larger in order to transfer molecules form the ink-pad to the stamp. Finally the molecules should be transferred to the target substrate, thus a larger adhesion of the molecules is needed. Note, that in some cases a complete wetting is not desired (discussed in Chapter 4.5.1. In order to have an ideal stamp for each kind of molecule the stamp materials were chosen such, that a kit with different water contact angles was available (Fig.4.26). The values are listed in table 4.1. As can be seen, only the water contact angle was measured. Thus it was not possible to determine the surface free energy as described in equation 2.1. The values given in the table are taken from literature sources or material data sheets. Although Zeonor, Zeonex, Topas and Affinity are all polyolefin plastomers, which should have a similar surface free energy, their water contact angle is different. This indicates, that the different composition of the materials, although having the same main components leads to a different wettability. A detailed investigation of the surface free energy using different liquids has not been part of this thesis. The contact angle of PDMS could be changed by plasma activation. After 15 s in a 200 W oxygen plasma the contact angle was below 10°. For the thermoplastic materials a changing of the contact angle by surface modification has not been investigated in this framework, but it is described by [Munzert et. al. 2003].

As a proof of concept high aspect ratio structures were fabricated using *Hot Embossing*. Topas was embossed into porous aluminum membranes. These mem-

branes were described and fabricated by [Wolfrum et. al. 2006]. Afterwards the aluminum was dissolved in potassium-hydroxide. Typically pores had diameters of 30 - 150 nm. The aspect height of patterns was mostly larger than 10. Depending on the size, structures were stable, laterally collapsed or completely collapsed (Fig.A.14). More detailed investigations are part of ongoing research. However these first results prove, that arrays of sub 100 nm polymeric nanopillar can be fabricated in an easy process, compromising only a few steps. [Zhang et. al. 2006] reported a process, that was used to fabricate similar polymeric nanopillar arrays. They used silicon nanopillar arrays as master, made a PDMS replica and used REM with epoxy or polyurethan materials. Thus this process compromises more steps than that reported here. In addition porous membranes are easier to fabricate and the size and distance of pores is easier tuneable than that of silicon nanopillars.

4.5 Printing

Printing denotes the process, where the molecules are transferred from the stamp to a substrate surface. Prior to printing an inking step is performed. Inking denotes the process, where molecules are brought onto the surface of the stamp. The ideal inking and printing process should fulfill the following requirements: a high, reproducible pattern fidelity; transfer of molecular monolayers; the functionality of molecules should not be affected by the printing process. Basically three kinds of inks were used: alkanethiols, proteins and gold (as a metal film). Alkanethiols were widely studied by many groups. Here they served as model molecules to get used to the procedures and familiar with problems arising. Proteins were the molecules of major interest for this thesis. Since they have a huge variety of different functionalities, they can be used for countless application. Of special interest here is the local addressing of their functionalities. The transfer of metals was studied in order to fabricate *Molecular Electronic* devices in a gentle manner.

PDMS stamps were used as model system since most results reported were obtained with it. Affinity VP polyolefin stamps were used, since it is the material with the highest Young´s modulus used for μCP so far. It served as reference system for the transfer of molecules with thermoplastic materials. Surlyn was used as a new system having a higher Young´s modulus than Affinity VP and a lower water contact angle. Thus different results are expected compared to Affinity VP. Stamps were 5 by 5 mm in size. The thickness was approximately 2 mm for PDMS and 0.1 - 1 mm for the thermoplastic materials. It was found to be reasonable to use a finger to apply a pressure on stamp and substrate. PDMS is soft enough, that it does completely adhere to a substrate due to its own weight. No additional force was needed

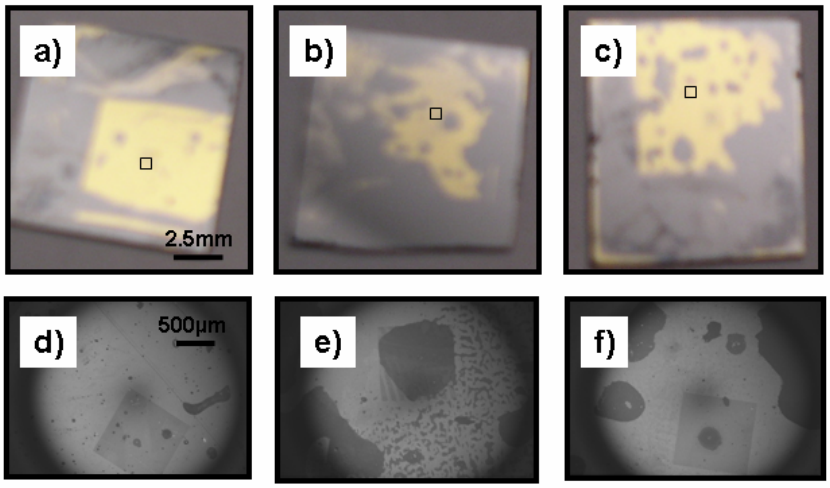

Figure 4.27: Conformal contact for POP and Surlyn
ODT was printed onto gold using different stamp materials. The stamps had a total size of 5 mm by 5 mm and a patterned area of 800 μm by 800 μm in the middle. After printing the gold was etched in a cyanide solution.
a),b),c) show photographic images of gold on the silicon chip after etching. Bright contrast indicates gold, dark contrast indicates silicon;
d),e),f) are SEM images (2 kV) of the patterned area.
a) transfer with an Affinity VP stamp
b) transfer with a Surlyn stamp
c) transfer with a Surlyn stamp with backplane

to achieve a conformal contact. An extra load up to 0.1 MPa was needed for Affinity VP stamps. But then homogenous contact could be established (Fig.4.27a). For thin Surlyn stamps this pressure was not enough to achieve a good contact. Trapped air bubbles resulted in a disrupted pattern (Fig.4.27b). By attaching a slab of PDMS on the backside of the Surlyn as a backplane the pressure could be more homogenously distributed. This resulted in a more uniform contact (Fig.4.27c). A further discussion of the homogeneity will be given in Section 4.5.3.

4.5.1 Printing of Organic and Biomolecules

Alkanethiols were used as model system for μCP. However, their low mass diffusion limits the pattern fidelity. That is why the heaviest commercial available alkanethiol, namely octadecanethiol (ODT), was chosen for all printing experiments (Fig.2.27). A standard 1 mM ethanolic solution of the molecules was used.

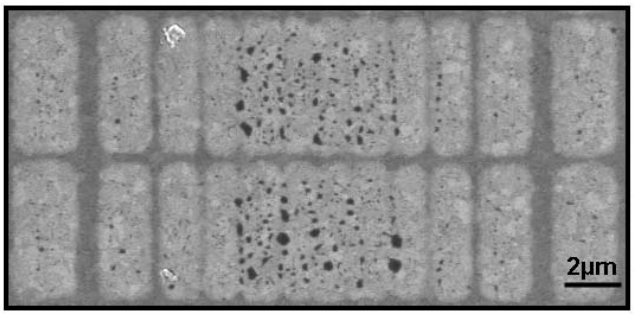

Figure 4.28: SEM image (2 kV) of ODT transferred onto gold with a PDMS stamp
A Sylgard stamp with the pattern shown in Fig.B.3 was used for *Contact Inking* of a 1 mM ODT solution. A contact between stamp and substrate was applied for 30 s. The image shows ODT molecules (bright contrast) transferred onto a gold substrate (dark contrast). Dark spots indicate unintentional transfer of non-crosslinked PDMS residues. In addition gold domains are visible.

Printing was always done onto silicon substrates covered with 5 nm chromium and 50 nm of gold (Appendix C). Since the molecules were partly destroyed in the SEM due to the energy deposition of the electron-beam, it was difficult to obtain high resolution images. Therefore ODT was used as an etch mask according to [Kumar et. al. 1992]. The etching was done until no more gold could be imaged by SEM in the unpatterned areas.

Contact Inking was performed using a PDMS ink-pad according to [Libioulle et. al. 1999]. The first issue to investigate was the inking time of the ink-pad. A time of 5 h - overnight immersion of the ink-pad in the thiol solution was found to be sufficient. As a first test Sylgard PDMS stamps were used. The stamps were brought into contact with the ink pad for 2 min. Shorter times led to unreproducible results. The stamp was pressed onto the substrate with 10 kPa. After a printing time of 30 s a spreading of line width due to diffusion was found (Fig.4.28). An increase of ≈ 700 nm can be seen for each line. [Bass et. al. 2004] reported a spreading of 60 nm after 10 s for ODT also using *Contact Inking* with PDMS stamps. This value is about 4 times smaller. This could be explained by the extra pressure applied here, while Bass et. al. only used the self-adhesion of stamps. It is a widely reported fact, that alkanethiol molecules diffuse into the PDMS during the inking step. The extra load could cause a higher transfer of molecules to the surface. Another experiment was performed using h-PDMS stamps. Printing was done for 25 s without extra load. Spreading of 100 nm was found (Fig.4.29). This is in agreement with the findings of [Bass et. al. 2004]. This further indicates, that the larger diffusion observed for PDMS was due to the extra pressure.

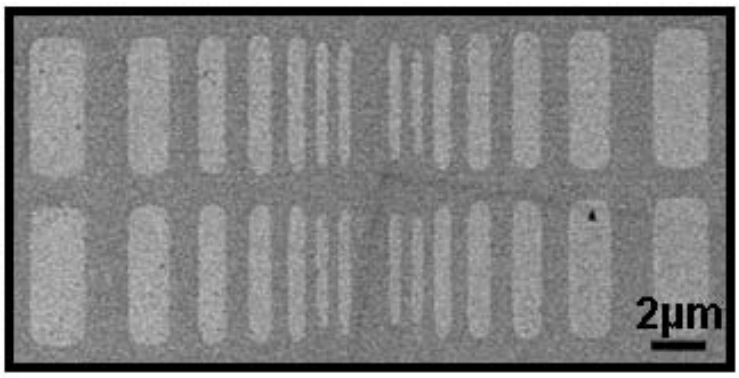

Figure 4.29: SEM image (2 kV) of ODT transferred onto gold with a h-PDMS stamp
A h-PDMS stamp with the pattern shown in Fig.B.3 was used for *Contact Inking* with a 1 mM ODT solution. The contact between stamp and substrate was 30 s. The image shows ODT molecules (bright contrast) transferred onto a gold substrate (dark contrast).

An issue of major importance was found to be the surface chemistry of the stamp material. The surface free energy can be qualitatively estimated by consideration of hydrophobicity with respect to the nature of the ink. For the hydrophobic materials PDMS and Affinity VP the ODT molecules seem to totally cover the patterns in a dense layer, while for Surlyn, which is rather hydrophilic only the edges of patterns are covered (Fig.4.30). This transfer at the edges leads to interesting patterns after etching. A 1 μm broad pattern results in a bowl with sidewalls of 60 nm (Fig.4.31). An edge transfer for ODT was also described by [Sharpe et. al. 2006]. They state, that for the edge transfer ofmobile inks such as alkanethiols a repellent, impermeable stamp material is needed. They proposed to use either chemically or anisotropically modified stamps. There anisotropic means, that the horizontal planes of stamps were coated with a titanium/titanium oxide layer. They used h-PDMS and PEE[14] as stamp materials. Although only 10 nm thick gold layers were used, they obtained 350 nm broad lines after etching. One concession they draw is the incorporation of a rigid support to better handle the stamps. With Surlyn a system could be found, which not only results in much smaller lines, but also does not need any additional surface modifications. At the same time it is stiff enough for high resolution patterning without additional rigid support layers. In this thesis the edge transfer effect was not studied in more detail, but just taken as an example, that for each kind of ink molecule pattern dimensions and stamp materials have to be chosen properly. Different effects might be observed for different molecules on different stamp materials. The final pattern is a function

[14] poly(butylene terephthalate-co-tetra(methylene oxide))

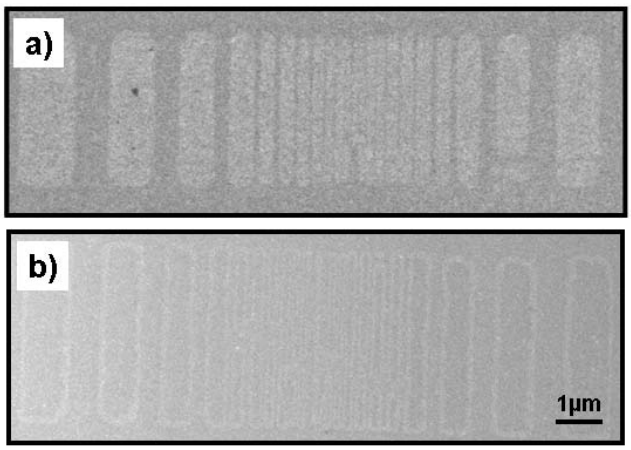

Figure 4.30: SEM images (2 kV) of ODT printed with Affinity POP and Surlyn
ODT was printed onto a gold substrate using stamps having the design Fig.B.4
contact inking: the stamp was in contact with the inkpad for 2 min
a) ODT printed with a Affinity POP stamp
b) ODT printed with a Surlyn stamp

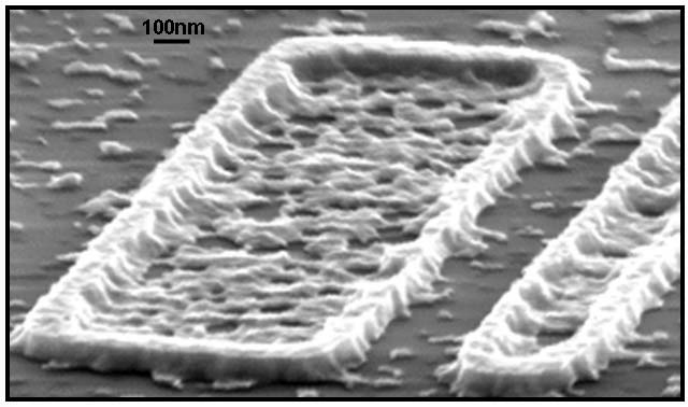

Figure 4.31: SEM image (10 kV) of a gold "bowl"
ODT was printed onto a gold substrate using a Surlyn stamp. After etching the uncovered gold in a cyanide solution the gold "bowl" structure was left. The etching time was short, thus some gold residues were left.

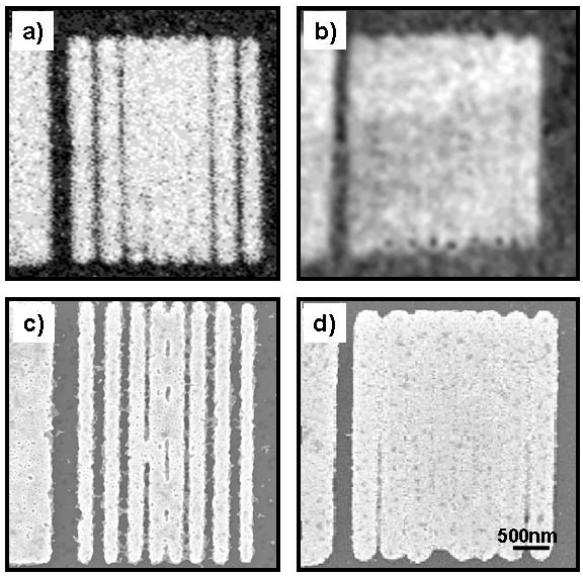

Figure 4.32: Variation of printing time for ODT
ODT printed onto a gold substrate using a POP stamp (Fig.B.4)
contact inking: the stamp was in contact with the ink-pad for 2 min
a) SEM image of ODT on gold; contact between gold and stamp 1 min
b) SEM image of ODT on gold; contact between gold and stamp 2 min
c) and d) SEM images of a) and b) after etching of the gold

of the respected combination of ink, stamp material and surface chemistry of both. To make μCP a powerful technique a repertory of stamp materials with different properties is needed.

The influence on the contact time was investigated using Affinity VP stamps. A printing time of 1 min led to a nice reproducible transfer (Fig.4.32a/c). The 75 nm trench was filled and the 100 nm trench partially. This means, that there was a diffusion of about 75 - 100 nm during 1 min printing time. A contact time of 2 min led to a diffusion around 200 nm (Fig.4.32b/d). Diffusion thus seems to be approximately linear and thus reasonable. This is only half of what was measured and reported for PDMS. This lower diffusion for POP might be reasonable since for PDMS it is known, that the molecules can diffuse into the PDMS while inking. Thus more molecules might be present during printing. This should not be the fact for thermoplastic materials such as POP. Therefore these materials might be very useful for limiting the diffusion in μCP.

For Surlyn this different since less molecules are transferred (Fig.A.11). After 1 min all trenches seemed to be free of diffusion, while after 2 min the 75 nm and

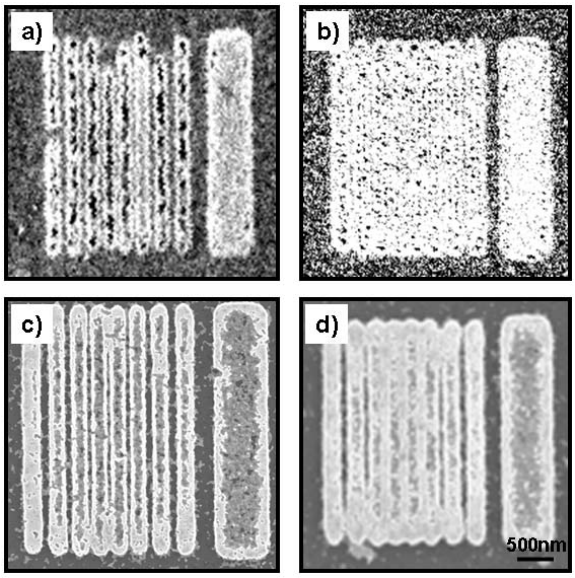

Figure 4.33: Variation of printing pressure for ODT
ODT printed onto a gold substrate using a Surlyn stamp with design Fig.B.4
a) SEM image of ODT on gold; contact between gold and stamp 200 kPa
b) SEM image of ODT on gold; contact between gold and stamp 400 kPa
c) and d) SEM images of a) and b) after etching of the gold

100 nm trenches were partially covered. This is reasonable since less molecules mean less diffusion.
The next parameter to change is the pressure used to bring stamp and substrate in contact. A pressure of 200 kPa resulted in a diffusion for trenches below 100 nm, while a pressure of 400 kPa resulted in diffusion for sub 200 nm trenches (Fig.4.33). This indicates, that less pressure is better suited to obtain perfect printing results. It is quite reasonable for PDMS not to apply any pressure at all, because the material is soft enough to completely adhere to a surface just by its own weight. For Affinity VP and Surlyn some pressure is necessary to remove the air bubbles that might be trapped between substrate and stamp. This is in agreement with [Trimbach et. al. 2003]. They also state, that a certain extra load is needed for harder stamp materials. The best results were obtained when the pressure was just high enough to remove trapped air bubbles (with optical control) and then release the pressure again. Because once in contact the stamp will stick to the substrate.

A closer look to the transferred molecules reveals, that they do not form sharp edges on the gold. They rather follow the shape of the gold grains (Fig.4.34). This is also an indication for diffusion.

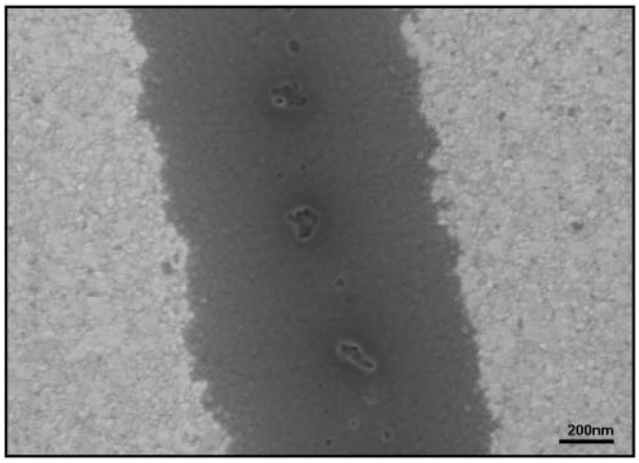

Figure 4.34: SEM image (2kV) of ODT on gold
ODT (bright contrast) printed onto a gold surface (dark contrast) with a PDMS stamp.

The printing of alkanethiols was also used to create chemical contrast on the gold substrates. Therefore a pattern of ODT was printed with either POP or Surlyn. Afterwards the gold chip was immersed into a solution of another thiol molecule, e.g benzenedithiol or mercapto-undecanoic acid (Fig.A.12). These SEM images reveal a nice patterning, but of course can not give any clue about the surface chemistry. Further investigations of these patterns are part of ongoing research.

Printing of Dendrimers

Dendrimers are organic macromolecules, that can be used as model systems of proteins. Here printing of dendrimers was demonstrated for as proof of concept for a specific application, namely the patterning of gold colloids onto a silicon substrate. Direct printing of a gold colloidal solution onto a silicon surface was not successful neither with *Wet* nor with *Contact Inking*. Therefore a different approach was taken, namely the printing of an adhesion promoter. Poly-amido-amid organo-silicon generation 4 dendrimer PAMAM-OS G4 was printed using *Contact Inking*. The organo-silicon groups allow an immobilization of the dendrimer on the silicon-oxide and the amino groups present in the dendrimer allow an immobilization of the colloids. After printing the substrate was immersed in the colloid solution for a few hours, rinsed and dried. The gold colloids were exclusively immobilized to the areas where the dendrimers were present (Fig.4.35). This result is in good agreement with [Li et. al. 2003]. They used the same approach with similar results.

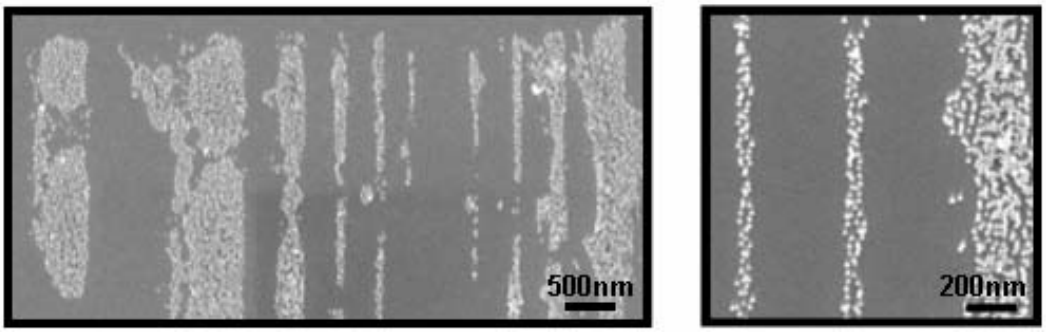

Figure 4.35: SEM images (10 kV) of gold colloids patterned onto a silicon surface PAMAM-OS G4 dendrimer was printed onto a silicon surface with a Surlyn stamp using *Wet Inking*. Afterwards 20 nm gold colloids were immobilized.

Printing of Proteins

Two protein functionalities of special interest for BE and ME, are binding/recognition and redox-activity. In addition proteins have a low mobility at surfaces, which allows a sub 100 nm patterning. Two types of proteins were investigated: cell adhesion proteins (albumin, poly-lysine, ECM gel, laminin) were studied as model molecules to introduce patterning to cell-culture. Therefore the conservation of binding/recognition as well as the patterning process of such proteins was investigated. Metalloproteins (cytochrome *c* and azurin) were investigated for their redox activity. This make them possible building blocks for future electronic devices. They served as a model system for a very fragile functionally. In addition the local addressing of their functionality was studied.

Since proteins are rather heavy printing was always successful by means of *Wet Inking* without diffusion to occur. Thus they were used to investigate sagging. Note, that for alkanethiol sagging is difficult to investigate since it is superimposed with diffusion. ECM gel was printed with a PDMS stamp onto a gold substrate. A load of 100 kPa was applied. Sagging could be observed for patterns i) (Fig.4.36), while for ii) no sagging was present. Note, that the small trenches were filled with protein. This was due to pairing present for such patterns of PDMS. Using equation 2.3 the left hand side is i) 0.15 and ii) 0.10. Thus the stamp pattern should be stable and no sagging should occur. Since sagging is observed, this equation is obviously not valid to describe this experiment. Actually the experimental proof of the equation was only given by means of larger and higher patterns [Sharp et. al. 2004]. [Decre et. al. 2005] report, that this equation overestimates the critical pressure.

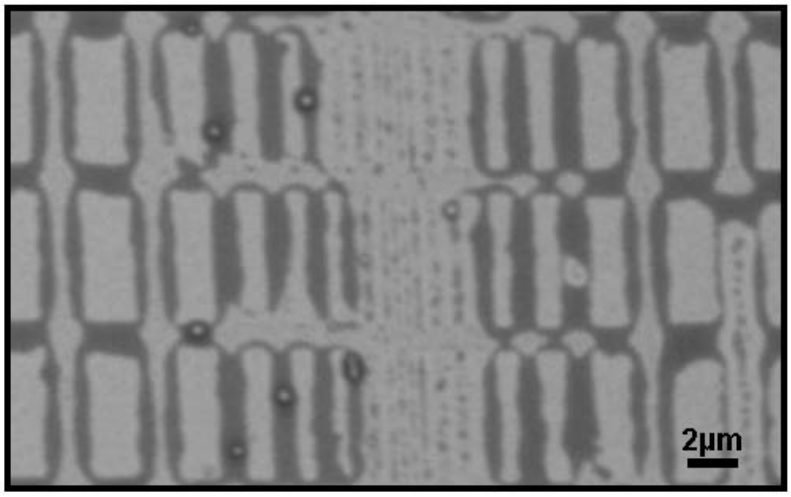

Figure 4.36: SEM image (2 kV) of ECM gel printed with *Wet Inking*
Extra cellular matrix gel (bright contrast) was printed onto a silicon substrate (dark contrast) with a PDMS stamp (design Fig.B.3). A typical sagging pattern can be seen.

	height	width	gap	Sagging†	left‡	right♮	expected♭
i)	440 nm	2 μm	1.5 μm	yes	0.2	1	no
ii)	440 nm	1.5 μm	1 μm	no	0.1	1	no

† sagging observed; ‡ left hand side of equation 2.3; ♮ right hand side of equation 2.3;
♭ sagging expected according to equation 2.3;

They present a numerical simulation describing their experimental data. But the dimensions they used were also rather large. [Bietsch et. al. 2000] present a calculation for sagging observed for PDMS stamps based on an equation describing deformation processes. They present a diagram for 450 nm height patterns with a widths of 500 nm, 1 μm and 2 μm, which is similar to the patterns used here. However, they indicate, that pressures necessary to obtain sagging are more than a factor of 5 higher than the pressure used here. This discrepancy between the predictions and the result presented here might be due to adhesion forces between stamp and substrate as discussed by [Huang et. al. 2005]. The authors state, that sagging is not only due to external load, but also due to adhesion forces. The influence of adhesion was not considered for equation 2.3 introduced by [Hui et. al. 2002]. However, since they used stamps having rather large dimensions adhesion forces might not play an important role. Since the dimensions used for the experiment presented here are much smaller, the impact of adhesion should be much larger. The equations presented by [Huang et. al. 2005] can not be applied here, since they only consider adhesion forces and do not consider an additional external load. Therefore a combination of both approaches would be needed to explain the results. For other stamp

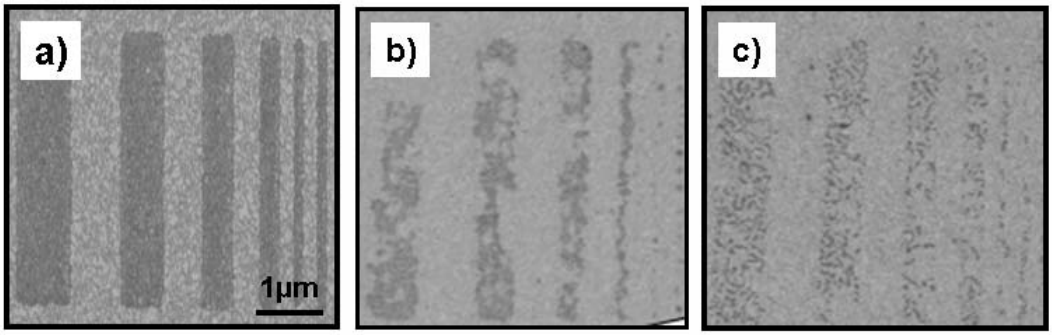

Figure 4.37: Printing of cytochrome *c* with different materials
Contact Inking was performed using
a) a Surlyn stamp with the design Fig.B.4 for 2 min
b) a Affinity VP stamp for 2 min
c) a Surlyn stamp for 5 s

materials used sagging was never observed (Fig.4.39). Affinity VP and Surlyn are stiff enough, that sagging did not occur for pattern dimensions used here. Note, that sagging also occurs for harder stamp materials, either if the gap between patterns becomes larger or a higher load is applied during printing. The later case will be discussed in Chapter 4.5.3.

The influence of sagging can be limited by *Contact Inking* as introduced by [Libioulle et. al. 1999]. So far it was only demonstrated for organic molecules. Here the influence of the *Contact Inking* process onto the functionality and pattern fidelity of proteins was investigated. Since the usage of PDMS is limited as discussed before, harder stamps materials, namely Affinity VP and Surlyn were used. Metalloproteins cytochrome *c* (cyt *c*) and azurin (Az) as well as cell adhesion protein laminin were used. The effect on their functionality was investigated. *Contact Inking* was performed similar to the procedure described for organic molecules. Cyt *c* was printed onto a MUA covered gold substrate. A pH 7 phosphate buffer was used, thus the protein as well as the MUA were charged. Cyt *c* was thus immobilized via electrostatic interaction. A PDMS ink-pad was immersed in the protein solution for at least 2 h. After drying of the ink-pad a stamp was brought into contact with it for 2 min. A printing time of 2 min using Surlyn stamps led to a good transfer of cyt *c* (Fig.4.37a), while for Affinity VP patterns are disrupted (see Fig.4.37b). This means, that cyt *c* needs a more hydrophilic stamp for a good transfer. Since most proteins have hydrophilic and hydrophobic domains it is not from the first clear, that type of stamp to use. A short transfer of only 5 s using Surlyn stamps led to an incomplete pattern (Fig.4.37c). This indicates, that the transfer of proteins from the stamp to the substrate takes longer than the

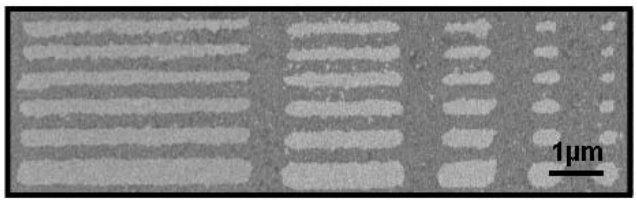

Figure 4.38: SEM image (2 kV) of cyt *c* printed with inverted patterns
Cyt *c* (dark contrast) was printed onto gold (bright contrast) using a Topas stamp with single cavity lines was used.

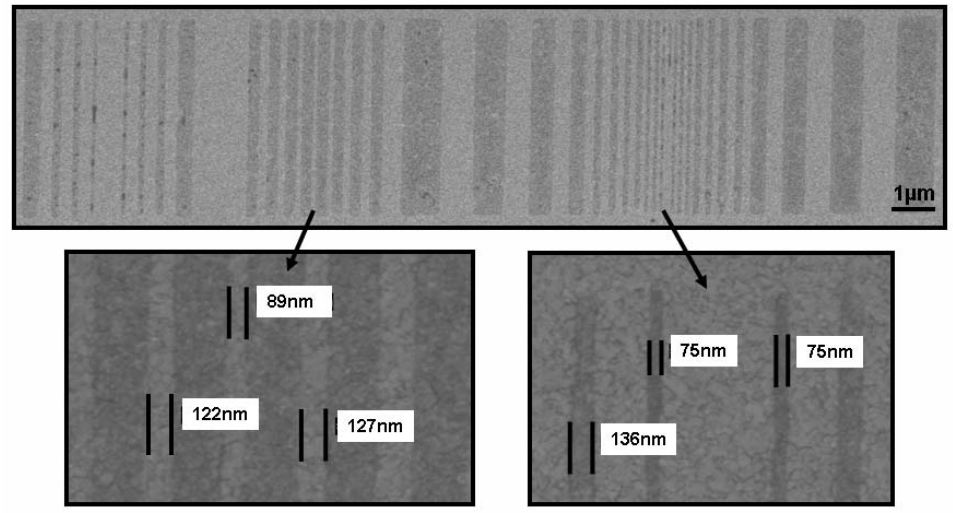

Figure 4.39: SEM images (2 kV) of Azurin on gold printed by *Wet Inking* using a Surlyn stamp

transfer of organic molecules. For alkanethiols printing times of as short as a few milliseconds were reported to be sufficient for the transfer [Helmuth et. al 2006]. Anyway the longer transfer times observed for proteins are reasonable, since their mass is much higher. No broadening of the line width could be observed. This is in agreement with [Bernard et. al. 1998]. Since the molecules are rather heavy diffusion is suppressed by many orders of magnitude. Therefore long transfer times (2 min) are best. The limited diffusion makes it possible to print large areas of molecules and just leaving out single lines uncovered. An inverted stamp design was used to print such patterns (Fig.4.38).

Pattern fidelity of proteins was further investigated via *Wet Inking* of azurin molecules. Azurin is a water soluble blue-copper protein with hydrophilic domains.

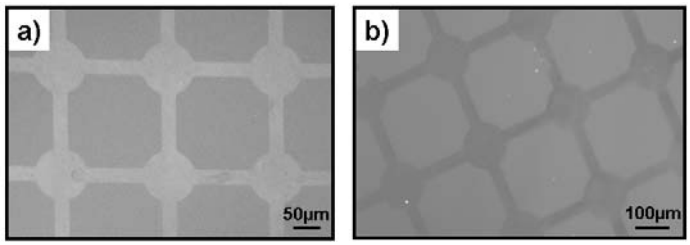

Figure 4.40: Protein transfer of micrometer patterns
Images of cyt *c* printed with *Wet Inking* using a Surlyn stamp with a design with umpty micron patterns onto gold.
a) SEM (2 kV)
b) optical microscope image taken in *Differential Interference Contrast* mode.

At a buffer pH of 4.6 azurin is not charged, since it is at its isoelectric point. Azurin was printed onto a bare siliconoxide substrate. Printing with Surlyn stamps worked best. This is expected, since hydrophilic molecules should more likely to be transferred with stamp materials of similar hydrophobicity. SEM images indicate, that the protein patterns are slightly smaller than expected (Fig.4.39). This is most probably caused by the fact, that the patterns on the Surlyn stamps have a rounded contour (Fig.4.23). Therefore the contact area of patterns to the surface is smaller. In addition it can be seen, that the 75 nm line of the **Variable Width** part is missing. This might be due to the fact, that this line is not of the same height like its neighboring lines (Fig.4.24). Obviously a pressure applied to the stamp of around 100 kPa using a finger is not sufficient to achieve a complete conformal contact. Therefore a novel printing technique was introduced. It will be described in Chapter 4.5.3.

Large patterns of cyt *c* were printed to investigate their homogeneity (Fig.4.40). 75 μm broad line patterns were transferred completely homogeneously. No dewetting effects were present. Dewetting is especially for larger patterns a problem. It happens if the hydrophobicity of the stamp material and ink molecule are too different. In case of cyt *c* Surlyn seems to be the perfect choice. Note, that typically proteins have hydrophilic and hydrophobic parts. Thus it is not always clear what type of stamp material to choose. For different molecules, stamp materials having different properties, namely contact angle, might be needed. An example of dewetting of the protein is given by [Reska 2005]. She showed, that the printing of concanavalin A printed with PDMS stamp resulted in a protein transfer mainly at the edges of the pattern. This is comparable to the edge transfer printing of ODT observed with Surlyn stamps as discussed before.

Furthermore AFM images were taken and compared with SEM images. Cyt

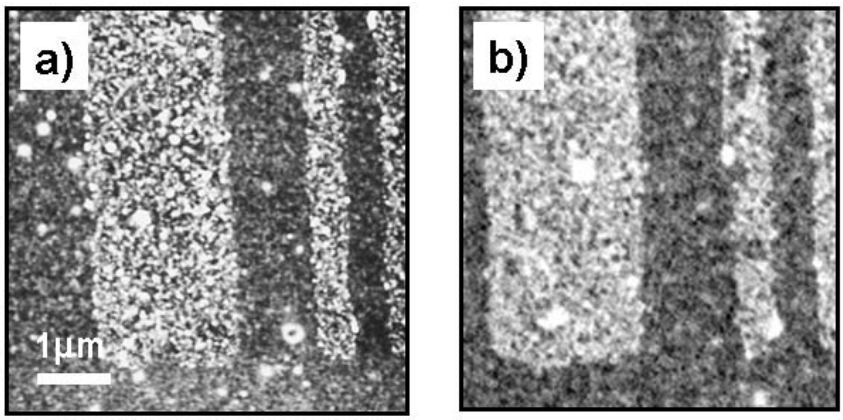

Figure 4.41: Comparison of AFM and SEM images of printed cyt *c*
a 12 μM cyt *c* solution in a 0.1 mM buffer was printed onto MUA covered gold with a Surlyn stamp using *Contact Inking* and 2 min printing time a) tapping mode AFM image, z-scale (white contrast) 10 nm
b) SEM image at 2kV (image contrast was inverted)

c was printed at low buffer concentrations. Images of equally prepared samples reveal, that equivalent information can be obtained (Fig.4.41). Obviously acceleration voltages of 2 kV allow takeing SEM images with good fidelity. Both images indicate the same kinds of defects, e.g. bright spots. These spots might be protein aggregates or salt crystals. These and other defects are discussed by [LaGraff et. al. 2006]. All kinds of defects discussed by the authors could be also found on the samples prepared in this thesis.

For further investigations the concentration of the phosphate buffer used for preparing the cyt *c* solution was changed. A strong dependence of the transfer results on the buffer concentration of was found. A transfer of a densely packed monolayer as indicated by AFM images was found for a weak buffer solution (Fig.4.42a). For higher buffer concentrations the proteins tend to agglomerate. This led to more disrupted patterns (Fig.4.42b). At pH 7, which was used for the buffer solution, cyt *c* is charged. A low buffer concentration means less screening of charges, thus the protein molecules are subject to electrostatic repulsion. In addition the electrostatic attraction to the charged MUA SAM was only slightly screened. A high buffer concentration means a stronger screening of charges. Thus the repulsion between protein molecules is stronger and the attraction to the MUA SAM is weaker. This leads to agglomerations. These results were further confirmed by means of surface plasmon resonance and other methods [Salomon 2006]. In these experiments proteins were immobilized from solution. Since the same effect (agglomeration) was observed after *Contact Inking* and solution assembling, the proteins must have

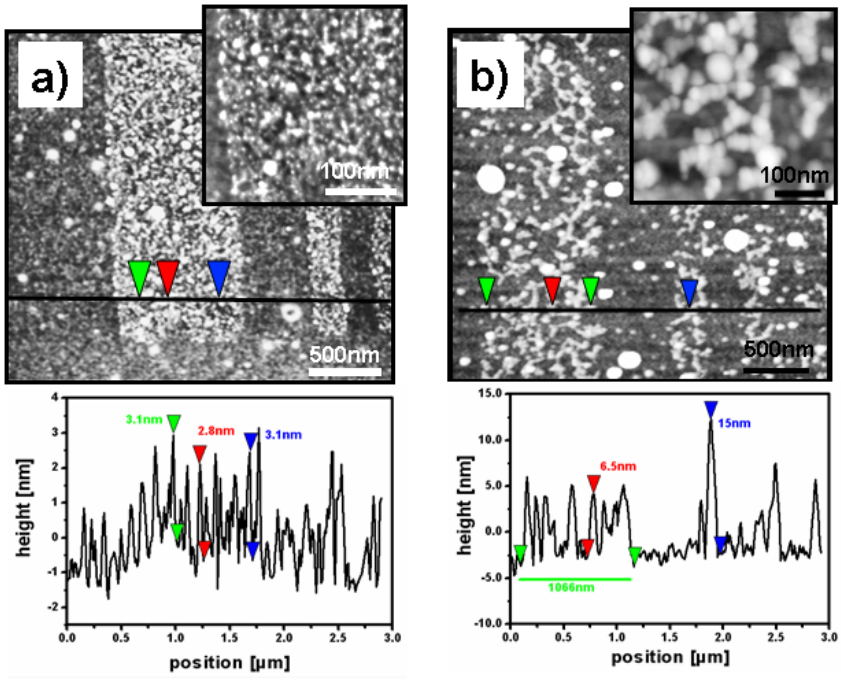

Figure 4.42: AFM images of printed cyt *c* with different buffer concentrations
a 12 μM cyt *c* solution was printed onto MUA covered gold with a Surlyn stamp using standard contact inking and 2 min printing time; imaging was done with tapping mode AFM
a) cyt *c* buffer concentration 0.1 mM; z-scale (white contrast) 10 nm
b) cyt *c* buffer concentration 30 mM; z-scale (white contrast) 30 nm

assembled on the ink-pad the same way they do on any other surface. This indicates, that the forces involved leading to the formation of agglomerations are the same on stamps, ink-pads or the substrate. Furthermore, these agglomerations once dried must have been transferred in the same way uniform layers of proteins do. Note, it is not clear from the first, that drying proteins on an ink-pad, transferring them to a stamp and successively transferring them to a substrate leads to the same observation than immobilizing them from solution to a substrate and subsequently drying them. This observation further proves, that there is no qualitative difference between *Contact* and *Wet Inking* although one more step and one more surface are involved. Fig.4.42, cyt *c* printed at low buffer concentrations, further indicates a height of approximately 3 nm, which is approximately the size of a native molecule. This indicates, that even though *Contact Inking* consist of several steps (drying the protein to the ink-pad, transferring it to the stamp, transferring to the substrate) the protein does not totally denature. Further investigations of the redox activity by means of cylic voltammetry will be discussed in the next section.

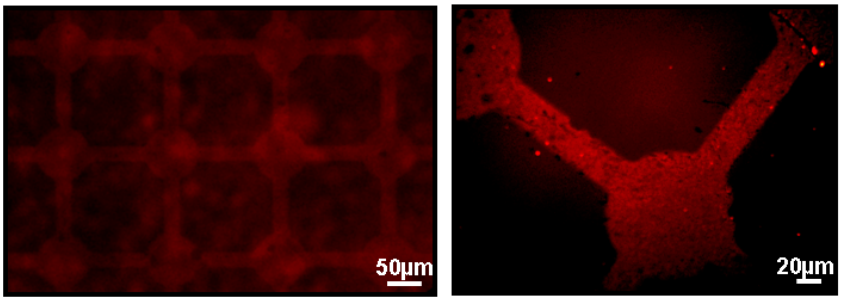

Figure 4.43: Fluorescence Microscope images of laminin
Laminin was printed with a Surlyn stamp onto glass using *Contact Inking*. Subsequently an antibody was immobilized and stained.

The redox activity of cyt *c* and azurin is a rather fragile functionality. In order to check a more robust functionality the recognition of antibodies was investigated by means of antibody-staining[15]. This functionality is of major importance for a huge variety of biological process and applications, e.g. cell adhesion. A staining protocol according to [Vogt 2003] was used. Mouse laminin in PBS buffer solution was printed via *Contact Inking* onto a glass coverslip. Afterwards the sample was immersed in a BSA solution to avoid unspecific binding. BSA thus covered all parts of the substrate, which were not covered by laminin. Then the sample was rinsed with PBS and immersed into an anti-mouse laminin antibody solution. The antibody specifically only binds to the laminin, where the counterpart is still present. Excess unbound antibodies were rinsed away with PBS. Afterwards a CY3 labeled goat-anti-rat secondary antibody was immobilized. It specifically binds to the first antibody. Since it carries a fluorescence marker, it thus stains the bound primary antibodies. Fluorescence was imaged with a fluorescence microscope using a *Rhodamin-filter*[16]. The printed pattern was clearly visible (Fig.4.43). This indicates, that the part of the laminin, responsible for the recognition of the antibody, was still present and functional after printing. This does not tell whether other parts of the protein suffered conformation changes or not. Note, that it is sufficient for most applications to have the recognition capability. Thus *Contact Inking* can be used for the transfer of proteins conserving their binding functionality. The conservation of such functionalities was also reported by [Bernard et. al. 1998]. They proved the functionality after *Wet Inking*. For most recognition capabilities they found 100 % functionality after printing. For the more fragile cyt *c* they reported a 100 % monolayer transfer by means of ellipsometry. In this context ellipsometry measures the height like AFM does. It has to be mentioned, that the height information is not a proof for the functionality. More than that, the denaturing depends on the kind of protein, and the surface properties of the stamp and inkpad used.

[15] More details about antibodies and the staining process can be found in [Harlow et. al. 1988].
[16] 545 nm excitation / 570 nm beam splitter, 605 nm emission

[Biasco et. al. 2005] report a reduction of the size of azurin printed onto gold using *Wet Inking*. The functionality of cyt *c* during μCP will be further discussed in the next section.

4.5.2 In-Situ Microcontact Printing

In conventional μCP the proteins are dried on stamp prior to the transfer. Proteins are macromolecules with 3D structure which strongly depends on physiological conditions like dampness, pH, salinity and temperature. Drying of proteins means changing their conformation and thus their functionality. More than that, drying is not reproducible. All publications dealing with the printing of proteins (or molecules in general) speak of "drying". But nobody exactly specifies what drying is. Drying could for example mean to use a pressure of 300 kPa to blow away any droplets in a few seconds. But it could also mean to use nitrogen at rather low pressures (below 100 kPa) to dry the solution for several minutes until no more solvent is left. Note, that these two extreme examples are qualitatively different. If the droplets on the stamp are blown away rapidly, only the molecules that are physisorbed on the stamp will stay. If the droplets on the stamp are dried without blowing them away, the coverage with molecules will be much higher. In addition the amount of surface water strongly depends on the drying procedure and duration. The amount of water on the other hand influences the conformation/functionality of the proteins, since most proteins need physiological conditions to keep their functionality. Of course the transfer strongly depends on the amount and state of the molecules on the stamp. In order to have a defined process to transfer proteins under full conservation of their functionality the drying of stamp was abolished.

Cytochrome *c* was chosen as a model molecule for this study since it has a pronounced functionality, namely its redox activity. The redox activity strongly depends on the conformation, miss-orientation and denaturation of the protein. The conformation of cyt *c* itself strongly depends on the humidity, pH and other factors. Redox activity is easily accessible by cycling voltammetry and thus easy to evaluate.[17]

Several groups report about the conservation of functionality of cyt *c* e.g. [Bernard et. al. 1998] or [Runge et. al. 2003]. Last named authors report, that the functionality of cyt *c* is lost using a hydrophobic stamp for the transfer onto indium tin oxide (ITO) substrates, whereas the activity is maintained using a hydrophilic stamp. The question about the real dryness of stamp and the fact, that the cyt *c*/ITO system is a very specific case make this study un-comparable to the results pre-

[17] the charge transfer of cyt *c* was further studied by [Salomon 2006]

sented here. The direct immobilization of cyt *c* onto ITO is very different to the immobilization onto gold via a alkanethiol layer. Conservation of protein functionality as reported by [Bernard et. al. 1998] is also difficult to compare. For cyt *c* they give ellipsometry measurements as a proof. But this does not tell anything about the redox activity. Other proteins having specific binding sites were also reported to fully conserve this functionality. These binding functionalities might be less fragile than e.g. a redox activity.

In the following different containers with ink solution or plain buffer solution were provided such, that all printing steps were performed in solution. The transfer times of the stamp from one container to the other was kept that short (few seconds), that the stamp conserved its dampness. Four possible process paths are proposed as alternatives to *Wet* or *Contact Inking* (Fig.4.44). For printing of cyt *c* a modification of Contact Inking provided the best results, but for over systems one or the other paths might give better results (Fig.4.44a). Here only method a) will be described in more details: Affinity VP or Surlyn stamps were prepared as described in Chapter 4.4. A PDMS ink-pad was immersed into the protein solution. After 2 h the stamp was gently pressed onto the ink-pad for 2 min in the vessel. Immediately after separating the stamp and the ink-pad, the stamp was transferred without drying into a beaker with buffer solution, containing the target substrate. The transfer time from one solution to the other was less than 5 s. The dampness of the surface film on the stamp was maintained during this time. The stamp was pressed onto the substrate for 2 min in order to transfer the proteins from the stamp to the modified gold surface. Finally, the substrate was put into a beaker containing fresh buffer solution in order to prevent unfolding and undesired adsorption of contaminations like dissolved molecules. The conservation of the proteins activity was proven by measuring the redox activity of the proteins after the transfer with cyclic voltammetry.

For the electrochemical characterizations[18] the proteins were printed onto an Au(111) single crystal which was subsequently used as a working electrode. Prior to printing the gold was covered with a mercapto-undecanoic acid SAM. This allows an electrostatic immobilization of cyt *c* via its lysine group. Thus the position of the redox center with respect to the gold surface is fixed. Measurements were performed by employing a PAR Model 283 potentiostat. The cyclic voltammograms were recorded in the hanging meniscus configuration. In this method the particular metal plane of the single crystal is brought into contact with the electrolyte by forming a meniscus. The advantage of this method is that just one face of the crystal is in contact with the electrolyte and contributes to the electrochemical response. A standard calomel electrode (SCE) and a platinum coil were used as reference and

[18] for a further description see [Salomon 2006]

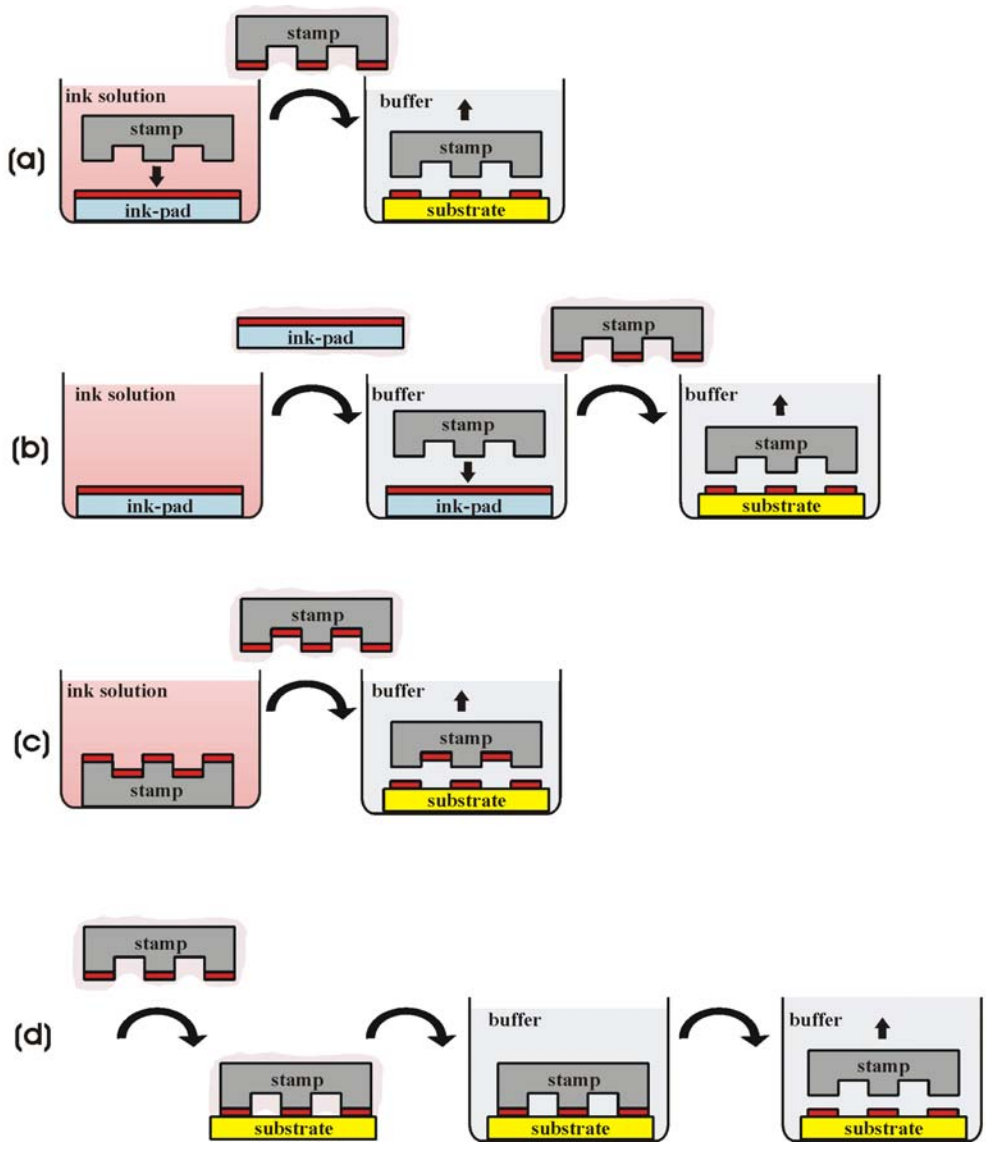

Figure 4.44: Possible schemes for *In-Situ Microcontact Printing*
a) and b) are modifications of *Contact Inking*
c) is a modifications of *Wet Inking*
d) after bringing the molecules on the stamp a),b) or c) stamp and substrate could be brought into contact before putting them into a buffer solution

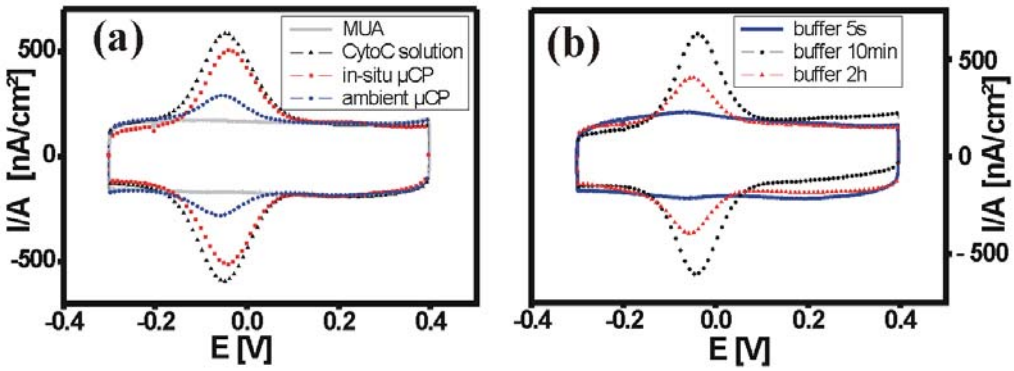

Figure 4.45: Voltammograms of in-situ printed cyt *c*
a) comparison between a bare surface (MUA), cyt *c* adsorbed of solution, in-situ printed cyt *c* and ambient printed cyt *c*
b) comparison of different retention times of the stamp in the buffer solution

counter electrode, respectively. The setup was placed in a Faraday cage in order to reduce electronic noise. The cyclic voltammograms apparent in Fig.4.45a) show the redox response of the modified gold surface for different processes. For a bare MUA/gold surface only the capacitive charging of the double layer could be observed. Adsorption of cyt *c* from either solution or μCP (in-situ and ambient) gave clear reversible redox peaks occurring at a formal redox potential of E_0 = -60 mV (SCE), which is in good agreement with previously reported literature results. The symmetrical peak shape and the uniform capacitive charging indicate the immobilization of the cyt *c* to the surface. The amount of protein adsorbed from solution was estimated[19] to be $1.2 \cdot 10^{-11}\, mol\, cm^{-2}$, which corresponds to a surface coverage of 88 %. For in-situ μCP the obtained current at the redox potential corresponds to a surface coverage with active proteins of 73 %. In contrast the peak of the CV after conventional μCP using *Wet Inking* is strongly reduced. The coverage with functional cyt *c* molecules is significantly lower (20 %) than after the in-situ printing process. This suggests, that through the drying process a fraction of the proteins experience irreversible conformational changes, which lead to a loss of the proper orientation and/or conformation of the protein/surface adsorbate complex. Note, although *Wet Inking* is used the functionality was lost. For Contact Inking of laminin the binding functionality was fully observed. This indicates, that the redox activity is more fragile than ability to binding antibodies. This is expected since the redox centers are rather complex and small distortions of geometry strongly influence the

[19] Assumptions: the diameter of a cyt *c* molecule is 3.5 nm; it has the shape of a cube, thus the area per protein is $(3.5\, nm)^2$; the charge per molecule is one elementary charge; this results in $1.3\, \mu C/cm^2$ surface charge. The diameter of the crystal used was 3.7 mm

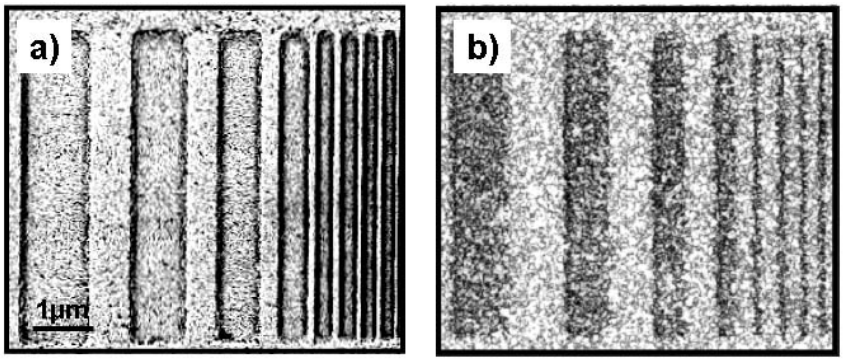

Figure 4.46: SEM image of in-situ printed cyt *c*
a) SEM image (10 kV) of a POP stamp (the stamp was covered with a sputtered gold film for imaging)
b) SEM image (2 kV) of cyt *c* (dark contrast) printed onto a MUA covered gold surface

process.
The retention time between inserting the inked stamp into the buffer solution containing the substrate and bringing it into conformal contact with the substrate has a large impact (Fig.4.45b). These results show, that the current at the formal redox potential decreases as the delay time increases, indicting, that the surface coverage with functional proteins decreases. This can be explained with the diffusion of the weakly absorbed proteins from the surface of the stamp. The tremendous concentration gradient of the pure buffer solution drives desorption of the water-soluble protein.

Furthermore *in-situ µCP* was tested for its structuring capabilities by imaging transferred protein patterns by means of SEM. For this purpose a structured Affinity VP stamp was used to print cyt *c* onto a polycrystalline gold substrate. The transferred pattern shows nicely resolved 150 nm broad lines with 150 nm gaps in between (Fig.4.46b). The transferred pattern corresponds well to the original stamp structure. Since there were no smaller stamp patterns, this result indicates, that the lateral resolution is mainly limited by the dimensions of the stamp pattern rather than by the technique itself. The transferred lines appear to be exact copies of the lines of the stamp. The broadening of the line width in Fig.4.46a) is most probably a result of the sputtered Au layer, which is needed for imaging of non-conductive samples with a SEM.

This patterns were also used for a *Scanning Ellipsometry* analysis. An image was taken under nulling conditions (Fig.4.47). Then the thickness was measured

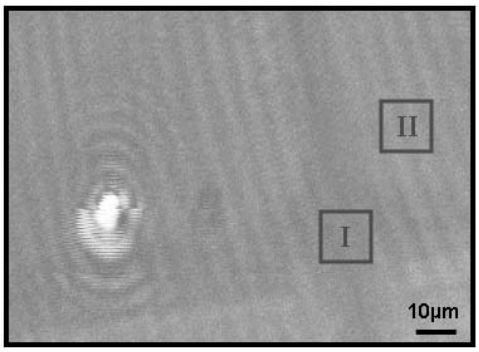

Figure 4.47: Ellipsometer image of *in-situ* printed pattern
I and II correspond to the areas which were used for the determination of the thickness

on top of a protein line and beside it. The absolute value of the thickness could not be determined due to a uncertainty about the exact value of the underlying gold film. 50 nm gold on silicon were taken as model for the substrate. To account for the uncertainty the difference between the measurements at the two different spots was used. The difference was found to be approximately 2 nm. Since the cyt *c* is around 3 nm in size, this indicates a monolayer coverage of 2/3.

The transfer of cyt *c* to a MUA modified Au surface is possible while retaining the redox response of the cyt *c*. The observed redox response is influenced by the retention time between the immersion of the inked stamp into the buffer and stamping the proteins onto the substrate. The conservation of the redox activity could by achieved by maintaining physiological conditions during all process steps. Although for some proteins the functionality is conserved by conventional printing techniques, it is not for molecules with more fragile functionalities. *In-situ μCP* should be applicable for such proteins. There is not indication, that this technique is limited to the system of cyt *c* printed onto MUA/gold. The critical dimensions of achieved transferred patterns were 150 nm. The lateral resolution seems to be mainly limited by the dimensions of the stamp´s pattern rather than by the technique itself, because the patterns on the stamp used were of the same dimensions. In general the in-situ μCP is expected to be applicable to other proteins and fragile bio-molecules, which require physiological conditions.

4.5.3 Air-Cushion Microcontact Printing

Almost all results reported in μCP were obtained using stamps made of poly-dimethylsiloxane (PDMS), although as previously discussed the usage for pattern-

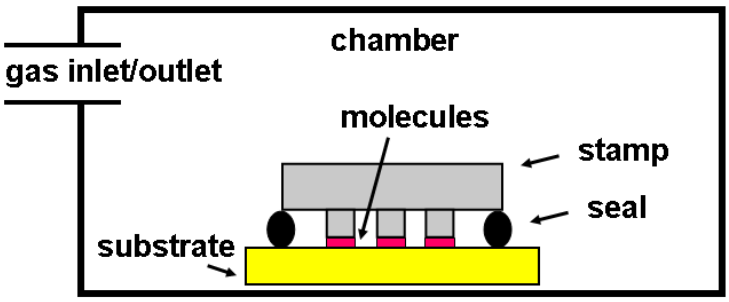

Figure 4.48: Scheme of the *Air-Cushion µCP* process

ing with dimensions below 200 nm is very limited due to its rather low Young´s modulus. Even the harder h-PDMS is not capable of reproducing arbitrary sub 100 nm patterns as shown before. [Csucs et. al 2003] and [Trimbach et. al. 2003] introduced thermoplastic materials such as Affinity VP as stamp materials for μCP. It could be shown, that they are suited for the printing of proteins and alkanethiol, and that sagging is limited. As previously discussed for the design shown in Fig.B.4 Affinity VP was found not to be stiff enough. Therefore stamp materials with much higher Young´s modulus were tested, namely Surlyn, Topas, Zeonor, Zeonex and Plexiglas (see Chapter 4.4). As discussed by [Trimbach et. al. 2003] the printing process for thermoplastic materials is slightly different compared with that of PDMS. While PDMS adheres to a surface by its own weight for the materials used by Trimbach et. al. an additional load of 10 kPa was necessary to obtain a conformal contact. This is in agreement with the experiments described here. For Affinity VP an extra load of 10 - 50 kPa was needed, while for the much stiffer Surlyn at least a pressure of 100 kPa was needed. Fig.4.39 shows, that although a conformal contact was established not all lines were transferred. The 75 nm lines in that experiment were not transferred. This is due to a problem with the stamp as indicated in Fig.4.24, namely the small lines are not of the same height as the larger lines. To obtain a better transfer a higher extra load is needed in order to deform the stamp. For other stamp materials, which are even stiffer than Affinity VP or Surlyn, a conformal contact could not be achieved using loads up to 200 kPa. Higher loads were needed to obtain a transfer. Since it is difficult to apply pressures of 0.1 - 5 MPa[20] in a uniform fashion a new process was needed.

A technique, which is used in NIL to apply pressure up to 4.5 MPa in uniform way, is the *Air Cushion Press* (ACP) technique as described by [Chou 2002] and [Tan et. al. 2004]. The basic idea behind this process is applying a load onto the

[20] This is equal to placing 1 - 50 kg weight onto a 1cm^2 area

substrate/mask using a fluid pressure (Fig.4.48). The advantage of fluid pressure is, that it is absolutely uniform and easy applicable. In order to obtain a difference pressure the volume between mask and substrate has to be sealed. In case of the commercially available NX-2000 tool, which was used for the experiments, sealing is done by placing substrate and mask between two silicone foils. Afterwards the assembly is placed into a chamber, where a pressure is applied. Pressures can range between 0 - 4.3 MPa. This system could demonstrate homogeneous imprint pressures on four inch wafers using hard molds [Tan et. al. 2004]. With soft PDMS molds uniform 1.6 μm patterns on a whole 12 inch wafer were demonstrated using thermal NIL [Chang et. al 2005].

All experiments were performed in the following way. The inked stamp was placed onto the substrate. The substrate lay on a first silicone foil. A second silicone foil fixed on a tenter was placed on top of the stamp. It was supported by springs, such that the two foils did not touch each other. This assembly was put into the chamber of the NX-2000. After evacuating the chamber for 10 s the two foils were pressed together and thus sealed substrate and stamp. This sealing is necessary since a force only occurs if there is a difference in absolute pressures. The sealing fixes the pressure in the stamp/substrate assembly. A higher pressure outside the seal thus leads to a force. For evacuation times shorter than 10 s the sealing was not perfect and thus the method did not work. Small cavities in the sealing allow the applied pressure to enter the stamp/substrate assembly. Thus the pressure inside and outside was equal and no force occurred. For evacuation times longer than 20 s the transfer was bad. This can be explained, because the vacuum led to an evaporation of surface water, which was left on the stamp. After it is completely evaporated the molecules might be too dry to be transferred. After this sealing step a pressure profile was applied. As a first step the pressure inside the chamber was raised to 200 kPa for 10 s, then it was increased up to the final pressure for 1 min. Afterwards the chamber was vented and substrate and stamp were separated.

In a first experiment Surlyn stamps were used to print cyt *c* onto gold substrates. At an final pressure of 1.0 MPa patterns smaller 150 nm were missing (Fig.4.49a). This is in agreement with the results obtained by applying the pressure with a finger. Using a final pressure of 1.8 MPa the 75 nm line in the **Variable Width** pattern is transferred, while the 75 nm lines in the **Variable Both** pattern are still missing (Fig.4.49b). A pressure of 2.5 MPa was needed to transfer all lines in a precise way (Fig.4.49c). A closer look reveals, that all patterns have the desired dimensions (Fig.A.15). Obviously the pressure resulted in a deformation of the stamp such, that the smaller lines were pressed in direction to the substrate until they also made a contact. This result is very homogeneously distributed over the

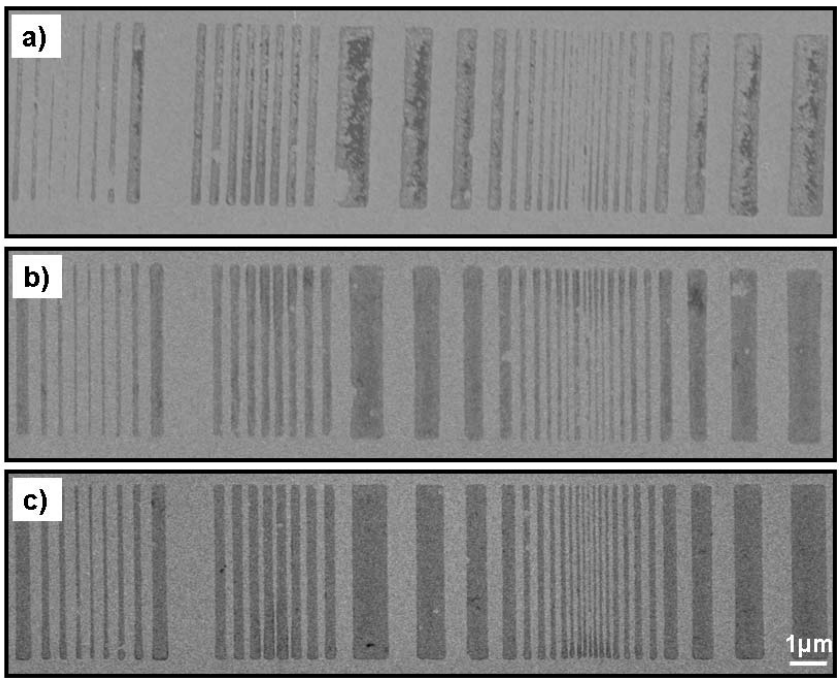

Figure 4.49: SEM images (2 kV) of cyt *c* printed with Surlyn with the *Air-Cushion µCP* process
a) Cyt *c* printed with a Surlyn stamp using an final pressure of 1.0 MPa
b) Cyt *c* printed with a Surlyn stamp using an final pressure of 1.8 MPa
c) Cyt *c* printed with a Surlyn stamp using an final pressure of 2.5 MPa

whole patterned area (Fig.A.17). Within the 800 μm by 800 μm are that is patterned, only a few defects were present. At all parts the transferred pattern is completely transferred.

Air-Cushion µCP is not limited to cyt *c*. An experiment performed with the same parameters to print ODT also revealed a nice transfer (FigA.16). The transfer is comparable to that achieved with conventional printing. Since Surlyn was used also an edge transfer was observed.

Fig.4.50 shows the influence of a dust grain on the transferred pattern. The stamp was nicely pressed into a close contact around this defect. That is why this grain only resulted in a small area of non-contact, rather than a large wedge-shape area of non-contact as discussed before.

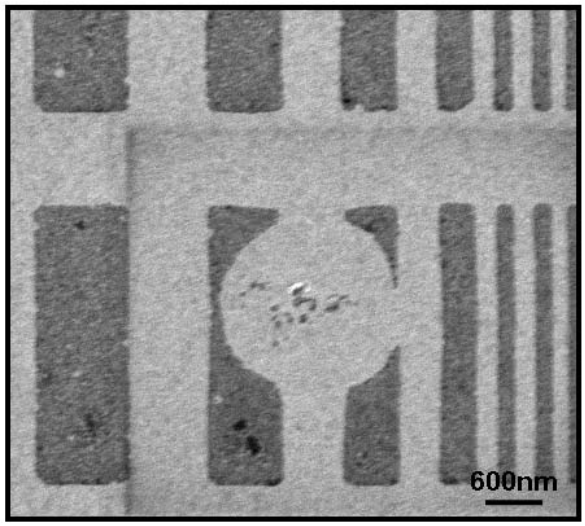

Figure 4.50: SEM image (2 kV) of a defect observed during an *Air-Cushion µCP* process
Cyt *c* was printed with a Surlyn stamp at 2.5 MPa onto gold.

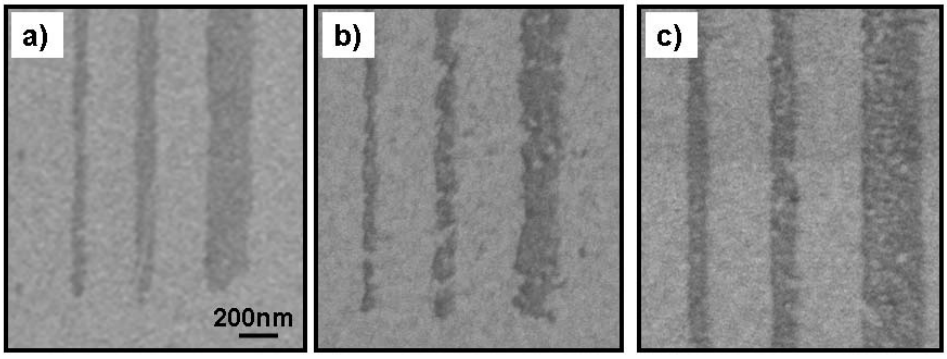

Figure 4.51: SEM images (2 kV) of cyt *c* printed with different stamp materials
Cyt *c* was printed with a 4.3 MPa *Air-Cushion µCP* process using a:
a) Topas 8007 stamp
b) Plexiglas 99530 stamp
c) Zeonex 48R stamp

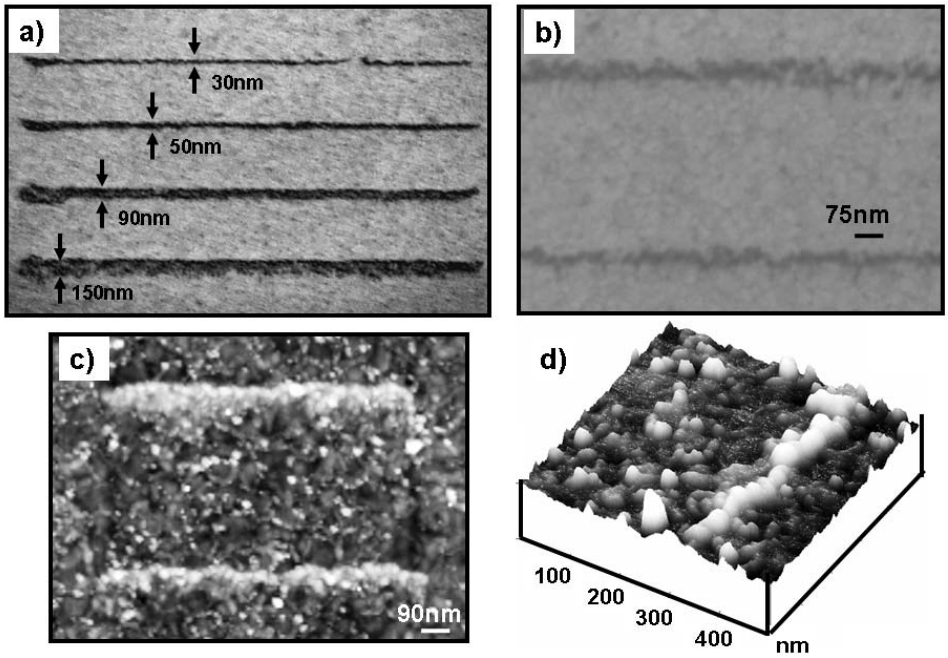

Figure 4.52: SEM (2 kV) and AFM images of sub 50 nm patterns printed with *Air-Cushion µCP*
a) SEM image (2 kV) of cyt *c* printed with a Topas stamp having the design of Fig.B.5 at 3.9 MPa.
b) SEM image (2 kV), closer view on a)
c) Tapping mode AFM image of b); data scale is 30 nm (white contrast)
d) Tapping mode AFM image surface plot; data scale is 17 nm (white contrast)

By applying a final pressure of 4.3 MPa it was possible to achieve a protein transfer with Topas, Zeonex and Plexiglas as stamp materials (Fig.4.51). This process was not optimized and just taken as a proof of concept. Obviously there is no limitation of μCP to certain stamp materials, as long as conformal contact can be achieved. The reason, that printing with this materials using a finger to apply pressure did not work, because the applied pressure were to small. SEM images of the cyt *c* transfer looks similar to the transfer, that was achieved with Surlyn. An additional benefit of the ACP process is, that substrate and stamp are held in place with respect to each other through the silicone foils. Thus a displacement or sliding until the conformal contact is established is not possible. Sliding is the major problem using e.g. Topas in conventional μCP processes. This made it impossible to apply higher pressure and thus to obtain a conformal contact.

Using Topas stamps carrying the design shown in Fig.B.5 and applying a final

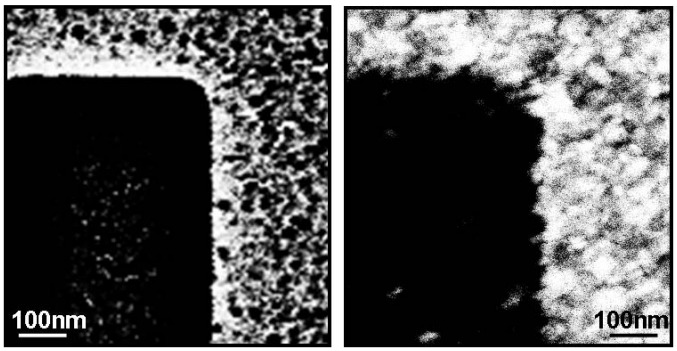

Figure 4.53: SEM images (2 kV) of a Topas stamp and cyt *c* printed with Topas
a) 400 nm line of a Topas stamp
b) cyt *c* printed with the stamp of a) at 3.9 MPa.

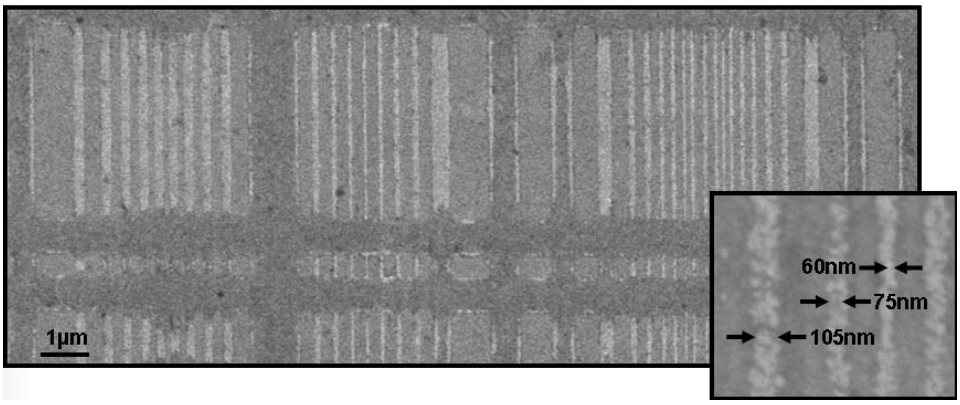

Figure 4.54: SEM images (2 kV) of sagging observed at 4.5 MPa
Cyt *c* was printed with a 0.4 mm thick Surlyn stamp at 4.5 MPa.

pressure of 3.9 MPa sub 30 nm patterns could be obtained printing cyt *c* (Fig.4.52). These lines are with the smallest patterns ever created by μCP. Evidently the edge roughness of these lines is rather larger. A closer look to the Fig.4.52b) indicates, that the protein pattern follows the gold domains[21]. This becomes clearer by looking at the stamp (Fig.4.53a) and at larger protein patterns (Fig.4.53b). It can be seen, that the stamps line edge roughness is much smaller. Apparently larger protein patterns show the same roughness than the 25 nm line. This indicates, that the roughness is a general problem and not a problem due to the resolution of the technique.

[21] Evaporated gold forms a polycrystalline layer.

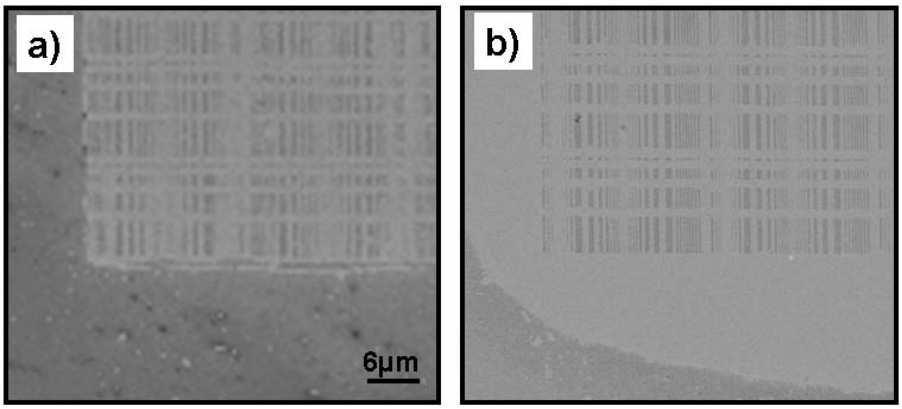

Figure 4.55: SEM images (2 kV) of a sagging observed during *Air-Cushion µCP process*
a) Cyt *c* was printed with a 0.4 mm thick Surlyn stamp at 1.8 MPa.
b) Cyt *c* was printed with a 0.7 mm thick Surlyn stamp at 3.6 MPa.

Since this technique allows to apply rather high pressures the impact of pressure and Young´s modulus can be observed through investigating of sagging. As indicated by equation 2.3 there is a critical pressure for sagging to occur. In case of a 0.4 mm thick Surlyn stamp at 4.3 MPa sagging is present down to 600 nm lines (Fig.4.54). Thus 60 nm patterns were formed. This is comparable to the procedure introduced by [Guo et. al. 2004]. They used an over pressure to obtain sagging and used it to fabricate small patterns out of stamps having large patterns. But they applied the pressure by adding weights. Comparing the observed sagging with equation 2.3 again proofs, that the equation is not adequate. For Surlyn (Young´s modulus = 180 MPa) with height = 125 nm and a pressure of 4.3 MPa the sagging should only occur for gaps larger 12 μm. Another possible approach is based on considering the equation for the flexure modulus[22]:

$$E_F = \frac{F_\perp \cdot l^3}{4 \cdot w \cdot t^3 \cdot y} \tag{4.2}$$

This equation is accounts for a three point measurement. A sample of width w and thickness t is laying on two support points separated by a length l. A force $F_\perp$ is applied perpendicular to the surface in the middle of the sample. The deflection obtained is y. In principle the height difference between the small lines (75 nm) and the larger lines could be taken as the deflection necessary to obtain nice transfer results. But this aspect could not be harmonized with equation 4.2. For sagging the deflection should be equal to the height of patterns. But also here a harmonization with the equation could not be found. The thickness of the sample

[22] which is almost equal to the Young´s modulus

has a major influence (to the power of three) on the force needed to obtain a certain deflection. However, for stamps it is not clear, whether the whole thickness of a stamp has to be taken into account. An equation describing the observed sagging for the thermoplastic materials could not be established. Further indications for sagging were found on the edges of the pattern. Since only a small square in the middle of the stamp carries the pattern, the rest of the stamp is not supported while printing. Therefore a homogeneous transfer of molecules around the pattern due to sagging should be obtained. The distance between the edge of the pattern and this homogeneous region is a measure for sagging. For i) a 0.4 mm Surlyn stamp used at 1.8 MPa immediately beside the pattern the stamp is sagged to the surface, while for ii) a 0.7 mm thick Surlyn stamp at 3.6 MPa a region of 15 - 20 μm separates them (Fig.4.55). Using equation 4.2 to calculate the ratio of the deflection of i) vs. ii) the result indicates, that the deflection of i) is 2.7 times larger than the deflection of ii) assuming, that all parameters are equal. This is in agreement with the images, since i) shows more sagging than ii).

The adaption of the ACP technique for μCP proofs to be valuable. The homogeneous applied pressure leads to homogenous printing results. Height deviations of stamp patterns can be compensated. Very stiff polymers with a Young´s modulus larger than 2 GPa could firstly be used as stamp materials. Protein as well as alkanethiols could be transferred. Sub 30 nm protein patterns could be obtained.

4.5.4 Printing of Metals using Shuttle-Transfer Printing

The printing of metal patterns is of major importance for the fabrication of *Molecular Electronic* devices based on molecules. Since many molecules, especially proteins, are fragile or do not form layers free of defects the evaporation of metal electrodes onto such layer is a problem. Direct filaments can form in defects and short the junction or molecules could be destroyed or denatured do to the vacuum needed for the evaporation. In addition evaporated metal molecules have a high energy and thus may harm the molecules. Printing provides a process, which allows the transfer of metal electrodes with low kinetic energy. Small defects in the molecular layer could be spanned by the pre-patterned metal layer.

A new process was developed in the course of this thesis in order to be able to transfer patterned metal films onto target surfaces. More specifically these target surfaces should comprise other patterned metal films and/or functional molecular layers. The application behind this idea is the building of *Crossbar* arrays (Xbar) with organic or biomolecules as functional interlayer. Metal electrodes are placed onto molecular films in a way, that molecules are neither harmed nor damaged.

Classically metal patterns are evaporated onto the molecules. [Stewart et. al. 2004] report about the molecule independent switching in *Crossbars* having molecular interlayers.

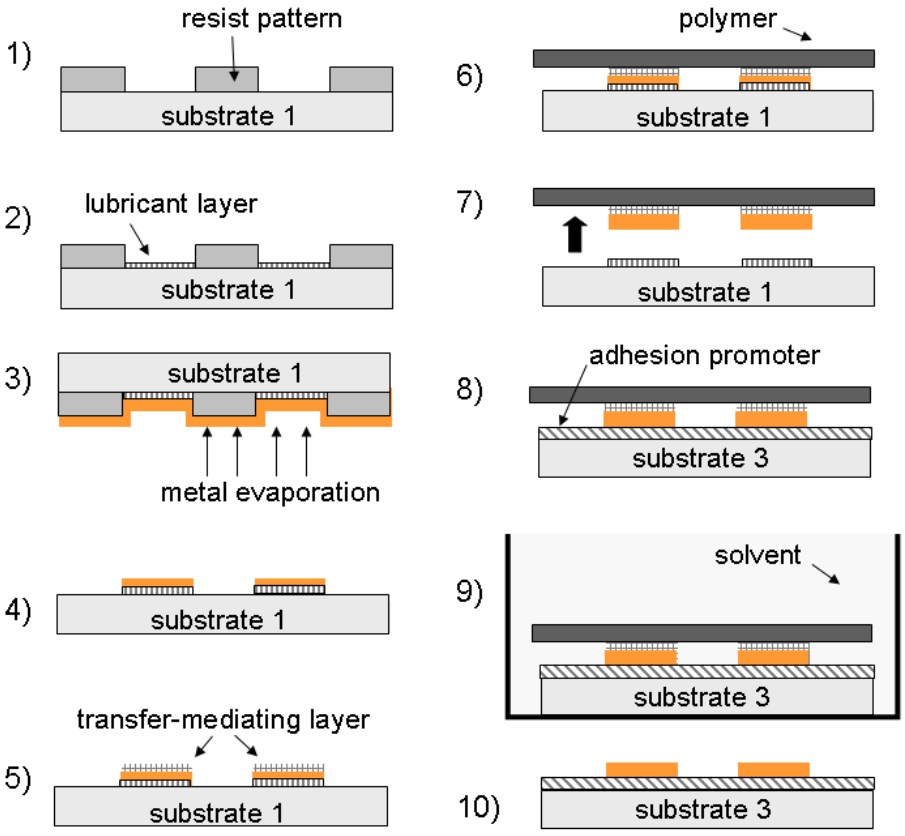

Figure 4.56: Schematics of the Shuttle-Transfer Printing Process

Like in nTP the basic idea is having an adhesion gradient between metal/stamp and metat/substrate. But instead of using the system PDMS stamp, gold and alkanedithiol covered GaAs reported by [Loo et. al. 2002a] or the non-covalent nTP system having different polymer surfaces reported by [Hur et. al. 2004], several intermediate steps and layers are used. [Ojima et. al. 2005] proposed the idea of using a release agent layer on the stamp[23] before depositing gold. With this step they could eliminate special surface preparations of the target substrate. By lowering the adhesion between gold and stamp a lower adhesion to the target substrate is needed. [Hines et. al. 2005] reported a process where gold was patterned on a surface and transferred at pressures higher than 1.5 MPa to plastic surfaces.

[23] They used a patterned silicon mold as stamp.

Another idea was proposed by [Meitl et. al. 2006]. They describe a transfer printing process. Thereby solid materials are picked of a donor (first substrate) with a piece of PDMS and are transfer to a receiver (target substrate). The control of adhesion is controlled by kinetic means namely the transfer rate (speed). Again this system is very specific. With the single parameter transfer-rate several selected solid objects could be transferred. But this is more or less due to coincides. In case of gold it could be lifted off a siliconoxide surface at a rather high speed, but with a low speed it could not be transferred back. The transfer rate in general is an additional parameter which can be used to slightly change the adhesion gradient. This system is very specific because up to now only PDMS was used. In addition as mentioned above the use of PDMS for replicating arbitrary patterns with a high resolution is limited by its softness. [Menard et. al. 2004] used composition stamps to increase the integrity of stamp, but the top layer still was PDMS. Here *Shuttle-Transfer Printing* (STP) is introduced. It expands, generalizes and supplements all ideas. Supplementing by defining the metal patterns with a high resolution process on a first substrate and afterwards transferring the patterns onto a target substrate using a polymeric substrate as shuttle. A schematics of this process is shown in Fig.4.56. The first step is defining a resist pattern on a first substrate (1). This is done by *Optical Lithography* for patterns above one micron or with *Electron Beam Lithography* for patterns below one micron. Other methods such as NIL could also be used. Then a lubricant layer is deposited to the first substrate (2). This could be done by vapor deposition of a fluoro-silane. The silane only bonds to the parts of the substrate which are not covered by resist. Subsequently a metal layer is deposited (3). This could be done by evaporation, electrochemical deposition or other techniques. After this step a lift-off is performed to remove the resist (4). After removing the resist only the lubricant and the metal inside the patterns stay on the substrate. Then a transfer-mediating layer is immobilized onto the metal surface (5). This could be done by self-assembly of an alkane-thiol. Further a polymer substrate is brought into conformal contact with the first substrate (6). By removing the polymer the metal (and transfer-mediating layer) stick to the polymer, the lubricant layer stays on the first substrate. Subsequently the polymer surface with the metal patterns can be contacted with a second substrate (8). This substrate could already have some metal patterns or functional layers and the contact with the polymer substrate could be aligned. Either before or after contacting both surfaces a solvent could be applied (9). The solvent should be chosen such, that the adhesion between metal and polymer is weakened and thus facilitate the transfer to the second substrate. Or if a transfer-mediating layer is used the solvent should change the properties of the layer. In addition the solvent has to be matched to the kind of functional layer used. If for example proteins are used, they might be harmed by organic solvents. In that case water buffer solutions should be used. Finally the polymer is removed and the metal stays on the second substrate.

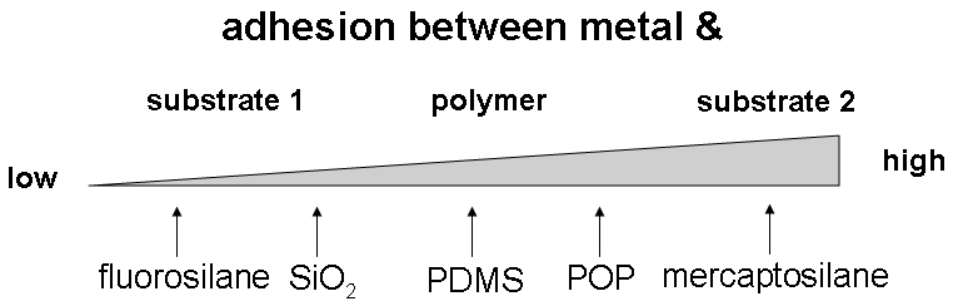

Figure 4.57: Adhesion gradient for the *Shuttle-Transfer Printing* process

The most crucial point of this technique is to find a system with a gradation of the metal adhesion (Fig.4.57): i) the adhesion between the metal and the first substrate should be very low; ii) the adhesion between the metal and the polymer has to be larger in order to transfer the metal of the substrate to the polymer; iii) the adhesion between the metal on the second substrate has to be greater than to the polymer. The first issue can be easily achieved by applying a release agent layer between the first substrate and the metal. The second issue can be controlled by choosing the type of polymer used or by selecting the right transfer-mediating layer. Polymers that guarantee a close conformal contact to surfaces such as PDMS, Affinity VP or Surlyn are required. The third issue can be address from two different directions. Either the second substrate could have a strong adhesion to the metal. This could be realized via covalent binding e.g. with a SAM with sulfur-headgroups or having a material with a larger surface free energy. On the other hand the adhesion between the metal and the polymer could be changed. This can be done by applying a solvent. If no transfer-mediating layer is used an alkane solution can be used to achieve a transfer [Schreiber 2006]. If a transfer-mediating layer is used, e.g water or ethanol might be sufficient to weaken the adhesion.

STP is a technique for transferring a metal electrode onto a molecular layer and thus well suited to create *Crossbar* arrays with molecular interlayers. STP was experimentally realized in the following way:
The first substrate was covered with PMMA resist and patterned with electron beam lithography. The design shown in Fig.B.8 was used. After development of the structures, 15 s of a 200 W oxygen plasma were used to make sure, that the trenches of the patterns were completely free of resist residues. Afterwards a fluoro-silane layer was applied using the procedure described in section 4.3. A 20 nm thick gold layer was then evaporated at a rate of 8 Å/s using an electron beam evaporation chamber. The lift-off process was performed with acetone and isopropanol. Different treatments were tested (Fig.4.58). By just immersion in

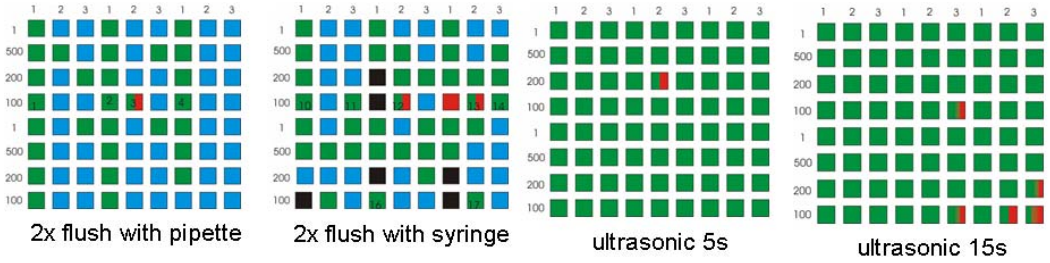

Figure 4.58: Illustration of different *lift-off* conditions for the Xbar fabrication Array of the design B.8
green indicates perfect lift-off, blue indicates metal residues between wires, red indicates broken wires, black indicates totally destroyed wires

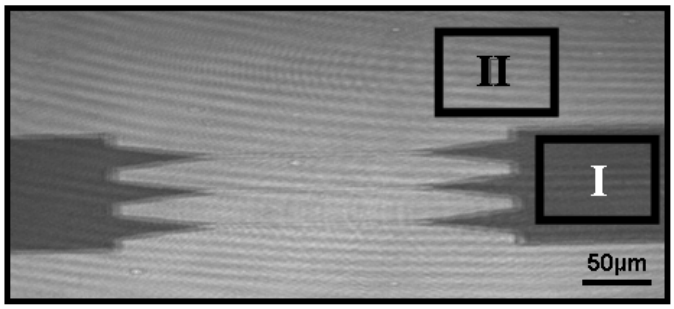

Figure 4.59: Ellipsometer image of the silane for Xbar fabrication

the acetone or flushing the acetone over the surface with a pipette or syringe the gold between neighboring wires could not be removed. Metal frazzles got stuck and could not be ruptured. By flushing air bubbles through a syringe or pipette all patterns were removed or damaged. Using ultrasonic assistance for the lift-off process all patterns were free of excess metal and almost no defects appeared. PDMS as well as Affinity VP and Surlyn were used as polymer surfaces. The adhesion between gold and Affinity VP is slightly stronger than for PDMS. It could be proven by ellipsometry, that after removing the gold of first substrate the thickness of the silane layer is still the same as before the gold evaporation (Fig.4.59). Therefore the thickness of the silane after lift-off was measured by taking the difference in height between the spot, where the silane was (I) and a spot aside (II). The initial silane height was measured on the same spot (I) before the evaporation of gold. This result indicates that the silane does not stick to the gold and the gold surface is still free of residues.

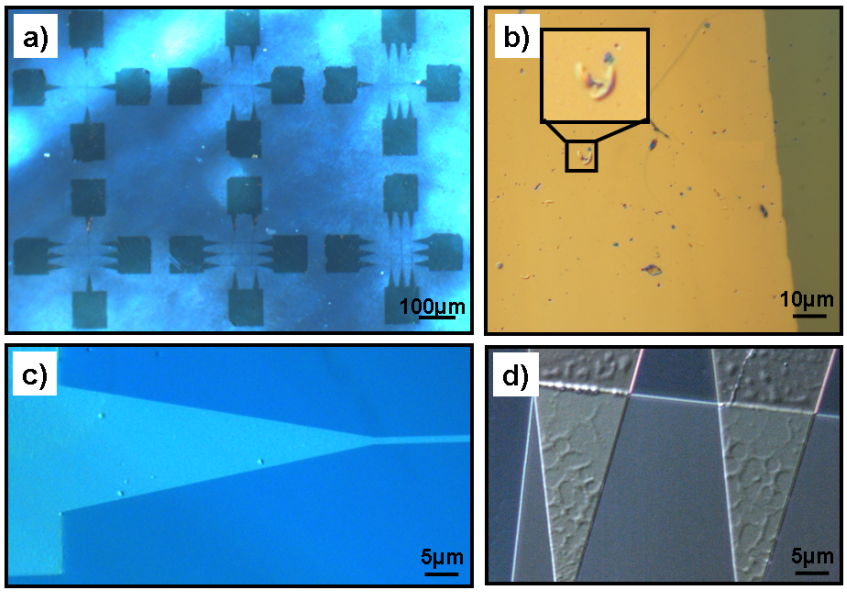

Figure 4.60: Microscope images of transferred gold patterns
a) gold Xbar arrays transferred onto Affinity VP
b) gold layer transferred onto siliconoxide using MUA as a transfer-mediating layer
c) gold Xbar electrode transferred from PDMS to a PAMAM covered siliconoxide sample
d) gold Xbar electrode transferred from Microset PDMS onto a Xbar array on siliconoxide

In order to fabricate Xbar arrays two different approaches were taken: i) Xbar arrays on polymer and ii) Xbar arrays on siliconoxide. Electronic components on plastic are of major interest for a new field called *Plastic Electronics*, which deals with devices such as flexible circuits, transparent displays or cheap, light devices such as RFID[24] tags. *Crossbars* on siliconoxide however allow an integration into commonly used *Silicon Technology*. For the first approach the gold electrodes on the polymer were immersed in a molecule solution for a certain time, rinsed and dry-blown. PDMS as well as Affinity VP or Surlyn could be used. Since PDMS is too soft, lots of cracks were present due bending. That is why Affinity VP is the polymer of choice. In addition the adhesion of gold is much stronger than with PDMS. This in agreement with [Hur et. al. 2004] since the surface free energy of Affinity VP is larger than for PDMS. Afterwards the polymer was brought into contact with an additional first substrate with gold patterns on a silane layer. The alignment was made such, that the gold wires crossed each other in a 90° angle thus forming Xbars using the FinePlacer. After removing the polymer surface of

[24] **R**adio **F**requency **ID**entification

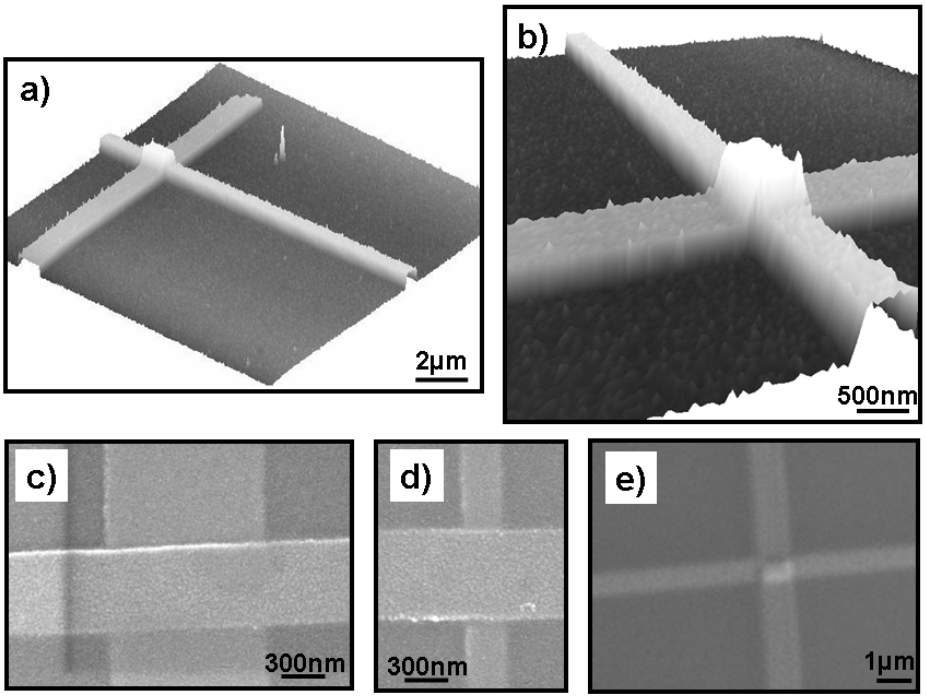

Figure 4.61: Images of *Crossbars* on siliconoxide after transfer
a) Tapping mode AFM image of a Crossbar with an alkanethiol interlayer
b) close-up of a)
c) SEM image (10 kV) of a 1 μm x 500 nm junction
d) SEM image (10 kV) of a 500 nm x 200 nm junction
e) Microscope image of a 1 μm x 1 μm junction

the substrate also the second gold patterns stuck to the polymer (Fig.4.60a). For the second approach a second substrate with the same patterns was used, but without a silane layer. In addition the silicon was covered with 400 nm - 1000 nm of siliconoxide as an insulating layer. Instead of 20 nm Au a stack of 5 nm titanium, 5 nm platinum and 20 nm gold is deposited. Titanium is an adhesion promoter for gold on siliconoxide and guarantees, that it is not removed or damaged by contacting it with a polymer. The electrodes on this substrate acted as bottom electrodes. They were immersed into a molecule solution to immobilize a molecular interlayer. The gold electrodes on the polymer were brought into contact with the bottom electrodes such, that the electrodes were aligned in a 90° angle. In case of Microset PDMS the top electrodes could be transferred onto the bottom electrodes without any solvents (Fig.4.60d). In case of Affinity VP a droplet of heptane had to be used for transferring the gold onto the bottom electrodes. Various Xbar junctions are shown in Fig.4.61.

Another promising strategy for the transfer of gold was printing onto a mercapto-silane SAM on siliconoxide. These experiments are part of ongoing research [Gilles 2006], [Schreiber 2006]. The gold should bind covalently to the sulfur-head groups. Since the covalent interaction is much stronger than non-covalent the transfer should work well. A molecule studied here for covalent binding was PAMAM and PAMAM-OS dendrimers. After applying solutions of it to a siliconoxide surface amino-groups are present on the surface. It was possible to transfer gold patterns onto it with PDMS as well as Affinity VP (Fig.4.60c). The usage of such a transfer strategy is very limited. If the covalent linker molecules are applied onto a siliconoxide surface, which already has the bottom electrodes, the linker molecules will also be present in the junction. No other molecules could be measured in such junctions. If the linker molecule is immobilized on siliconoxide without prepatterned electrodes, both the top and the bottom electrodes have to be transferred in two successive steps. Since each transfer is not perfect, the yield of such a strategy is low. Therefore the printing onto PAMAM was not optimized in this thesis. Another idea pursuit was lowering the adhesion between polymer shuttle and metal by immobilizing an SAM onto the gold before it is transferred. By using a mercapto-undecanoic acid SAM on the gold, it was still possible to transfer the gold of the fluoro-silane onto the Affinity VP surface. By applying a few drops of isopropanol it was possible to transfer this gold onto a siliconoxide surface (Fig.4.60b). Note, that without the MUA between gold and Affinity VP the transfer does not work, even with isopropanol. So obviously the SAM allows the isopropanol to enter into the cleft and weaken the adhesion. Since this process provides several parameters for optimization, it was still not completely investigated. Further studies are part of ongoing research.

The smallest lines that could be transferred so far was a 50 nm gold electrode (Fig.4.62). This result seemed not be limited by the transfer technique itself, but rather by the electron-beam writing and the lift-off procedure. This experiment was a proof of concept and thus not optimized.

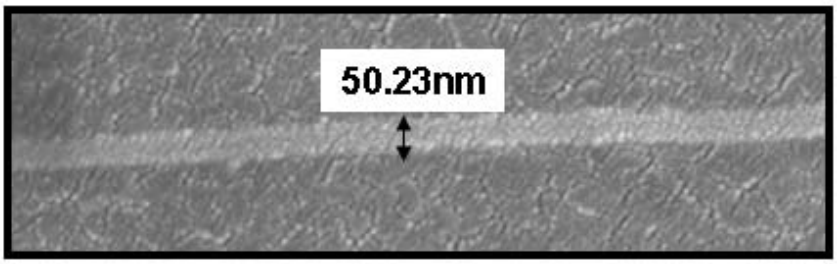

Figure 4.62: 50 nm gold electrode transferred onto Affinity VP using STP

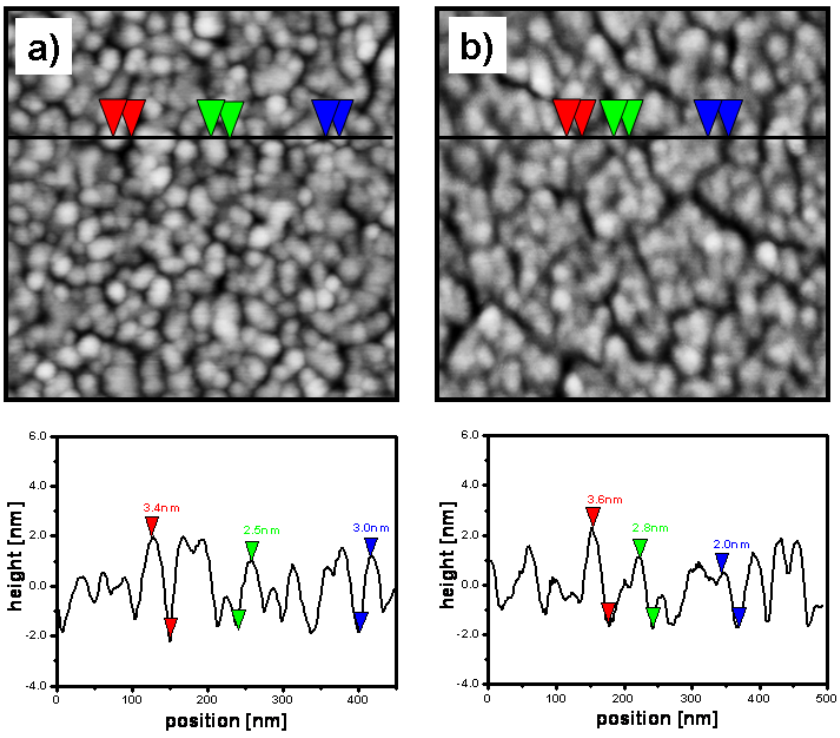

Figure 4.63: Tapping mode AFM images of gold surfaces
The contrast scale is 15 nm in height.
a) 20 nm gold deposited onto siliconoxide at 8 Å/s with electron beam evaporation
b) 20 nm gold deposited onto a fluor-silane SAM under the same conditions

The roughness of the gold is one of the most important issues in applying the electrodes for Molecular Electronic devices. Therefore the roughness of the gold was monitored through the different process steps with AFM. The typical rms roughness of gold deposited by electron-beam evaporation at 8 Å/s onto a siliconoxide surface was found to be 9 Å (Fig.4.63a). Circular domains with a diameter in the range of 25 - 30 nm could be observed. This is very common for such films. The roughness of gold evaporated onto a siliconoxide covered with a fluro-silane SAM was almost the same (Fig.4.63b). But a clustering of domains forming patterns in the range of 100 nm in size can be seen. The roughness of gold after transferring it from the silane layer to a piece of Affinity VP is slightly smaller (Fig.4.64a). The rms roughness was 7 Å. Note, that this surface is smoother, because it was been in contact with the smooth silane layer. This proves, that the roughness is not increased by the deposition of gold onto the silane. The roughness is neither increased by the transfer process onto the Affinity VP and nor through the Affinity VP surface itself. After transferring the gold back onto a siliconoxide surface covered by a PAMAM dendrimer, the rms roughness was 8 Å (Fig.4.64b).

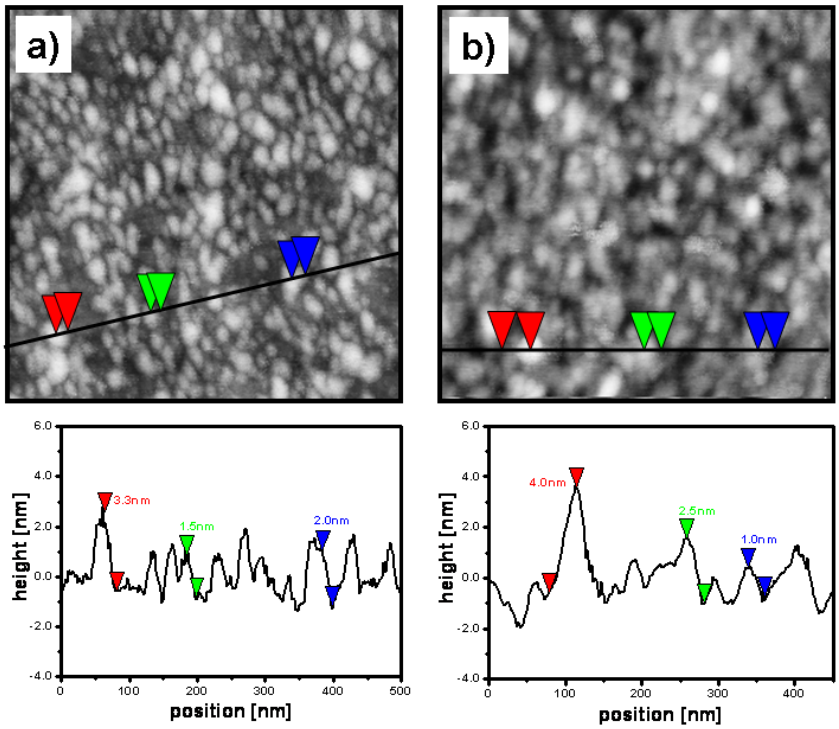

Figure 4.64: Tapping mode AFM images of gold surfaces
The contrast scale is 15 nm in height.
a) the film of Fig.4.63b) transferred to a piece of Affinity VP
b) the film of a) transferred to a PAMAM layer immobilized to a siliconoxide surface

Obviously the roughness is not influenced by the transfer process. Note, that in this case the smoother surface was facing the molecules.

Testing of the *Crossbars* was performed with a manual probe station. An apparent problem occurring is the electrical contact between tips and the thin gold bond-pads. For probing on polymer there is the additional problem of bending. The tips will introduce a force to the surface, which will lead to a deformation (Fig.4.65b). The deformation might lead to cracks in the gold. These cracks will lead to uncontrollable electrical behavior, because the separation of the electrodes might lead to tunneling similar to the break-junction experiments. Since the force of the tip is not fixed, there is a time-dependence and this effect leads to unreproducible results. Therefore a droplet of a gallium-indium alloy is placed onto the contact pads (Fig.4.65a). It is liquid at room-temperature and has a good conductivity and makes an ohmic contact to gold. The gallium-indium can be placed by dipping the tips into a drop and then softly contacting the place, there

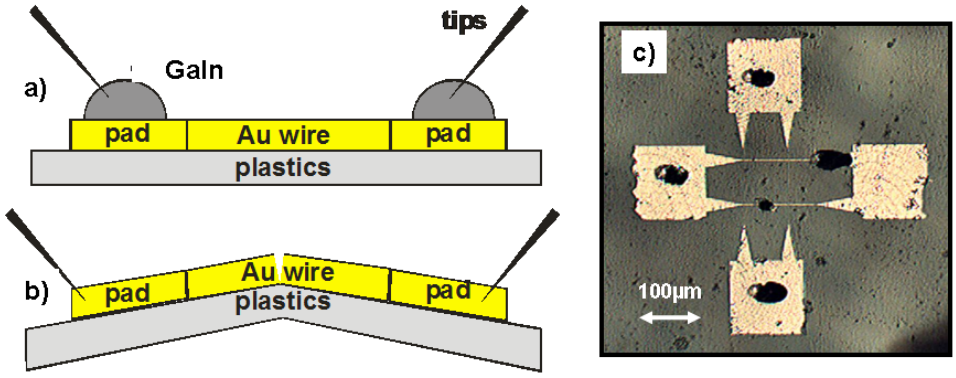

Figure 4.65: Testing strategy using GaIn alloy
a) A droplet of GaIn is placed onto the bond pads. Thus the tips do not have to touch the bond pad.
b) If the tips touch the bond pads a compression of the polymer is applied, which might lead to cracks in the metal.
c) Droplets of GaIn can be placed as small as 30 μm.

the droplet should be positioned. This also can be used to repair cracks in wires. Droplets as small as 20 μm could be placed (Fig.4.65c). Note, that cracking of electrodes could be also avoided by using different or thicker electrodes materials. It is much likely for a 20 nm gold film to be subject to cracks.

A universal printing process for metal patterns has been demonstrated based on an adhesion gradient. STP was used for the transfer of gold patterns to siliconoxide surfaces. Gold electrodes were fabricated by EBL and lift-off. To decrease the adhesion between the gold and the substrate a fluoro-silane release agent was used. The gold electrodes could easily be transferred onto polymeric shuttle substrates without increasing the rms roughness. Note, that the roughness is given by the evaporation process, rather than the transfer process. Afterwards the gold electrodes could be transferred onto target substrate. Here the target substrate compromised electrodes covered with a functional molecular layer. Thus *Crossbar* junctions were formed. However, there should not be a limitation to gold or the formation of *Crossbars*. STP compromises several parameters, namely release agent layers, auxiliary layers, polymeric materials, solvents and target substrate modifications, which can be adapted to the respective material or application. The application of STP for Crossbars is demonstrated in the next chapter.

4.5.5 Alignment

Alignment is an important issue for addressing of functional materials to supporting device structures. Alignment of patterns with respect to the substrate was done with the FinePlacer[25]. One substrate is lying on the stage, the stamp is held on an arm perpendicular to the stage. A microscope with a beam-splitter allows to simultaneously image both. The images are superimposed. By moving the stage with micrometer screws one sample can be aligned with respect to the other. By carefully doing this a resolution of a few microns precision was achieved (Fig.4.66). The resolution is limited by several facts: the resolution of the microscope, the minimum adjustment of the micrometer screws and additional misplacement through slackness by moving the arm towards the first sample. For μCP additional problems are introduced by the stamps. Non-parallel surfaces, a thickness variation or bent surfaces may lead to non-uniform alignment. Only the patterns next to the alignment marks are accurate. Lines further away are subject to larger misplacement.

The FinePlacer was also used for printing. Different pressures were applied by changing the force to the lever. In order to hold the stamp on this lever arm sticky Sylgard 1:40 slabs were used as backplanes to "glue" the stamp to the arm.
For a more sophisticated approach an EVG 620[26] aligner was tested. Therefore the two samples were mounted parallel to each other. They were brought into a defined separation distance of several ten microns. The upper sample had to be

[25] device sold by Finetech
[26] EV Group, Austria

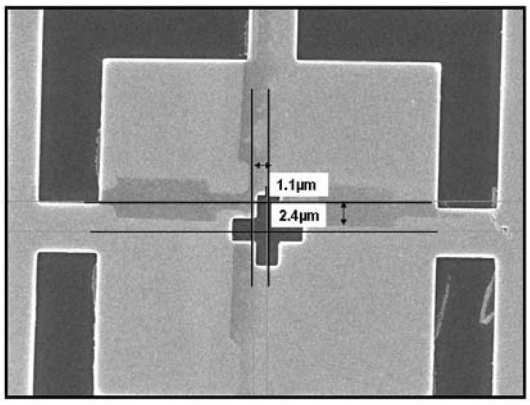

Figure 4.66: SEM image (2 kV) of cyt *c* printed onto gold
Cytochrome *c* (dark contrast) is printed onto a gold substrate with a stamp having an alignment cross as pattern. The substrate is patterned with corresponding alignment marks. Alignment of stamp and substrate was done with the FinePlacer device.

transparent, because a microscope was used to image the patterns for above. With this setup an accuracy of 500 nm should be possible. Nevertheless, an accuracy of only 6 μm was achieved, since two mandatory requirements had been missing: the stamp should have an area of at least 3 or 4 inch to guarantee easy handling and the total thickness variation over the area should be well below 20 μm. Since master, stamps and methods described above were designed as testing structures in the centimeter range it was not possible to make appropriate stamps for alignment tests. The thickness variation of the stamps used here was in the range of $>50\,\mu$m. Since the separation distance used for the 500 nm alignment accuracy is typically 20 μm it is clear, that such stamps were inappropriate.

To further increase the alignment accuracy moire techniques have to be used instead of imaging the ordinary alignment marks with optical microscopy. To pave the way for implementing and testing the moire technique for μCP moire alignment marks were designed and transferred into the polymer. The realization of moire assisted alignment is a part of ongoing research. However, first prototypes of masters and stamps were fabricated.(Fig.A.10).

Summary

To briefly summarize the printing results:

- The stamp material should be chosen such, that it matches the properties of the molecules to be transferred. Rule by thumb: hydrophilic molecules need hydrophilic stamp materials and vice versa. The stiffness of the material has to be chosen such, that no pairing or sagging defects occur. This depends on the pattern design and dimensions.
- *Contact Inking* using polyolefin stamps is the method of choice for the printing of alkanethiols. Very small patterns can be created by taking advantage of the *Edge Transfer* observed for printing with Surlyn stamps. Shorter printing times are preferable.
- *Wet Inking* using polyolefin or Surlyn stamps is the method of choice for the printing of proteins. Longer printing times are preferable. For patterns with larger gaps, for which sagging is expected, *Contact Inking* is better suited. For proteins with very fragile functionalities neither of these methods works. Therefore *In-situ μCP* is the method of choice.
- For the formation of colloid patterns an indirect method works best. An adhesion promoter should be printed and the colloids should be immobilized from solution.

- For printing of sub 50 nm patterns or for the printing of patterns on large areas *Air-Cushion Printing* is the method of choice using stamp materials with a Young´s modulus larger than 1 GPa.
- *Shuttle-Transfer Printing* is the method of choice for the transfer of metal layers. The choice of parameters depends on the metal used and application.
- Alignment down to dimensions of 1 μm is straight forward using the Fine-Placer with any type of stamp. For higher precision larger stamps with very precise dimensions have to be used. In addition specially designed alignment marks e.g. Moire patterns are needed.

Chapter 5

Crossbar Junctions with Molecular Interlayer

Commonly *Crossbar Arrays* were fabricated by evaporation of the top electrodes onto the assembled molecules. Defects in the molecular layer or the evaporation process itself often led to direct filaments. These filaments represent short circuits influencing the properties of the junction. As reported by [Hsu et. al. 2003] a printing of electrodes using nTP avoids this problem. Since STP was introduced as a generalization and expansion of nTP, the usage of STP for the fabrication of Crossbar arrays with various molecular interlayers will be demonstrated in this chapter.

5.1 Characterization of Electrodes

As previously described electrodes with the design shown in Fig.B.8 were prepared by EBL and transferred by means of *Shuttle-Transfer Printing* using a piece of Affinity VP or Microset PDMS as shuttle. The electrodes were made by evaporation of 20 nm gold at a rate of 8 Å/s. Characterization was done with a probe station through placing two tips onto the bondpads measuring the IV[1] characteristic with a two point setup. The resistance was used to calculate the resistivity ρ according to:

$$\rho = \frac{R \cdot A}{l} \tag{5.1}$$

Here A is the cross-section of the wire, l is its length and R the resistance measured. IV plots and the values of the resistivity are given in Fig.5.1. Note, that the width of the wires was slightly larger than expected. It is given in the upper left corner of each plot. Due to the RIE process used in fabrication, the width of the

[1] Current vs. Voltage

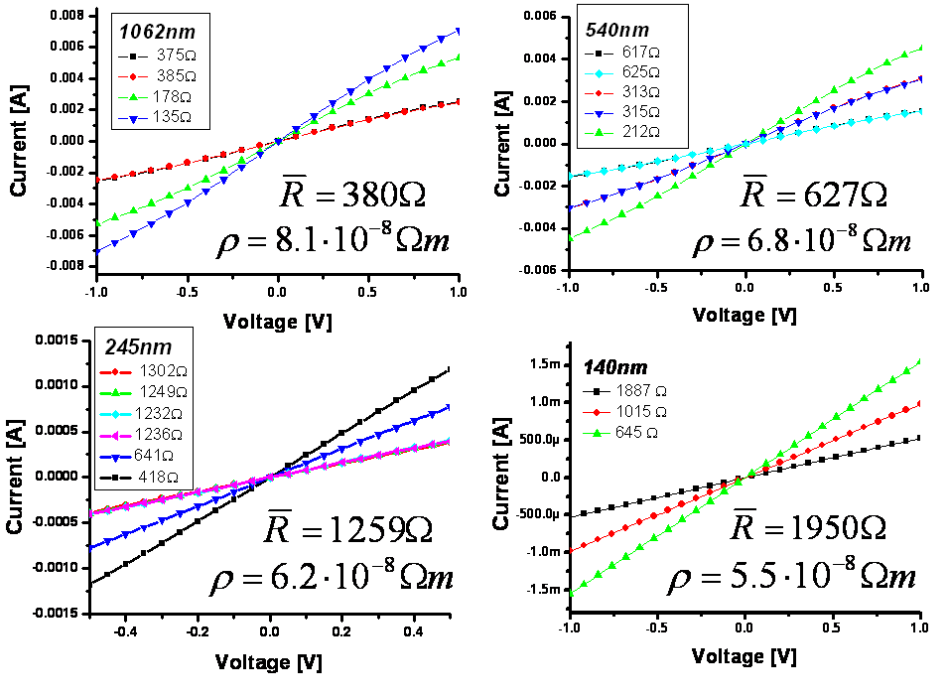

Figure 5.1: Current vs. voltage characteristic for a gold electrodes on Affinity POP 20 nm thick gold electrode with the design shown in Fig.B.8 were transferred onto Affinity VP. The resistance was measured and used to calculate the resistivity.

resist patterns increase. For all calculations in this chapter, the measured width was used, rather than the nominal width. However, the nominal width will be used to denote the electrodes. Also note, that for each width there are electrodes having one, two or three wires between the bondpads. As expected three different values for the resistance were observed. Their ratio was 1:2:3 as expected. The resistance for a respective single electrode was used to calculate the mean value. The largest electrodes show a bending of the curve for large voltages. Since this is most prominent for the highest currents it can be attributed to the heating of the wires. Using equation:

$$R = R(T_0) \cdot (1 + \alpha T) \tag{5.2}$$

which describes the impact of heating on the resistance, it is possible to calculate the heating of the electrodes. Here $R(T_0)$ is the resistance at initial temperature T_0 and α is the temperature coefficient describing the increase of resistance with temperature. For gold α is $3.99 \cdot 10^{-3}\,\Omega/°C$. Considering the blue line in the upper left corner of Fig.5.1, namely the characteristic of three parallel 1062 nm electrodes, a heating of $40\,°C$ is observed. Note, that this measurement was rather fast and only took 1.5 s.

The resistivity of bulk gold is supposed to be $2.2 \cdot 10^{-8}\,\Omega m$. Thin polycrystalline films are known to have a resistivity 2-3 times higher. This is in agreement with the measurements shown here. Interestingly the broader the electrodes are, the larger is their resistivity. In principle one would expect the resistivity to become smaller, since conduction of a broader piece should be better. The larger resistivity can only be explained with defects. Obviously for larger electrodes more defects such as crinkles are present, which increase resistivity. However, this deviation is not significant, especially since junctions with molecular interlayer will have resistances in the range of $M\Omega$ to $T\Omega$.

5.2 Crossbar Junctions on Affinity VP

As described in Chapter 4.5.4 some Xbar arrays were completely fabricated on Affinity VP slabs. Depending on the specific system this method is suited or un-suited. Since 20 nm thin gold layers were used some major problems arose. Since Affinity VP is rather flexible the electrodes were subject to compression and dilation, which led to crinkles and cracks of the electrodes. Especially these cracks were a problem, because they acted as *Break-Junctions* and created tunneling currents[2]. In addition vibrations and tensions led to a further moving of the cracks. This led to time-dependent signals. In fact most results obtained on Affinity VP were neither reproducible nor stable. Applying GaIn alloy onto the bondpads as described on page 121 could minimize these problems, but not solve them completely. Two examples of such unreproducible measurements are given in Fig.A.18 and Fig.A.19. One measurement showed a NDR[3] like behavior and one a pronounced switching. Each of these measurements were only observed once. Thus they might not correspond to any molecular properties of the interlayer, but rather be due to the unique properties of the polymer/Xbar/molecule setup.

On the other hand Affinity VP was subject to melting, if the currents were to high. For currents above μA the POP obviously started to melt. This indicates, that electrodes must have heated above 70 °C. A typical image indicating the heating is given in Fig.5.2. Clearly a discoloration can be seen radial to the electrode. Stepwise taken images are shown in Fig.A.20. The discoloration starts above 1.3 V and currents in the nA range. The diameter of the discoloration becomes larger until in a range of 2 - 3 V the wire completely breaks. Sometimes the breaking of the wires occurred at more than 5 V. In that cases the Affinity VP must have melted around the wire preventing a early fusing.

[2] In fact *Break-Junctions* are formed very similar

[3] **N**egative **D**ifferential **R**esistance

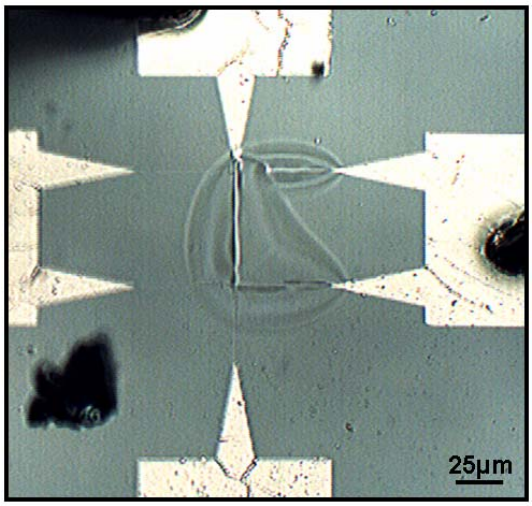

Figure 5.2: Microscope image of a Xbar array on Affinity VP after break-down

This method is a indicator for temperature. Since a measurement took around 50 s it is difficult to compare it with the temperature increase observed for electrodes without molecules as discussed above. Note, that the measurement speed depends on the current range. Since the *Crossbar* junctions here have molecular interlayer, the resistance increase can not be sole associated with a temperature increase. A comparison or estimating with classical equations was not reasonable. Just assuming Joule´s heating due to the applied voltage and current flowing and using the heat capacity of gold, the temperature should be millions of kelvins. Obviously the wire is too small and the system is too complex to make a classical calculation. The heat conduction to the tips and Affinity VP, as well as heat radiation seem not be negligible.

Affinity VP is not suited for high current or high voltage applications due to the melting. However, it might be useful for different metal/polymer devices since it provides inertness, transparency, flexibility, adhesion and is cheap.

5.3 Crossbar Junctions on SiO_2

In order to have a more defined system Xbar junction were formed on siliconoxide. It is rigid, isolating and patterned or coated in a precise manner.
The easiest system of molecular interlayer are alkanethiols. They are easy to

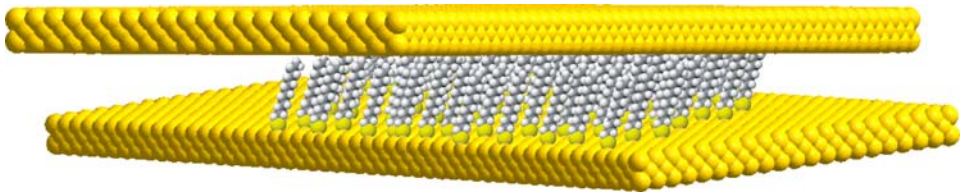

Figure 5.3: Schematic of a Xbar junction having a DDT interlayer

immobilize, form dense monolayer, are available with different lengths and functional groups and they are widely studied. Their characteristic was investigated with many different techniques and they were thus often used as model system to characterize new devices or techniques. The following alkanethiols were studied as interlayer for Xbar junctions:

propanethiol	PT	$CH_3-(CH_2)_2-SH$
butanethiol	BT	$CH_3-(CH_2)_3-SH$
hexanethiol	HT	$CH_3-(CH_2)_5-SH$
octanethiol	OT	$CH_3-(CH_2)_7-SH$
dodecanethiol	DDT	$CH_3-(CH_2)_{11}-SH$
hexadecanethiol	HDT	$CH_3-(CH_2)_{15}-SH$
octadecanethiol	ODT	$CH_3-(CH_2)_{17}-SH$
octanedithiol	OdiT	$SH-(CH_2)_8-SH$
benzenedithiol†	BDT	$SH-phenyl-SH$
thiobisbenzenethiol†	TBBT	$SH-phenyl-S-phenyl-SH$

† junctions having these molecules as interlayer will be discussed on page 140.

The dependency of the current versus the distance of the electrodes was instigated by using molecules having different chain lengths. The effect of the contact between molecules and metals was investigated using mono- and dithiol molecules. For monothiols the thiol group was covalently bound to the bottom-electrode while only a tunneling link was formed to the top-electrode, since it was not covalently bound. For dithiol molecules covalent binding should occur for top- and bottom-electrodes. The molecules were assembled to the bottom electrode. The junctions was fabricated by transferring the top electrode with Microset PDMS or Affinity VP and heptane (as described in Chapter 4.5.4) onto the bottom electrodes. Thus a monolayer of the molecules was formed inside the junction as indicate in Fig.5.3.

The thiol was immobilized by dipping the sample having the bottom electrodes into a 1 mM solution for 10 min. 1 mM is the standard concentration commonly used for thiols throughout the literature. 10 min was chosen for fabrication issues.

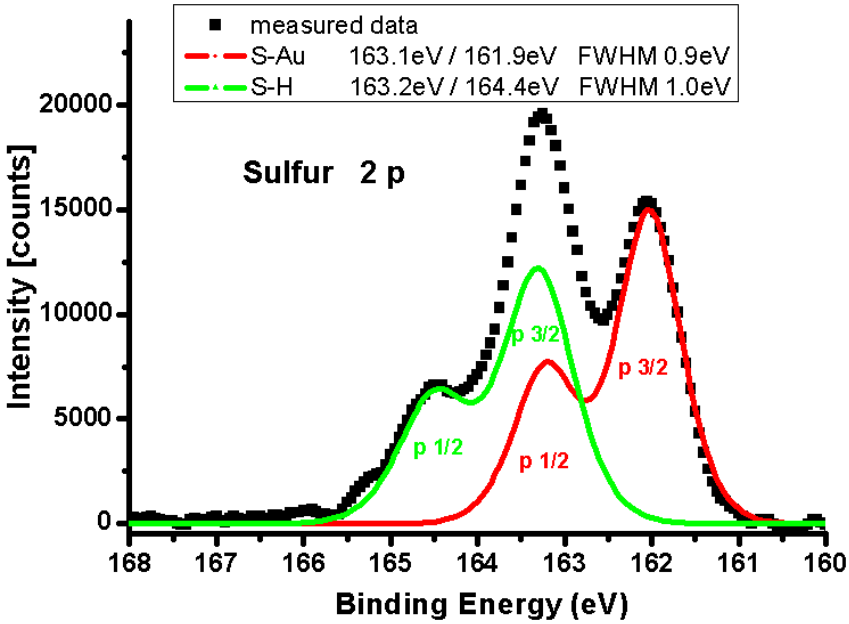

Figure 5.4: XPS spectrum of the sulfur 2p component of BDT immobilized to a gold bottom electrode

It is known, that within 10 min alkanethiols assemble on gold. However, especially for long alkanethiols this first assembly might not be the best packing. Therefore assembling time up to 50 h were used. For the dithiol molecules it is important, that after immobilization the molecules form a upright standing layer. Note, that it is also possible, that the molecules lay flat on a substrate and both thiols are covalently bound to this substrate. In order to investigate the immobilization conditions for BDT XPS[4] was used. The spectrum of the sulfur 2p peak after immobilization to the bottom-electrode shows two components, one at 161.87 eV / 163.07 eV, which can be attributed to sulfur bound to gold, and 163.15 eV / 164.35 eV, which can be attributed to -SH groups (Fig.5.4). Note, that since the p component is used a doublet 1/2 and 3/2 is present. The peak area for both peaks is the same. This indicates, that all molecules stand upright and the immobilization conditions are suited.

A first observation made is, that although the thiols should not interact with the siliconoxide, somehow the surface properties are changed (e.g. the water contact angle was larger than 10°). Thus the yield of the transfer of the top-electrode is worse with either methods. Typically some of the bondpads are broken and only part of the wires were transferred (Fig.A.22). In case of transferring only single

[4] **X**-ray **P**hotoelectron **S**pectroscopy

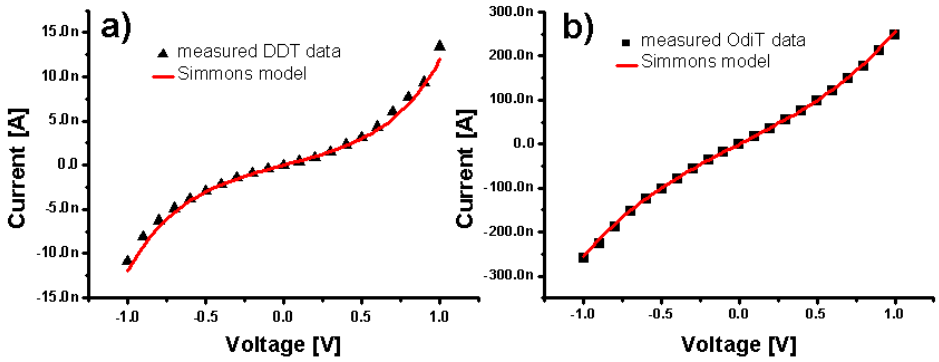

Figure 5.5: Measured current vs. voltage characteristic for typical junctions
the red curve corresponds to a fit using equation 2.8
a) a 1 μm by 1 μm DDT junction
b) a 1 μm by 500 nm OdiT junction

wires, reproducible contacts were made directly by touching them with a tip. In case also the bondpads were transferred and more than one wire, the bondpad was separated, that only one junction was measured at a time. Two or more junction in a serial or parallel connection or in a more complex network are to difficult to investigate, as long as the behavior of a single junction is not fully determined.

Many of the junctions showed a short circuit behavior, namely currents equal to the currents observed in the absence of molecules. The yield of junctions having non-short behavior was found to strongly dependent on the chain length of the molecules as well as on the area of the electrodes. For butanethiol 17 out of 21 junctions were short circuit, while for hexadecanthiol only 2 out of 12 junctions were short circuits. For short molecules (less than 8 C-atoms) areas larger than 0.5 μm^2 always resulted in shorts. For butanethiol useful junctions could only be formed of 100 nm and 200 nm wires resulted. These findings are reasonable since shorter molecules are known to result in less order SAMs. In addition the roughness of the electrodes should stronger contribute to the characteristics. Since defects scale with the area, it is reasonable to find more shorts for larger areas.

All junctions with non-short behavior showed a tunneling like characteristic (Fig.5.5). The data was fitted using Simmons equation 2.8. Therefore α and φ_0 were used as fit parameters. The thickness of the interlayer was assumed to be equal to the nominal chain length of the molecules used. The current density was converted into a current by assuming a junction area, which is the product of the widths of the electrodes. Some typical values are:

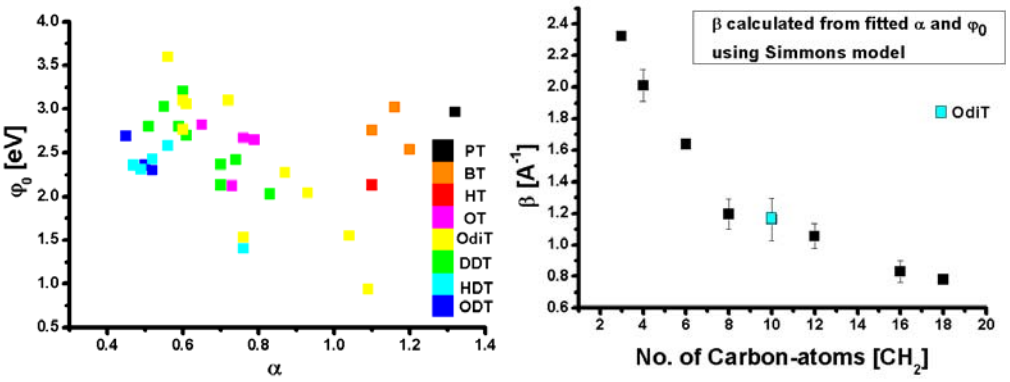

(a) (b)

Figure 5.6: Non-short Xbar junctions fitted by Simmons equation
a) φ_0 vs. α
b) β_0 vs. chain length
Note since OdiT is longer than OT it was plotted on the position, which corresponds to its length rather than the number of its CH_2-groups.

molecule	$\varphi_0[eV]$	α	$\beta_0[\text{Å}^{-1}]$
ODT	2.5	0.45	0.73
HDT	2.3	0.52	0.80
DDT	2.8	0.63	1.09
OT	2.4	0.89	1.40
OdiT	2.7	0.80	1.35

β_0 was calculated using equation 2.10. As discussed by [Wang et. al. 2005] the fitted parameters are not unique. Other combinations result in a similar performance of the fit. However, β_0 should be the same for such pairs of φ_0 and α. Plotting φ_0 vs. α for all non-short junctions indicates, that α strongly depends on the chain length (Fig.5.6a). The longer molecules are the smaller is α. Fitted values ranges between 0.4 - 1.4 . φ_0 is more or less independent on the chain length, but for a certain molecule it varies between 0.8 eV - 3.6 eV (OdiT). [Wang et. al. 2005] summarized characteristic parameters for alkanethiol tunneling junctions gathered by different methods. However, these fluctuations are much smaller than observed here. Especially the huge range for α is indication for a problem. It should not as strongly depend on the chain length. In addition a value larger 1 is not physical. Since the reduced mass in a rectangular potential is given by $m^* = \alpha^2 m$ $\alpha > 1$ means, that the reduced mass is larger than the real mass. The values of α and φ_0 were used to calculated β_0. It was plotted against the chain length of the molecules (Fig.5.6b). An exponential decay was found. Theoretically β_0 should be independent on the chain length. This is a strong indication, that there is a problem. Since

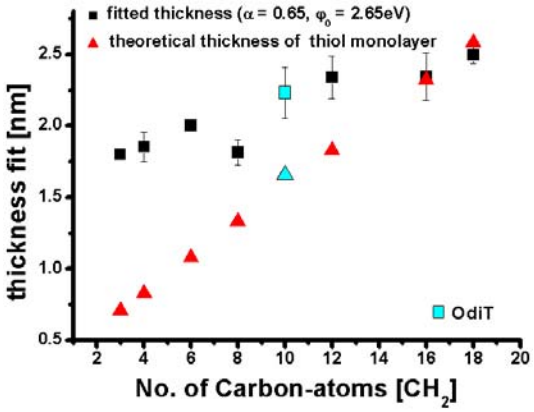

Figure 5.7: Thickness fitted in Simmons model vs chain length
Note since OdiT is longer than OT it was plotted on the position, which corresponds to its length rather than the number of its CH_2-groups.

the chain length enters into Simmons equation exponentially, this indicates that the assumption of electrodes separated by a distance equal to the chain length of the molecules in this junction is inappropriate. All data were fitted again fixing α as 0.65 and φ_0 as 2.65 eV[5]. This time the thickness was used a fit parameter. The fitted thickness for ODT and HDT was found to be approximately equal to the chain length of the molecules (Fig.5.7). For short molecules however, the fitted thickness was in a range of 1.7 nm - 2.3 nm. This is clearly larger than the chain length of these molecules. This finding indicates, that for molecules shorter than HDT the electrodes are not in contact as close as possible. Obviously the roughness of the gold dominated the distance in this region. Remember, that the rms roughness of the electrodes inside the junction was 7 - 8 Å and the maximum peak-peak height was about 3.5 nm.

The simple fitting of the thickness assuming a constant α and φ_0 is not adequate, since Simmons equation described the current density. If the mean distance between the electrodes with a junction is really a few nm for shorter molecules only a few molecules might be directly contacted by the top electrode. Thus the assumption, that all molecules contribute is inadequate. A new factor N has to be introduced to the fit equation to account for the percentage of area, which contributes to the charge transport. Using this parameter the values for the fitted thickness or fitted α and φ_0 are changed without changing the quality of the fit. Assuming that only 10 % of the molecules in a ODT junction contribute to the charge transfer α and φ_0 are reduced and β is 0.63 $Å^{-1}$ instead of 0.73 $Å^{-1}$. However, a full fit using all four parameters could not be established. Thus the

[5] This means fixing β as 1 $Å^{-1}$.

absolute values for the fitted thickness or α and φ_0 could be slightly different. In addition β and the thickness are highly correlated. A small variation in the thickness leads to a different value for β. Since the real β is not known, the fitted value for the thickness is not 100 % appropriate. However, since the thickness for ODT and HDT seems to be reasonable, their α, φ_0 and β values should be right. φ_0 was found to be in a range between 2 - 2.6 eV, α is 0.45 - 0.7 and β is 0.75 - 0.9 $Å^{-1}$. These values are in agreement with values obtained by other techniques summarized by [Salomon et. al. 2003] and [Wang et. al. 2005]. Since the HOMO-LUMO gap for alkanethiols is approximately 7 - 8 eV, a barrier height of 1 - 3 eV as difference between LUMO and Fermi level seems to be reasonable. In addition it is smaller than the work function of gold which is ≈ 4.7 eV.

The observed IV characteristics did not give an indication for hysteresis, switching effects or direct contacts. Such effects were observed for Xbar arrays made with Ti electrodes [Richter et. al. 2005] or for evaporated gold electrodes [Hsu et. al. 2003]. This is a further indication, that the properties obtained can be fully addressed to the molecules. In addition this indicates, that the observations for short molecules are due to roughness effects rather than filamentary growth.

Expecting a certain area of non-contact seems to be quite reasonable for the electrodes used. The electrodes were transferred onto a siliconoxide surface. It is known, that the adhesion between gold and siliconoxide is rather poor. In addition most contact areas were formed by monothiols. Thus the top electrodes were laid onto a layer of methylene groups. It is known, that the interaction between gold and methylene is also very weak. This means, that the gold is not constrained into a close contact. This could be changed by using a substrate, that allows covalent binding of the gold, for example a mercapto-silanized siliconoxide sample. Covalent binding in the junction as obtained by using octanedithiol did not seem to improve the situation. This phenomenon is further strengthened by the observation, that it was sometimes possible to move top electrodes with the tip over the surface. Such an event is shown in Fig.A.21. Further investigation of this phenomenon could not be pursued since there is not suited methods. *Optical Microscopy* does not have resolution to make direct observation. Since the Xbar arrays are formed on siliconoxide an additional metal layer has to be sputtered on the samples for investigations with a SEM. In AFM junctions can be observed, but the image processing is rather difficult. Ideally objects such as wires should be scanned perpendicular to the scan direction. In case of Xbars it is not possible to scan both wires perpendicular, of course. A 45° angle works best for scanning, but then it is difficult to process the raw image. Operations such as *Flatten* and *Planefit* are difficult to perform for such images. After each processing the view of the image is different and thus it is difficult to tell, what the real surface looks like. Using the calculated values for α,

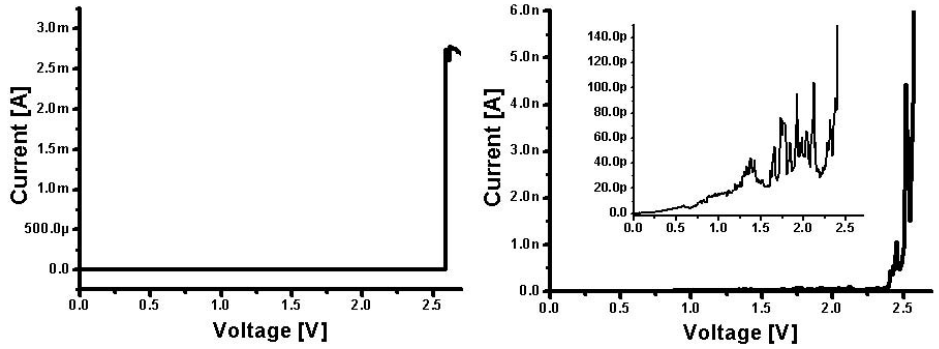

Figure 5.8: Typically break-down characteristic for a alkanethiol junction Hexadecanethiol in a 140 nm by 1 μm junction. The right plot is a magnification of the left one. The inset shows even more details.

φ_0 and β to develop and investigate a model what junctions with short molecules look like is difficult. Since the real values are not known (remember that reported values differ be a factor of up to three) a valid model could not be established. These difficulties are part of ongoing research.

The electrical break-down of the alkanethiol SAMs was investigated by increasing the voltage until the current reached the short circuit level (Fig.5.8). Typically in a range between 0 and 1.2 V the current increased exponentially as expected for a tunneling characteristics. Above 1.2 V peaks occurred. The current increased to a certain extend and decreased again. In the range below 2 V these peaks increased at most to 300 % of the current. Above 2 V sharp exponential increases of the current could be observed. They were looked like a break-down, but the current decreased again. Typically two or three such sharp peaks occurred. Afterwards the real break-down happened with an increase of the current to that of a short between the two electrodes. In case of Hg/HDT/HDT/Ag [Haag et. al. 1999] observed a exponential increasing current and a clear, steep break-down. Since different electrodes and a thicker organic layer was used, it is difficult to compare these result. In case of the observations reported here electro-migration of gold might lead to the formation of filaments (or parts). These increase the current by decreasing the distance to the other electrode. Once the current flows through these filaments they might be destroyed again. This decreases the current again. Above a certain threshold voltage the filaments might be large enough to make a physical contact to the other electrode. This results in a short between the electrodes. Other phenomena involved in this process might be the temperature increase and electro-stimulated desorption. From the experiments of Xbars on Affinity VP described above it is known, that above a few nA the temperature of the wire is above 50 °C. The heating could lead to a desorption of the molecules.

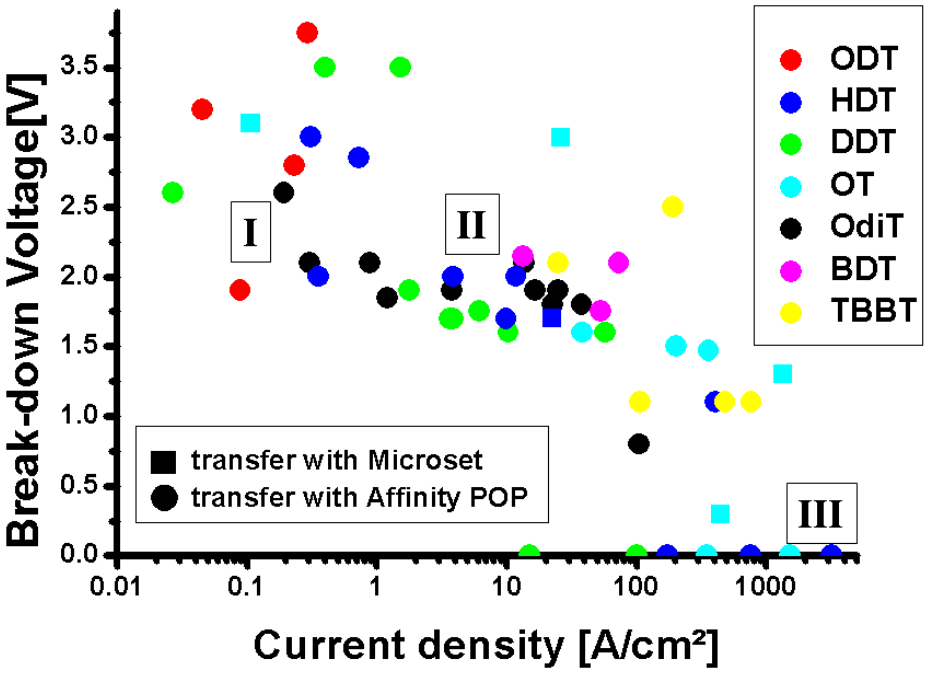

Figure 5.9: Break-down voltage vs. current density for various alkanethiols

The break-down voltage for different molecules was compared using the current density (Fig.5.9). Three distinct regions were observed: I) for current densities below 1 A/cm^2 there was a spread of break-down voltages in the range of 2 - 3.5 V; II) between 1 A/cm^2 and 100 A/cm^2 the break-down voltage was almost independent on the current density; III) above 100 A/cm^2 most junctions showed a strange break-down (indicate as 0 V), or they broke immediately. A dependency on the chain-length could not be determined. There was also no difference between the mono- and dithiols apparent as well as no difference between aliphatic and conjugated molecules. The transfer with Microset PDMS or with POP and heptane did not show any influence as well. [Haag et. al. 1999] reported a dependency of the break-down voltage on the chain length. This can be explained since the chain length influences the current and thus the current density. In addition the electric field is reduced with increasing chain length. They did not observe differences between aliphatic and aromatic molecules, and did not see any difference for different solvents used. This is in agreement with the results obtained here. The absolute value reported by Haag et. al. for a Hg/OT/OT/Au junction was 0.7 ± 0.2 V. This is way smaller the value of around 2 - 3 V that was observed here for HDT. Obviously the stability in their system was mainly determined by the

mercury droplet.

Another observation to be drawn from Fig.5.9 is, that the current density for each molecule has a rather large spread. Ideally it should be more or less identical for junctions with different areas. A dependance between the junction area and the current density could not be observed. Especially for the junctions with short interlayer molecules the density varies by up to three orders of magnitude. This again can only be explained with a "wrong" contact area. For calculating the current density the geometric area was used. Three orders of magnitude in current density mean, that the area was overestimated by a factor of thousand. In other words the contact area was only tenth of a percent. This could be explained consistent with the finding of too large separations observed for the junctions with short molecules. Obviously the distance is influenced by the roughness and thus only some of the molecules are in contact with both electrodes. This seems to be reasonable, since the current densities for ODT are in the same order of magnitude.

Another method to determine the tunneling decay parameter was to compare the single molecule resistance for different molecules. For each measurement the current at 400 mV was plotted against the area of the contact (Fig.5.10). The current observed should scale with the area of the junction. The area was just taken as the product of the two electrode widths. The break-down voltage was used as an additional property of each point. Measurements with a strange break-down, e.g. the break-down did not reach the short current, are indicated by black symbols. They were neglected as well as points with a way to high current. The other points were used to make a linear fit $y(x) = mx$ through zero:

molecule	m [A/μm^2]
ODT	$8.8 \pm 0.6 \cdot 10^{-10}$
HDT	$1.2 \pm 1.1 \cdot 10^{-8}$
DDT	$3.2 \pm 0.8 \cdot 10^{-8}$
OT	$6.2 \pm 0.4 \cdot 10^{-7}$
OdiT	$1.1 \pm 0.4 \cdot 10^{-7}$

For propanethiol and hexanethiol only one non-short circuit junction could be measured and thus a fitting was not possible. Currents at 400 mV bias were taken to calculate the single molecule resistance, assuming that the area is completely covered. Each molecule was assumed to cover 21 Å^2. The values are plotted in Fig.5.11 against the number of CH_2 groups. For propanethiol and hexanethiol the single measurement was used. For octadecane-, hexadecane-, dodecane-, octanethiol and octanedithiol the fitted currents were used. For butanethiol the

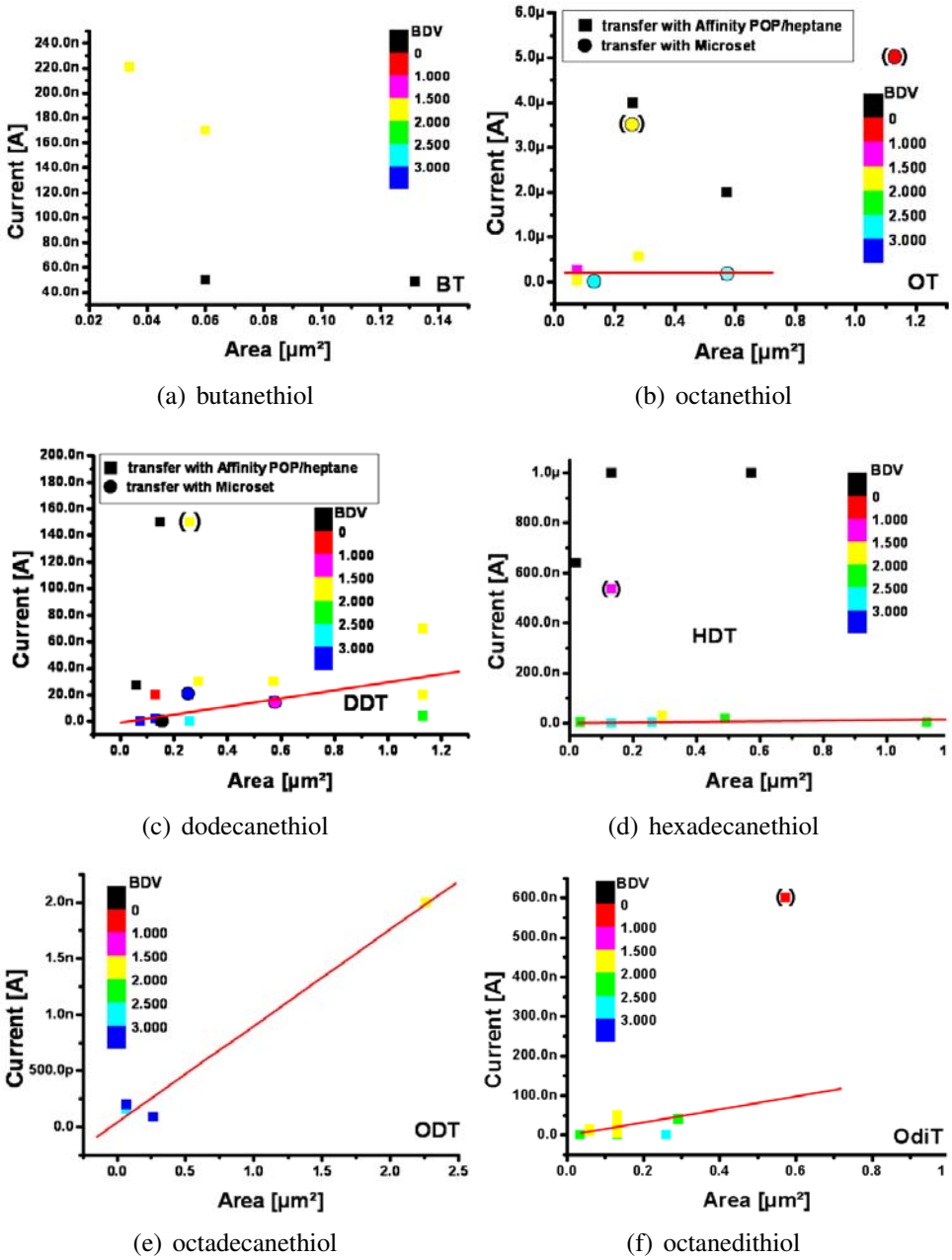

(a) butanethiol (b) octanethiol

(c) dodecanethiol (d) hexadecanethiol

(e) octadecanethiol (f) octanedithiol

Figure 5.10: Current vs. area plots for aliphatic alkanethiols
The red line is a linear fit through zero. The current was measured at 400 mV. The color indicates the break-down voltage of the respective measurement.

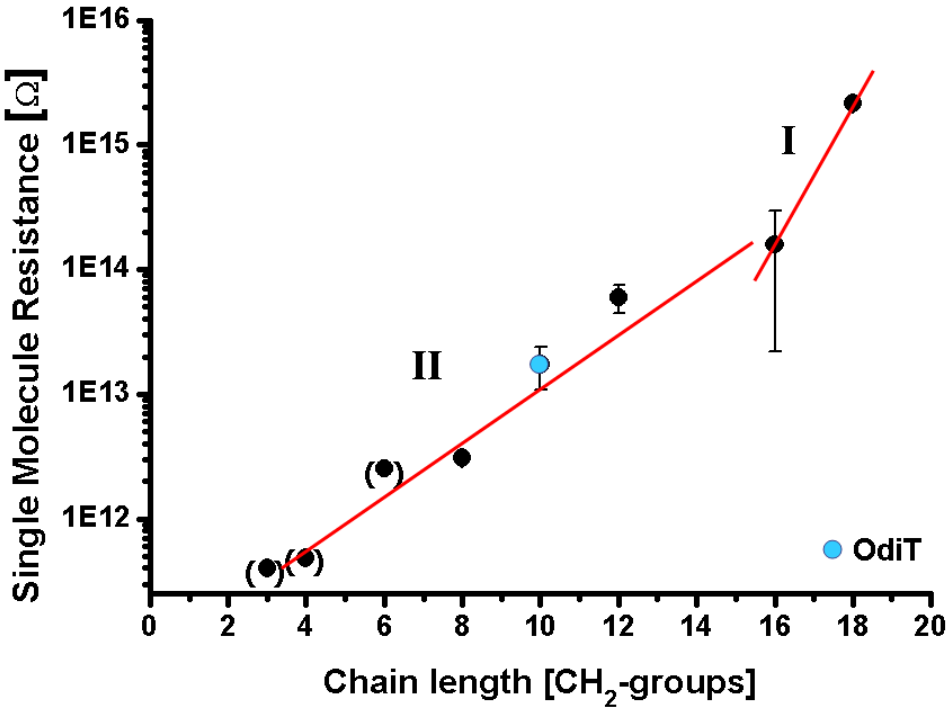

Figure 5.11: Single molecule resistance of *Crossbar* junctions having various alkanethiol interlayers
Note since OdiT is longer than OT it was plotted on the position, which corresponds to its length rather than the number of its CH_2-groups.

mean current was used.

Several effects can be seen in Fig.5.11. For octadecane- and hexadecanethiol a straight line with a slope of 1.13 $Å^{-1}$ can be plotted (I). The slope of this line corresponds to the tunneling parameter β. The single resistance of a octadecanethiol molecule of $4 \cdot 10^{15}\,\Omega$ is close to values reported by other techniques [York et. al. 2003]. Note, that the error-bar for hexadecanethiol is rather large, because the current vs. area plot does not show a clear trend. Therefore within the error the value of β could be between 0.82 $Å^{-1}$ and 2 $Å^{-1}$. A more detailed statistical analysis is not possible since only two points were used for this fit. As discussed before a β value larger 1 $Å^{-1}$ is in the range of reported results [Wang et. al. 2005], although most results were in a range of 0.8 - 0.9 $Å^{-1}$. Junctions with a interlayer of shorter thiols obviously did not follow the same trend (II). The values for dodecane- and octanethiol indicate a slope of around 0.44 $Å^{-1}$. Values for hexane-, butane- and propanethiols seem to confirm this trend. This value is smaller than expected. This is a further indication for a problem of junctions with short molecules. The single molecule resistance for these shorter molecules is too high. This could

simply be caused by overestimating the number of molecules per junction. This is again an indication, that the true contact area is most likely to be smaller than the geometric one.

The dithiol molecule OdiT showed a resistance as expected corresponding to its length. Since the top thiol groups should covalently bind to the top electrode a better contact was expected, thus a larger current resulting in a smaller resistance [Salomon et. al. 2003]. Either the top thiol-gold bond was not formed here, or the effect of a higher current was compensated by an even smaller contact area. This can be explainable using the following idea: Assuming, that the polymeric transfer shuttle is slightly bent, the metal forms a cavity during the first contact. In case of dithiols covalent bonds are formed, thus a closer contact can not be established. In case of monothiols through further force applied the contact area could be increased.

If the concept of not perfect contact between the Xbar electrodes is right, the smallest current density is most likely the true one, since higher current density indicate, that the surface area was overestimated. Using the smallest current density values of octadecane-, dodecane- and octanethiol β becomes 0.85 per methylene-group or 0.74 $Å^{-1}$. This value is in agreement with [Wang et. al. 2005]. This indicates again, that the model of a non perfect contact area suits the problem. In addition this indicates, that the separation apparent in Fig.5.11 into two regions with a different slope is just coincidence in a sense, that something happened between dodecane- and hexadecanethiol junctions. Obviously it should be possible to describe all thiol with one decay parameter. For shorter thiols than octanethiol this trend could not be confirmed. The quantity of non-short circuit junctions was too small (only one or two junctions were found). So just by coincidence none of these junctions showed the real current density. Another explanation could be, that for shorter thiols it even gets more complicated to obtain a full contact. This again would indicate, that the roughness plays a more important role for junction consisting of shorter molecules.

Junctions fabricated by the Microset PDMS transfer or the Affinity VP transfer showed the similar behavior and comparable currents/break-down voltages (Fig.5.10c). Thus both kinds of measurements were taken equally for further calculations. This finding was not expected since [Rampi et. al. 1998] report, that polar solvents such as heptane are trapped between the SAMs of *Mercury-Droplet* junctions. The situation there is slightly different since two SAMs are involved. Obviously such trapping of heptane is not be observed here, since only a single SAM was used.

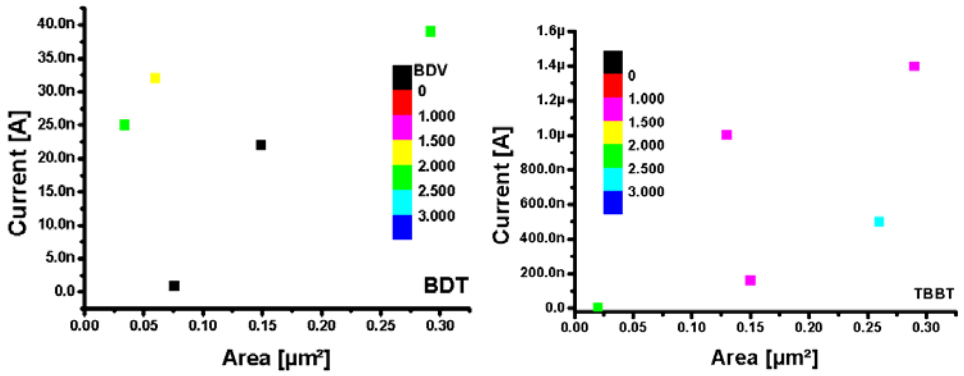

(a) benzenedithiol (b) thiobisbenzenethiol

Figure 5.12: Current vs. area plots for conjugated alkanethiols
The red line is a linear fit through zero. The current was measured at 400 mV.

Furthermore aromatic alkanethiols BDT and TBBT were used as interlayer. Like observed for the aliphatic alkanethiols also here for the rather short BDT most of the junctions formed showed short-circuit behavior, while for the longer TBBT only a few short circuit junctions were observed. Fitting of α and φ_0 revealed similar results as observed for the aliphatic molecules. For BDT φ_0 was found in a range between 1.4 - 2.4 eV, while α was found to be $1.3 - 1.9$. As discussed before such values are none physical. Calculated β values were around 2.4 $Å^{-1}$. For TBBT φ_0 was found in a range between 1.4 - 2.4 eV and α was found in a range between 0.65 - 0.9. Calculated β values were 1.1 - 1.3 $Å^{-1}$. Due to these deviation of α and β as discussed for aliphatic alkanethiols the thickness was fitted using fixed values for α and φ_0. This indicated, that the real distance of the top and bottom electrodes in case of BDT was about 2 nm. The distance in case of TBBT is fitted to approximately 1.8 nm, which is about 4 Å larger than the molecules length. This finding nicely corresponds to the finding for the aliphatic molecules and indicates, that the conjugated molecules are subject to the same effect than the aliphatic ones.

Since the HOMO-LUMO gap for conjugated molecules is only around 3 eV the tunneling efficiency should be higher and thus β should be lower (0.2 - 0.6 $Å^{-1}$). For BDT the current density, breakdown voltage and single molecules resistance was comparable to those of short aliphatic molecules. For TBBT the observed current was similar to that observed for OT, which has approximately the same length. In addition current densities, breakdown voltages and single molecule resistivity were in the same order of magnitude. This indicates, that since BDT and TBBT are shorter than the fitted thickness, the contact between top electrodes and molecules is less than expected. Thus coupling of the molecules π-conjugated system to the electrodes is not established. This explains why the β value corresponds to β of

aliphatic molecules and no conjugated coupling is observed.
In order to investigate the influence of conjugated molecules to the tunneling characteristic molecules with a length of at least 2 nm have to be used. Unfortunately such molecules were not available for these experiments.

In conclusion, it is possible to fabricate Xbar arrays with *Shuttle Transfer Printing* having alkanethiols as molecular interlayer. Current/voltage characteristic clearly showed, that the mechanism of conduction is tunneling. There were no indications for filaments. Tunneling decay parameters, barrier height and effective mass calculated were in agreement with values obtained by different techniques. Nevertheless, for short molecules (shorter than 2 nm) the roughness of electrodes seemed to dominate the characteristic, since the fitted thickness was much larger than the chain length of the molecules. Further indications for a insufficient contact for short molecules were also obtained by other considerations. The break-down of junctions occurred typically above 2 V. Additional information about the surface area and thickness of junctions is needed for more insides. One possibility to obtain such information is by measuring the capacity. The capacity of such a configuration is simply given by:

$$C = \varepsilon_0 \varepsilon_r \frac{A}{d} \tag{5.3}$$

ε_r for thiol SAM is approximately 2.6; assuming the area A to be 500 nm by 500 nm and a C10 SAM with a thickness of 1.2 nm results in a capacity of $5 \cdot 10^{-15}$ F. This is way to small to be measured with the setup used. Larger electrodes with at least five microns would lead to reasonable capacities. However, this measurement could only provide the ratio of area and thickness. Since both parameters are correlated several measurements e.g. impedance spectroscopy have to be used to fully determine both parameters. On the other hand electrode areas could be increase to access the capacitance or they could be decreased to measure real single molecule properties and further limit the influence of defects.

PAMAM Junctions on SiO_2

To further investigate the Xbar junctions dendrimers were used as molecular interlayer. Dendrimers are macromolecules with different functionalities. Here PAMAM-OS dendrimers were used as model system for proteins.

PAMAM-OS dendrimers were applied to bottom electrodes fabricated on siliconoxide as describe in Chapter 4.5.4. Therefore a 1 mM ethanolic solution was used. Top electrodes could be transferred onto this layer. The adhesion of gold onto the PAMAM was much larger than on bare siliconoxide. This is reasonable,

since amino-groups and gold form rather stable bonds. A good adhesion between gold and dendrimer is also reported by [Li et. al. 2005]. Thus Xbar junctions with PAMAM molecules in between were formed. The junctions showed unpredictable, unreproducible results. Some junctions had an ohmic behavior, some tunneling characteristic, some only capacitive behavior and many showed switching events. This different behavior can be attributed to the difficulty to handle thickness of the PAMAM layer. The top electrodes were transferred after a very brief rinsing, because after a longer rinsing the transfer did not work at all. Thus the layer was sometime thick or thinner. Often successive sweeps led to different results. This indicates, that the conformation of the layer changed. This could be for example due to the heating as also observed for Xbars on Affinity VP. [Schreiber 2006] also observed such a behavior for 20 nm thick spin-coated PAMAM layers. Using different generations of dendrimers did not indicate any trend.

In fact the nature of immobilized PAMAM-OS layer is not perfectly understood. PAMAM-OS is a macromolecule with amino groups in the inner part and organo-silicon groups exposed to the outside [Kohli et. al. 2004]. Thus these groups are responsible for the binding to siliconoxide. Since the adhesion of gold onto PAMAM-OS is rather good, this indicates, that somehow amino-groups must be exposed to the outside as well. This indicates a deformation of the dendrimer molecules. For valuable Xbar junctions a very precise interlayer is needed. The formation of precise dendrimer layers is part of ongoing research.

Cytochrome *c* Junctions on SiO_2

Cytochrome *c* was used as an interlayer to demonstrate the applicability of these technique to proteins. Therefore in a first step 1 mM MUA solution was immobi-

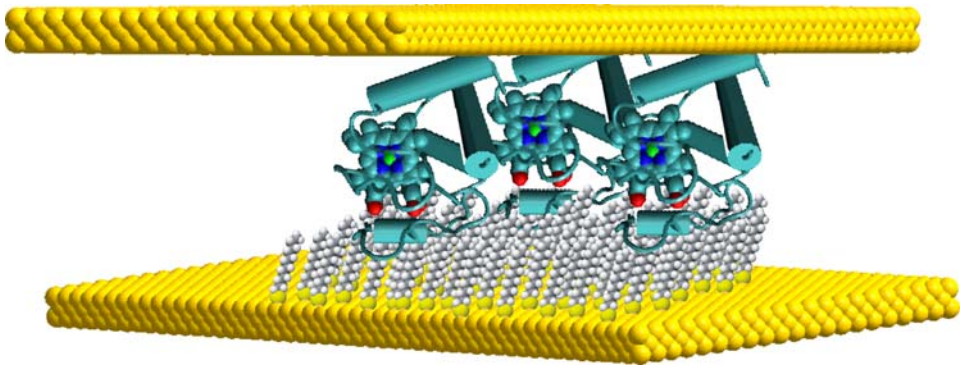

Figure 5.13: Schematic of a Xbar having a cyt *c* interlayer

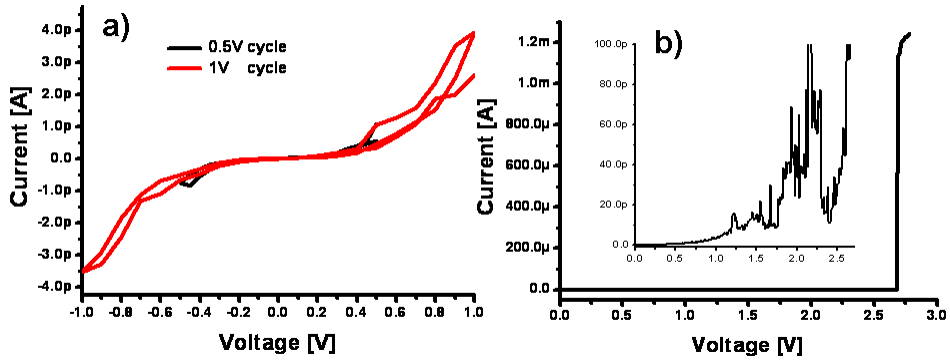

Figure 5.14: Current vs. voltage characteristic for a cytochrome *c* interlayer
Cyt *c* was immobilized on a MUA SAM in a Xbar junction. The transfer was performed with Affinity VP and heptane.
a) IV characteristic for a 0.5 V cycle and a 1 V cycle
b) break-down characteristic; the inset gives the details between 0 - 2.7 V

lized onto the bottom electrode for 10 min as described before. After rinsing bovine heart cytochrome *c* was immobilized onto the MUA SAM via electrostatic interaction. Afterwards the top electrode was transferred using Affinity VP and heptane.

The current vs. voltage characteristic was measured for several junctions as well as the break-down behavior. Tunneling-like behavior was found for all junctions (Fig.5.14). No short circuits were observed. The IV characteristic was very similar to that observed for alkanethiols. In addition very similar break-down voltages could be observed. Taking a closer look onto a plot of the current at 0.4 V against the junction area, two different behaviors can be seen. Points laying on a slope (i) having a "high" current, and points laying on a slope (ii) with less current (Fig.5.15a). The current per area of slope (i) fits into plot (Fig.5.11). It can be assumed that this current corresponds to a SAM having something around ten C-atoms. This indicates, that this behavior corresponds to a pure MUA interlayer, which has eleven C-atoms. A possible explanation is, that there was too much heptane in the junction during the transfer step. This might have somehow removed the cytochrome *c*.

Taking a closer look to the measurements with a lower current reveals, that there is not a clear indication for a certain slope (Fig.5.15b). This might be explained by two facts. Since too much heptane is able to completely remove the cytochrome *c*, smaller amounts might remove it partially. In addition there is the problem of a unknown surface area discussed in the last section. Thus it is not clear which measurements correspond to a full cytochrome *c* layer. Anyway the IV curves of

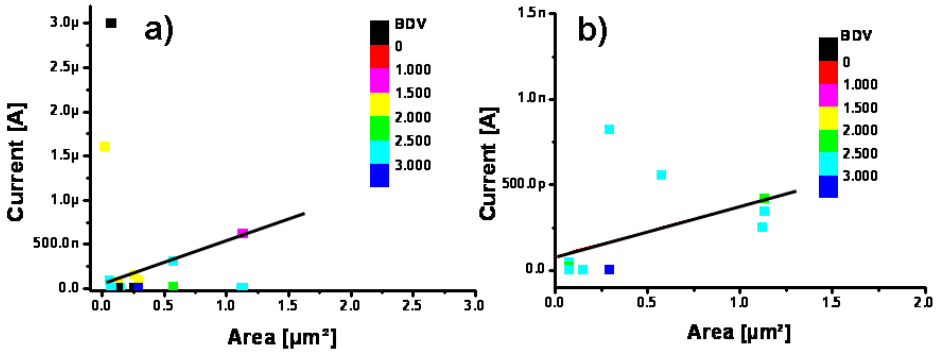

Figure 5.15: Current vs. junction area for a cytochrome c interlayer

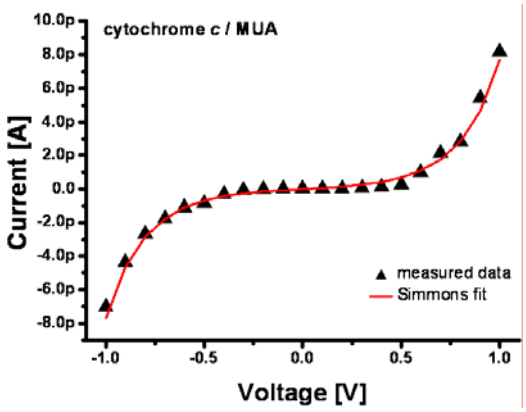

Figure 5.16: Current vs. junction area for a cytochrome c interlayer

such junctions could be fitted using Simmons equation assuming a thickness of 4.8 nm[6] (Fig.5.16). Fitted values for the junctions with low current and appropriate break-down voltage are:

φ_0	α	β
2.2	0.36	0.55
1.6	0.45	0.60
1.6	0.46	0.55
2.6	0.33	0.54
1.3	0.52	0.60

These β values can be harmonized with other reports about the tunneling decay parameter in proteins [Gray et. al. 1995]. In general two processes contribute to the charge transfer through peptides: *Hopping* and *Superexchange*. For short peptides β values of $\sim$1.4 Å^{-1} are reported due to the *Superexchange* mechanism, for longer peptides β decreases to 0.2 Å^{-1} due to the *Hopping* mechanism [Malak et. al. 2004]. This decrease was observed for chains with a length of 2 nm. The β value of 0.5 - 0.6 Å^{-1} observed here suggests, that the *Hopping* mechanism is not dominant. It rather suggests, that the *Superexchange* mechanism makes a major contribution to the overall electron transfer through cyt *c*. A similar observation was reported by [Sek et. al. 2006]. They observed $\beta = 0.5$ for a 3 nm long α-helical peptide and came to the same conclusion. The electron transfer through peptides is still not understood in all details [Long et. al. 2005]. The system of electrode, immobilization layer (MUA), redox protein cyt *c* and top electrode is much more complex than a simple peptide chain on a substrate and thus even more difficult to understand. It is expected, that a stronger electron transfer is present in comparison to proteins without a redox center. Also note, that since cyt *c* was dried and measured in a two electrode setup, the results obtained here can not be 1:1 compared to the electron transfer experiments performed by cyclic voltammetry.
Note, that the problems discussed for alkanethiol interlayers should not contribute here, since the interlayer thickness is much thicker. But it is not clear, whether the junctions with the lower current values correspond to dense cyt *c* layer or are only partial covered. Thus the number of cyt *c* could have been overestimated. Other independent measurements are needed to further confirm these results. Due to the strong correlation between the thickness and β deviations in the thickness directly contribute to the fitted β value. Note, that these measurements could be also fitted with a thickness of 1.8 nm[7] obtaining the same quality for the fit. In that case β=1.2 Å^{-1} is obtained. This would indicate a pure alkanethiol interlayer. The lower currents observed for these junctions however indicate, that the thickness of

[6] cyt c $\approx$ 3 nm + MUA $\approx$ 1.8 nm
[7] =thickness of MUA

4.8 nm is more likely to be true value.

Another approach taken to analyze the data was fitting a linear slope through all points in Fig.5.15b) with low current behavior. By assuming a dense cyt *c* layer a current of 0.9 fA can be estimated for each molecule. Just assuming, that the MUA and cyt *c* form an alkanethiol-like tunneling barrier (4.8nm thick), the current should be smaller by several orders of magnitude. This is in agreement with the expectation, that the tunneling rates will be enhanced by transitions that involve redox processes [Lindsay 2005]. The absolute value of 0.9 fA however is by 3-4 orders of magnitude larger than expected. The value for the electron transfer for cyt *c* is approximately $3\,s^{-1}$ [Salomon 2006]. But these values were measured in buffer solution by means of EC methods. Here the protein is in a dry state and the setup having bottom and top electrode contacts is different to the typical three electrode EC setup. Thus the results are not comparable.

A first demonstration of *Crossbar* junctions having a MUA/cytochrome c interlayer could be given. Junctions showed tunneling like behavior. Part of the junctions were found to have a larger current. These junctions had the same characteristic than pure alkanethiol junctions. Thus it is concluded, that these junctions correspond to a bare MUA layer, where the cyt *c* was washed away during fabrication. The junctions with a low current behavior were fitted with Simmons equation. β=0.5 - $0.6\,Å^{-1}$ were obtained for these junctions. This indicates, that the *Superexchanges* mechanism plays a major roll in the electron transfer. Further investigations, experiments and analysis to fully determine and understand the behavior of these junction are part of ongoing research.

Chapter 6

Nanocontact Printing for patterned Cell Culture

A major effort in Bio-Electronics is the growth of defined neuronal networks via the culture of neurons. Such networks could be for example combined with silicon based electronic components [Lauer et. al. 2001]. Two approaches to be used to bring patterning into the growth of neurons: *bottom-up* and *top-down*. The *bottom-up* approach investigates the conditions needed for cells to adhere to a substrate. Individual focal adhesion points were addressed by means of nano-structures [Spatz 2003]. The *top-down* approach uses μCP to pattern proteins, that guide the growth of neurons and neurites, by introducing a gradient between cell adhesive and cell aversive sites. If the substrate is cell aversive neurons will exclusively grow on the patterns of cell adhesion protein. In addition neurites will only grow along patterns. Typical cell adhesive biomolecules used are polylysine, laminin or ECM gel. Printing so far was exclusively done with PDMS stamps. Since the critical dimensions of patterns that can be achieved with μCP were expanded by introducing new stamp materials and techniques a combination between the top-down and bottom-up approach was pursued.

Two questions were addressed in the framework of this thesis:
Are the new developed printing methods and stamp materials compatible with cell culture conditions?
Can the growth be affected by patterns having dimensions below one micron?

Therefore *Wet Inking* with Affinity VP and Surlyn stamps using a mixture of poly-D-lysine and ECM gel solution was performed onto glass cover slips. After printing rat neurons were plated onto these cover slips. This process is described in full details by [Decker 2006]. After 12 days in cell culture the cell were fixated

according to [Hoeller 2005] and investigated with the SEM.
The first observation was, that neurons grow on protein patterns transferred with Affinity VP or Surlyn stamps. Cell vitality does not seem to be reduced. Thus the used stamp materials are not cell toxic. The cell density however, was very low. Although *Wet Inking* was used, the amount of proteins transferred seems to be less than with PDMS stamp. The transfer process with Affinity VP and Surlyn stamps was not further optimized and investigated here. This is part of ongoing research.
The influence of the pattern design and dimensions was tested by using stamps with the pattern shown in Fig.B.4. Fig.6.1a) and c) show neurons growing on this pattern. Due to the low coverage only a few neurons on the pattern could be observed. The neurons growing on the pattern were attached to the area with the largest patterns. This seems to be reasonable, since the neurons, obviously prefer the areas with the highest protein coverage per area. Another observation is, that some directions seem to be preferred for the growth of branches. Fig.6.1a) shows eight branches growing in the direction of the line pattern, three perpendicular and four in other directions. Fig.6.1c) shows five branches in line direction, one perpendicular and three in any other direction. Eight out of thirteen of the branches grew in line direction grew on the lines having a width of one micron, two branches grew on the lines with a width of 800 nm and one branch on the right hand side of c) follows a zigzag between the micron line and 800 nm lines. This is a clear indication, that neurites seem to be prefer protein patterns broader than 800 nm. Two branches grew along the 75 nm lines in the **Variable Both** and **Variable Gap** region respective. Since printing was done with an Affinity VP stamps pairing is expected for these patterns (compare Fig.4.22). Thus the patterns there were much broader or completely filled with proteins. Fig.6.1d) shows, that at 1 μm to 600 nm lines a separating of branches occurred. Single neurites grew perpendicular out of a broader bundle. Fig.6.1b) shows, that near a one by one micron pattern a splitting of a bundle occurred.
These result indicate, that the methods and materials introduced in Chapter 4 are compatible with the needs for cell culture, namely a process under sterile conditions and non-cell-toxic materials. Furthermore sub five micron pattern can be used to introduce certain effects such as guiding, separation or splitting. The design Fig.B.4 is not specific enough to fully determine the dependency but gives some first indications for interesting phenomena to occur. A new design based on the transfer of sub 50 nm patterns to directly address focal adhesion points combined into larger patterns to guide the growth is part of ongoing research, but the results obtained here are very promising for this further research.

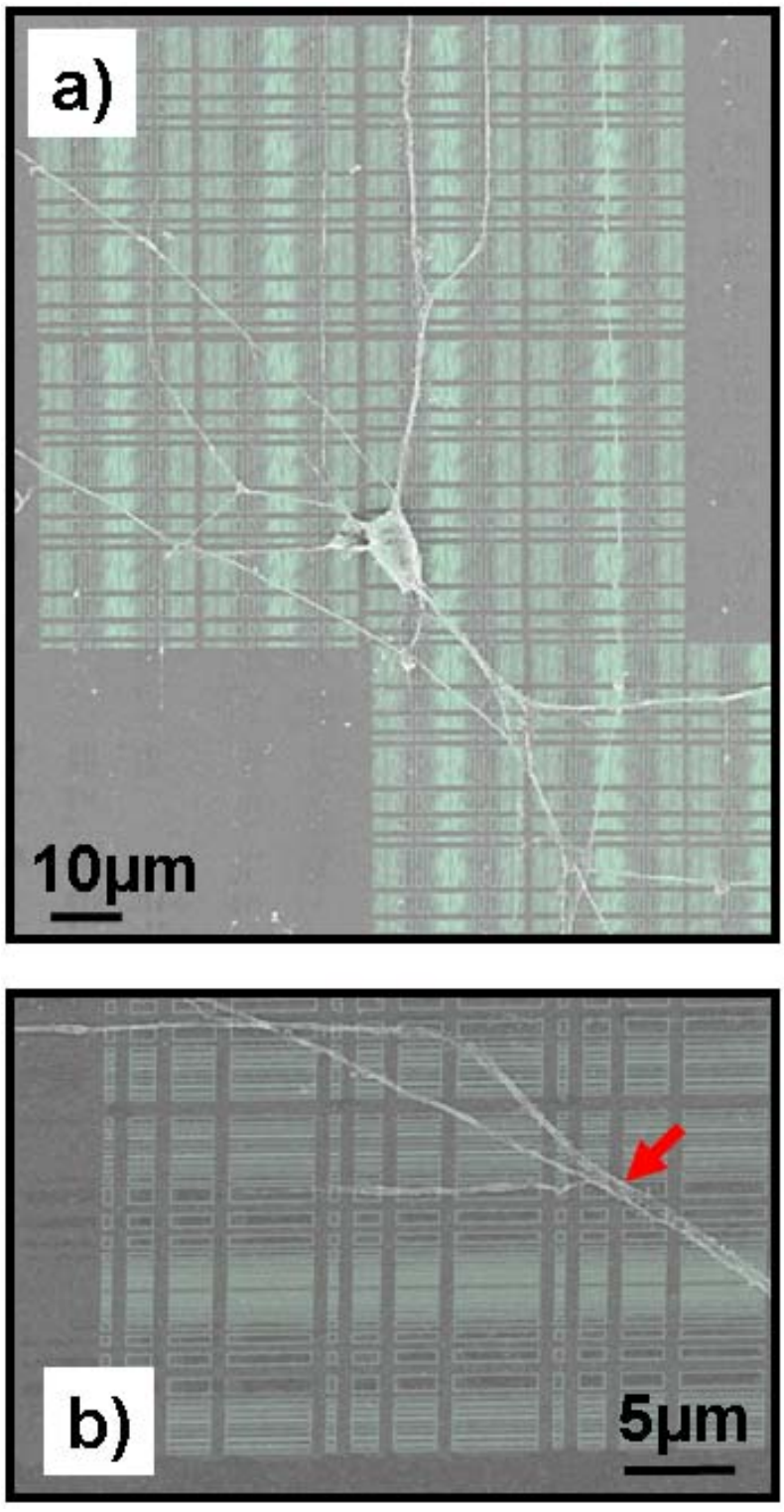

Figure 6.1: SEM images (10 kV) of neurons cultured on patterned proteins
Polylysine/ECM gel was printed onto a glass coverslip with an Affinity VP stamp. After fixation a gold film was deposited onto the sample. The pattern design (green lines) was superimposed with the images to guide the eye.

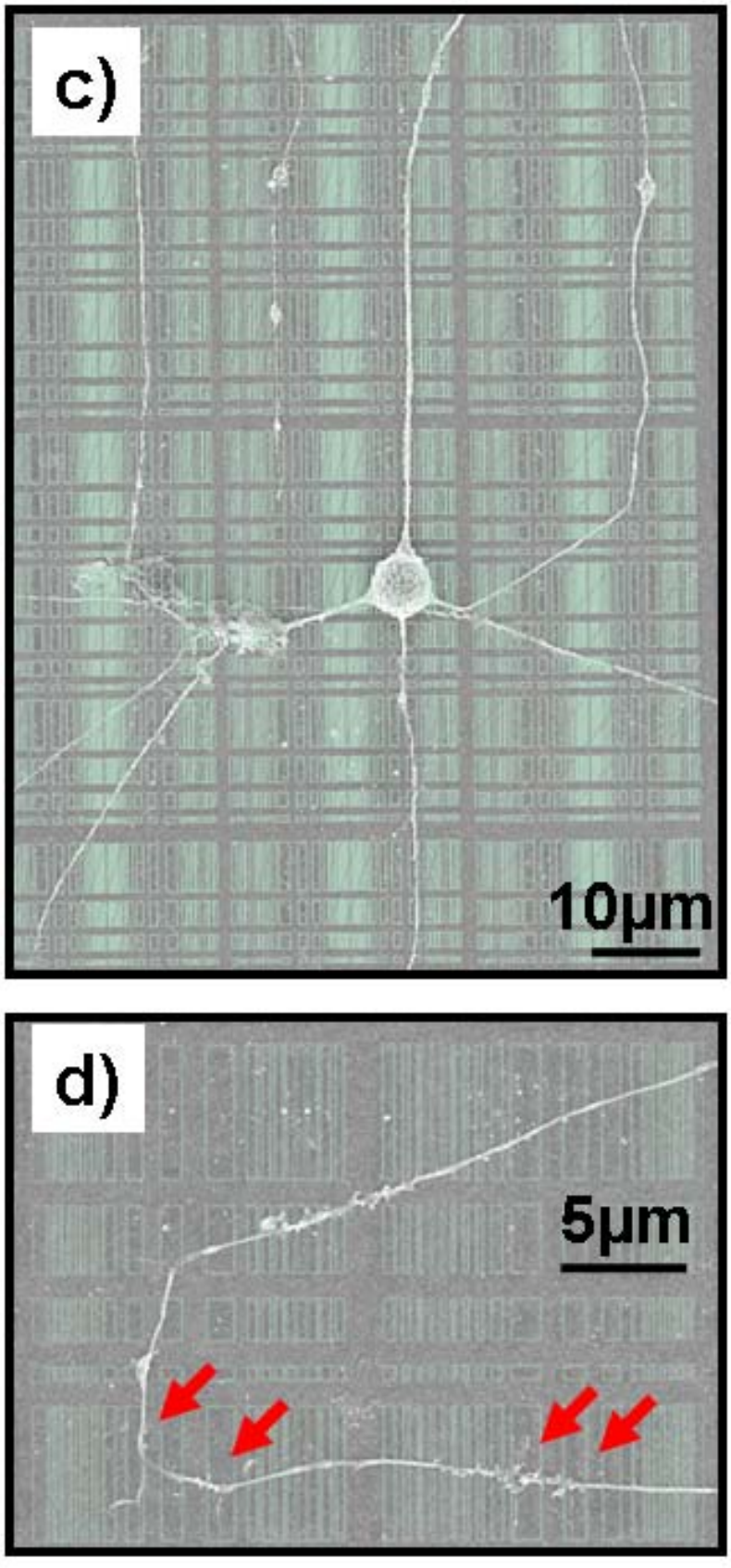
c)
10µm
d)
5µm

Chapter 7

Conclusion and Outlook

The aim of this thesis was establishing *Soft Lithography*, mainly *Microcontact Printing*, as a powerful patterning technique for *Molecular* and *Bio-Electronics*. Especially patterns having sub 100 nm dimensions were subject of this thesis. Therefore a main issue addressed was the adoption of stamp materials with a Young´s modulus larger than 100 MPa that allowed the transfer of patterns with low critical dimensions. The Young´s modulus of these materials was more than an order of magnitude larger than that of materials commonly used. From a functional point of view emphasis was laid on the transfer of proteins. A process was to be developed that allowed the transfer of fully functional protein patterns. In addition the influence of *Contact Inking* on the functionality of transferred proteins was investigated. Beside that, protein patterns were used to demonstrate the influence of sub 1 μm patterns on the cell culture of neurons. Another major object of this thesis was the establishment of a technique to transfer metal patterns to arbitrary surfaces. Commonly used methods only work with a specific choice of stamp material, metal and target surface. The concept proposed and demonstrated in this thesis was more universal. *Crossbar* junctions having molecular interlayers were demonstrated as one application for this process.

The following paragraphs will shortly summarize the findings of this thesis:

- A design based on single lines having different widths and gaps proved to be useful for the investigation of different effects. *Pairing*, *Sagging*, *Diffusion* as well as the results of EBL and etching could easily be analyzed by comparing SEM or AFM images with the nominal design. The dimensions of patterns, where problems occurred were estimated by just counting the lines and comparing the result with their nominal size.

- EBL and RIE proved to be the ideal combination for the fabrication of mas-

ters. HSQ resist was found to be very difficult to apply for the designs used in this thesis. An ideal set of process parameters could not be established. Proximity correction, which was found to be a critical issue for HSQ, did not lead to the expected improvements.
PMMA resist on the other hand provided good results after EBL. However, the development of exposed patterns turned out to be a critical issue. Resist residues stayed especially inside the smaller trenches. These residues could be removed by applying a megasonic treatment with 2 MHz and 300 W.
Etching of polysilicon using a ICP RIE process with a HBr plasma provided good selectivity against PMMA and HSQ. The polysilicon was completely etched through to a siliconnitrid etch stop. The nitride was not harmed at all. Thus the bottom of the trenches was very smooth and plane, thus fulfilling the major requirements. The edges of the patterns were slightly tilted. Performing the etch process in 30 s runs was found to be necessary to avoid melting and deformation of the PMMA resist pattern.

- Vacuum deposition of TFTS proved to be the ideal process for covering the master surface with a release agent. No sticking or damage of stamps was observed, as well as no decrease of quality even after fifty *Hot Embossing* or *Casting* cycles. A slow evaporation process of the silane at 4.5 kPa provided better result than a process performed at lower vacuum pressures and thus higher silane vapor pressures. A smooth, complete coverage was observed with AFM. Liquid deposition of silanes as well as the vapor deposition of NFDC were found to leave aggregates up to 50 nm and more on the surface.

- Stamps made of various types of PDMS fabricated by a *Casting* process showed pairing of small patterns. This pairing is in good agreement with various publications and theoretical predictions. As predicted pairing for h-PDMS was found to be less pronounced than for Sylgard 184. A self-build *Hot Embossing* device made of glass was successfully used to replicate stamps. Affinity VP stamps fabricated by *Hot Embossing* were found to be subject to pairing. This was puzzling since it cannot be harmonized with the theories describing pairing observed for PDMS stamps. Since the Young´s modulus of Affinity VP is 80 times larger than for PDMS, no pairing should occur. Materials with a larger Young´s modulus such as Surlyn, Topas, Zeonor, Zeonex and Plexiglas were also successfully patterned by means of *Hot Embossing*. The patterns were faithfully replicated and no pairing for the design used was observed. While for Surlyn the shape of rectangular trenches was not exactly reproduced, for Topas and other materials the shape of patterns was almost rectangular.

- The transfer of alkanethiols with PDMS stamp was found to be comparable with the findings of various other groups. Diffusion in the order of 4 nm per second was observed. Longer printing times resulted in larger diffusion areas. Applying an extra load onto the stamp during the printing step was also found to increase diffusion as expected. However, for Affinity VP stamps diffusion was less pronounced. This can be explained by the different composition of the thermoplastic material compared to the rubber PDMS. Printing with Surlyn stamps resulted in a very precise, reproducible edge transfer of the thiol molecules. This is attributed to a different wetting behavior due to the smaller hydrophobicity. A 1 μm broad line was used to create 60 nm pattern. Surlyn is stiffer than all stamp materials used so far in μCP. For printing an extra load of up to 0.1 MPa was needed.
  For printing of proteins no pattern enlargement due to diffusion could be found as expected. Longer printing times were needed for a complete transfer. The formation of a dense layer was found to depend on the stamp material used. In case of cytochrome *c* Surlyn was the material of choice. Sagging was observed for the *Wet Inking* with PDMS stamp, but it could not be explained by any of the theories describing sagging. For all other stamp materials *Wet Inking* was applicable without any sagging occurring for the used pattern designs.
  For the first time *Contact Inking* of proteins was demonstrated. AFM images proved, that the thickness of cytochrome *c* was not changed through the transfer. The functionality of the protein, namely the redox activity was partially destroyed. However, the redox activity was found to be that fragile, that it was even lost after *Wet Inking*. Another kind of functionality, namely the antibody recognition was found to be still functional after *Contact Inking*. This was proven by a antibody staining of printed mouse laminin. For cytochrome *c* a dependency of protein aggregation on the buffer concentration after printing was found. A high buffer concentration led to large agglomerations, while for a low concentration a dense monolayer was formed. This is in good agreement with other measurements and theory.

- The conservation of the functionality of fragile proteins was further investigated using the redox activity of cytochrome *c*. A novel process called *In-situ Microcontact Printing* was developed. All process steps were performed in a buffer solution and thus a drying of the proteins was avoided. It was shown, that this process is capable of transferring the protein under full conservation of their functionality, while still being able to pattern them. Patterns of 150 nm have been demonstrated. The redox activity was found to to be comparable to proteins adsorbed from solution.

- A novel process called *Air-Cushion Microcontact Printing* was demonstrated

based on the *Air Cushion Press* used for NIL. With this process for the first time materials with a Young´s modulus larger 1 GPa were used for as stamp materials in μCP. Different materials tested all gave comparable transfer results for cytochrome *c* or octadecanethiol. A certain pressure was needed to obtain a perfect transfer for all patterns. This pressure made the stamp compensate some minor defects, imperfections or dust grains. As expected a dependency on the thickness of the stamps and the applied pressure could be found. For very high pressures a complete sagging comparable to the Overpressure μCP was seen. It resulted in 60 nm patterns not covered with proteins.
With hard stamp materials a transfer of sub 30 nm protein patterns was achieved. Further investigations indicated, that the roughness of these patterns is determined by the structure of the domains on the substrate.

- A novel process called *Shuttle-Transfer Printing* was developed to address the transfer of patterned metal films to arbitrary target surfaces. Therefore a system having gradient of adhesion was applied. The transfer of gold electrodes to form *Crossbar* junctions was demonstrated as model application. The gold electrodes were fabricated on a fluoro-silane layer and were transferred with PDMS, Affinity VP or Surlyn from the silane layer to another substrate. This substrate already had a pattern of gold electrodes modified with organic molecules. Thus crossbars with molecular interlayers were formed.

- *Crossbars* electrodes transferred onto Affinity VP slabs showed a resistivity as expected for thin gold films. However, for larger voltages/currents melting of the POP was observed.
  Currents observed for alkanethiol junctions showed tunneling behavior. No indication for filaments was observed. Fitting of the measured characteristics using Simmons equation indicated tunneling parameters in agreement with other publications for long thiols (ODT and HDT). For shorter thiols the roughness of electrodes seems to dominate the characteristics. Breakdown voltages between 1 -3 V were observed. Calculated single molecule resistances further proved the indications found by applying Simmons equation. For ODT and HDT the values were reasonable, while for shorter thiols the resistance was too high, indicating an overestimation of the number of molecules contributing to the charge transfer. For conjugated thiols an improved charge transfer was not observed. This was expected, since they were much shorter than HDT and thus the roughness made the major contribution. For MUA/cyt *c* interlayers two major trends were found. Some junctions showed a current similar to that of alkanethiols. It is assumed, that for these junctions the cyt *c* was washed away due to fabrication issues and only the bare MUA contributed to the transfer. Other junctions showed a much smaller

current. These junctions showed tunneling behavior. The decay parameter indicates, that *Superexchange* mechanism makes a major contributing to the charge transfer of cyt *c*. The current per cyt *c* was found to be 0.9 fA. Although this is larger than the electron transfer observed by EC methods, they seem to be reasonable, since a different setup was used.

- The culture of neurons on transferred cell adhesion proteins was possible. The density of neurons on these patterns was found to be rather low. However, the neurons observed were attached to the largest patterns. The growth of neurites was found to be preferably in direction of patterns. There neurites especially followed the 1 μm and 800 nm lines. For a neurite bundle growing perpendicular to the pattern direction separations at the 1 μm and 800 nm were observed.

The designs and patterns proposed here can and will be further miniaturized. Ultimate limitations given by EBL and RIE are in the range of 10 - 15 nm. With hard stamp materials as proposed here such patterns should be reproducable in a precise manner. Having such stamps there is no obvious reason why a transfer of 15 nm or 10 nm protein patterns should not be possible. In addition there are many other thermoplastic materials, which can be applied as stamp materials. New effects, such as the edge transfer obtained with Surlyn, might be observed for other materials, using other inks. Using *Air-Cushion µCP* the stamp material is no longer restricted to elastomeric and thermoplastic materials. In principle other polymers and even solids should be applicable as long as they are thin and flexible enough to somehow conform to the substrate. *In-situ µCP* was only demonstrated on one system up to now, namely the printing of cytochrome *c* onto MUA covered gold, but there is no obvious limitation to this system. A variety of other systems or applications could make use of this process. Proteins printed under full conservation of functionality might be used for several applications. Protein patterns with sub 1 μm dimensions seem to influence the growth of neurons and neurites. These phenomena can be further investigated using more sophisticated pattern designs. Sub 50 nm patterns can be utilized to further investigate the cell attachment and neurite growth. *Shuttle-Transfer Printing* might be useful for several applications. There is no obvious reason, why this process should only work for the transfer of gold. To increase the yield of the gold transfer, further experiments are needed to find better suited transfer-mediating layers and surface treatments for the target substrate, increasing the adhesion. More investigations are necessary to fully determine the behavior and characteristics of *Crossbar* junctions formed by *Shuttle-Transfer Printing*. However other molecular interlayers can be applied for further investigations, especially molecules longer than 2 nm should be used. The roughness of the electrodes could be reduced by different evaporation or post-evaporation processes. In addition there is no obvious limitation to gold as electrode material. Finally *Crossbar Arrays* could be used for logic operations and integrated into *Silicon Technology* processes.

The application, utilization and expansion of the methods developed here for *Molecular* and *Bio-Electronics* is part of ongoing research.

Appendix A

Images

Master

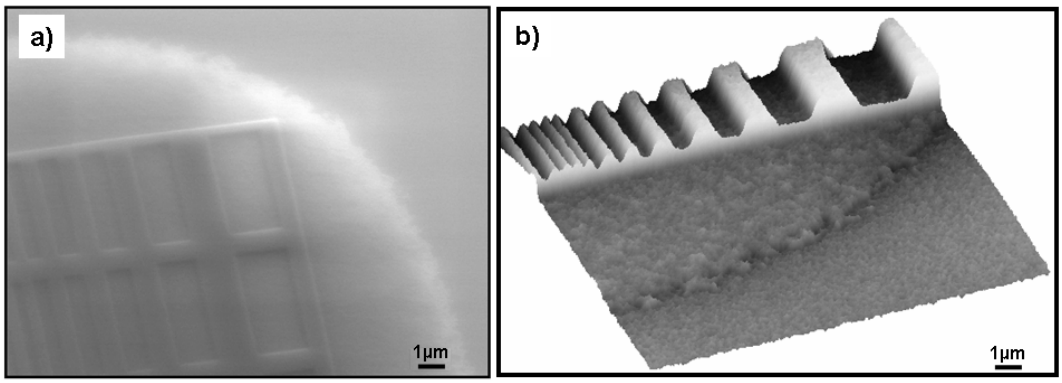

Figure A.1: Proximity effect observed with HSQ resist
a) SEM image (10 kV) of HSQ on a silicon wafer pattern with the design Fig.B.3
b) Tapping mode AFM image of the same surface. The height scale of the image is 300 nm.

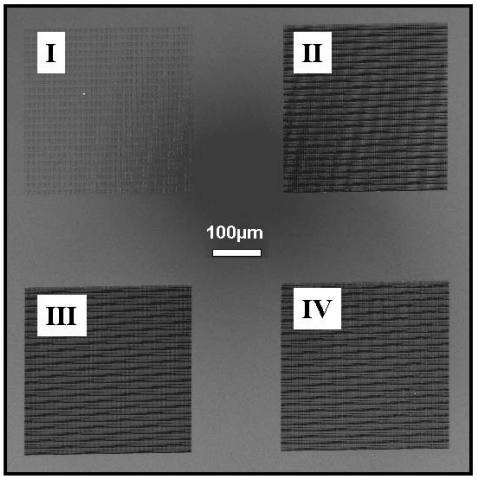

Figure A.2: Arrangement of the design B.4 for HSQ
SEM image (10 kV) of HSQ on a polysilicon surface after HBr-RIE etching
I) Design B.5 II) Variable Gap
III) Variable Width IV) Variable Both

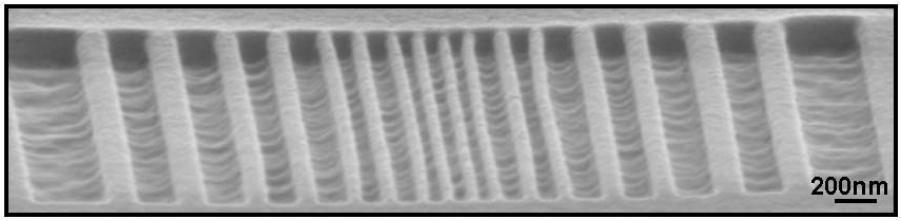

Figure A.3: SEM image (10 kV) of a PMMA master developed using a 1MHz megasonic process at 35 % power. The image is taken under a 70 ° angle with the SE2 detector.

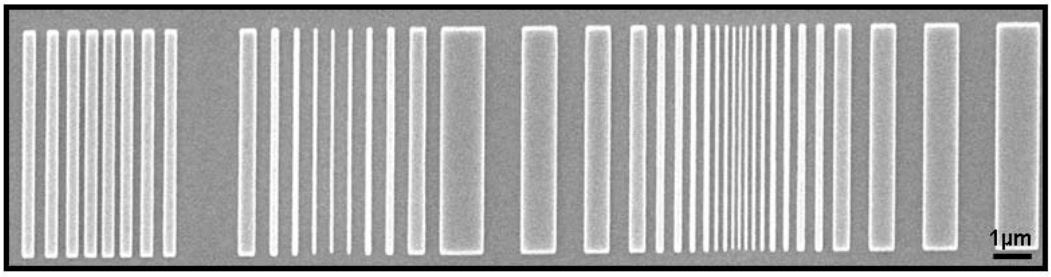

Figure A.4: SEM image (10 kV) of PMMA patterned with the inverted design Fig.B.4 Compared to the PMMA patterns presented in Chapter 4 here the an inverted pattern was written. Nevertheless, the pattern looks well exposed and developed. A sputtered gold film was deposited onto the PMMA for imaging.

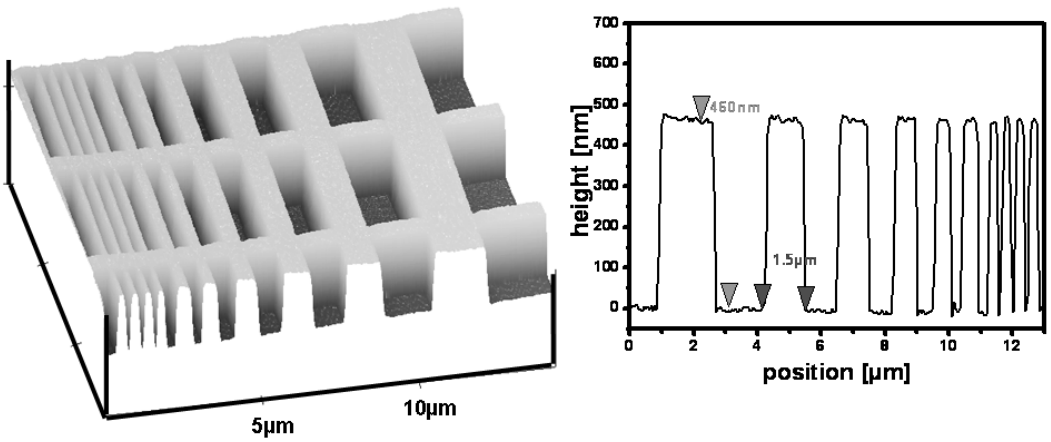

Figure A.5: AFM image of PMMA patterned on silicon with the design Fig.B.3
Due to geometry of the tip the 200 nm broad trenches could not be completely resolved.

Release Agent

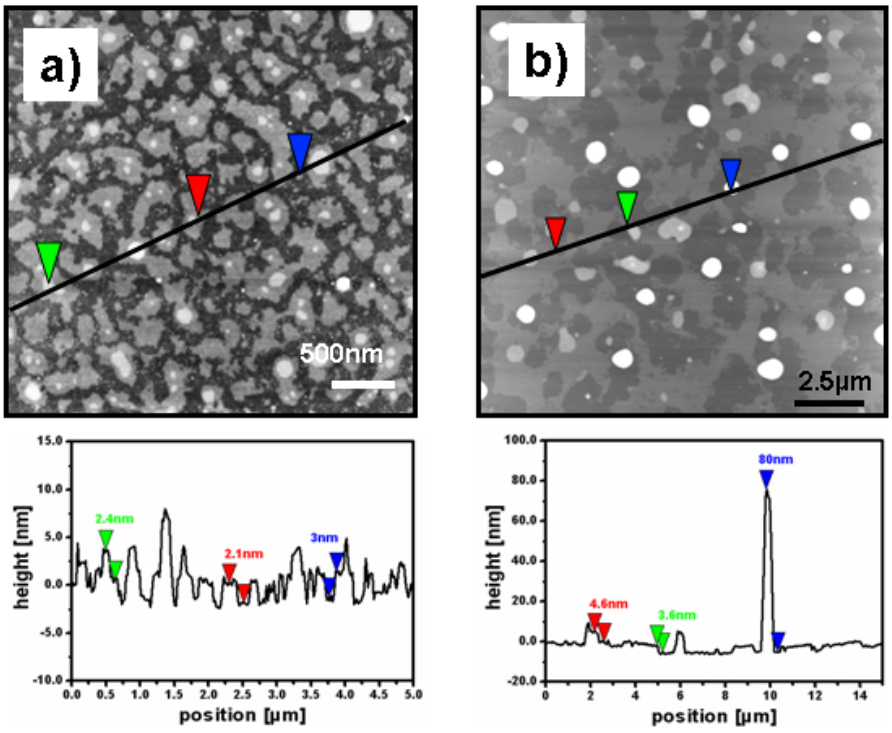

Figure A.6: AFM image of a fluoro-silanized surfaces
TFTS deposited onto siliconoxide surfaces by vapor deposition (results obtained before the glovebox was used) imaged by tapping AFM
a) 4.5 kPa for 1 h; z-scale (white contrast) 20 nm
b) 100 Pa for 1 h; z-scale (white contrast) 150 nm

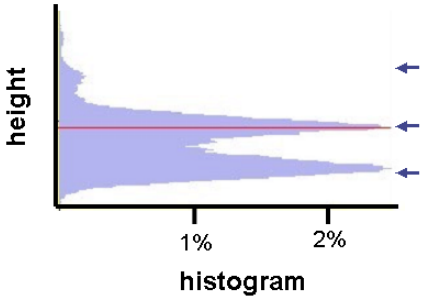

Figure A.7: Histogram of the depths of Fig.A.6a)
Three distinct equidistant heights can be seen. These might correspond to substrate, monolayer and bilayer respective.

Stamps

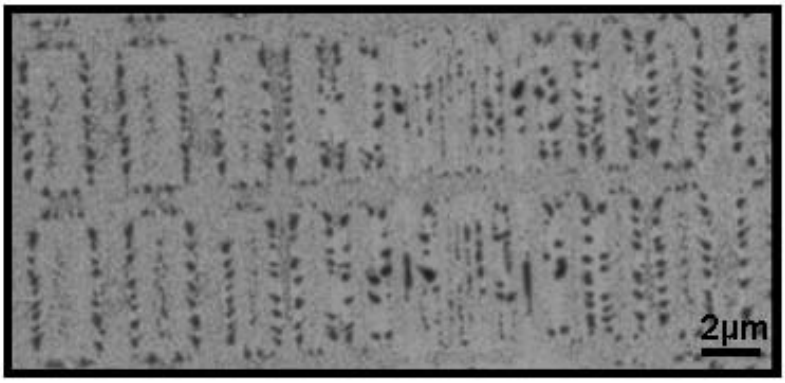

Figure A.8: SEM image (2kV) of residual transfer with Microset PDMS
A Microset stamp was prepared as described in Chapter 4. It was brought into conformal contact with a gold surface without applying an ink. Clearly a pattern transfer can be seen which is due to non-crosslinked PDMS residues.

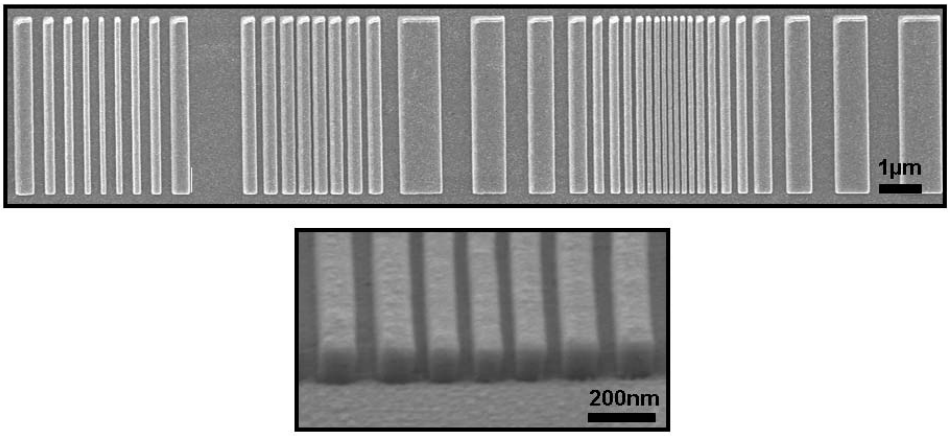

Figure A.9: SEM images (10 kV) of a Topas stamp
Topas embossed at 140 °*C* and 0.2 MPa with a depth of 100 nm and design Fig.B.4. The stamp was covered with a sputtered gold film. The lower images shows a magnification under a 70 ° angle.

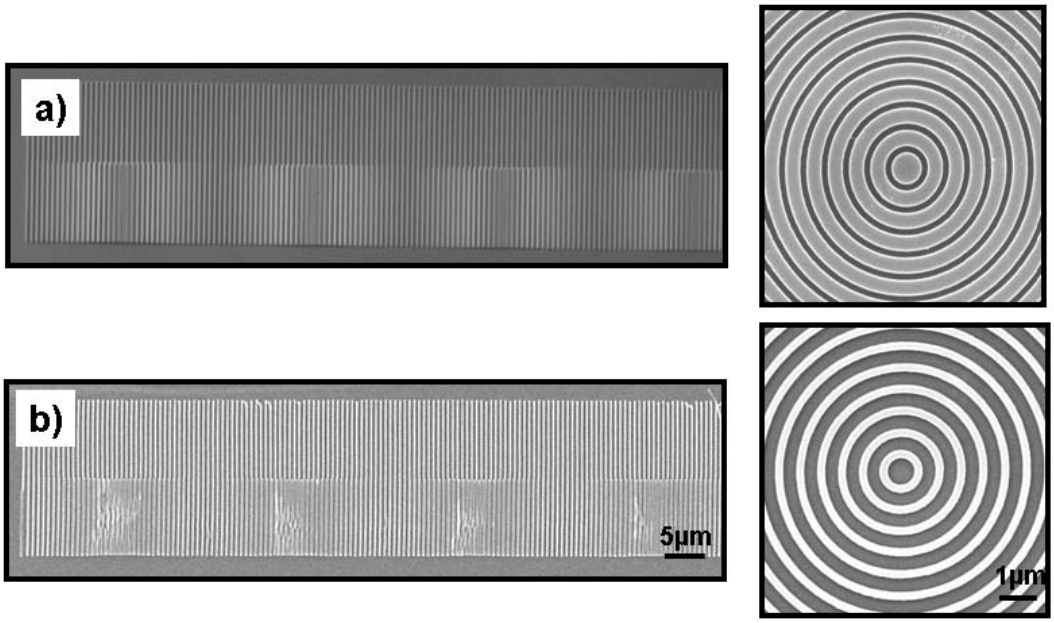

Figure A.10: SEM images (10 kV) of master and stamps with Moire patterns according to [Moers 2006]
the line width is 200 nm, the pitch is 750 nm
a) master patterned with PMMA and etched with the CHF_3/CF_4 process
b) Surlyn stamp embossed with the master of a)

Printed Patterns

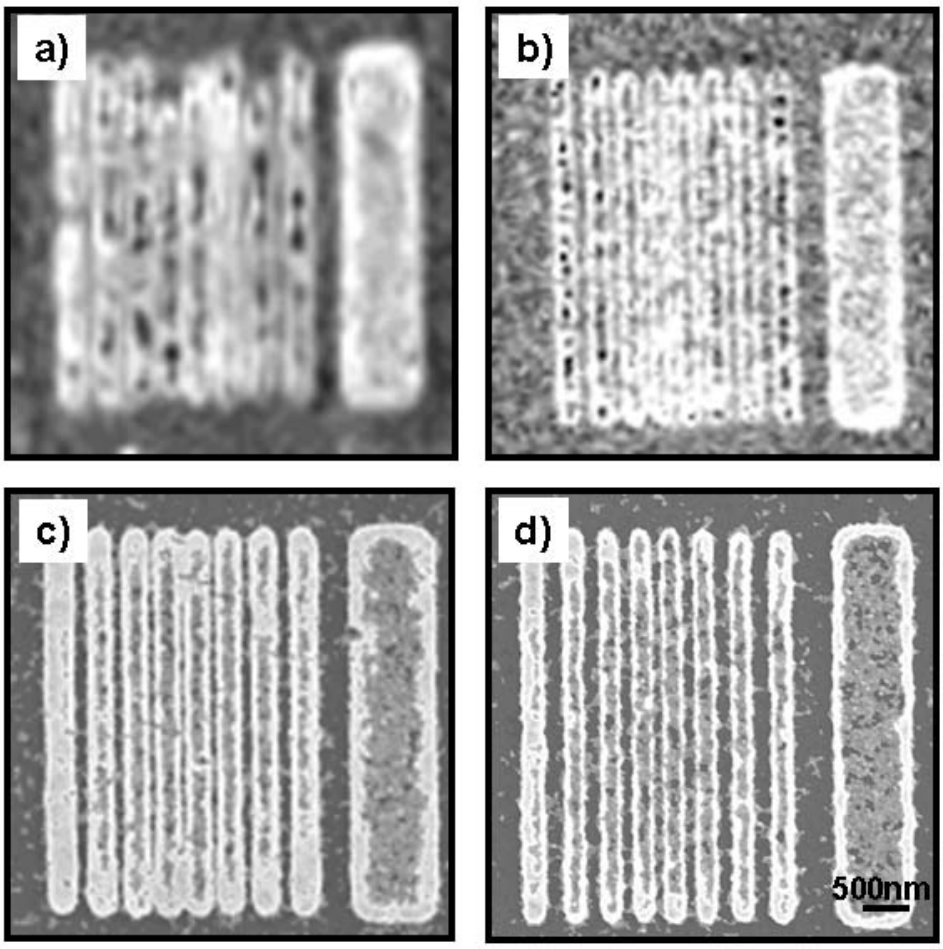

Figure A.11: Variation of printing time for ODT
ODT printed onto a gold substrate using a Surlyn stamp Fig.B.4
contact inking: the stamp was in contact with the inkpad for 2 min
a) SEM image of ODT on gold; contact between gold and stamp 2 min
b) SEM image of ODT on gold; contact between gold and stamp 1 min
c) and d) SEM images of a) and b) after etching the gold

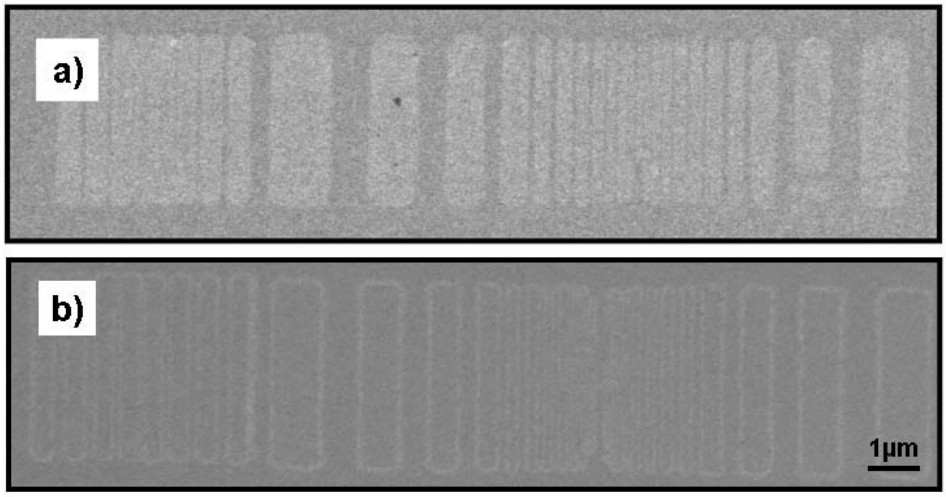

Figure A.12: SEM images (2 kV) of a chemical contrast on a gold surface
ODT was printed onto a gold substrate
a) with a POP stamp. Afterwards it was immersed into a mercapto-undecanoic acid solution
b) with a Surlyn stamp. Afterwards it was immersed into a benzenedithiol solution

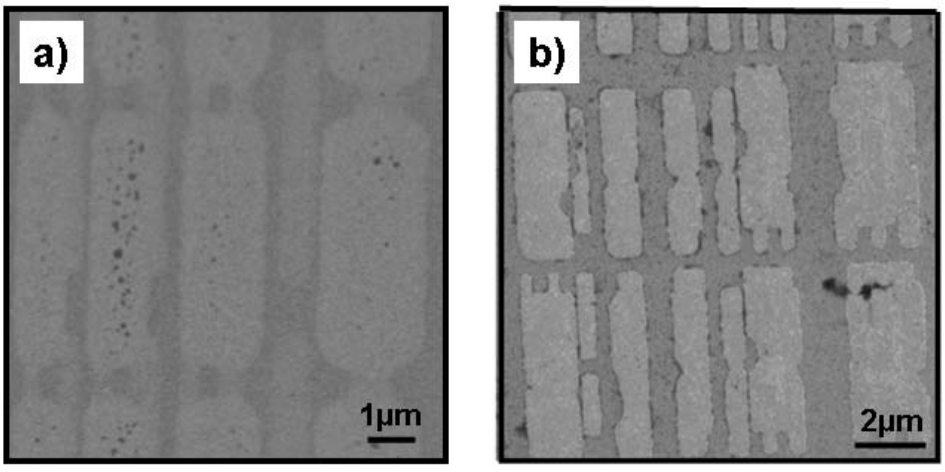

Figure A.13: SEM images (2 kV) of multiple prints
Accidentally the stamp moved will printing resulting in two contact sites leaving two patterns displaced by a few microns.
a) ODT on gold b) ODT was printed onto gold. The gold was etched in a cyanide solution leaving a gold pattern on silicon.

Miscellaneous

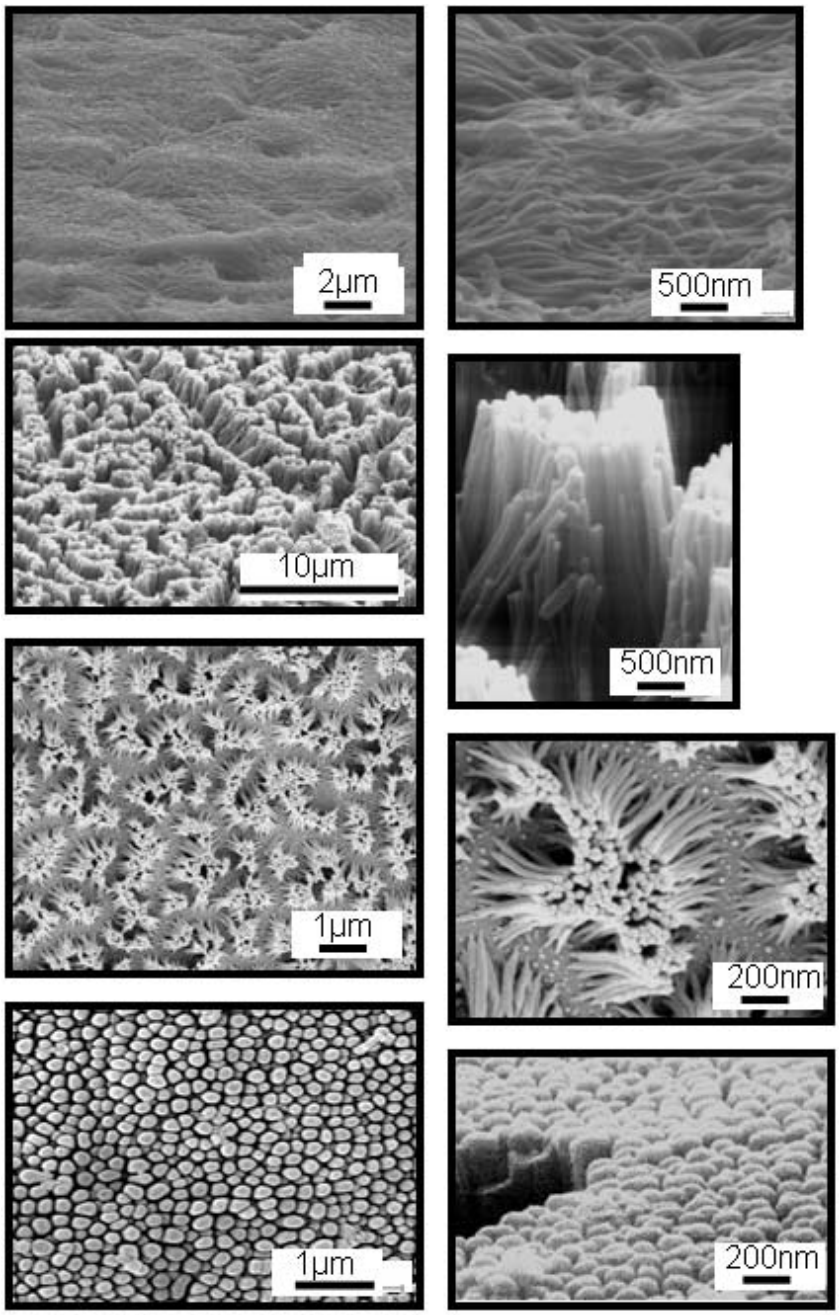

Figure A.14: *Hot Embossing* of polymers into porous Aluminum layer
Topas was hot embossed into porous aluminum membranes with different pore size, distance and depth. From top to bottom of the image the aspect ratio gets smaller

Air-Cushion μCP

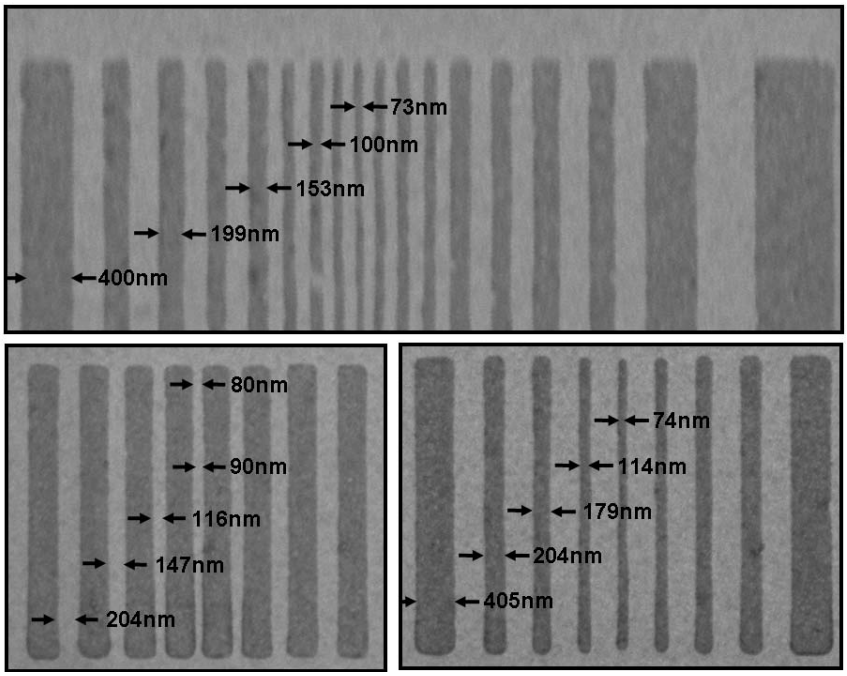

Figure A.15: SEM images (2 kV) of the 75 nm design printed with *Air-Cushion μCP*
Cyt *c* was printed with a Surlyn stamp using a 2.5 MPa Air Cushion process onto gold.

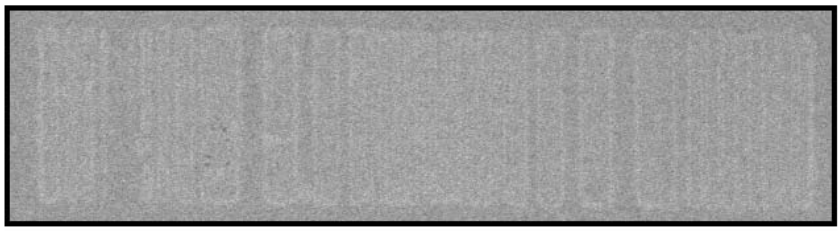

Figure A.16: SEM image (2 kV) of ODT printed with Air Cushion μCP
ODT printed with Surlyn stamp using a 2.5 MPa Air Cushion process onto gold.

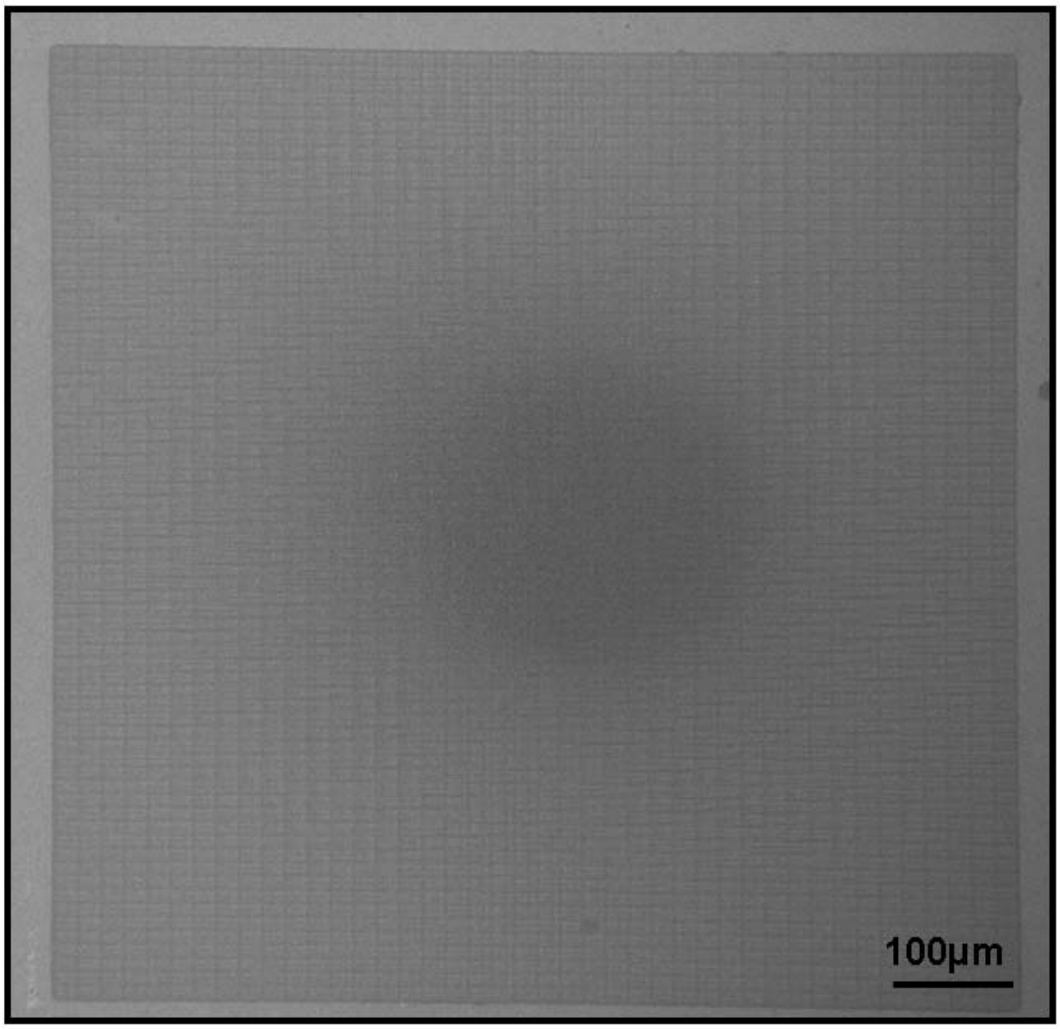

Figure A.17: SEM image (2 kV) of a protein transfer on a 800 μm$*$800μm area
Cyt *c* was printed with *Wet Inking* and *Air-Cushion µCP* using a Surlyn stamp having the design shown in Fig.B.4 onto gold. A very homogeneous result was achieved all over the area. Only three defects can be seen.

Crossbars

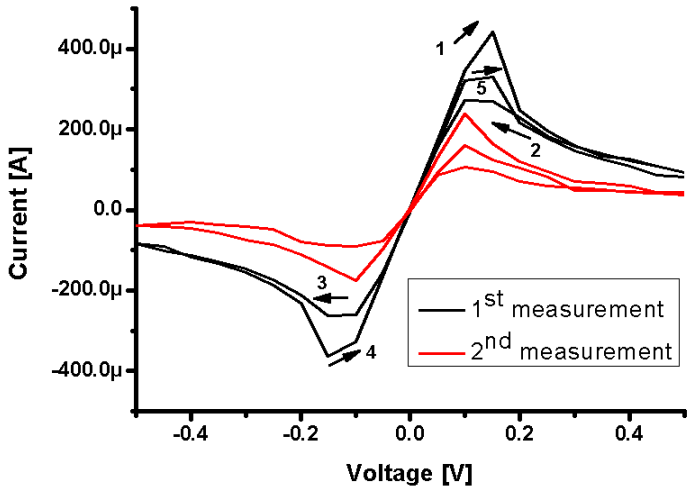

Figure A.18: IV characteristic of a Xbar junction on Affinity VP
A Xbar junction formed on Affinity VP with a MUA/cyt *c* interlayer. This NDR-like characteristic was only observed for this particular junction.

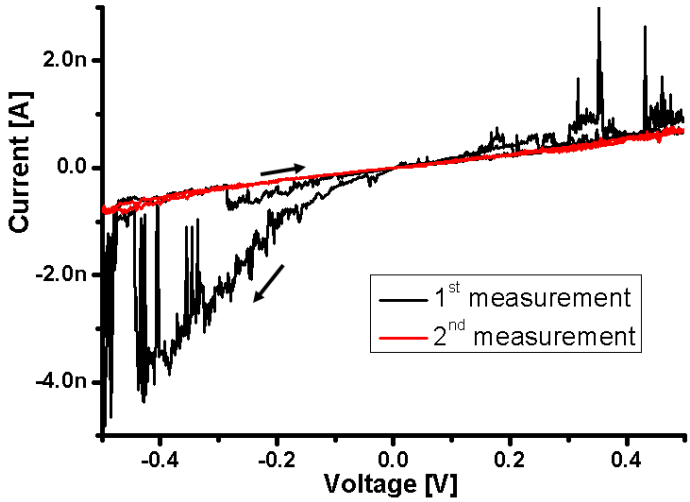

Figure A.19: IV characteristic of a Xbar junction on Affinity VP
A Xbar junction formed on Affinity VP with a MUA/cyt *c* interlayer. This switching characteristic was only observed for this particular junction.

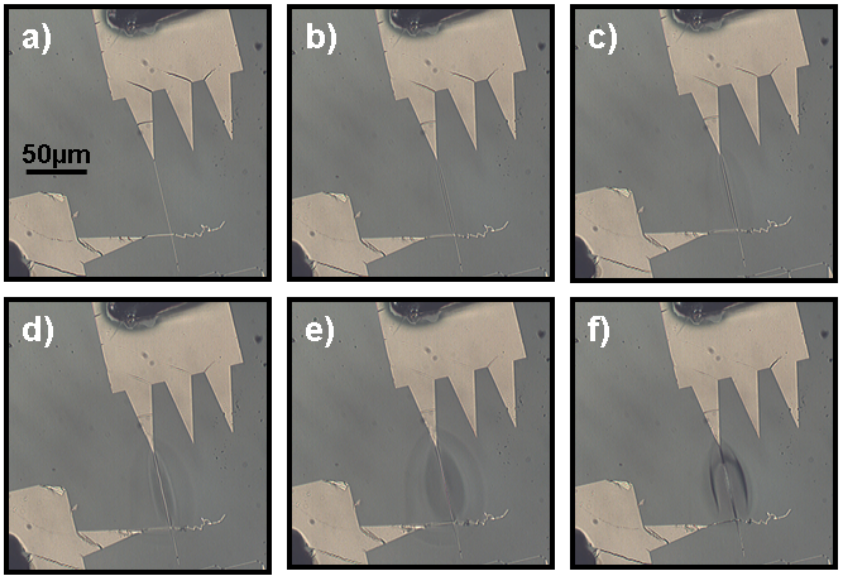

Figure A.20: Microscope images showing the melting of Affinity VP
A voltage was applied between two bondpads. It was swept between 0 - 3 V. At around 1.5 V a current of nA was reached and Affinity VP started to melt. At around 2.7 V the wire broke.

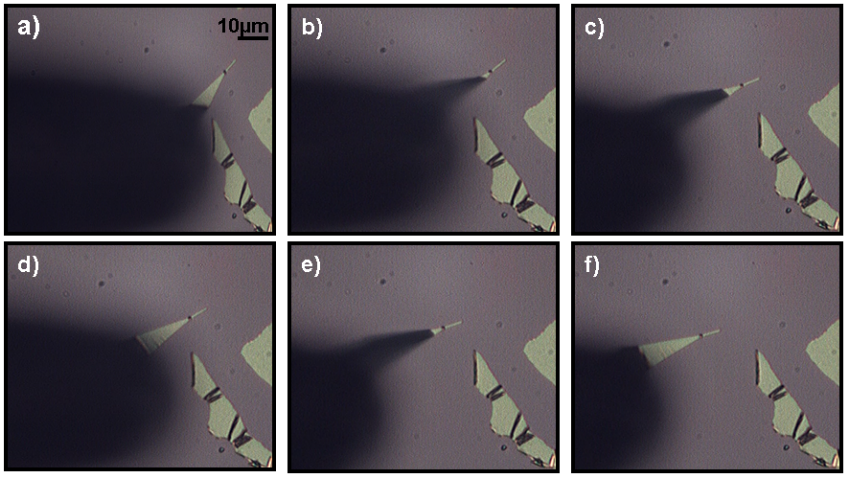

Figure A.21: Microscope images showing the displacement of a top electrode on siliconoxide
The top electrode was transferred with Microset PDMS onto siliconoxide. It stuck to a tungsten tip modified with a droplet of GaIn alloy. The gold could be lifted and moved over the surface without rupturing.

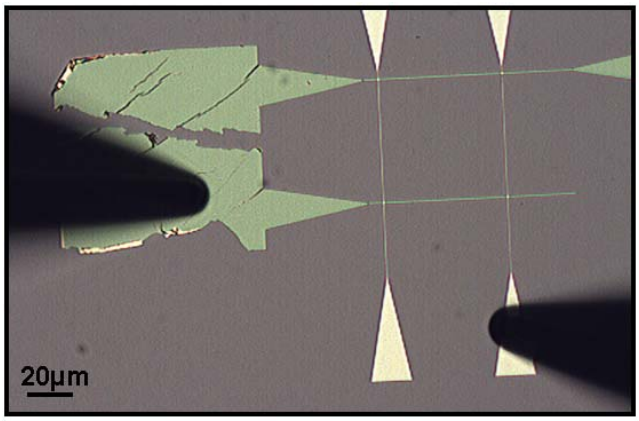

Figure A.22: Microscope image of a typical Xbar array after transfer

Appendix B

Designs

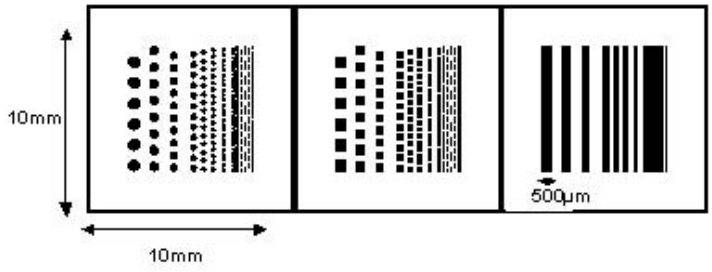

Figure B.1: Design for *micron masters* with squares, dots and lines ranging between 5 μm and 500 μm
This design is realized on a mask for *Optical Lithography*.

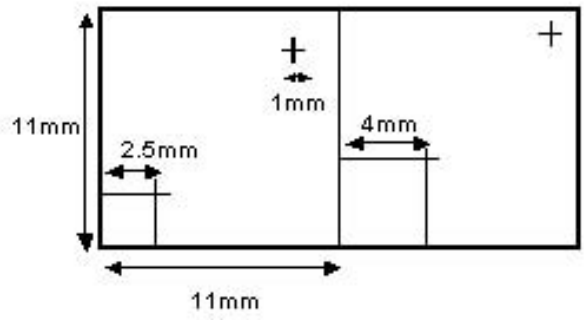

Figure B.2: Design for the gold substrates
This design is realized on a mask for *Optical Lithography*.

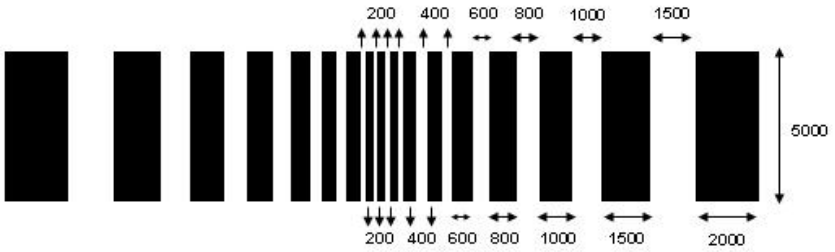

Figure B.3: Design for the *200 nm master*
The design consists of bars of 5 μm length; the width is varied between 200 *nm* and 2 μm; the gap between two bars is also between 200 nm and 2 μm, such that the gap equals the width of the prior bar. Each bar corresponds to a trench in the master.

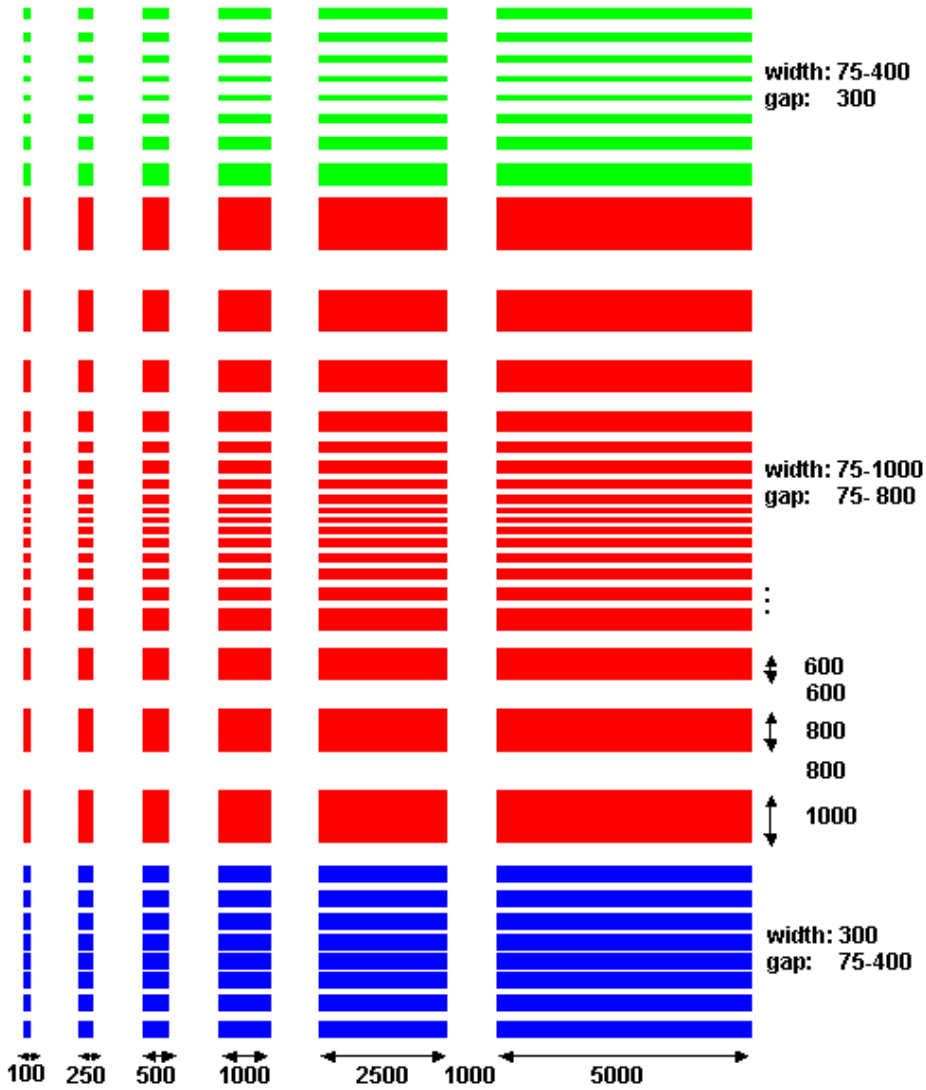

Figure B.4: Design for the *75 nm master* **all values in nm**
The design consists of bars with different lengths, widths and gaps between them. Each bar corresponds to a trench in the master.
a) the gap is 300 nm, the width is varied between 75 *nm* and 1 μm red
b) the width is 300 nm, the gap is varied between 75 *nm* and 1 μm green
c) the width and the gap are both varied between 75 *nm* and 1μm, such that the gap equals the width of the prior bar blue
The lengths are varied between 100*nm* and 5μm

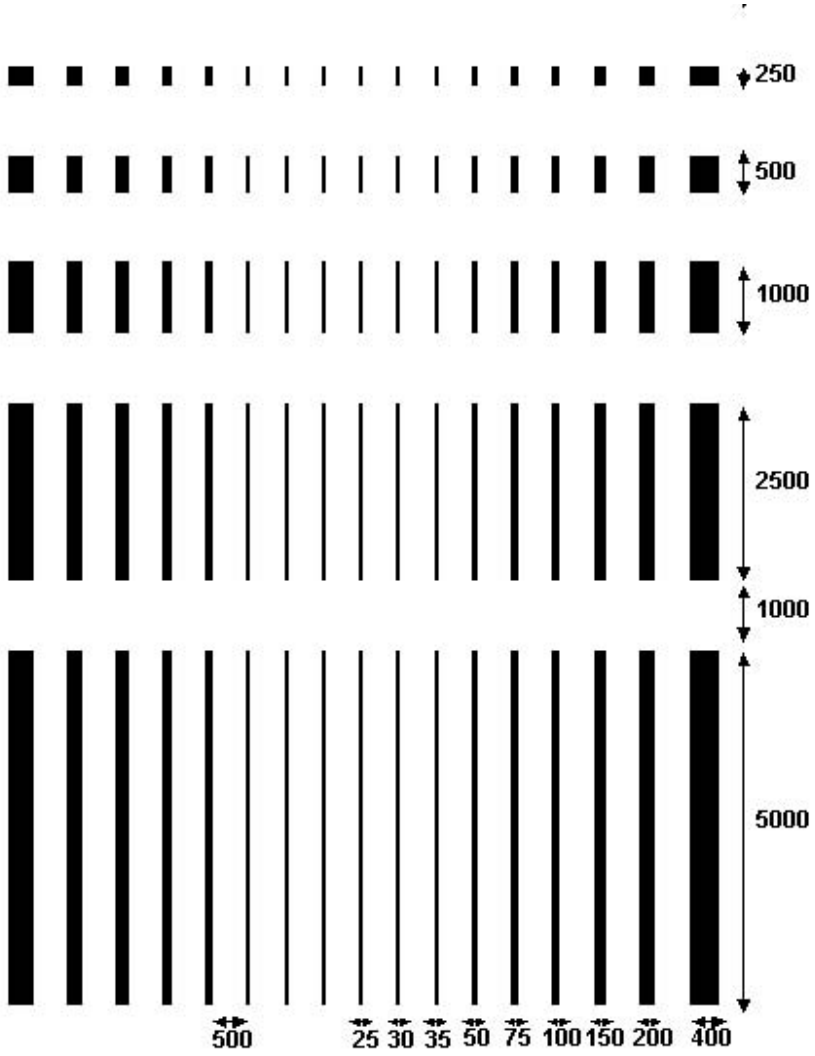

Figure B.5: Design for the *25 nm master*
The design consists of bars separated by a 500 nm gap; the width is varied between 25 *nm* and 400 *nm*; their length is varied between 50 *nm* and 5 μm.

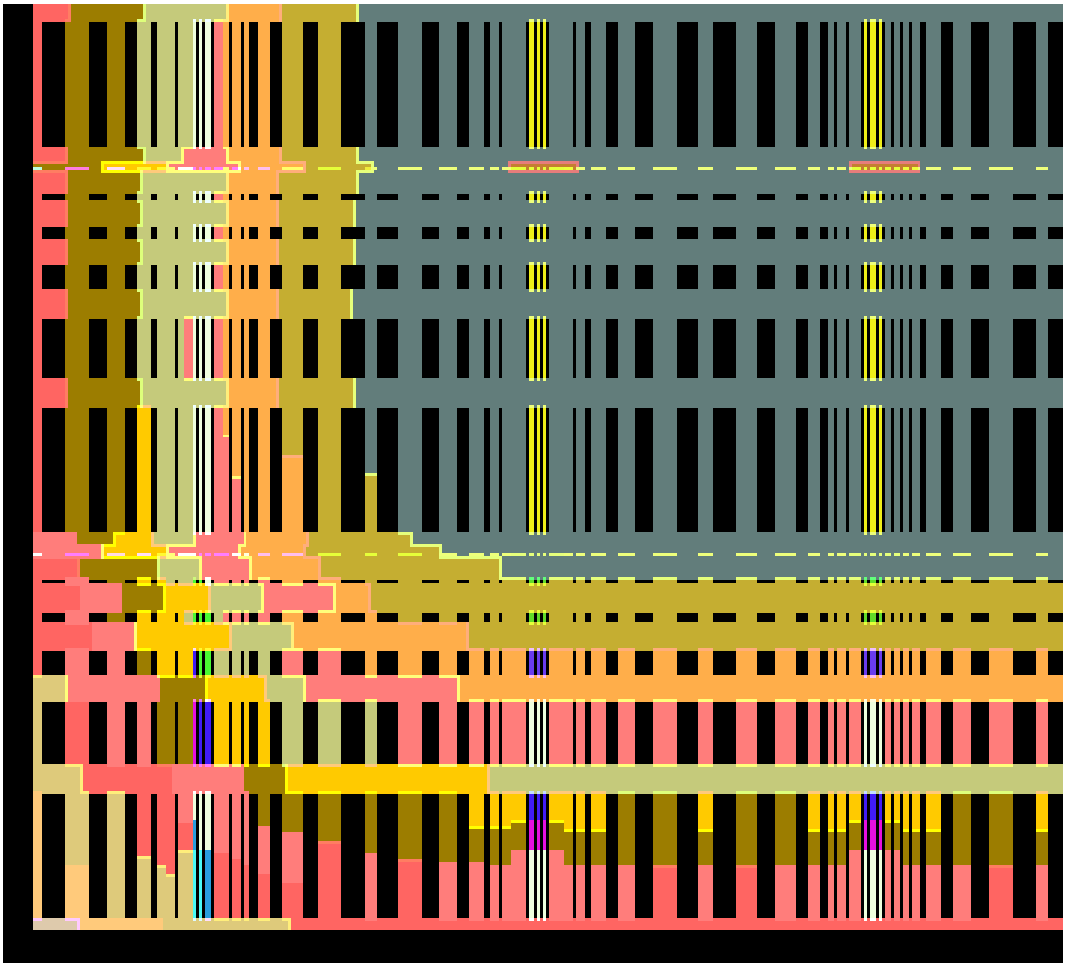

Figure B.6: Proximity corrected doses for 75 nm design
The design is inverted for writing a negative resist (HSQ). Thus all colored lines are written. Each color represents a different dose factors. These factors are multiplied with a basis dose to get the actual doses. Thus different parts of the design are written using different doses.
Proximity correction is necessary to account for the profile of exposure and scattering effects.

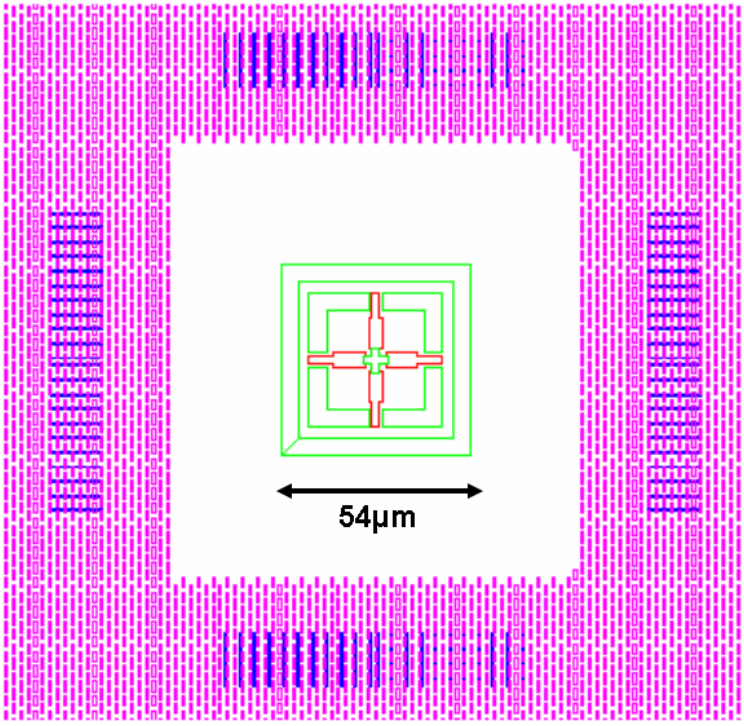

Figure B.7: Design for testing the alignment
green and blue indicate patterns on the substrate
pink and red are patterns on the stamp

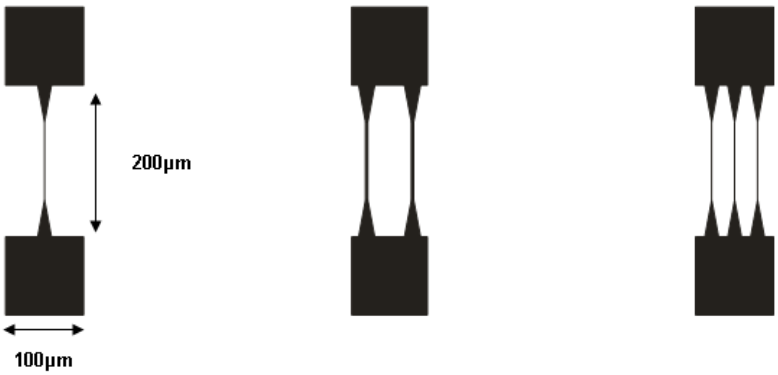

Figure B.8: Design for the *Crossbar* Electrodes.
100 μm bond pads are connected by wires. The wires have taper-triangulares at both ends. The width of wires is varied between 1 μm and 100 nm.

Appendix C

Recipes

Gold substrates

design:	Figure B.2
material:	p-silicon ⟨100⟩
resist	AZ5214 4000 rpm
pre-bake	115 °C / 60 s
exposure:	7 mW, 365 nm, 4.2 s
development:	MIBK 45 s
metal deposition:	5 nm chromium / 50 nm gold
lift off:	acetone 30 min / isopropanol 2 min

Micron master

design:	Figure B.1
material:	p-silicon ⟨100⟩
	400 nm wet oxide
resist:	AZ5214 4000 rpm
pre-bake:	115 °C / 60 s
exposure:	7 mW, 365 nm, 4.2 s
development:	MIBK 45 s
reactive ion etching:	O_2 200 W 2 s; CHF_3/CF_4 200 W 5:30 min; O_2 200 W 20 s
stripping:	acetone, isopropanol

PMMA for direct usage as master

design:	Figure B.3 or B.4
material:	p-silicon ⟨100⟩
resist:	PMMA AR-P661.04 4000 rpm
pre-bake:	$180\,°C\,/\,90\,s$
e-beam:	50 kV 250 μC/cm^2
development:	AR 600.55S 45 s Megasonic 2 MHz 100 % power

PMMA as etch mask for a siliconoxide etch

design:	Figure B.3 or B.4
material:	p-silicon ⟨100⟩
	150 nm wet oxide
resist:	PMMA AR-P661.04 4000 rpm
pre-bake:	180 °C / 90 s
e-beam:	50 kV 250 μC/cm^2
development:	AR 600.55S 45 s Megasonic 2 MHz 100 % power
reactive ion etching:	O_2 200 W 2 s; CHF_3/CF_4 200 W 5:30 min; O_2 200 W 20 s
stripping:	acetone, isopropanol

PMMA as etch mask for a silicon etch

design:	Figure B.4
material:	p-silicon ⟨100⟩
	150 nm silicon-nitride
	100 nm n-polysilicon
resist:	PMMA AR-P641.04 4000 rpm
pre-bake:	180 °C / 90 s
e-beam:	50 kV 250 μC/cm^2
development:	AR 600.55S 45 s Megasonic 2 MHz 100 % power
reactive ion etching:	HBr 50 W bias; 750 W ICP; 2:30 min
stripping:	acetone, isopropanol

PMMA master with 25nm design

design	Figure B.5
material:	p-silicon ⟨100⟩
resist:	PMMA AR-P661.04 4000 rpm
pre-bake:	180 °C / 90 s
e-beam:	50 kV 250 μC/cm^2
development:	AR 600.55S 45 s Megasonic 2 MHz 100 % power
stripping:	acetone, isopropanol

Crossbar Master Top Electrode

design:	Figure B.8
material:	p-silicon ⟨100⟩
resist:	PMMA AR-P661.04 4000 rpm
pre-bake:	180 °C / 90s
e-beam:	50 kV 250 μC/cm^2
development:	AR 600.55S 45 s Megasonic 2 MHz 100 % power
reactive ion etching:	O_2 200 W 15 s
release agent:	fluoro-silanization, 40 μL, 4.5 kPa, 1 h
metal deposition:	20 nm gold at 8 Å/s
lift-off:	acetone 5 s ultrasonic, isopropanol

Crossbar Master Bottom Electrode

design:	Figure B.8
material:	p-silicon ⟨100⟩
resist:	PMMA AR-P661.04 4000 rpm
pre-bake:	180 °C / 90 s
e-beam:	50 kV 400 μC/cm^2
development:	AR 600.55S 45 s Megasonic 2 MHz 100 % power
reactive ion etching:	O_2 200 W 15 s
metal deposition:	5 nm titanium, 5 nm platinum, 20 nm gold
lift-off:	acetone 5 s ultrasonic, isopropanol

HSQ master 75nm design

design:	Figure B.4
material:	p-silicon ⟨100⟩
	150 nm silicon-nitride
	100 nm n-polysilicon
resist:	FOx12 1:4 MIBK 4000 rpm
pre-bake:	150 °C / 2 min and 220 °C / 2 min
e-beam:	50 kV proximity correction
development:	MF-CD26 1 min
reactive ion etching:	HBr 50 W bias, 750 W ICP; 1 min
	HBr:O_2 = 50 : 1 100 W bias, 2000 W ICP; 35 s
stripping:	1 % HF 1 min

HSQ master 25nm design

design:	Figure B.5
material:	p-silicon ⟨100⟩
	150 nm silicon-nitride
	100 nm n-polysilicon
resist:	FOx12 1:4 MIBK 4000 rpm
pre-bake:	150 °C / 2 min and 220 °C / 2 min
e-beam:	50 kV proximity correction
development:	MF-CD26 1 min
reactive ion etching:	HBr 50 W bias, 750 W ICP; 1 min
	HBr:O_2 = 50 : 1 100 W bias, 2000 W ICP; 35 s
stripping:	1 % HF 1min

Bibliography

[Andrade et. al. 1986] ANDRADE, J. D. ; HLADY, V. : Protein Adsorption and Materials Biocompatibility: A Tutorial Review and Suggested Hypotheses. In: *Adv. in Polym. Sci.* 79 (1986)

[Angst et. al. 1991] ANGST, D. L. ; SIMMONS, G. W. : Moisture Adsorption Characteristics of Organosiloxane Self-Assembled Monolayers. In: *Langmuir* 7 (1991), p. 2236–2242

[Aviram et. al. 1974] AVIRAM, A. ; RATNER, M. A. : Molecular Rectifiers. In: *Chem. Phys. Lett.* 29 (1974), p. 277–283

[Austin et. al. 2005] AUSTIN, M. D. ; ZHANG, W. ; GE, H. X. ; WASSERMAN, D. ; LYON, S. A. ; CHOU, S. Y. : 6 nm half-pitch lines and 0.04 mu m(2) static random access memory patterns by nanoimprint. In: *Nanotechnology* 16 (2005), p. 1058–1061

[Balgar et. al. 2003] BALGAR, T. ; BAUTISTA, R. ; HARTMANN, N. ; HASSELBRINK, E. : An AFM study of the growth kinetics of the self-assembled octadecylsiloxane monolayer on oxidized silicon. In: *Langmuir* 11 (1995), p. 4393–4399

[Balmer et. al. 2005] BALMER, T. E. ; SCHMID, H. ; STUTZ, R. ; DELAMARCHE, E. ; MICHEL, B. ; SPENCER, N. D. ; WOLF, H. : Diffusion of Alkanethiols in PDMS and Its Implications on Microcontact Printing. In: *Surf. Sci.* 532-535 (2005), p. 963–969

[Banga et. al. 1995] BANGA, R. ; YARWOOD, J. ; MORGAN, A. M. ; EVANS, B. ; KELLS, J. : FTIR and AFM Studies of the Kinetics and Self-Assembly of Alkyltrichlorosilanes and (Perfluoroalkyl)trichorosilanes onto Glass and Silicon. In: *Langmuir* 11 (1995), p. 4393–4399

[Bard et. al.] BARD, A. J. ; FAULKNER, L. R. : Electrochemical Methods. *John Wiley Sons, Inc.* New York, Chichester, Brisbane, Toronto, Singapore (1980)

[Basch et. al. 2005] BASCH, H. ; COHEN, R. ; RATNER, M. A. : Interface Geometry and Molecular Junction Conductance: Geometric Fluctuation and Stochastic Switching. In: *Nano Letters* 9 (2005), p. 1668–1675

[Bass et. al. 2004] BASS, R. B. ; LICHTENBERGER, A. W. : Microcontact printing with octadecanethiol. In: *Appl. Surf. Sci.* 226 (2004), p. 335–340

[Bender et. al. 2000] BENDER, M. ; OTTO, M. ; HADAM, B. ; VRATZOV, B. ; SPANGENBERG, G. ; KURZ, H. . : Fabrication of Nanostructures using a UV-based imprint technique. In: *Microelectr. Eng.* 53 (2000), p. 233–236

[Berg et. al. 2006] BERG, J. M. ; TYMOCZKO, J. L. ; STRYER, L. : Biochemistry. *W. H. Freeman & Company* 6th edition (2006)

[Bernard et. al. 1998] BERNARD, A. ; DELAMARCHE, E. ; SCHMID, H. ; MICHEL, B. ; BOSSHARD, H. R. ; BIEBUYCK, H. : Printing Patterns of Proteins. In: *Langmuir* 14 (1998), p. 2225–2229

[Bernard et. al. 2000] BERNARD, A. ; RENAULT, J. P. ; MICHEL, B. ; BOSSHARD, H. R. ; DELAMARCHE, E. : Microcontact Printing of Proteins. In: *Adv. Mater.* 12 (2000), p. 1067–1070

[Biasco et. al. 2005] BIASCO, A. ; PISIGNANO, D. ; KREBS, B. ; CINGOLANI, R. ; RINALDI, R. : Microcontact printing of metalloproteins. In: *Synthetic Metals* 153 (2005), p. 21–24

[Biebuyck et. al. 1997] BIEBUYCK, H. ; LARSEN, N. B. ; DELAMARCHE, E. ; MICHEL, B. : Lithography beyond light: Microcontact printing with monolayer resists. In: *IBM J. Res. Dev.* 41 (1997), p. 159–170

[Bietsch et. al. 2000] BIETSCH, A. ; MICHEL, B. : Conformal contact and pattern stability of stamps used for soft lithography. In: *J. Appl. Phys.* 88 (2000), p. 4310–4318

[Bonnell 2001] BONELL, D. : Scanning Probe Microscopy and Spectroscopy. *Wiley-VCH* 2nd Ed. , (2001)

[Bratkovsky 2005] BRATKOVSKY, A. M. : Theory of electron current rectification, switching, and a role of defects in molecular devices. In: *Appl. Phys. A* 80 (2005), p. 1363–1372

[Büttiker et. al. 1985] BÜTTIKER, M. ; IMRY, Y. ; LANDAUER, R. ; PINHAS, S. : Generalized many-channel conductance formula with application to small rings. In: *Phys. Rev. B* 31 (1985), p. 6207–6215

[Bunker et. al. 2000] BUNKER, B. C. ; CARPICK, R. W. ; ASSINK, R. A. ; THOMAS, M. L. ; HANKINS, M. G. ; VOIGT, J. A. ; SIPOLA, D. ; DE BOER, M. P. ; GULLEY, G. L. : The Impact of Solution Agglomeration on the Deposition of Self-Assembled Monolayers. In: *Langmuir* 16 (2000), p. 7742–7751

[Burdinski et. al. 2005] BURDINSKI, D. ; DECRE, M. M. J. ; BRANS, H. J. H. : Single etch patterning of stacked silver and molybdenum alloy layers on glass using microcontact wave printing. In: *J. Am. Chem. Soc.* 127 (2005), p. 10786–10787

[Carter 1983] CARTER, F. L. : Molecular Fabrication techniques and molecular electronic devices. In: *J. Vac. Sci. Technol. B* 1 (1983), p. 959–968

[Chang et. al 2005] CHANG, J. H. ; CHEN, F. S. ; CHAO, C. C. ; WENG, Y. C. ; YANG, S. Y. ; WANG, L. A. : Direct imprinting using soft mold and gas pressure for large areas and curved surfaces. In: *J. Vac. Sci. Technol. A* 23 (2005), p. 1687–16900

[Chen et. al 1999] CHEN, J. ; REED, M. A. ; RAWLETT, A. M. ; TOUR, J. M. : Large On-Off Ratios and Negative Differential Resistance in a Molecular Electronic Device. In: *Science* 286 (1999), p. 1550–1552

[Chen et. al 2003] CHEN, Y. ; JUNG, G. Y. ; OHLBERG, D. A. A. ; LI, X. ; STEWART, D. R. ; JEPPESEN, J. O. ; NIELSEN, K. A. ; STODDART, J. F. ; WILLIAMS, R. S. : Nanoscale molecular-switch crossbar circuits. In: *Nanotechnology* 14 (2003), p. 462–468

[Cherniavskaya et. al. 2002] CHERNIAVSKAYA, O. ; ADZIC, A. ; KNUTSON, C. ; GROSS, B. J. ; ZANG, L. ; LIU, R. ; ADAMS, D. M. : Edge Transfer Lithography of Molecular and Nanoparticle Materials. In: *Langmuir* 18 (2002), p. 7029–7034

[Childs et. al 2005] CHILDS, W. R. ; NUZZO, R. G. : Large-Area Patterning of Coinage-Metal Thin Films Using Decal Transfer Lithography. In: *Langmuir* 21 (2005), p. 195–202

[Choi et. al. 2004] CHOI, Y. H. ; KIM, Y. K. : A nanoscale scalable memory architecture for molecular electronics. In: *Nanotechnology* 15 (2004), p. 639–644

[Chou et. al 1996a] CHOU, S. Y. ; KRAUSS, P. R. ; RENSTROM, P. J. : Nanoimprint Lithography. In: *J. Vac. Sci. B* 14 (1996), p. 4129–4133

[Chou et. al 1996b] CHOU, S. Y. ; KRAUSS, P. R. ; RENSTROM, P. J. : Imprint lithography with 25-nanometer resolution. In: *Science* 272 (1996), p. 85–87

[Chou 2002] CHOU, S. Y. : Fluid Pressure Imprint Lithography. US patent 6,482,742 Nov 2002

[Clark et. al. 1997] CLARK, R. A. ; BOWDEN, E. F. : Voltammetric Peak Broadening for Cytochrome c/Alkanethiolate Monolayer Structures: Dispersion of Formal Potentials. In: *Langmuir* 13 (1997), p. 559–565

[Clavier et. al 1980] CLAVIER, J. ; FAUVE, R. ; GUINET, G. ; DURAND, R. : Preparation of monocrystalline Pt microelectrodes and electrochemical study of the plane surfaces cut in the direction of the 111 and 110 planes. In: *J. Electroanal. Chem.* 107 (1980), p. 205–209

[Coburn et. al 1982] COBURN, J. W. : Plasma etching and reactive ion etching. American Vacuum Society monograph series (1982)

[Colburn et. al 1999] COLBURN, M. ; JOHNSON, S. ; STEWART, M. ; DAMLE, S. ; BAILEY, T. ; CHOI, B. ; WEDLAKE, M. ; MICHAELSON, T. ; SREENIVASAN, S. V. ; EKERDT, J. ; WILLSON, C. G. : Step and flash imprint lithography: A new approach to high-resolution patterning. In: *EMERGING LITHOGRAPHIC TECHNOLOGIES* III (1999), p. 379–389

[Collier et. al 1999] COLLIER, C. P. ; WONG, E. W. ; BELOHRADSKY, M. ; RAYMO, F. M. ; STODDART, J. F. ; KUEKES, P. J. ; WILLIAMS, R. S. ; HEATH, J. R. : Electronically configurable molecular-based logic gates. In: *Science* 285 (1999), p. 391–394

[Crozatier et. al 2006] CROZATIER, C. ; LE BERRE, M. ; CHEN, Y. : Multi-colour micro-contact printing based on microfluidic network inking. In: *Micro. Eng.* 83 (2006), p. 910–913

[Csucs et. al 2003] CSUCS, G. ; KUENZLER, T. ; FELDMAN, K. ; ROBIN, F. ; SPENCER, N. : Microcontact Printing of Maromolecules with Submicrometer Resolution by Means of Polyolefin Stamps. In: *Langmuir* 19 (2003), p. 6104–6109

[Dameron et. al 2005] DAMERON, A. A. ; HAMPTON, J. R. ; SMITH, R. K. ; MULLEN, T. J. ; GILLMOR, S. D. ; WEISS, P. S. : Microdisplacement Printing. In: *Nano Letters* 5 (2005), p. 1834–1837

[Decker 2006] DECKER, T. : Dissertation in preparation (2006), RWTH Aachen university

[Decre et. al. 2004] DECRE, M. M. J. ; SCHNEIDER, R. ; BURDINSKI, D. ; SCHELLEKENS, J. ; SAALMINK, M. ; DONA, R. : Wave Printing (I): Towards Large-Area, Multilayer Microcontact Printing. In: *Mat. Res. Soc. Symp. Proc.* EXS-2 (2004), p. 59–61

[Decre et. al. 2005] DECRE, M. M. J. ; TIMMERMANS, P. H. M. ; VAN DER SLUIS, O. ; SCHROEDERS, R. : Numerical and Experimental Study of Critical Roof Collapse Conditions in Soft Lithography. In: *Langmuir* 21 (2005), p. 7971–7978

[Delamarche et. al. 1998] DELAMARCHE, E. ; SCHMID, H. ; BIETSCH, A. ; LARSEN, N. B. ; ROTHUIZEN, H. ; MICHEL, B. ; BIEBUYCK, H. : Transport Mechanisms of Alkanethiols during Microcontact Printing on Gold. In: *J. Phys. Chem. B* 102 (1998), p. 3324–3334

[Delamarche et. al. 2003] DELAMARCHE, E. ; DONZEL, C. ; KAMOUNAH, F. S. ; WOLF, H. ; GEISSLER, M. ; STUTZ, R. ; SCHMIDT-WINKEL, P. ; MICHEL, B. ; MATHIEU, H. J. ; SCHAUMBURG, K. : Microcontact Printing Using Poly(dimethylsiloxane) Stamps Hydrophilized by Poly(ethylene oxide) Silanes. In: *Langmuir* 19 (2003), p. 8749–8758

[Devaprakasam et. al. 2004] DEVAPRAKASAM, D. ; SAMPATH, S. ; BISWAS, S. K. : Thermal Stability of Perfluoroalkyl Silane Self-Assembled on a Polycrystalline Aluminum Surface. In: *Langmuir* 20 (2004), p. 1329–1334

[Di Carlo et. al. 2005] DI CARLO, A. ; PECCHIA, A. ; LATESSA, L. ; FRAUENHEIM, T. ; SEIFERT, G. : Tight-Binding DFT for Molecular Electronics (gDFTB). In: *Introducing Molecular Electronics* Springer (2005), S. 117–151

[Di Felice et. al. 2005] DI FELICE, R. ; CALZOLARI, A. ; VARASANO, D. ; RUBIO, A. : Electronic Structure Calculations for Nanomolecular Systems. In: *Introducing Molecular Electronics* Springer (2005), S. 77–116

[Dorogi et. al. 1995] DOROGI, M. ; GOMEZ, J. ; OSIFCHIN, R. ; ANDRES, R. P. A. ; REIFENBERGER, R. : Room-temperature Coulomb blockade from a self-assembled molecular nanostructure. In: *Phys. Rev. B* 52 (1995), p. 9071–9077

[O´Dwyer et. al. 2004] O´DWYER, C. ; GAY, G. ; VIARIS DE LESEGNO, B. ; WEINER, J. : The Nature of Alkanethiol Self-Assembled Monolayer Adsorption on Sputtered Gold Substrates. In: *Langmuir* 120 (2004), p. 8172–8182

[Ellenbogen et. al 2000] ELLENBOGEN, J. C. ; LOVE, J. C. : Architectures for Molecular Electronic Computers: 1.Logic Structures and an Adder Designed from Molecular Electronic Diodes. In: *Proc. IEEE* 88 (2000), p. 386–426

[Evans et. al 1949] EVANS, M. G. ; GERGELY, J. : A discussion of the possibility of bands of energy levels in proteins. In: *Biochim. Biophys. Acta* 3 (1949), p. 188–197

[Fedurco 2000] FEDURCO, M. : Redox reactions of heme-containing metalloproteins: dynamic effects of self-assembled monolayers on thermodynamics and kinetics of cytochrome *c* electron-transfer reactions. In: *Coord. Chem. Rev.* 209 (2000), p. 263–331

[Felmet et. al. 2004] FELMET, K. ; LOO, Y. L. ; SUN, Y. : Patterning conductive cooper by nanotransfer printing. In: *Appl. Phys. Lett.* 85 (2004), S. 3316–3318

[Gates et. al. 2003] GATES, B. ; WHITESIDES, G. M. : Replication of Vertical Feature Smaller than 2nm by Soft Lithography. In: *J. Am. Chem. Soc.* 125 (2003), p. 14986–14987

[Gates et. al. 2004] GATES, B. ; XU, Q. ; LOVE, J. C. ; WOLFE, D. B. ; WHITESIDES, G. M. : Unconventional Nanofabrication. In: *Annu. Rev. Mater. Res.* 34 (2004), p. 339–372

[Geissler et. al. 2002] GEISSLER, M. ; SCHMID, H. ; BIETSCH, A. ; MICHEL, B. ; DELAMARCHE, E. : Defect-Tolerant and Directional Wet-Etch System for Using Monolayer as Resists. In: *Langmuir* 18 (2002), p. 2374–2377

[Geissler et. al. 2003] GEISSLER, M. ; KIND, H. ; SCHMIDT-WINKEL, P. ; MICHEL, B. ; DELAMARCHE, E. : Direct Patterning of NiB on Glass Substrates Using Microcontact Printing and Electroless Deposition. In: *Langmuir* 19 (2003), p. 6283–6296

[Geissler et. al. 2003b] GEISSLER, M. ; WOLF, H. ; STUTZ, R. ;DELAMARCHE, E. ; GRUMMT, U. W. ; MICHEL, B. ; BIETSCH, A. : Fabrication of Metal Nanowires Using Microcontact Printing. In: *Langmuir* 19 (2003), p. 6301–6311

[Geissler et. al. 2004] GEISSLER, M. ; XIA, Y. : Patterning: Principles and Some New Developments. In: *Adv. Mater.* 16 (2004), p. 1249–1269

[Geissler et. al. 2005] GEISSLER, M. ; MCLELLAN, J. M. ; XIA, Y. : Edge-Spreading Lithography: Use of Patterned Photoresist Structures to Direct the Spreading of Alkanethiols on Gold. In: *Nano Letters* 5 (2005), p. 31–36

[Gilles 2006] GILLES, S. : Diploma thesis in preparation. (2006), University of Freiberg

[Glasmaestar et. al. 2003] GLASMAESTAR, K. ; GOLD, J. ; ANDERSSON, A. ; SUTHERLAND, D. S. ; KASEMO, B. : Silicone Transfer during Microcontact Printing. In: *Langmuir* 19 (2003), p. 5475–5483

[Goldstein et. al. 2003] GOLDSTEIN, J. ; NEWBURY, D. E. ; JOY, D. C. ; LYMAN, C. E. ; ECHLIN, P. ; LIFSHIN, E. ; SAWYER, L. C. ; MICHAEL, J. R. : Scanning Electron Microscopy and X-ray Microanalysis. *Springer* 3rd Edition, (2003)

[Graham et. al. 2002] GRAHAM, D. J. ; PRICE, D. D. ; RATNER, B. D. : Solution Assembled and Microcontact Printed Monolayers of Dodecanethiol on Gold: A Multivariate Exploration of Chemistry and Contamination. In: *Langmuir* 18 (2002), p. 1518–1527

[Gray et. al. 1995] GRAY, H. B. ; WINKLER, J. R. : Electron Transfer in Proteins. In: *Ann. Rev. Biochem.* 65 (1995), p. 537–561

[Guo et. al. 2004] GUO, Q. ; TENG, X. ; YANG, H. : Overpressure Contact Printing. In: *Nano Letters* 4 (2004), p. 1657–1662

[Haag et. al. 1999] HAAG, R. ; RAMPI, M. A. ; HOLMLIN, R. E. ; WHITESIDES, W. M. : Electrical Breakdown of Aliphatic and Aromatic Self-Assembled Monolayers Used as Nanometer-Thick Organic Dielectrics. In: *J. Am. Chem. Soc.* 121 (1999), p. 7895-7906

[Habuka et. al. 2005] HABUKA, H. ; SUZUKI, K. ; OKAMURA, S. ; SHIMADA, M. ; OKUYAMA, K. : Quartz Crystal Microbalance for Silicon Surface Organic Contamination. In: *J. Electr. Soc.* 154 (2005), p. 241-245

[Haller et. al. 1968] HALLER, I. ; HATZAKIS, M. ; SRINIVASAN, R. : High-resolution positive resists for electron-beam exposure. In: *IBM J. Res. Develop.* 12 (1968), p. 251

[Harlow et. al. 1988] HARLOW, E. ; LANE, D. Eds. : Antibodies: A Laboratory Manual. *Cold Spring Harbor Laboratory Press* (1988)

[Heath et. al 1998] HEATH, J. R. ; KUEKES, P. J. ; SNIDER, G. S. ; WILLIAMS, R. S. : A Defect-Tolerant Computer Architekture: Opportunities for Nanotechnology. In: *Science* 280 (1998), p. 1716–1721

[Heath et. al 2003] HEATH, J. R. ; RATNER, M. A. : Molecular Electronic. In: *Physics Today* May (2003), p. 43–49

[Heckele et. al 2004] HECKELE, M. ; SCHOMBURG, W. K. : Review on micro molding of thermoplastic polymers. In: *J. Micromech. Microeng.* 14 (2004), p. 1–14

[Helmuth et. al 2006] HELMUTH, J. A. ; SCHMID, H. ; STUTZ, R. ; STEMMER, A. ; WOLF, H. : High-Speed Microcontact Printing. In: *J. Am. Chem. Soc.* 128 (2006), p. 9296–9297

[Henschel et. al 2003] HENSCHEL, W. ; GEORGIEV, Y. M. ; KURZ, H. : Study of a high contrast process for hydrogen silesquioxane as a negative tone electron beam resist. In: *J. Vac. Sci. Technol. B* 21 (2003), p. 2018–2025

[Heule et. al 2004] HEULE, M. ; SCHÖNHOLZER, U. P. ; GAUCKLER, L. J. : Patterning colloidal suspensions by selective wetting of microcontact-printed surfaces. In: *J. Euro. Cera. Soc.* 24 (2004), p. 2733–2739

[Hines et. al. 2005] HINES, D. R. ; MEZHENNY, S. ; BREBAN, M. ; WILLIAMS, E. D. ; BALLAROTTO, V. W. ; ESEN, G. ; SOUTHARD, A. ; FUHRER, M. S. : Nanotransfer printing of organic and carbon nanotube thin-film transistors on platics substrates. In: *Appl. Phys. Lett.* 86 (2005), art.no. 163101

[Hoeller 2005] HOELLER, M. : Biophysikalische Charakterisierung des Zell-Transistor-Kontaktes Diploma thesis (2005) , RWTH Aachen university

[Holmlin et. al. 2001] HOLMLIN, R. E. ; HAAG, R. ;CHABINYC, M. L. ; ISMAGILOV, R. F. ; COHEN, A. E. ; TERFORT, A. ; RAMPI, M. A. ; WHITESIDES, G. M. : Electron Transport through Thin Organbic Films in Metal-Insulator-Metal Junctions Based on Self-Assembled Monolayers. In: *J. Am. Chem. Soc.* 123 (2001), p. 5075–5085

[Hovis et. al 2000] HOVIS, J. S. ; BOXER, G. S. : Patterning barriers to lateral diffusion in supported lipid bilayer membranes by blotting and stamping. In: *Langmuir* 16 (2000), S. 894–897

[Hsu et. al. 2003] HSU, J. W. P. ; LOO, Y. L. ; LANG, D. V. ; ROGERS, J. A. : Nature of electrical contacts in a metal-molecule-semiconductor system. In: *J. Vac. Sci. Technol. B* 21 (2003), p. 1928–1935

[Hsu et. al. 2005] HSU, J. W. P. ; LANG, D. V. ;WEST, K. W. ; LOO, Y. L. ; HALLS, M. D. ; RAGHAVACHARI, K. : Probing Occupied States of the Molecular Layer in Au-Alkanedithiol-GaAs Diodes. In: *J. Phys. Chem. B* 109 (2005), p. 5719–5723

[Hu et. al. 2004] HU, W. ; SARESWARAN, K. ; LIEBERMAN, M. ; BERNSTEIN, G. H. : Sub-10nm electron beam lithography using cold development of poly(methylmethacrylate). In: *J. Vac. Sci. Technol. B* 22 (2004), p. 1711–1716

[Hu et. al. 2004b] HU, S. ; REN, X. ; BACHMAN, M. ; SIMS, C. E. ; LI, G. P. ; ALLBRITTON, N. L. : Tailoring the Surface Properties of Poly(dimethylsiloxane) Microfluidic Devices. In: *Langmuir* 20 (2004), p. 5569–5574

[Hua et. al. 2004] HUA, F. ; SUN, Y. ; GAUR, A. ; MEITL, M. A.; BILHAUT, L. ; ROTKINA, L. ; WANG, J. ; GEIL, P. ; SHIM, M. ; ROGERS, J. A.; SHIM, A. : Polymer Imprint Lithography with Molecular-Scale Resolution. In: *Nano Letters* 4 (2004), p. 2467–2471

[Huang et. al. 2004] HUANG, J. ; TAHOORI, M. B. ; LOMBARDI, F. : On the Defect Tolerance of Nano-scale Two-Dimentsional Crossbars. In: *Proceedings. 19th IEEE International Symposium on Defect and Fault Tolerance in VLSI Systems* (2004), p. 96–104

[Huang et. al. 2005] HUANG, Y. Y. ; ZHOU, W. ; HSIA, K. J. ; MENARD, E.; PARK, J. U. ; ROGERS, J. A. ; ALLEYNE, A. G. : Stamp Collapse in Soft Lithography. In: *Langmuir* 21 (2005), p. 8058–8068

[Hui et. al. 2002] HUI, C. Y. ; JAGOTA, A. ; LIN, Y. Y. ; KRAMER, E. J. : Constraints on Microcontact Printing Imposed by Stamp Deformation. In: *Langmuir* 18 (2002), p. 1394–1407

[Hur et. al. 2004] HUR, S. H. ; KHANG, D. Y. ; KOCABAS, C. ; ROGERS, J. A. : Nanotransfer printing by use of noncovalent surface forces: Applications to thin-film transistors that use single-wall carbon nanotube networks and semiconduting polymers. In: *Appl. Phys. Let.* 85 (2004), p. 5730–5732

[Hush 2003] HUSH, N. S. : An Overview of the First Half-Century of Molecular Electronics. In: *Ann. N.Y. Acad. Sci.* 1006 (2003), p. 1–20

[Jacobs et. al. 2001] JACOBS, H. O. ; WHITESIDES, G. M. : Submicrometer patterning of charge in thinfilm electrets. In: *Science* 291 (2001), p. 1763–1766

[James et. al. 1998] JAMES, C. D. ; DAVIS, R. C.; KAM, L. ; CRAIGHEAD, H. G. ; ISAACSON, M. ; TURNER, J. N. ; SHAIN, W. : Patterned protein layers on solid substrates by thin stamp microcontact printing. In: *Langmuir* 14 (1998), p. 741–744

[Jaszewski et. al. 1999] JASZEWSKI, R. E. ; SCHIFT, H.; SCHNYDER, B. ; SCHNEUWLY, A. ; GRÖNING, P. : The deposition of anti-adhesive ultra-thin teflon-like films and their interaction with polymers during hot embossing. In: *Appl. Surf. Sci.* 143 (1999), p. 301–308

[Junarsa et. al. 2005] JUNARSA, I. ; STOYKOVICH, M. P. ; NEALEY, P. F. ; YUANSHENG, M. ; CERRINA, F. ; SOLAK, H. H. : Hydrogen silsesquioxane as a high resolution negative-tone resist for extreme ultraviolet lithography. In: *J. Vac. Sci. Technol. B* 23 (2005), p. 138–143

[Jung et. al. 2004] JUNG, G. Y. ; GANAPATHIAPPAN, S. ; OHLBERG, D. A. A. ; OLYNICK, D. L. ; CHEN, Y. ; TONG, W. M. ; WILLIAMS, R. S. : Fabrication of a 34x34 Crossbar Structure at 50nm Half-pitch by UV-based Nanoimprint Lithography. In: *Nano Letters* 4 (2004), p. 1225–1229

[Jung et. al. 2005] JUNG, G. Y. ; LI, Z. ; WU, W. ; CHEN, Y. ; OLYNICK, D. L. ; WANG, S. Y. ; TONG, W. M. ; WILLIAMS, R. S. : Vapor-Phase Self-Assembled Monolayer for Improved Mold Release in Nanoimprint Lithography. In: *Langmuir* 21 (2005), p. 1158–1161

[Jung et. al. 2006] JUNG, G. Y. ; JOHNSTON-HALPERIN, E. ; WU, W. ; YU, Z. ; WANG, S. Y. ; TONG, W. M. ; LI, Z. ; GREEN, J. E. ; SHERIFF, B. A. ; BOUKAI, A. ; BUNIMOVICH, Y. ; HEATH, J. R. ; WILLIAMS, R. S. : Circuit fabrication at 17nm half-pitch by Nanoimprint Lithography. In: *Nano Letters* 6 (2006), p. 351–354

[Kandallu.R.S. 2006] KANDALLU.R.S., R. : Electrochemical characterization of Pseudomonas aeruginosa azurin on Au(111) electrodes using various immobilization strategies. Master thesis ; Aachen University of Applied Science (2006)

[Kawai et. al. 1998] KAWAI, S. ; TORII, Y. : Highly precise alignments using moire diffraction methods . In: *Jap. Jour. Appl. Phys.* 37 (1998), p. 3691-3694

[Kohli et. al. 2004] KOHLI, N. ; DVORNIC, P. R. ; KAGANOVE, S. N. ; WORDEN, R. M. ; LEE, I. : Nanostructured Crosslinkable Micropatterns by Amphiphilic Dendrimer Stamping. In: *Macromol. Rapid Commun.* 25 (2004), p. 935-941

[Kraus et. al. 2005] KRAUS, T. ; STUTZ, R. ; BALMER, T. E. ; SCHMID, H. ; MALAQUIN, L. ; SPENCER, N. D. ; WOLF, H. : Printing Chemical Gradients. In: *Langmuir* 21 (2005), p. 7796–7804

[Kuekes et. al. 2005] KUEKES, P. J. ; STEWART, D. R. ; WILLIAMS, R. S. : The crossbar latch: Logic value storage, restoration, and inversion in crossbar circuits. In: *J. Appl. Phys.* 97 (2005), art.no. 034301

[Kuekes et. al. 2005b] KUEKES, P. J. ; SNIDER, G. S. ; WILLIAMS, R. S. : Crossbar nanocomputers. In: *Sci. Am.* 293 (2005), p. 48–55

[Kuekes et. al. 2006] KUEKES, P. J. ; ROBINETT, W. ; WILLIAMS, R. S. : Defect tolerance in resistor-logic demultiplexers for nanoelectronics. In: *Nanotechnology* 17 (2006), p. 2466–2474

[Kumar et. al. 1992] KUMAR, A. ; BIEBUYCK, H. A. ; ABBOTT, N. L. ; WHITESIDES, G. M. : The Use of Self-Assembled Monolayers and a Selective Etch to Generate Patterned Gold Features. In: *J. Am. Chem. Soc.* 114 (1992), p. 9188–9189

[Kumar et. al. 1993] KUMAR, A. ; WHITESIDES, G. M. : Features of gold having micrometer to centimeter dimensions can be formed through a combination of stamping with an elastomeric stamp and an alkanethiol "ink" followed by chemical etching. In: *Appl. Phys. Lett.* 63 (1993), p. 2002–2004

[Kushmerick et. al. 2002] KUSHMERICK, J. G. ; HOLT, D. B. ; YANG, J. C. ; NACIRI, J. ; MOORE, M. H. ; SHASHIDHAR, R. : Metal-molecule contacts and charge transport across monomolecular layers: Measurement and theory. In: *Phys. Rev. Lett.* 89 (2002), art. 086802

[LaGraff et. al. 2006] LAGRAFF, J. R. ; LAGRAFF, Q. C. : Scanning Force Microscopy and Fluorescence Microscopy of Microcontact Printed Antibodies and Antibody Fragments. In: *Langmuir* 22 (2006), p. 4685–4693

[Lange et. al. 2004] LANGE, S. A. ; BENES, V. ; KERN, D. P. ; HÖRBER, J. K. ; BERNARD, A. : Microcontact Printing of DNA Molecules. In: *Anal. Chem.* 76 (2004), p. 1641–1647

[Langowski et. al. 2005] LANGOWSKI, B. A. ; UHRICH, K. E. : Oxgen Plasma-Treatment Effects on the Si Transfer. In: *Langmuir* 21 (2005), p. 6366–6372

[Larsen et. al. 1997] LARSEN, N. B. ; BIEBUYCK, H. ; DELAMARCHE, E. ; MICHEL, B. : Order in Microcontact Printed Self-Assembled Monolayers. In: *J. Am. Chem. Soc.* 119 (1997), p. 3017–3026

[Lau et. al. 2005] LAU, C. N. ; STEWART, D. R. ; BOCKRATH, M. ; WILLIAMS, R. S. : Scanned probe imaging of nanoscale conducting channels in Pt/alkanoic acid monolayer/Ti devices. In: *Appl. Phys. A* 80 (2005), p. 1373–1378

[Lauer et. al. 2001] LAUER, L. ; INGEBRANDT, S. ; SCHOLL, M. ; OFFENHÄUSSER, A. : Aligned Microcontact Printing of Biomolecules on Microelectronic Device Surfaces. In: *IEEE Trans. Biomed. Eng.* 48 (2001), p. 838–842

[Leatherman et. al. 1999] LEATHERMAN, G. ; DURANTINI, E. N. ; GUST, D. ; MOORE, T. A. ; MOORE, A. L. ; STONE, S. ; ZHOU, Z. ; REZ, P. ; LIU, Y. Z. ; LINDSAY, S. M. : Carotene as a molecular wire: Conducting atomic force microscopy . In: *J. Phys. Chem. B* 103 (1999), p. 4006–4010

[Lee et. al. 2004] LEE, M. H. ; KIM, Y. K ; CHOI, Y. H. : A Defect-Tolerant Memory Architecture for Molecular Electronics. In: *IEEE Trans. Nanotec.* 3 (2004), p. 152–157

[Li et. al. 2002] LI, H. W. ; KANG, D. J. ; BLAMIRE, M. G. ; HUCK, W. T. S. : High-Resolution Contact Printing with Dendrimers. In: *Nano Letters* 2 (2003), p. 347–349

[Li et. al. 2003] LI, H. W. ; MUIR, B. V. O. ; FICHET, G. ; HUCK, W. T. S. : Nanocontact Printing: A Route to Sub-50-nm-Scale Chemical and Biological Printing. In: *Langmuir* 19 (2003), p. 1963–1965

[Li et. al. 2003b] LI, X. M. ; PETER, M. ; HUSKENS, J. ; REINHOULDT, D. N. : Catalytic Microcontact Printing without Ink. In: *Nano Letters* 3 (2003), p. 1449–1453

[Li et. al. 2003c] LI, H. W. ; KANG, D. J. ; BLAMIRE, M. G. ; HUCK, W. T. S. : Focused ion beam fabrication of silicon print masters. In: *Nanotechnology* 14 (2003), p. 220–223

[Li et. al. 2005] LI, X. ; HUANG, F. ; CURRY, M. ; STREET, S. C. ; WEAVER, M. L.: Improved adhesion of Au thin films to SiOx/Si substrates by dendrimer mediation. In: *Thin Solid Films* 473 (2005), p. 164–168

[Libioulle et. al. 1999] LIBIOULLE, L. ; BIETSCH, A. ; SCHMID, H. ; MICHEL, B. ; DELAMARCHE, E. : Contact-Inking Stamps for Microcontact Printing of Alkanethiols on Gold. In: *Langmuir* 15 (1999), p. 300–304

[Liebau et. al. 2001] LIEBAU, M. ; HUSKENS, J. ; REINHOUDT, D. N. : Microcontact Printing with Heavyweight Inks. In: *Adv. Funct. Mater.* 11 (2001), p. 147–150

[Likharev 2003] LIKHAREV, K. K. : Electronics Below 10nm. In: *Nano and Giga Challenges in Microelec.* (2003), p. 27–68

[Lindsay 2005] LINDSAY, S. : Single-Molecule Electronic Measurements with Metal Electrodes. In: *J. Chem. Edu.* 82 (2005), p. 727–733

[Liou et. al. 1998] LIOU, H. C. ; PRETZER, J. : Effect of curing temperature on the mechanical properties of hydrogen silesquioxane thin films. In: *Thin Solid Films* 335 (1998), p. 186–191

[Long et. al. 2005] LONG, Y. T. ; ABU-IRHAYEM, E. ; KRAATZ, H. B. : Peptide Electron Transfer: More Questions than Answers. In: *Chem. Eur. J.* 11 (2005), p. 5186–5194

[Loo et. al. 2002a] LOO, Y. L. ; WILLETT, R. L. ; BALDWIN, K. W. ; ROGERS, J. A. : Interfacial Chemistries for Nanoscale Transfer Printing. In: *J. Am. Chem. Soc.* 124 (2002), p. 7654–7655

[Loo et. al. 2002b] LOO, Y. L. ; WILLETT, R. L. ; BALDWIN, K. W. ; ROGERS, J. A. : Additive, nanoscale patterning of metal films with a stamp and a surface chemistry mediated transfer process: Applications in plastic electronics. In: *Appl. Phys. Lett.* 81 (2002), p. 562–564

[Loo et. al. 2002c] LOO, Y. L. ; HSU, J. W. P. ; WILLETT, R. L. ; BALDWIN, K. W. ; WEST, K. W. ; ROGERS, J. A. : High-resolution transfer printing on GaAs surfaces using alkane dithiol monolayers. In: *J. Vac. Sci Technol. B* 20 (2002), p. 2853–2856

[Loo et. al. 2003a] LOO, Y. L. ; LANG, D. ; ROGERS, J. A. ; HSU, J. W. P. : Electric Contacts to Molecular Layers by Nanotransfer Printing. In: *Nano Letters* 3 (2003), p. 913–917

[Loo 2003b] LOO, Y. L. : NSF Workshop; April 2003; University of Rochester, NY.

[Luo et. al. 2002] LUO, Y. ; COLLIER, C. P. ; JEPPESEN, J. O. ; NIELSEN, K. A. ; DELONNO, E. ; HO, G. ; PERKINS, J. ; TSENG, H. R. ; YAMAMOTO, T. ; STODDART, J. F. ; HEATH, J. R. : Two-Dimensional Molecular Electronics Circuits. In: *Chem. Phys. Chem* 3 (2002), p. 519–525

[Maile et. al. 2000] MAILE, B. E. ; HENSCHEL, W. ; KURZ, H. ; RIENKS, B. ; POLMAN, R. ; KAARS, P. : Sub-10 nm linewidth and overlay performance achieved with a fine-tuned EBPG-5000 TFE electron beam lithography system. In: *Jpn. J. Appl. Phys.* 39 (2000), p. 6836–6842

[Malak et. al. 2004] MALAK, R. A. ; GAO, Z. ; WISHART, J. F. ; ISIED, S. S. : Long-Range Electron Transfer Across Peptide Bridges: The Transition from Electron Superexchange to Hopping. In: *J. Am. Phys. Soc.* 126 (2004), p. 13888–13889

[Marrian et. al. 2003] MARRIAN, C. R. K. ; TENNANT, D. M. : Nanofabrication. In: *J. Vac. Sci. Technol. A* 21 (2003), p. 207–215

[Maruccio et. al. 2005] MARUCCIO, G. ; BIASCO, A. ; VISCONTI, P. ; BRAMANTI, A. ; POMPA, P. P. ; CALABI, F. ; CINGOLANI, R. ; RINALDI, R. ; CORNI, S. ; DI FELICE, R. ; MOLINARI, E. ; VERBEET, M. R. ; CANTERS, G. W. : Towards protein field-effect transistors: Report and model of prototype. In: *Adv. Mater.* 17 (2005), p. 816–822

[Matsui et. al. 2003] MATSUI, S. ; IGAKU, Y. ; ISHIGAKI, H. ; FUJITA , J. ; ISHIDA, M. ; OCHIAI, Y. ; NAMATSU, H. ; KOMURO, M. : Transfer printing by kinetic control of adhesion to an elastomeric stamp. In: *Nature Mat.* 5 (2006), p. 33–38

[Mayer 2006] MAYER, D. : personal communication. (2006), IBN2-BE Forschungszentrum Jülich

[Meitl et. al. 2006] MEITL, M. A. ; ZHU, Z. T. ; KUMAR, V. ; LEE, K. J. ; FENG, X. ; HUANG, Y. Y. ; ADESIDA, I. ; NUZZO, R. G. ; ROGERS, J. A. : Improved Surface Chemistries, Thin Film Deposition Techniques, and Stamp Designs for Nanotransfer Printing. In: *Langmuir* 20 (2004), p. 6871–6878

[Menard et. al. 2004] MENARD, E. ; BILHAUT, L. ; ZAUMSEIL, J. ; ROGERS, J. A. : Improved Surface Chemistries, Thin Film Deposition Techniques, and Stamp Designs for Nanotransfer Printing. In: *Langmuir* 20 (2004), p. 6871–6878

[Meyer et. al. 2002] MEYER, P. ; EL-KHOLI, A. ; SCHULZ, J. : Investigations of the development rate of irradiated PMMA microstructures in deep X-ray lithography. In: *Microelectr. Engin.* 63 (2002), p. 319–328

[Michel et. al. 2001] MICHEL, B. ; BERNARD, A. ; BIETSCH, A. ; DELAMARCHE, E. ; GEISSLER, M. ; JUNCKER, D. ; KIND, H. ; RENAULT, J. P. ; ROTHUIZEN, H. ; SCHMID, H. ; SCHMID-WINKEL, P. ; STUTZ, R. ; WOLF, H. : Printing meets lithography: Soft approaches to high-resolution patterning. In: *IBM J. Res. and Dev.* 45 (2001), p. 697–719

[Moers 2006] MOERS, J. : personal communication IBN1, FZ Juelich

[Mulliken et. al. 1969] MULLIKEN, R. S. ; PERSON, W. B. : Donor acceptor complexes. In: *Ann. Rev. Phys. Chem.* 30 (1969), p. 107–1026

[Munzert et. al. 2003] MUNZERT, P. ; SCHULZ, U. ; KAISER, N. : Transparent thermoplastic polymers in plasma-assisted coating processes. In: *Surf. Coat. Technol.* 174-175 (2003), p. 1048–1052

[Namatsu et. al. 1998] NAMATSU, H. ; YAMAGUCHI, K. ; NAGASE, M. ; YAMAZAKI, K. ; KURIHARA, K. : Nano-Patterning of Hydrogen Silesquioxane Resist with Reduced Linewidth Fluctuations. In: *Microelectron. Eng.* 41/42 (1998), p. 331–334

[Nitzan 2001] NITZAN, H. : Electron Transmission through Molecules and Molecular Interfaces. In: *Ann. Rev. Phys. Chem.* 52 (2001), p. 681–750

[Ojima et. al. 2005] OJIMA, K. ; OTSUKA, Y. ; MATSUMOTO, T. ; KAWAI, T. ; NAKAMATSU, K. ; MATSUI, S. : Printing electrode for-contact molecular junction. In: *Appl. Phys. Let.* 87 (2005), art. 234110

[Parikh 1979a] PARIKH, M. : Corrections to proximity effects in electron beam lithography. I.Theory In: *J. Appl. Phys.* 50 (1979), p. 4371–4377

[Parikh 1979b] PARIKH, M. : Corrections to proximity effects in electron beam lithography. II. Implementation In: *J. Appl. Phys.* 50 (1979), p. 4378–4382

[Parikh 1979c] PARIKH, M. : Corrections to proximity effects in electron beam lithography. III. Experiments In: *J. Appl. Phys.* 50 (1979), p. 4383–4387

[Park et. al. 2002] PARK, J. ; PASUPATHY, A. N. ; GOLDSMITH, J. I. ; CHANG, C. ; YAISH, Y. ; PETTA, J. R. ; SETHNA, J. P. ; ABRUNA, H. D. ; MCEUEN, P. L. ; RALPH, D. C. : Coulomb blockade and the Kondo effect in single-atom transistors. In: *Nature* 417 (2002), p. 722–725

[Paul et. al. 2003] PAUL, K. E. ; PRENTISS, M. ; WHITESIDES, G. M. : Patterning Spherical Surfaces at the Two-Hundred-Nanometer Scle Using Soft Lithography. In: *Adv. Funct. Mater.* 13 (2003), p. 259–263

[Piner et. al. 1999] PINER, R. ; ZHU, J. ; XU, F. ; HONG, S. ; MIRKIN, C. A. : "Dip-Pen" Nanolithography. In: *Science* 283 (1999), p. 661–663

[Rai-Choudhury Ed. 1997] RAI-CHOUDHURY, P. Ed. : Handbook of Microlithography, Micromachining, and Microfabrication Vol I. *SPIE Press* (1997)

[Rakshit et. al. 2004] RAKSHIT, T. ; LIANG, G. C. ; GHOSH, A. W. ; DATTA, S. : Silicon-based Molecular Electronics. In: *Nano Letters* 4 (2004), p. 1803–1807

[Rampi et. al. 1998] RAMPI, M. A. ; SCHUELLER, O. J. A. ; WHITESIDES, G. M. : Alkanethiols self-assembled monolayers as the dielectric of capacitors with nanoscale thickness. In: *Appl. Phys. Let.* 72 (1998), p. 1781–1783

[Rampi et. al. 2002] RAMPI, M. A. ; WHITESIDES, G. M. : A versatile experimental approach for understanding electron transport through organic materials. In: *Chem. Physics* 281 (2002), p. 373–391

[Reed et. al. 1997] REED, M. A. ; ZHOU, C. ; MULLER, C. J. ; BURGIN, T. P. ; TOUR, J. M. : Conductance of a Molecular Junction. In: *Science* 278 (1997), S. 252–253

[Renault et. al. 2003] RENAULT, J. P. ; BERNARD, A. ; BIETSCH, A. ; MICHEL, B. ; BOSSHARD, H. R. ; DELAMARCHE, E. ; KREITER, M. ; HECHT, B. ; WILD, U. P. : Fabricating Arrays of Single Protein Molecules on Glass Using Microcontact Printing. In: *J. Phys. Chem. B* 107 (2003), p. 703–711

[Reska 2005] RESKA, A. : Elektrophysiologische Charakterisierung neuronaler Netzwerke von Insekten in vitro. Diploma thesis; RWTH Aachen university (2005)

[Richter et. al. 2005] RICHTER, C. A. ; STEWART, D. R. ; OHLBERG, D. A. A. ; WILLIAMS, R. S. : Electrical charcterization of Al/AlOx/molecule/Ti/Al devices. In: *Appl. Phys. A* 80 (2005), p. 1355–1362

[Rinaldi et. al. 2003] RINALDI, R. ;BIASCO, A. ;MARUCCIO, G. ; ARIMA, V. ; VISCONTI, P. ; CINGOLANI, R. ; FACCI, P. ; DE RIENZO, F. ; DI FELICE, R. ; MOLINARI, E. ; VERBEET, M. R. ; CANTERS, G. W. : Electronic rectification in protein devices . In: *Appl. Phys. Lett.* 82 (2003), p. 472–474

[Rinaldi et. al. 2004] RINALDI, R. ; CINGOLANI, R. : Electronic nanodevices based on self-assembled metalloproteins. In: *Physica E* 21 (2005), p. 45–60

[Roca-Cusachs et. al. 2005] ROCA-CUSACHS, P. ; RICO, F. ; MARTINEZ, E. ; TOSET, J. FARRE, R. ; NAVAJAS, D. : Stability of Microfabricated High Aspect Ratio Structures in Poly(dimethylsiloxane). In: *Langmuir* 21 (2005), p. 5542–5548

[Runge et. al. 2003] RUNGE, A. F. ; SAAVEDRA, S. S. : Comparision of Microcontact-Printed and Solution-Adsorbed Cytochrome *c* Films on Indium Tin Oxide Electrodes. In: *Langmuir* 19 (2003), p. 9418–9424

[Salomon et. al. 2003] SALOMON, A. ; CAHEN, D. ; LINDSAY, S. ; TOMFOHR, J. ; ENGELKES, V. B. ; FRISBIE, C. D. : Comparison of Electronic Transport Measurements on Organic Molecules. In: *Adv. Mater.* 15 (2003), p. 1881–1890

[Salomon 2006] SALOMON, O. : Charakterisierung des Ladungstransfers von immobilisiertem Cytochrom c. Dissertation (2006), RWTH Aachen university

[Santhanam et. al. 2004] SANTHANAM, V. ; ANDRES, R. P. : Microcontact Printing of Uniform Nanoparticle Arrays. In: *Nano Letters* 4 (2004), p. 41–44

[Schmid et. al. 2000] SCHMID, H. ; MICHEL, B. : Siloxane Polymers for High-Resolution, High-Accuracy Soft Lithography. In: *Macromolecules* 33 (2000), p. 3042–3049

[Schmid et. al. 2003] SCHMID, H. ; WOLF, H. ; ALLENSPACH, R. ; RIEL, H. ; KARG, S. ; MICHEL, B. ; DELAMARCHE, E. : Preparation of Metallic Films on Elastomeric Stamps and Their Application for Contact Processing and Contact Printing. In: *Adv. Funct. Mater.* 13 (2003), p. 145–153

[Schreiber 2000] SCHREIBER, F. : Structure and growth of self-assembling monolayers. In: *Prog. Surf. Sci.* 65 (2000), p. 151–256

[Schreiber 2006] SCHREIBER, A. : personal communication (2006), MSL, Sony Deutschland

[Sek et. al. 2006] SEK, S. ; MISICKA, A. ; SWIATEK, K. ; MAICKA, E. : Conductance of α-Helical Peptides Trapped within Molecular Junctions. In: *J. Phys. Chem. B* (2006)

[Seunarine et. al. 2006] SEUNARINE, K. ; GADEGAARD, N. ; RIEHLE, M. O. ; WILKINSON, C. D. W. : Optical heating for short hot embossing cycle times. In: *Microelect. Engineering* 83 (2006), p. 859–863

[Sharp et. al. 2004] SHARP, K. G. ; BLACKMAN, G. S. ; GLASSMAKER, N. J. ; JAGOTA, A. ; HUI, C. Y. : Effect of Stamp Deformation on the Quality of Microcontact Printing: Theory and Experiment. In: *Langmuir* 20 (2004), p. 6430–6438

[Sharpe et. al. 2004] SHARPE, R. B. A. ; BURDINSKI, D. ; HUSKENS, J. ; ZANDVLIET, H. J. W. ; REINHOUDT, D. N. ; POELSEMA, B. : Spreading of 16-Mercaptohexadecanoic Acid in Microcontact Printing. In: *Langmuir* 20 (2004), p. 8646–8651

[Sharpe et. al. 2006] SHARPE, R. B. A. ; TITULAER, B. J. F. ; PEETERS, E. ; BURDINSKI, D. ; HUSKENS, J. ; ZANDVLIET, H. J. W. ; REINHOUDT, D. N. ; POELSEMA, B. : Edge Transfer Lithography Using Alkanethiol Inks. In: *Nano Letters* 6 (2006), p. 1235–1239

[Shwartzman et. al. 1985] SHWARTZMAN, S. ; MAYER, A. : Megasonic Particle Removal from Solid-State Wafers. In: *RCA Review* 46 (1985), p. 81–105

[Simmons 1963] SIMMONS, J. G. : Generalized Formula for the Electric Tunnel Effect between Similar Electrodes Separated by a Thin Insulated Film. In: *J. Appl. Phys.* 34 (1963), p. 1793–1803

[Slowinski et. al. 1999] SLOWINSKI, K. ; FONG, H. K. Y. ; MAJDA, M. : Mercury-Mercury Tunneling Junctions. 1. Electron Tunneling across Symmetric and Asymmetric Alkanethiolae Bilayers. In: *J. Am. Chem. Soc.* 121 (1999), p. 7257–7261

[Smith et. al. 2004] SMITH, R. K. ; LEWIS, P. A. ;WEISS, P. S. : Patterning self-assembled monolayers. In: *Prog. Surf. Sci.* 75 (2004), p. 1–68

[Snider et. al. 2005] SNIDER, G. ; KUEKES, P. ; HOGG, T. ; WILLIAMS, R. S. : Nanoelectronic architectures. In: *Appl. Phys. A* 80 (2005), p. 1183–1195

[Song et. al. 1993] SONG, S. ; CLARK, R. A. ;BOWDEN, E. F. : Characterization of cytochrome c/alkanethiolate structures prepared by self-assembly on gold. In: *J. Phys. Chem.* 97 (1993), p. 6564–6572

[Sotomayor Torres *Ed*. 2003] SOTOMAYOR TORRES, C. M. : Alternative Lithography: Unleashing the Potentials of Nanotechnology. *Kluwer Academic* (2003)

[Spatz 2003] SPATZ, J. P. : Cell-Nanostructure interactions. In: *Nanobiotechnology* Wiley VCH, Weinheim (2003), p. 53–65

[Stan et. al. 2003] STAN, M. R. ; FRANZON, P. D. ; GOLDSTEIN, S. C. ; LACH, J. C. ; ZIEGLER, M. M. : Molecular Elelctronics: From Devices and interconnects to Circuits and Architecture. In: *Proc. IEEE* 91 (2003), p. 1940–1956

[Stewart et. al. 2004] STEWART, D. R. ; OHLBERG, D. A. A. ; BECK, P. A. ; CHEN, Y. ; WILLIAMS, R. S. ; JEPPESEN, J. O. ; NIELSEN, K. A. ; STODDART, J. F. : Molecule-Independent Electrical Switching in Pt/Organic Monolayer/Ti Devices. In: *Nano Letters* 4 (2004), p. 133–136

[Stokbro et. al. 2005] STOKBRO, K. ; TAYLOR, J. ; BRANDBYGE, M. ; GUO, H. : Ab-inition Non-Equilibrium Green´s Function Formalism for Calculating Electron Transport in Molecular Devices. In: *Introducing Molecular Electronics* Springer (2005), S. 117–151

[Straka 2005] STRAKA, J. : personal communication. SONOSYS Ultraschallsysteme GmbH

[Strukov et. al. 2005] STRUKOV, D. B. ; LIKHAREV, K. K. : CMOL FPGA: a reconfigurable architecture for hybrid digital circuits with two-terminal nanodevices. In: *Nanotechnology* 16 (2005), p. 888–900

[Sun et. al. 2004] SUN, Y. ; ROGERS, J. A. : Fabricating Semiconductor Nano/Microwires and Transfer Printing Ordered Arrays of Them onto Plastic Substrates. In: *Science* 93 (1941), p. 609–611

[Szent-Gyorgi 1941] SZENT-GYORGI, A. : Towards a new biochemistry?. In: *Nano Letters* 4 (2004), p. 1953–1959

[Takahagi et. al. 1996] TAKAHAGI, T. ; SHINGUBARA, S. ; SAKAUE, H. ; HOSHINO, K. ; YASHIMA, H. : Study on the adsorption behavior of organic contaminations on silicon surface by gas chromotography mass spectrometry. In: *Jap. J. Appl. Phys.* 35 (1996), p. 818–821

[Tallal et. al. 2005] TALLAL, J. ; PEYRADE, D. ; LAZZARINO, F. ; BERTON, K. ; PERRET, C. ; GORDON, M. ; GOURGON, C. ; SCHIAVONE, P. : Replication of sub-40nm gap nanoelectrodes over an 8-in. substrate by nanoimprint lithography. In: *Microelec. Engin.* 78-79 (2005), p. 676–681

[Tan et. al. 2004] TAN, H. ; KONG, L. ; LI, M. ; STEERE, C. ; KOECHER, L. : Current Status of Nanonex Nanoimprint Solutions. In: *SPIE´s The International Society for Optical Engineering: Emerging Lithographic Technologies* VIII (2004), p. 213-221

[Tans et. al. 1998] TANS, S. J. ; VERSCHUEREN, A. R. M. ; DEKKER, C. : Room-temperature transitor based on a single carbon nanotube. In: *Nature* 393 (1998), p. 49

[Tarlov et. al. 1991] TARLOV, M. J. ; BOWDEN, E. F. : Electron-transfer reaction of cytochrome c adsorbed on carboxylic acid terminated alkanethiol monolayer electrodes. In: *J. Am. Chem. Soc.* 113 (1991), p. 1847–1849

[Tien et. al. 2002] TIEN, J. ; NELSON, C. M. ; CHEN, C. S. : Fabrication of aligned microstructures with a single elastomeric stamp. In: *PNAS* 99 (2002), p. 1758–1762

[Tomfohr et. al. 2002] TOMFOHR, J. K. ; SANKEY, O. F. : Simple Estimates of the Electron Transport Properties of Molecules. In: *Phys. Stat. Sol. B* 233 (2002), p. 59–69

[Trellenkamp 2003] TRELLENKAMP, S. : Entwicklung und Charakterisierung vertikaler Double-Gate-MOS-Feldeffekttransistoren. Dissertation (2003), RWTH Aachen university

[Trimbach et. al. 2003] TRIMBACH, D. ; FELDMAN, K. ; SPENCER, N. D. ; BROER, D. J. ; BASTIAANSEN, C. W. M. : Block Copolymer Thermoplastic Elastomers for Microcontact Printing. In: *Langmuir* 19 (2003), p. 10957–10961

[Trimbach et. al. 2004] TRIMBACH, D. C. ; AL-HUSSEIN, M. ; DE JEU, W. H. ; DECRE, M. ; BROER, D. J. ; BASTIAANSEN, C. W. M. : Hydrophilic Elastomer for Microcontact Printing of Polar Inks. In: *Langmuir* 20 (2004), p. 4738–4742

[Tripp et. al. 1993] TRIPP, C. P. ; VEREGIN, R. P. N. ; HAIR, M. LS. : Effect of Fluoroalkyl Substituents on the Reaction of Alkylchlorosilanes with Silica Surfaces. In: *Langmuir* 9 (1993), p. 3518–3522

[van Delft et. al. 2000] VAN DELFT, F. C. M. J. M. ; WETERINGS, J. P. ; VAN LANGEN-SUURLING, A. K. ; ROMIJN, H. : Hydrogen silsesquioxane/novolak bilayer resist for high aspect ratio nanoscale electron-beam lithography. In: *J. Vac. Sci. Technol. B* 18 (2000), p. 3419–3423

[van Delft 2002] VAN DELFT, F. C. M. J. M. : Delay-time and aging effects on contrast and sensitivity of hydrogen silsesquioxane. In: *J. Vac. Sci. Technol. B.* 20 (2002), p. 2932–2936

[van Kan et. al. 2006] VAN KAN, J. A. ; BETTIOL, A. A. ; WATT, F. : Proton Beam Writing of Three-Dimensional Nanostructures in Hydrogen silsesquioxane. In: *Nano Letters* 6 (2006), p. 579–582

[Vieu et. al. 2000] VIEU, C. ; CARCENAC, F. ; PEPIN, A. ; CHEN, Y.; MEJIAS, M. ; LEBIB, A. ; MANIN-FERLAZZO, L. ; COURAUD, L. ; LAUNOIS, H. : Electron beam lithography: resolution limits and applications. In: *Appl. Surf. Sci.* 164 (2000), p. 111–117

[Vilan et. al. 2002] VILAN, A. ; CAHEN, D. : Soft Contact Deposition onto Molecularly Modified GaAs. Thin Metal Film Flotation: Principles and Electrical Effects. In: *Adv. Funct. Mater.* 12 (2002), p. 795–807

[Vogt 2003] VOGT, A. K. : Synaptic Connectivity in Micropatterned Networks of Neuronal Cells. Dissertation (2003), Mainz University

[Wang et. al. 2005] WANG, W. ; LEE, T. ; REED, M. A. : Electron tunneling in self-assembled monolayers. In: *Rep. Prog. Phys.* 68 (2005), p. 523–544

[Wahlbrink et. al. 2005] WAHLBRINK, T. ; MOLLENHAUER, T. ; GEORGIEV, Y. M. ; HENSCHEL, W. ; EFAVI, J. K. ; GOTTLOB, H. D. B. ; LEMME, M. C. ; KURZ, H. ; NIEHUSMANN, J. ; HARING BOLIVAR, P. : Highly selective etch process for silicon-on-insulator nano-devices. In: *Microelec. Engin.* 78-79 (2005), p. 212–217

[Weisenhorn et. al. 1992] WEISENHORN, A. L. ; MAIVALD, P. ; BUTT, H. J. ; HANSMA, P. K. : Measuring adhesion, attraction, and repulsion between surfaces in liquids with an atomic-force microscope. In: *Phys. Rev. B* 45 (1992), p. 11226–11232

[Wolfrum et. al. 2006] WOLFRUM, B. ; MOURZINA, Y. ; SOMMERHAGE, F. ; OFFENHÄUSSER, A. : Suspended Nanoporous Membranes as Interfaces for Neuronal Biohybrid Systems. In: *Nano Letters* 6 (2006), p. 453–457

[Workman et. al. 2004] WORKMAN, R. K. ; MANNE, S. : Molecular Transfer and Transport in Noncovalent Microcontact Printing. In: *Langmuir* 20 (2004), p. 805–815

[Wu et. al. 2005] WU, W. ; JUNG, G. Y ; OLYNICK, D. L. ; STRAZNICKY, J. ; LI, Z. ; LI, X. ; OHLBERG, D. A. A. ; CHEN, Y. ; WANG, S. Y. ; LIDDLE, J. A. ; TONG, W. M. ; WILLIAMS, R. S. : One-kilobit cross-bar molecular memory circuits at 30-nm half-pitch fabricted by nanoimprint lithography. In: *Appl. Phys. A* 80 (2005), p. 1173–1178

[Wu 1973] WU, S. : Polar and Nonpolar Interactions in Adhesion. In: *J. Adhesion* 5 (1973), p. 39–55

[Xia et. al. 1995] XIA, Y. ; ZHAO, X. M. ; KIM, E. ; WHITESIDES, G. M. : A Selective Etching Solution for Use with Patterned Self-Assembled Monolayers of Alkanethiolates on Gold. In: *Chem. Mat.* 7 (1995), p. 2332–2337

[Xia et. al. 1998] XIA, Y. ; WHITESIDES, G. M. : Soft Lithography. In: *Annu. Rev. Mater. Sci* 28 (1998), p. 153–184

[Xiao et. al. 2004] XIAO, X. ; XU, B. ; TAO, N. J. : Measurement of Single Molecule Conductance: Benzendithiol and Benzenedimethanethiol. In: *Nano Letters* 4 (2004), p. 1267–271

[Yan et. al. 1999] YAN, L. ; HUCK, W. T. S. ; ZHAO, X. M. ;WHITESIDES, G. M. : Patterning thin films of poly(ethylene imine) on a reactive SAM using microcontact printing. In: *Langmuir* 15 (2004), p. 1208–1214

[Yan et. al. 2004] YAN, L. ; HUCK, W. T. S. ; WHITESIDES, G. M. : Self-Assembled Monolayers (SAMs) and Synthesis of Planar Micro- and Nanostructures. In: *J. Macromolec. Sci.* 44 (2004), p. 175–206

[Yeung et. al. 2001] YEUNG, C. K. ; LAUER, L. ; OFFENHÄUSSER, A. ; KNOLL, W. : Modulation of the growth and guidance of rat brain stem neurons using patterned extracellular matrix proteins. In: *Neurosci. Let.* 301 (2001), p. 147–150

[York et. al. 2003] YORK, R. L. ; SLOWINSKI, K. : Tunneling conductivity of one- and two-component alkanethiol bilayers in Hg/Hg junctions. In: *J. Electroanal. Chem.* 550-551 (2003), p. 327–336

[Young et. al. 1988] YOUNG, B. R. ; PITT, W. G. ; COOPER, S. L. : Protein Adsorption on Polymeric Biomaterials. In: *J. Coll. Int. Sci.* 124 (1988), p. 28–43

[Zaumseil et. al. 2003] ZAUMSEIL, J. ; MEITL, M. A. ; HSU, J. W. P. ; ACHARYA, B. R. ; BALDWIN, K. W. ; LOO, Y. L. ; ROGERS, J. A. : Three-Dimensional and Multilayer Nanostructures Formed by Nanotransfer Printing. In: *Nano Letters* 3 (2003), p. 1223–1227

[Zeiss 2005] Manual SmartSEM V5.0. Carl Zeiss SMT (2005)

[Zhang et. al. 2002] ZHANG, J. ; WANG, Z. L. ; LUI, Y. ; CHEN, S. ; LIU, G. Y. : Self-assembled Nanostructures. *Kluwer Academic* (2002)

[Zhang et. al. 2006] ZHANG, Y. ; LO, C. W. ; TAYLOR, J. A. ; YANG, S. : Replica Molding of High-Apsect-Ratio Polymeric Nanopillar Arrays with High Fidelity. In: *Langmuir* (2006)

[Zhitenev et. al. 2006] ZHITENEV, N. B. ; JIANG, W. ; ERBE, A. ; BAO, Z. ; GARFUNKEL, E. ; TENNANT, D. M. ; CIRELLI, R. A. : Control of topography, stress and diffusion at molecule-metal interfaces. *Nanotechnology* 17 (2006), p.1272–1277

[Zhong et. al. 2003] ZHONG, Z. ; WANG, D. ; CUI, Y. ; BOCKRATH, M. W. ; LIEBER, C. : Nanowire Crossbar Arrays as Address Decoder for integrated Nanosystems. In: *Science* 302 (2003), p. 1377–1379

[Ziegler et. al. 2003] ZIEGLER, M. M. ; STAN, M. R. : CMOS/Nano Co-Design for Crossbar-Based Molecular Electronic Systems. In: *IEEE Trans. Nanotec.* 2 (2003), p. 217–230

Abbreviations

β	tunneling decay parameter
φ_0	barrier height for a rectangular tunneling barrier
ρ	resistivity
E	Young´s modulus
I	current
J	current density
R	resistance
V	voltage
Ac	acetone
AFM	Atomic Force Microscopy
azurin	azurin from pseudonomas aeruginosa
BE	Bioelectronic
BDT	bezenedithiol
BSA	bovine serum albumin
cyt *c*	horse or bovine heart cytochrome C
CY3	indocarbocyanin
DDT	dodecanethiol
DFT	Density Function Theory
e-beam	Electron Beam
EBL	Electron Beam Lithography
EC	electrochemical
ECM gel	extracellular matrix gel
EtOH	ethanol
FIB	Focussed Ion Beam
HDT	hexadecanethiol
HE	Hot Embossing
HF	hydrofluoric acid
HOMO	highest occupied molecular orbital
HSQ	hydrogensilesquioxane
HT	hexanethiol
ICP	inductive coupled plasma
LPCVD	low pressure chemical vapor deposition
LUMO	lowest unoccupied molecular orbital
ME	Molecular Electronic
MIBK	Methylisobutylketon
μCP	Microcontact Printing
MPA	mercapto-propionic acid
MUA	mercapto-undecanoic acid
NFDC	nonofluoro-hexyl-dimethyl-chlorosilane
NIL	Nanoimprint Lithography

nTP	Nanotransfer Printing
ODT	octadecanethiole
OdiT	octanedithiol
OL	Optical Lithography
OT	octanethiol
PAMAM	polyamido-amid dendrimer
PBS	phosphate buffered salt solution
PDMS	polydimethylsiloxane
PMMA	poly(methylmethacrylate)
POP	polyolefine plastomer
PT	propanethiol
RIE	Reactive Ion Etching
rms	root mean square
rpm	rounds per minute
SAM(s)	self-assembled monolayer(s)
SCE	standard calomel electrode
SEM	Scanning Electron Microscopy
SIMS	Secondary Ion Mass Spectroscopy
SL	Soft Lithography
STP	Shuttle-Transfer Printing
STM	Scanning Tunneling Microscopy
TBBT	4,4´-thiobisbenzenethiol
TFTS	Tridecafluoro-octyltrichlorsilane
UHV	Ultra High Vacuum
Xbar	Crossbar
XPS	X-ray Photoelectron Spectroscopy

Acknoledgements/Danksagung

Zunächst möchte ich mich an dieser Stelle bei allen bedanken, die zum Gelingen dieser Arbeit beigetragen haben. Insbesondere bei...

Prof. Dr. A. Offenhäusser, der mir dieses interessante Thema gestellt hat und immer mit Rat und Tat zur Seite stand.

Dr. D. Mayer, der mich betreut hat und bei allen Problemen stets zur Stelle war.

Dr. A. Yasuda, Dr. J. Wessels, Dr. G. Kron, Dr. M. Riedl, Dr. B. Luessem, A. Schreiber und Z. Karipidou von Sony Deutschland GmbH, Material Science Lab in Stuttgart, die mein Projekt nicht nur finanziell unterstützt haben sondern auch aktiv daran mitgewirkt haben.

Dr. P. Berlin, Dr. S. Böckert-Meffert, Dr. H. Bohn, Dr. H. Bousack, Dr. S. Ingebrandt, Dr. A. Jung, Dr. J. Krause, Dr. F. Nakamura, Dr. Y. Murzina, Dr. M. Papst, Dr. P. Schulte, Dr. B. Wolfrum, Dr. G. Wrobel und allen anderen wissenschaftlichen Mitarbeitern am IBN2 für die gute Zusammenarbeit und das gemeinsame Problemlösen.

M. Banzet, S. Bippus, R. Helpenstein, D. Lomparski, M. Prömpers, S. Schaal, R. Stockmann für die Unterstützung bei der praktischen Umsetzung der Arbeiten.

S. Bunte, K.-H. Deussen, A. v.d.Hart, Dr. J. Moers, J. Mohr, J. Müller, M. Nonn, F. Ringelmann, A. Steffen, H. Wingens und der übrigen Reinraum-Mannschaft für die Unterstützung bei allen angefallenen Reinraumarbeiten

E. Brauweiler-Reuters, H.-P. Bochem, Dr. M. Marso für der Unterstützung am REM und der Probe-Station

F. Amberger, K. Adamiak, D. Borstlap, T. Decker, S. Eick, S. Gilles, Y. Han, B. Hofmann, Dr. S. Meyburg, Dr. O. Salomon, F. Sommerhage, M. Schindler, Dr. S. Weigel, sowie allen anderen Doktoranden, Diplomanden und Masterstudenten für ein angenehmes, interessantes Arbeitsklima.

den technisches Werkstätten, insbesondere bei D. Strobl und G. d´Orsaneo, sowie dem Elektronik-Labor und dem ZCH.

meiner Familie, die mir das Studium ermöglich hat und mich zu jeder Zeit unterstützt hat.

meiner Frau Michaela, die immer für mich da war, grosses Verständnis für meine Arbeit aufbrachte und mich in jedlicher Art und Weise immer unterstützt hat.

Lebenslauf

Daniel Christian Johannes Wendelin Schwaab

geboren:	11.September 1979 in Landau in der Pfalz
wohnhaft:	Wesseling
08.1986-06.1990	Grundschule
08.1990-06.1999	Leibniz Gymnasium Neustadt/Weinstrasse
10.1999-08.2003	Physik-Studium Johannes Gutenberg Universität Mainz
08.2002-08.2003	Diplomarbeit in der Arbeitsgruppe von Uni-Prof. Dr.rer.nat von Harrach Thema: *Ausbau des A4-Bleifluoridkalorimeters und Untersuchung einer bestimmten Form von Strahlenschäden in Bleifluoridkristallen* Institut für Kernphysik, Johannes Gutenberg Universität Mainz
09.2003-12.2003	Graduate Student in der Arbeitsgruppe von Prof. Ferbel High Energy Physics, University of Rochester, Rochester USA
01.2004-09.2006	Promotion in der Arbeitsgruppe von Uni-Prof. Dr.rer.nat. Offenhäusser Thema: *Surface patterning by means of Soft Lithography for Molecular and Bio-Electronics* Institut für Bio- und Nanosysteme 2, Forschungszentrum Jülich
seit 10.2006	Senior Associate Financial Risk Management, KPMG DTG AG